Abstract

Palaeoenvironmental reconstruction using foraminifera relies on the assumption that assemblages reflect the ecological conditions at the time of deposition. However, the distribution of taxa can be greatly affected by transport and reworking of tests. This is particularly important in high energy environments such as submarine canyon and fan systems, which are major pathways for sediment transported from the continental shelf to the abyssal plain. Traditionally, these assemblages have been abandoned as hopelessly taphonomically corrupted, but it is possible that these assemblages contain useful hydraulic information. This project aims to develop the fundamental concepts needed to extract this information, via a series of classical particle hydraulics experiments on empty tests in static water and unidirectional currents. Hyaline foraminifera have been selected for these experiments, as they are the most abundant tests found in shelf and upper-slope environments and consequently are most likely taxa to be entrained into gravity flows.

Static water experiments have shown that settling velocities are significantly different between taxa, meaning that assemblages are likely to fractionate according to species during transportation. Settling velocities range from 0.01 to 0.06 ms^{-1} with larger specimens falling faster than smaller ones. *Elphidium crispum* exhibited the fastest average settling velocity of 0.03 ms^{-1} while *Planorbulina mediterranensis* fell with the lowest average settling velocity of 0.01 ms^{-1}. The occurrence of spatial separation of taxa within a single flow is directly tested using a flume where a spatially waning turbidity current is simulated by a saline density flow. Results show that the slowly settling tests such as *P. mediterranensis* and *Cibicides lobatulus* remain suspended in the current for longer, and are thus transported further than more rapidly settling taxa such as *E. cripsum* and *Ammonia beccarii.*

The experiments have shown that there are significant statistical differences in settling velocity of foraminiferal species and this does result in significantly distinct travelling distances between species in a turbidite. This information is related to the oceanic environment in the Gulf of Cadiz. The signal of fractionation is then identified in core data from Trinidad supplied by Ichron showing that useful assemblage data can be extracted to interpret the depositional environment.

Table of Contents

Table of Figures

Table of Tables

1 Rational and aims

1.1 Rationale

Amongst the most abundant, diverse and well preserved fossils from marine sediments are those of the single-celled Protists, Foraminifera. These microfossils are particularly useful in reconstructing past environmental oceanic conditions, not only due to their diversity and wide geographical distribution but also as a result of their small size and short life span (Sen Gupta, 2002). Consequently, many foraminifera can be relied upon to represent the presence of a specific ecological niche when they are recovered from a particular level in a sedimentary formation. However, before the shells, known as tests, of foraminifera can be used to reconstruct past environments, it is essential that it is considered whether the assemblage under study reliably reflects ecological conditions at the site and the time of study (Murray, 2006). The specific taphonomy of the fossil population, in other words the processes that have occurred during the transformation of the living assemblage into the fossil assemblage, must first be considered before palaeoenvironmental reconstruction is attempted. In particular, the proportion of species in a sedimentary deposit can be greatly affected by transport and reworking of tests due to turbulence and currents before final deposition and accumulation on the sea floor (Murray, 2006). This is particularly relevant in high energy environments such as submarine canyons and fans which are major pathways for sediments being transported from the continental shelf to the abyssal plain (Mullenbach *et al.,* 2004). Thus, assemblages from these environments rarely pass the "test of taphonomy" and generally are considered inadequate for palaeoenvironmental reconstruction (Murray & Alve, 1999).

Post-mortem transport of foraminifera from the continental shelf to the deep sea has been well documented (Harman, 1964; Murray *et al.*, 1982; Venec-Peyre & Le Calvez, 1986: Stanley *et al.,* 1986; Brunner & Ledbetter, 1987; Schafer *et al.,* 1989; Wynn *et al.,* 2002; Hayward *et al.*, 2004; Fontanier *et al.,* 2005; Schroder-Adams *et al.,* 2008). An extreme case of turbidite deposition has been reported at a depth of

8053m in the Palau Trench. Here, Yamamoto *et al.* (1988) found transported calcareous reefal foraminifera well below the carbonate compensation depth. Consequently, although most benthic foraminifera live on continental shelves and slopes at depths up to 1000m (Armstrong & Brasier, 2005) their tests contribute to fossil foraminiferal assemblages across vast areas of the oceans abyssal plains. Not only does this make palaeoenvironmental reconstruction from off-shore sediments a risky proposition, but sediments from these settings provide many of the source, reservoir and seal formations for the world's most significant accumulations of hydrocarbons (Talling *et al.,* 2007). The result is that some of the most potentially important sediments in the geological record are amongst the least likely to be open to normal micropalaeontological assessment.

The traditional view that assemblages from submarine canyon and fan environments are abandoned as hopelessly taphonomically corrupt has been challenged by recent work on the Tertiary deposits of Spain (Rogerson *et al*., 2006) and recent turbidites from the eastern North Atlantic (Talling *et al.,* 2007) which indicate that these assemblages may contain useful information. To extract this information, an understanding of recolonisation of defaunated surfaces and post-mortem transport processes affecting the distribution and final deposition of foraminifera in deep sea environments are necessary. It is the latter that the research described in this thesis is concerned with. Experiments that investigate movement of foraminifera in off-shore environments will enable assessments to be made as to the degree to which assemblages are modified by post-mortem transport and of the processes that modified them. This project aims to develop the fundamental concepts needed to extract this information.

1.2 Aims of thesis

The main barrier to understanding turbidite foraminiferal assemblages lies in differentiating colonising and transported taxa, making understanding of the transportation dynamics of benthic foraminifera a critical consideration. This project aims to develop the fundamental knowledge needed to understand post mortem transport of benthic foraminifera, via a series of classical particle hydraulics

experiments on empty tests. If the palaeoenvironmental information contained within these assemblages can be fully unlocked, new insights into processes of oceanic sediment transportation can be brought to light. This is especially important for hydrocarbon exploration, as off-shore sand deposits provide the reservoir formations for the worlds most significant accumulations of hydrocarbons.

The hydrodynamics of foraminifera are investigated by studying the response of differently shaped benthic foraminiferal tests to unidirectional water currents. Hyaline foraminifera have been selected for these experiments, as they are the most abundant tests found in shelf and upper-slope environments and consequently are most likely taxa to be entrained into gravity flows.

Terminal settling velocities of variously shaped and sized foraminifera are examined in a settling tube to determine differences in settling between species to establish which are most buoyant and likely to remain in suspension longest. Once differences are established experiments are then carried out using a flume where a spatially waning turbidity current is simulated by a saline density flow. This ascertains the possible relationship between settling velocity of foraminifera and the sedimentation sequence of species under turbulent, unidirectional flow conditions. How the results fit into field data is then explored using core data from the Gulf of Cadiz. This contourite oceanic environment is used as a case study to apply the laboratory work to a naturally occurring system. Having related the experimental work to the field, a model is used on a sample of material from an actively producing petroleum field in offshore Trinidad. This enables the sedimentology of the field to be analysed in relation to the hydrodynamics of the foraminifera present.

These results have implications for palaeoenvironmental interpretations and may help towards understanding the energy regime under which sediments are laid down. Being able to differentiate between an autochthonous and a transported assemblage would provide important information on the extent of cap rocks to hydrocarbon fields during drilling campaigns. This "palaeohydraulic micropalaeontology" may provide new insights into processes of oceanic sediment transportation and past ocean-bottom current activity.

1.3 Thesis outline

Chapter 2 is an introduction to the literature surrounding this topic. It includes an explanation of how foraminifera are utilized in the petroleum industry and the use in reconstruction in marine palaeoenvironments. Geographic areas where foraminifera are found is examined as well as taphonomy and particle hydraulics. **Chapter 3** describes the methods and equipment used during the laboratory work. This chapter aims to give details of how the foraminifera are prepared and how they are used in settling velocity procedures and within flume experiments.

Analysis of settling velocity results are given in **Chapter 4**. Comparisons are made between foraminifera taxa in relation to spheres and how this impacts on their hydrodynamic behaviour. It is proposed that the depositional sequence in which they are found in the sedimentary environment reflects post mortem transport where fractionation occurs due to different settling velocities.

Chapter 5 examines the results of flume experiments where the hydrodynamics of the foraminifera are examined with differences in down slope deposition enable comparison between taxa. The results are explored further to investigate the main variables in the flow to understand what causes the foraminifera to either remain in suspension or settle out. The pattern of behaviour down flume is then related to the oceanic environment in **Chapter 6**. Size and shape fractionation in a "real world" setting are discussed from Gulf of Cadiz data where significant post mortem transport can be observed.

Evidence from the experimental work is then related to drilling records from offshore Trinidad in **Chapter 7**. Here different assemblage data within biostratigraphical summaries enables comparisons to be made between turbidites and pelagic muds on the sea floor. This work is then summarized in **Chapter 8** and potential future developments from this study are discussed.

2 Introduction

2.1 Biostratigraphy and its application in the petroleum industry

Biostratigraphy is defined as *"the classification of sediment units according to observable variations in fossil content"* (Lowe & Walker, 1997) and enables a sediment sequence to be divided into biostratigraphic units or biozones, each characterised by a distinctive fossil assemblage. In the context of petroleum exploration, the primary use of biostratigraphy is to provide a means of identifying isochrons within sedimentary successions that contain diachronous formations and/or are laterally variable in terms of sedimentology (Jones, 1996). Biozonations are often local or regional, and effective only for single subsidence basins or for basins over continental-scale regions. However, the International Commission on Stratigraphy (http://www.stratigraphy.org/) is engaged in ongoing development of a global summary of stratigraphic distributions for major microfossil groups for the Palaeozoic, Mesozoic and Cenozoic.

Foraminifera, with their small size, global ecological extent and rapid evolutionary turnover provide an excellent means of biozonation (Kennett & Srinivasan, 1983). Generally the upper to middle slope environments are characterised by buliminides; lower slope environments by rotaliides; and abyssal environments, especially below the carbonate compensation depth, by arenaceous foraminifera (Jones, 2006). Deep-water agglutinated foraminifera have been used during hydrocarbon explorations since the 1970's when the first Deep Sea Drilling Programme (DSDP) established their value for both biostratigraphical and palaeoenvironmental studies (Gradstein & Berggren, 1981). Recent innovations in industrial foraminiferal biostratigraphy have focused on the palaeoenvironmental potential of benthic foraminifera, however this potential hinges on the ability of benthic foraminiferal assemblages to delineate and map environmental conditions at the time of deposition (Murray, 2006).

Benthic foraminifera are strongly controlled by the environment in which they live, with each taxon being restricted to a particular environmental niche; their

presence/absence can therefore be exploited as a palaeoenvironmental proxy (Murray, 2001). Different species colonise a wide range of marine habitats from shallow tidal marshes and lagoons to deep-sea trenches (Gooday *et al.*, 1992; Linke & Lutze, 1993) with first-order controls on distribution being temperature, alkalinity, salinity, depth, dissolved oxygen, photic conditions, nutrient levels (organic matter), substrate character, water turbidity and the presence/absence of toxic substances (Murray, 1991; Boltovskoy *et al.*, 1991; Alve, 1995; De Stigter *et al.*, 1998; Jorissen, 2002; Platon *et al.*, 2005; Mojtahid *et al.*, 2009). Adaption to the considerable range of niches presented by the marine environment has resulted in extensive physiological innovation amongst benthic foraminifera (Hottinger, 2000). Environmental biostratigraphy therefore relies on our ability to identify individual foraminifera to at least genus, if not species, level.

2.2 Foraminiferal taxonomy

The principle criteria used in the suprageneric classification of foraminifera are wall structure, coiling mode and apertural form. There are a large number of subgroups, with the principle ones being agglutinating (Texulariina - Loeblich & Tappan, 1964; Astrorhizida and Lituolida - Haynes, 1981), microgranular and porcellaneous foraminifera (Fusulinina and Miliolina - Loeblich & Tappan, 1964) and hyaline foraminifera (Rotaliina - Loeblich & Tappan, 1964; Nodosariida, Buliminda, Robertinida, Rotaliida and Globigerinida - Haynes, 1981). Fig.2-1 shows a summarised taxonomy of foraminiferal orders as presented by Sen Gupta (2002).

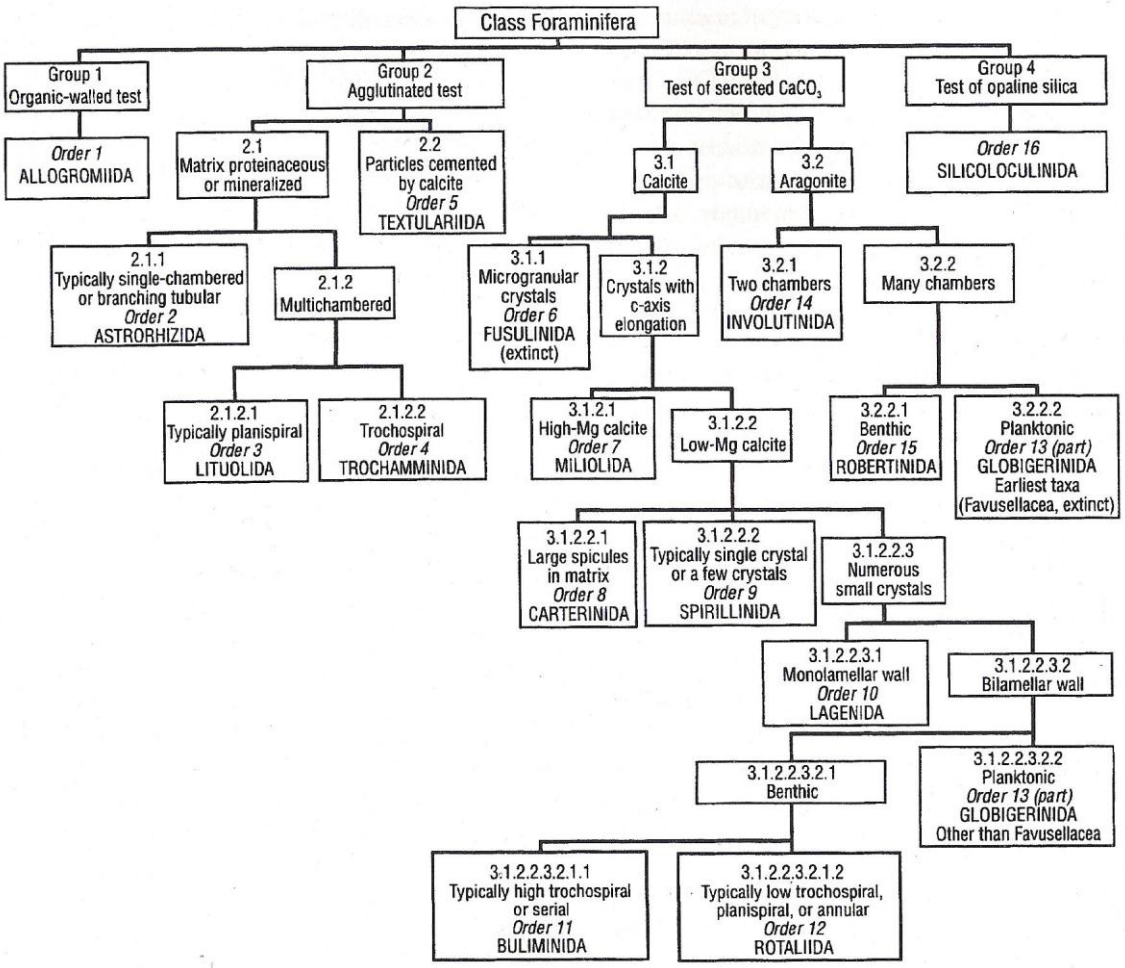

Figure 2-1 Orders of modern foraminifera (Sen Gupta, 2002).

The majority of shelf-sea foraminifera are hyaline and agglutinated forms (Fig.2-2). On shelf environments agglutinated forms have a low preservation potential as the organic cement of taxa degrades upon burial, consequently hyaline foraminifera are the most abundant type in shelf studies (Corliss, 1985; Murray, 2006).

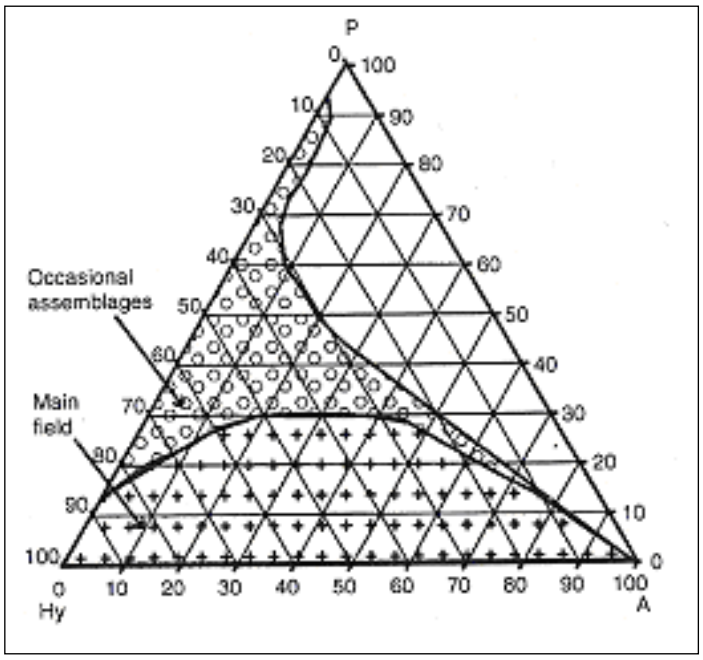

Figure 2-2 Ternary plot for shelf-seas foraminifera test type; P = porcellaneous, A = agglutinated, Hy = hyaline forms (Murray, 2006).

Study of diversity and growth plans by Brasier (1982) recognised three patterns: non-septate contained growth (i.e. a single near-spherical chamber), non-septate continuous growth (i.e. a single tubular chamber) and septate growth (multichambered) (see Fig.2-3). Other features include changes in coiling axis, external surface sculpture and aperture shape (Topa & Tyszka, 2002; Armstrong & Brasier, 2005).

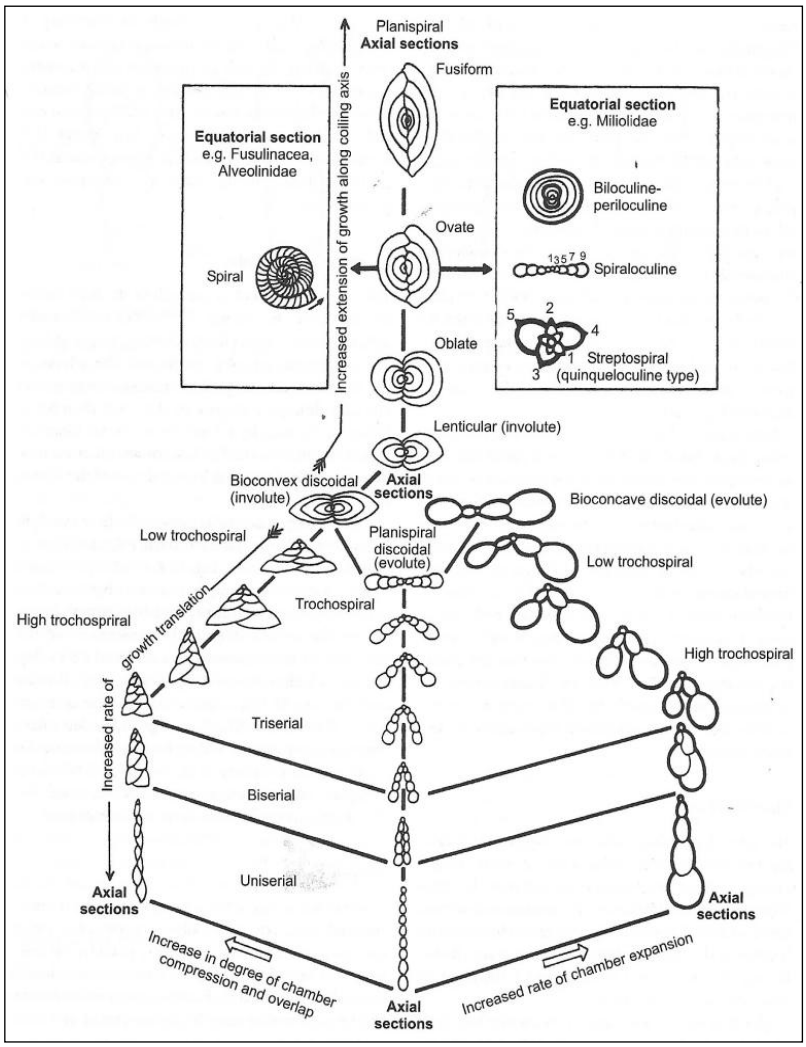

Figure 2-3 Growth forms of multilocular foraminifera. Axial sections are those cut parallel to and including the main axis of symmetry and growth. Equatorial sections are cut at right angles to the axis, at the widest point on the test (Armstrong & Brasier, 2005).

Topa & Tyszka (2002) present a simple geometric model based on isometric growth with chambers being represented by circles or spheres and are described in terms of 'morphospace'. These have been developed further to attempt to simulate foraminiferal shape and growth (Tyszka & Topa, 2005; Tyszka, 2006; Kaminski *et al.*, 2011) as a means of quantification of taxonomy. Describing the morphology of foraminifera and understanding their form, shape and function increases understanding of biological processes and contributes to a better understanding of foraminiferal morphogenesis and evolution.

2.3 Micropalaeontological reconstruction of marine palaeoenvironments

Biological proxies depend on there being a well-defined relationship between the abundance of an organism or community and the magnitude of a given environmental factor (Murray, 2006). For extinct taxa, an approach based on concepts of functional morphology must be adopted (Hottinger, 2000). This method relies upon the relation between test morphology and microhabitat enabling reconstruction of palaeoenvironments (Sen Gupta, 2002). However, it must be recognised that the functional morphology approach would only be effective in roughly 75% of cases for extant taxa (Buzas *et al.*, 1993).

In high energy environments, tests tend to have robust thick shells with heavily ornamented tests of lenticular or globular shape (Wetmore, 1987; Murray, 2006). Epifaunal taxa living in the photic zone often have tests that are flattened on one or both sides while infaunal species tend to be lenticular or elongate (Hottinger, 2000; Armstrong & Brasier, 2005). Plano-convex and biconvex shapes are suggested to be advantageous for attachment at the sediment-water interface during times of bottom turbulence for stability in travelling on or near the surface (Corliss & Chen, 1988).

Several foraminifera taxa are known to exhibit both ecophenotypy (an organisms observable characteristics) and cryptospeciation (Murray, 2006). Haynes (1992) described an ecophenotype as *'a phenotype exhibiting non-genetic adaptations associated with a given habitat or to a given environmental factor'*, and this behaviour can arise from virtually any external factor, for example light intensity in symbiont-bearing forms (Larsen, 1976; Hallock, 1979). Variants of *Amphisteginids* are more spherical in shallow water, being robust and ovate, becoming flatter in deeper waters with thinner test walls reflecting decreased light levels at greater depth (Hallock, 1980, 1983; Leutenegger, 1984). Recent investigations of molecular genetic analysis have shown that morphologically similar forms may be genetically different (Holzmann & Pawlowski, 1997; Holzmann, 2000; Hayward *et al.*, 2004) and the planktonic morphospecies *Globigerina bulloides* is now known to exhibit at least 15 genetic cryptospecies (Kucera *et al.*, 2002). Darling &Wade (2008) state

high cryptic diversity occurs in planktic foraminifera with at least 54 genetic types occurring among 18 planktic foraminiferal morphospecies. In the Northwest Pacific 36 genetic types were identified from 21 morphospecies in planktic foraminifera (Ujiie & Lipps, 2009). It is therefore apparent that further studies are required before morphological and genetic variation can be deciphered and used as a tool for palaeoenvironmental interpretation (Murray, 2006).

The effect of disturbance or tranquility on the sea floor has been shown to influence the distribution of foraminifera, particularly simple agglutinated forms, providing a means of assessing the lateral extent of mudrocks from a single outcrop / core to basin scale (Kaminski, 1985). *'Rhabdammina'* or 'flysch-type' faunas of the abyssal and hadal depositional environments and are often associated with submarine fans (Jones, 2006). Beneath the lysocline mudstones deposited in deep water settings during short intervals of time between successive turbidites have simple agglutinated foraminiferal assemblages dominated by suspension feeders. Mudstones deposited under longer time intervals and quiescent pelagic conditions have a more complex community structure dominated by detritivores (Holmes, 1999). Consequently, the relative abundance of detritivore 'morphogroups' has been used to identify lateral and/or vertical heterogeneity of reservoirs and delineate critical boundary surfaces (Kaminski *et al.,* 1988; Holmes, 1999).

2.4 Deep sea sand formations

Sedimentation in the deep ocean generally reflects the interplay of distal riverine and aeolian sediment supply with biogenic particle production, and is therefore generally fine grained (Reading, 1996). Deposition of sand within these low-energy environments requires significant focusing of current energy, and consequently only occurs under specific conditions involving either gravity transport down relatively steep slopes (Piper *et al,* 1999) or the activity of oceanic currents along them (Stow *et al.,* 1996). The product of these processes, having enhanced porosity and permeability relative to the oceanic oozes they are emplaced into, are prime targets for hydrocarbon exploration (Selley, 2004). So-called 'turbidite' systems, in particular, comprise laterally continuous, stacked sandstones with persistent

mudstones, and as a result present potential source, reservoir and seal lithologies within a single stratigraphic package (Wakefield *et al*, 2001). These packages require only burial to maturation depth to become prolific hosts for hydrocarbon reserves. An estimated 1200 to 1300 oil and gas fields, including discoveries and producing fields, were already known from deep-water turbidite and related systems over a decade ago (Stow & Mayall, 2000).

Turbidites are sedimentary deposits laid down by turbidity currents consisting of high-density flows in which sediment is supported by the upward component of fluid turbulence (Mulder & Alexander, 2001). The 'Bouma cycle' is an idealised sequence of sedimentary structures to describe the transport, deposition and post-depositional processes observed in turbidity-current deposits under waning current conditions (Fig.2-4). The coarsest sands and sometimes gravel is deposited in the proximal part of the fan with flow deposits typically comprising of sand overlain by mud (Selley, 2004). Sequences grade from coarse grains (A) deposited in high energy environments to fine grained muds (E) forming under quiescent conditions. Grain size declines distally downslope as submarine fans grade out into pelagic muds of the basin floor (Kelling & Stanley, 1976).

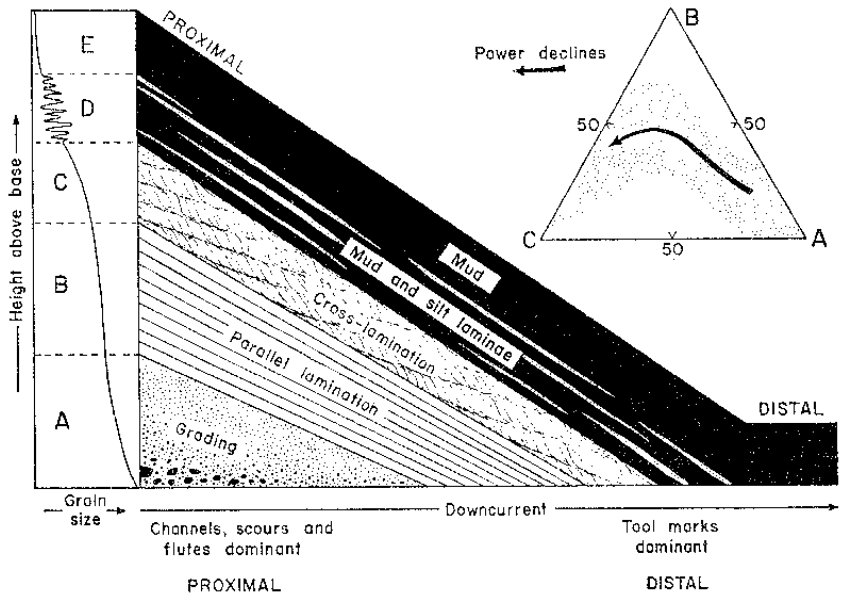

Figure 2-4 Bouma cycle: vertical and lateral (downcurrent) variation in an ideal turbidite bed (Allen, 1977).

Entire sequences are not common and the depositional conditions under which different structures and sequences are laid down results in complex stratigraphy. (Baas *et al.*, 2000; Wynn *et al.*, 2002; Kneller & McCaffrey, 2003; Baas, 2004; Baas *et al.*, 2005; Amy *et al.*, 2006; Talling *et al.*, 2007; Sumner *et al.*, 2008). In high energy flows Bouma-like turbidite deposits are often accompanied by debris flows which have a higher sediment concentration that suppresses turbulence, often containing a cohesive mudflow able to carry large clasts (Iverson, 1997; Talling *et al.*, 2007).

Deep sea depositional environments include slope apron, submarine canyons and ramps, contourite drifts and basin plains (Stow *et al.*, 1996). Submarine channels or canyons dissect the continental slope, often cutting well back into the shelf, and continue down through the continental slope finally debouching their sediment load onto a submarine fan (Selley, 2004). These canyons are major pathways for sediment and organic material to be transported from the continental shelf and upper slope to the deep sea (van Weering *et al.*, 2002). In some systems, canyon erosion via the passage of multiple turbidity currents (where sediment is supported primarily by fluid turbulence) produces degradational morphologies that share many attributes with sub-aerial landscapes produced by surface runoff (Mitchell, 2005).

Submarine fans are a constructional feature on the sea floor that develop as sediment flows from debris and turbidity currents down a canyon from a major point source or from a multiple sourced ramp. They vary from muddy to sand rich depending on the grain size of available sediment and the nature of the supplying system (Reading & Richards, 1994). Mud rich fans are generally enormous (extending over radii of up to 3,000km) and are fed by large volume, far travelling, relatively low density turbidity currents (Stow *et al.*, 1996). Submarine ramps are distinguished from fans in that they have multiple sources from a well supplied sediment shelf and are relatively short-lived progradational and aggradational sequences derived from a multiplicity of switching channels (Reading & Richards, 1994).

Contourites or sediment drifts are fine grained flows that tend to follow the bathymetric contours and bottom currents caused by thermohaline circulation forces

(Stow & Lovell, 1979). Contourite drifts comprise of extensive low-relief accumulations that either fill abyssal basins or occur against continental margins (Habgood *et al.*, 2003) and are volumetrically the most significant deposits associated with contour currents, with giant elongate drifts being tens to hundreds of kilometers long (Faugeres *et al.,* 1993). In addition to these aggradational features, contourite channels can occur as erosive features formed by the action of bottom currents where flows are restricted and velocities are increased (Hernandez-Molina *et al.,* 2006). Both contourite drifts and turbidity currents can result in similar features on the sea floor making differentiation and interpretation a complex task (Shanmugam, 2000). However, contourite deposits generally present fine sandy and muddy facies, in contrast to turbidites which are characterised by sporadic powerful turbidity currents depositing a very broad range of grain sizes (Stow *et al*., 2002). This characterization between contourites and turbidites remains controversial and the recognition of deep-water coarse-grained deposits as contourites requires further investigation (Viana *et al.,* 2007). Due to their distinct reservoir properties, mapping of the limits between turbidites and contourites is critical for reservoir characterization and is of great economic importance (Moreas *et al.,* 2007).

The internal architecture of submarine canyons, fans and contourite drifts are all complicated due to an array of erosion, bypass, deposition and remobilization processes that operate within submarine systems. Understanding has traditionally rested upon sedimentology from core records, seabed sonar (and allied imaging systems) and 3D seismic data (Klaucke *et al.,* 2000; Babinneau *et al.,* 2002; Kenyon *et al.,* 2002; Habgood *et al.,* 2003; Booth *et al*., 2003; Prather, 2003; Klaucke *et al*, 2004). Due to variability of sediment through canyon systems these approaches have not provided a complete picture of environments dominated by turbidite deposition. Consequently, in recent years micropalaeontological tools have been applied to address outstanding conceptual difficulties of discrimination of canyon, fan and open slope (Wakefield *et al*, 2001: Rogerson *et al*., 2005; Jones, 2011). This project may contribute towards a greater understanding of these deep-water processes.

2.5 Taphonomy

Taphonomy is the study of fossilization that encompasses processes during death, pre-burial and post-burial (Doyle, 2004). The main post mortem processes affecting foraminifera are 1) destruction of tests, 2) transport and 3) mixing (Murray, 2006).

2.5.1 Destruction of tests

Destruction of test can be brought about by biological, physical and chemical processes due to predation, infestations by parasites, bioerosion, abrasion and chemical stress (Martin & Liddell, 1991; Barbieri, 2001; Buzas-Stephens & Buzas, 2005; Murray, 2006; Fontanier *et al.,* 2008). Calcareous species are well preserved in most oceanic sediments, except for abyssal depths beneath the carbonate lysocline (Corliss, 1985). The change from well-preserved to poorly preserved assemblages is marked across the lysocline, where differential dissolution of delicate tests and departure to more robust species completely changes the assemblage character (Roth & Berger, 1975). Deep-Water Agglutinated Foraminifera (DWAF) are among the most common benthic organisms recovered from sediments deposited beneath the lysocline due to the chemical stability of their tests (Gradstein & Berggren, 1981).

Peebles and Lewis (1988) described abrasion and dissolution textures as distinctively differentiated: abrasion results in minute scratches and pits and a surface 'polish' in carbonate environments (Cottey & Hallock, 1988; Peebles & Lewis, 1991; Perry, 2000); dissolution produces a coarsened test surface, 'leaving a texture that resembles karst topography' (Peebles & Lewis, 1991). For calcitic tests, dissolution depends on wall thickness, wall structure, mineralogy and chemical composition (Peebles & Lewis, 1991). Low-Mg calcite of hyaline taxa is generally less soluble than the high-Mg calcite of porcelaneous taxa (Hecht *et al.,* 1975; Milliman, 1975; Berner *et al.,* 1976; Peebles & Lewis, 1991; Smith & Nelson, 2003). The correspondence between patterns of larger-scale test loss and patterns of surface alteration suggest that most structural losses are due to dissolution (Berkeley *et al.,* 2009). Both surface dissolution and structural losses are closely related to test architecture, being most common on porous chamber walls, as opposed to nonporous

suture-associated areas and chamber tips (Berkeley *et al.,* 2009). The small size fraction dissolved significantly quicker than the large size fraction (Hecht *et al.,* 1975, Berkeley *et al.,* 2009; Nguyen *et al.,* 2009). Yamashiro (1975) found that larger, heavier, faster settling tests were commonly the most resistant to solution and the lighter, more delicate, slowly settling taxa were the least resistant. As more robust species are more resistant to breakage and solution, as fossils they tend to have a broader distribution than more fragile forms (Thomas & Schafer, 1982).

Experiments have shown that even over long distances, damage to tests does not make benthic foraminifera unrecognizable (Kotler *et al.,* 1992). Transport in suspension selectively affects small tests which generally remain undamaged, resulting in smaller individuals being well preserved and in excellent condition (Murray, 2006; Zhang *et al.,* 1993). In low energy environments such as mud flats or deeper offshore settings abrasion is limited compared to channel near shore high energy locations (Murray & Alve, 1999; Vilela, 2003). Bed load transport is more likely to result in abraded and damaged tests. However, even in high energy systems, abrasion is not an effective mechanism for seriously damaging tests (Martin & Liddell, 1991). Dissolution and abrasion acting together are more effective taphonomic agents than either agent acting alone but only the most fragile species are totally destroyed (Kotler *et al.,* 1992).

2.5.2 Transport

All oceanic environments are dynamic, resulting in the transport of foraminifera by waves and tidal systems, contour currents, turbidity currents and activities of other organisms (Murray, 1991). Whole-assemblage transport of suspended foraminifera in shallow water environments is known to supply individuals that lived on the inner shelf into estuaries, where they accumulate in silty muds in low energy settings (Murray & Hawkins, 1976; Culver & Banner, 1978; Murray, 1980, 1987; Brasier, 1981; Wang & Murray, 1983; Cearreta, 1988, 1989; Gao & Collins, 1995). Within these systems, there is a correlation between the tidal regime of a receiving estuary and the quantity of incoming transported tests (Murray, 1991). In microtidal estuaries, where shelf seas are not subject to powerful tidal, current or wave

disturbances there are typically few allochthonous taxa. Shelf environments protected from cyclones and storms are less likely to exhibit transported tests due to erratic current directions and low bottom current velocities (Snyder *et al.,* 1990; Scoffin, 1993). Mesotidal and macrotidal estuaries, (areas influence of modest and powerful currents) may have more than 50% dead assemblages derived from the adjacent shelf (Wang & Murray, 1983: Murray 1987). Locations affected by storms have been shown to exhibit transport of sediment and winnowing of smaller specimens from these sites (Wilson, 2006; Wilson & Wilson, 2011). The transported component is easily recognizable from its limited size range <200μm and lack of living representatives (Murray, 2006). More recent quantitative research has been carried out on modern larger benthic foraminifera, showing hydrodynamic behaviour of tests is an important factor controlling their distribution in recent environment as well as in the fossil record (Hohenegger & Yordanova, 2001; Yordanova & Hohenegger, 2007; Briguglio & Hohenegger, 2009).

As well as waves, tides and currents foraminifera can also be transported on floating seaweed and seagrass (Boltovskoy & Lena, 1969; Bock, 1970; Spindler, 1980). Foraminifera living on submarine plants in shallow water are subject to transport when the plants are uprooted during storms (Murray, 1991). Tests often remain attached whether living or dead resulting in dispersal into new areas and contribute to the underlying sediment when they die (Bock, 1970). Wind is also an effective agent for transporting foraminifera. Murray (1991) found *Cibicides lobatulus* in bioclastic dunes at Dog's Bay, Connemara, Ireland. On Low Island Reef, northern Great Barrier Reef, Australia the high number of medium sand-sized *Calcarina* and *Amphistegina* tests deposited in the vegetated sands on the edge of the reef flat was a reflection of sorting action by wind (Schueth & Frank, 2008). Goudie and Sperling (1977) found Pleistocene foraminifera were transported up to 800 km into the Thar Desert, northwest India.

On continental slopes, transport and displacement by turbidity currents and within submarine canyons is greatly increased (Schroder-Adams *et al.,* 2008). Bandy (1964) considered that displaced shelf tests formed ~3% of typical basin floor assemblages, but ~25% of submarine fan assemblages and up to 78% of submarine fan sand

assemblages. Vertical variation in submarine fans is manifested by transition from essentially allochthonous assemblages associated with turbidites to interpreted autochthonous assemblages associated with hemipelagites (Jones, 2006).

Brunner & Ledbetter (1987) studied the late Pleistocene levee of the Monerey Fan, Central California and found that turbiditic muds could be distinguished from hemipelagic muds due to hydraulic sorting of benthic foraminifera. Fossil assemblages were biased and sorted in turbidite muds where the tests were small (generally <150μm) and well sorted. The shape varied from platy in silts to more compact and elongate in muds. There were few large specimens and many small tests of similar size. In contrast hemipelagic samples contained larger specimens and varied more in size. (There was a larger mean size and larger standard of error of the mean). They concluded that sorting by shape and size was measureable and statistically significant, but subtle enough so it was difficult to recognize by qualitative, visual inspection.

2.5.3 Mixing

Post-mortem mixing of species caused by transport, reworking of residual sediment and bioturbation causes “blurring” of palaeoenvironmental boundaries (Horton *et al.*, 1999). Bioturbation remains a serious issue when calibrating proxy data and when interpreting the palaeorecord of recent centuries. Most sea floor sediments are dated with radiocarbon, and the sediment is assumed to be zero-aged (modern) when the signal of atmospheric testing of nuclear weapons is present (Fraction modern (Fm) > 1). Keigwin & Guilderson (2009) state that even with Fm >1, half of the planktonic foraminifera on the sea floor can be centuries old because of bioturbation. In paleoenvironmental studies of marine sediments bioturbation is often neglected and/or only treated as a diffusion-like process affecting only the uppermost sediment with decreasing intensity with depth (Leuchner *et al.*, 2002). Deep dwelling animals, like the *Zoophycos* producing animal, however, affect the sediment composition by transporting material over vertical distances of up to 1 m below the seafloor. In Arabian Sea sediment cores (Leuschner *et al.*, 2002) found a significant downward transport of particles by *Zoophycos*. Within the burrows the faunal composition of

both planktonic and benthic foraminiferal assemblages produced radiocarbon ages of up to 10 000 years younger than those from the background sediment.

The bathymetric distribution of foraminifera is used as a tool to estimate paleodepths but downslope transportation and redeposition of individuals can adversely affect interpretations (Mackensen, 1987; Hohenegger, 2005). In modern environments when shallow living species are found with deeper living species they are regarded as transported (Hohenegger, 2005). It is also widely accepted that when live and dead individuals are both counted in a deposit, dead species will often contain representatives of taxa that are not living in situ (Hohenegger, 2005). For this reason, Murray (2000) strongly recommends against using total assemblages in ecological studies, and states that only living assemblages should be used. In view of this it has been found that when allochthonous tests are included in calculations depth is strongly underestimated, but becomes more precise after eliminating dead shallow species (Hohenegger, 2005).

2.6 Particle hydraulics

Particle hydraulics is the study of motion of particles in air, water or other fluids. The process of erosion, transport and deposition of sediment particles by water are controlled essentially by the characteristics of the moving fluid (Robert, 2003). The classical equation used to quantify the importance of forces within a flow is the dimensionless Reynolds number. The Reynolds number describes the dynamics of flow as a measure of the ratio of initial forces compared to viscous forces (Williams, 1996; Robert, 2003; Taylor, 2005) and consequently quantifies the relative importance of these two types of forces for given flow conditions. Under laminar flow viscous forces dominate whereas in turbulent flows inertial forces become more significant (Bridge, 2003). The criterion which determines whether a flow is viscous or turbulent is the quantity $\rho ul/\mu$ (ρ density; u velocity; l characteristic length in the system under consideration; μ dynamic viscosity) which can also be written as ul/ν where ν is the kinematic viscosity ($\nu = \mu/\rho$) (Douglas *et al.*, 2005). The transition from laminar to turbulent flow occurs at a Reynolds number of 500–2000 (Reynolds, 1883).

2.6.1 Settling

The dynamic behaviour of solid grains in fluids is a function of their size, shape and density (Le Roux, 2005) and the turbulent nature of the fluid. For irregular shaped grains, such as foraminifera, size is particularly difficult to quantify. There are various ways to describe dimensional parameters measuring surface or cross-sectional areas and different intersections or projections (Krumbein, 1941: Sneed & Folk, 1958: Matthews, 1991) but more useful measurements for irregular shaped particles include volume and settling velocity *V* parameters (Wadell 1932, 1933). Wadell (1932) introduced volume as a 'nominal diameter' in the equation $D_n = \sqrt[3]{6V/\pi}$. Yordanova & Hohenegger (2007) developed this idea to the measure size of foraminifera using the equation $D_n = 2(3V/4\pi)^{1/3}$. Size, when determined by settling velocity analysis, is expressed in terms of the equivalent sedimentation or fall diameter (D_W), which is the diameter of a sphere with the same settling velocity (Le Roux & Brodalka, 2004). It is generally assumed that the settling velocity of a particle is a more fundamental dynamic property than any geometrically defined measure of size with reference to its behaviour in the hydrodynamic environment (McCave & Syvitski, 1991).

The settling velocity of sediment is one of the key variables in the study of sediment transport, especially when suspension is the dominant process, since it serves to characterize the restoring forces opposing turbulent entraining forces of a particle (Jimenez & Madsen, 2003). For very small particles where the particle Reynolds number is approximately equal to 0.2 (corresponding to sediment $D \sim 100\mu m$ in water (Gibbs *et al.*, 1971)) settling behaviour of spheres can be described using Stokes' Law (Stokes, 1951) as:

$$W_S = \frac{gD^2(\rho s - \rho)}{18\mu} \qquad (2.1)$$

where W_S is settling velocity, g is the acceleration due to gravity, D is particle diameter, ρ_s and ρ are the sediment and fluid densities and μ is the dynamic viscosity

of the liquid. Under these conditions the drag coefficient (C_D) is inversely proportional to the particle Reynolds number and the settling velocity varies as the square of the grain diameter (Robert, 2003). Within the Stokes range (Re < 0.2) the drag on a smooth sphere settling in a fluid can be expressed as:

$$C_D = 24/\mathrm{Re} \tag{2.2}$$

where Re = DW_S/v and v is the kinematic viscosity of the fluid. Outside this region when the drag coefficient does not vary linearly with the particle Reynolds number Stokes Law no longer applies (Paterson, 1997).

Larger particles, including foraminifera, fall within a transitional regime which is neither fully laminar nor fully turbulent. Under fully turbulent conditions the drag coefficient again becomes constant ~ 0.5 when Re >1000 (corresponding to gravel sized sediment (Richards, 1982)) but below this the drag coefficient is not constant and the resistance of the particle to the flow changes non-linearly with velocity (Kravtsov, 1968). In these cases, for spheres the Allen flow equation for settling velocity can be used:

$$Ws = \sqrt{\frac{4gD(\rho s - \rho)}{3\rho C_D}} \tag{2.3}$$

where C_D is the drag coefficient which varies with the particle Reynolds number (Fig.2-5)

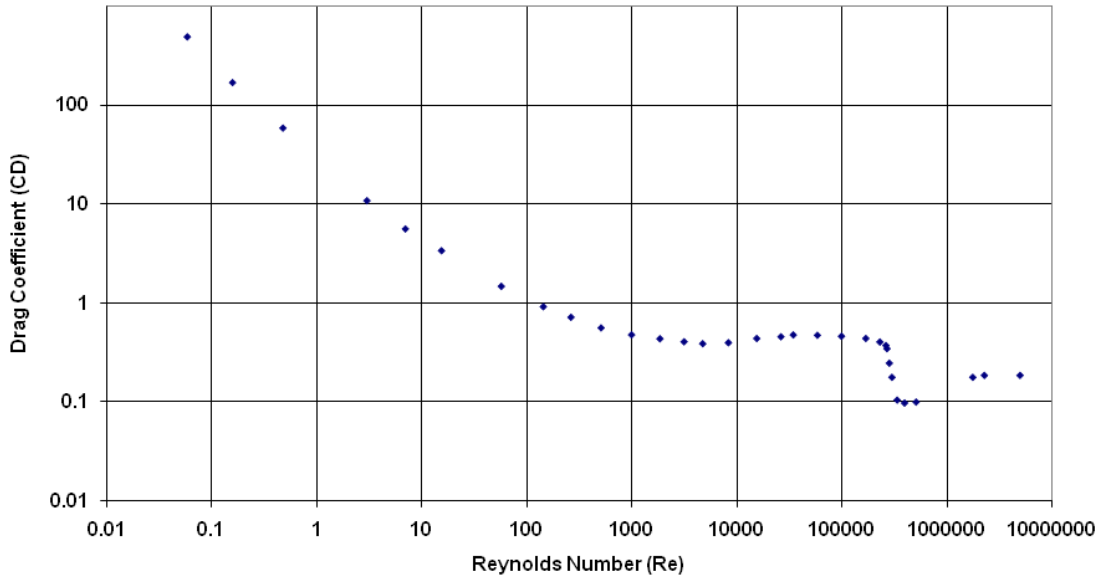

Figure 2-5 Variation of the drag coefficient CD as a function of the Reynolds number for a smooth sphere.

Yordanova & Hohenegger (2007) incorporated volume and area in the following formula to yield different settling velocities for ellipsoid and lenticular shaped larger foraminiferal tests.

$$Ws = \sqrt{\frac{2g\ M(\rho_{test} - \rho)}{C_D \rho\ \ A\, \rho_{test}}} \qquad (2.4)$$

where g is the gravitational force, ρ the density of the test and water, M/ ρ_{test} indicates test volume, A the test area being in horizontal position during sinking and C_D the drag coefficient (Allen, 1984). This equation uses three parameters – test density (ρ_{test}), volume and form, expressed in the area horizontal to the sinking direction, together with the drag coefficient $C_{D.}$

Deviation from sphericity results in setting velocities being lower than that of a sphere with the same nominal diameter. The result is that more non-spherical a particle is, the greater the reduction in its settling velocity (McNowan & Malaika, 1950; Maiklem, 1968; Komar & Reimers, 1978; Jimenez & Madsen, 2003). This is attributed to drag variations due to flow separation as the particle falls and development of turbulence in the wake of the particle. This depends on the geometry

of the solid body, and specifically how streamlined it is (Ganguly, 1990; Le Roux, 2005). At higher particle Reynolds numbers than the upper limit of the Stokes law (the transitional range), settling velocity is strongly influenced by shape, consequently additional shape factors are required to embrace the dynamics of irregularly shaped particles (Bridge, 2003a; Borah & Chhabra, 2005), including foraminifera.

Two distinct approaches have been used to correlate the settling velocity of irregularly shaped particles with some shape parameter. The first compares the settling velocity of a non-spherical particle with that of an equal volume sphere diameter under identical conditions. In this case, the ratio of the two velocities is related to the sphericity of the particle and to some measure of the orientation of the particle relative to its downward fall direction (Borah & Chhabra, 2005). The second relies on developing relationships which associate Reynolds number with drag coefficients in order to endeavour to reconcile drag data for variously shaped particles into one curve, akin to the standard drag curve for spheres (Chhabra *et al.*, 1999).

In order to compensate for shape effects, various shape factors have been invoked (Corey, 1949; McNown *et al.*, 1951; Briggs *et al.*, 1962; Janke, 1966; Mantz, 1977; Melhta *et al.*, 1980); the most widely used being the Corey Shape Factor where c/√ab, (shortest diameter divided by the square root of the longest and intermediate diameters). A shape factor value of with zero indicates a 2D plate, and a value unity represents a sphere. Many formulas for predicting settling velocities include coefficients *A* and *B* , which are obtained by experimental data for sediments within the transitional range. These include functions for shape (CSF) and roundness (*P*) (Dietrich, 1982; Zhu & Cheng, 1993; Cheng, 1997; Le Roux, 1997, 2002; Ahrens, 2000; Guo, 2002; Jimenez & Madsen, 2004; She *et al.*, 2005; Zhiyao *et al.*, 2008). An established formula for calculating the settling velocity of natural sediments is expressed by the formula:

$$\mathrm{W}s = \frac{v}{d} d_*^3 \left[\left(\frac{3A}{4} \right)^{2/n} + \left(\frac{3B}{4} d_*^3 \right)^{1/n} \right]^{-n/2} \qquad (2.5)$$

where d is the particle diameter, d_* is the dimensionless particle diameter ($d_* = (\Delta g/\nu^2)^{1/3} d$), n is an exponent and ν is the fluid kinematic viscosity (Camenen, 2007; Zhiyao *et al.*, 2008). Using coefficient data where A=32.2, B=1.17 and n=1.75, Zhiyao *et al.*, (2008) derived the settling velocity formula from experimental data of settling velocities of natural sediment particles:

$$Ws = \frac{\nu}{d} d_*^3 \left[38.1 + 0.93 d_*^{12/7}\right]^{-7/8} \quad (2.6)$$

This was shown to obtain a higher degree of accuracy than previously published formulas.

2.6.2 Entrainment

The movement of a resting particle entrained by flow is based on the balance of forces between the weight of the particle and the drag forces extended by the flow on the particle (Li, 1994). For a fluid to begin transporting sediment that is currently at rest on a surface, the boundary (or bed) shear stress exerted by the fluid must exceed the critical shear stress for the initiation motion of grains at the bed. This is typically represented by a comparison between a dimensionless shear stress (τ_b*) and a dimensionless critical shear stress (τ_c*). This balancing of shear stress is classically described by the Shields diagram (Fig.2-6). Shields (1936) used experimental data from the transport of non-cohesive, nearly uniform grains to calculate the dimensionless critical shear stress. The non-dimensionalisation is in order to compare the driving forces of particle motion (shear stress) to the resisting forces that would make it stationary (particle density and size). This dimensionless shear stress, τ*, is given by $*= \tau/(\rho_s - \rho)gD$. The dimensionless critical shear stress is related to particle Reynolds number (where D is the grain size and δ_o is the thickness of the laminar sublayer). This shear stress varied with the ratio between the boundary roughness and the thickness of the viscous sublayer (a very thin region next to the boundary where turbulent mixing is impeded) associated with the flow.

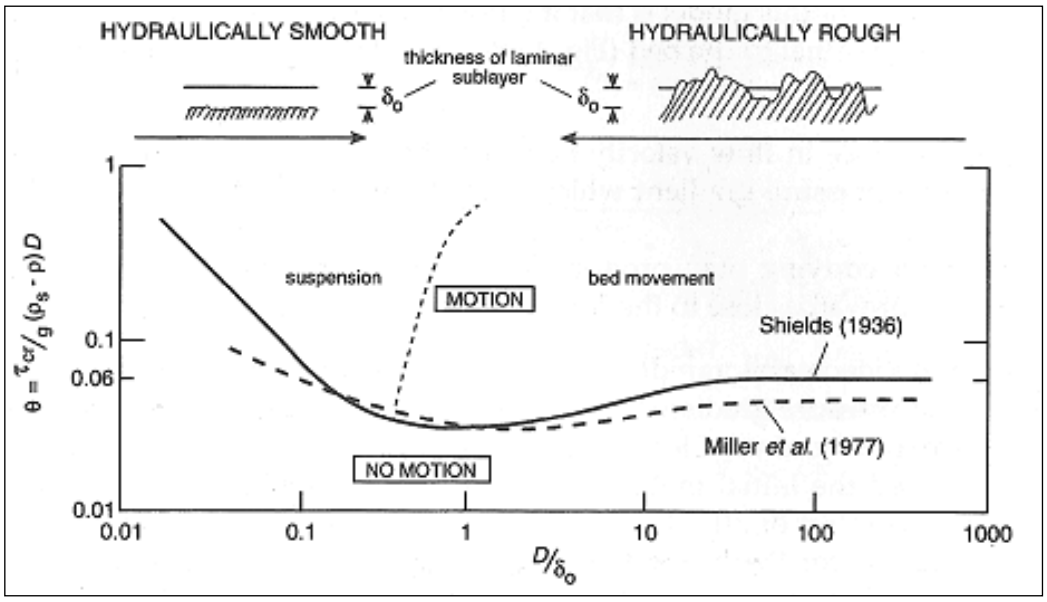

Figure 2-6 The Shields entrainment function. Dashed line represents the Shields curve modified by Miller et al., (1977).

For small particles and foraminifera, entrainment thresholds occur on the top left hand part of the diagram where very small stresses will entrain the sediment into suspension. Application of the Shields diagram to determine threshold movement of irregularly shaped biogenic particles has limitations and many authors have moved away from using critical shear stress to explain initial movement of grains and instead studied threshold friction stresses incorporating drag coefficients (Yalin, 1972; Miller *et al.,* 1977; Collins & Rigler, 1982; Komar & Clemens 1986; Paphitis *et al.,* 2002; Tompkins *et al.,* 2005).

2.7 Hydraulics of foraminifera

It has long been recognized that the hydrodynamic qualities of foraminifera vary from one species to another and that assemblages of species with similar hydrodynamic qualities could be evidence of post-mortem transport (Boucot, 1953). Shape, size and density are major factors in determining entrainment, transport and settling of benthic foraminifera (Baba & Komar, 1981; Kontrovitz *et al.,* 1978; Yordanova & Hohenegger, 2007). Snyder *et al.,* (1990) identified three significant shapes that influenced entrainment from a study of 31 common species on the Washington continental shelf. Equi-dimensional tests were the most easily entrained

at calculated velocities ~0.04-0.07 ms^{-1}, elongate, inflated or coiled became entrained at intermediate velocities ~0.069-0.09 ms^{-1}, while flattened-discoidal and coiled or elongate-compressed forms were the most difficult to entrain at velocities ~0.09-0.13 ms^{-1}. The more spherical the tests, the lower the entrainment velocities which are required, meaning that tests which exhibit the most deviation is shape from a sphere require the greater entrainment velocities (Kontrovitz *et al.*, 1978; Martin & Liddell, 1991; Wallbridge, 1998; Yordanova & Hohenegger, 2007).

Relatively low densities result in biogenic particles being more easily entrained than equivalently sized mineral grains (Oehmig, 1993; Prager *et al.*, 1996). Oehmig (1993) found that tests with relative densities (ρ_s/ρ) of 1.3-1.8 required shear stress velocities of around 0.08 ms^{-1} before entrainment occurred. As relative density increased towards that of quartz (2.6) the entrainment velocity of the tests became similar to that of sand particles of the same diameter, being closer to 0.1 ms^{-1}. Foraminifera with lower densities required lower shear stress to initiate transport compared to quartz sands of similar size while an increase in density resulted in an increase in shear stress velocity (Oehmig, 1993).

Once in motion transport is greatly influenced by the density of foraminiferal tests. Thin walled tests with low densities and high buoyancy and low settling velocities remain in the water column longer and therefore are transported further before being deposited. Yordanova & Hohenegger (2007) found that although flat shapes are more difficult to entrain (see above), once in the water column they travelled further, resulting in thin lenticular tests being transported further than thick lenticular tests. Test size was also related to distance travelled, with smaller tests being transported the greatest distances (Yordanova & Hohenegger, 2007).

Deposition of tests begins once the flow or shear velocity falls below the settling velocity for that particle, which for a given particle size is less than that required for entrainment, particularly within the finer fractions (Knighton, 1998). Settling curves for foraminifera show that larger tests settle faster than smaller ones, although there is considerable scatter due to different shapes and densities (Maiklem, 1968). Foraminifera larger than 1000 μm fall ~0.04-0.13 ms^{-1}, while at 1000 μm velocities

vary from 0.039-0.051 ms^{-1} while small tests between 500-300 μm fall ~0.02-0.002 ms^{-1} for various benthic and planktonic taxa (Fok-Pun & Komar, 1983; Oehmig 1993; Yordanova & Hohenegger, 2007). Generally the larger the test size the greater the deviation from the quartz grain density and settling behaviour (Oehmig, 1993). Biogenic particles travel further and faster than sands of similar size resulting in deposition within smaller sand and silt sizes, which is a logical consequence of their lower density (Prager *et al.* 1996).

During settling, particles commonly orientate themselves with their smallest axis vertical and with the maximum facial area to the flow (Dietrich, 1982). Settling velocities are affected by fall modes which vary according to shape; larger flat disc shaped tests with low densities oscillate down with a falling leaf pattern, lengthening the distance travelled (Maiklem, 1968; Wallbridge, 1998). Faster settling velocities occur with cone and rod shaped tests which settle smoothly with their long axis horizontal unless heavier at one end, in which case they spiral down the heavy end leading, settling with the long axis slightly tilted (Maiklem, 1968).

3 Methods

3.1 Source of Foraminifera for Experiments

Specimens used for all the experiments in this study were picked from core tops from the Gulf of Cadiz, off southwest Spain. The area is characterized by contourites composed of fine sand, silt and muds which develop as the Mediterranean Outflow decelerates and descends along the continental slope from the Strait of Gibraltar (Kenyon & Belderson, 1973). Five different shapes of common foraminifera were identified for transport analysis as shape is one of the fundamental parameters which influences the behaviour of solid grains in fluids (Le Roux, 2005). These included a range of morphologies including flat disc, hemispherical, conical, oval and lenticular and each has a different architecture and test wall structure and therefore are likely to have varying transport behaviour. The taxa selected for experimentation are *Elphidium crispum, Ammonia beccarii* and *Planorbulina mediterranensis* which are all typical of inner shelf environments (0-100 m) (Murray, 2006) and also *Cibicides lobatulus* and *Uvigerina peregrina,* which occur in the outer shelf (100-200 m) and upper slope (200-2000 m) (Murray, 2006).

The tests are all hyaline from the category *Buliminida* and *Rotaliida*; i.e. they are perforate, multichambered and composed of numerous crystals of elongate low magnesium calcite, forming bilamellar walls (Sen Gupta, 2002). *Buliminida* and *Rotaliida* are separated by multiple characteristics, with *Buliminida* having typically a high trochospiral test with a loop-shaped aperture that projects internally as a toothplate. *Rotaliida* has a low trochospiral test with a slit-like aperture and no toothplate (Loeblich & Tappan, 1992). Images of foraminifera are shown in Figure 3-1. More information about the architecture of these foraminifera can be found in Appendix 9.1.

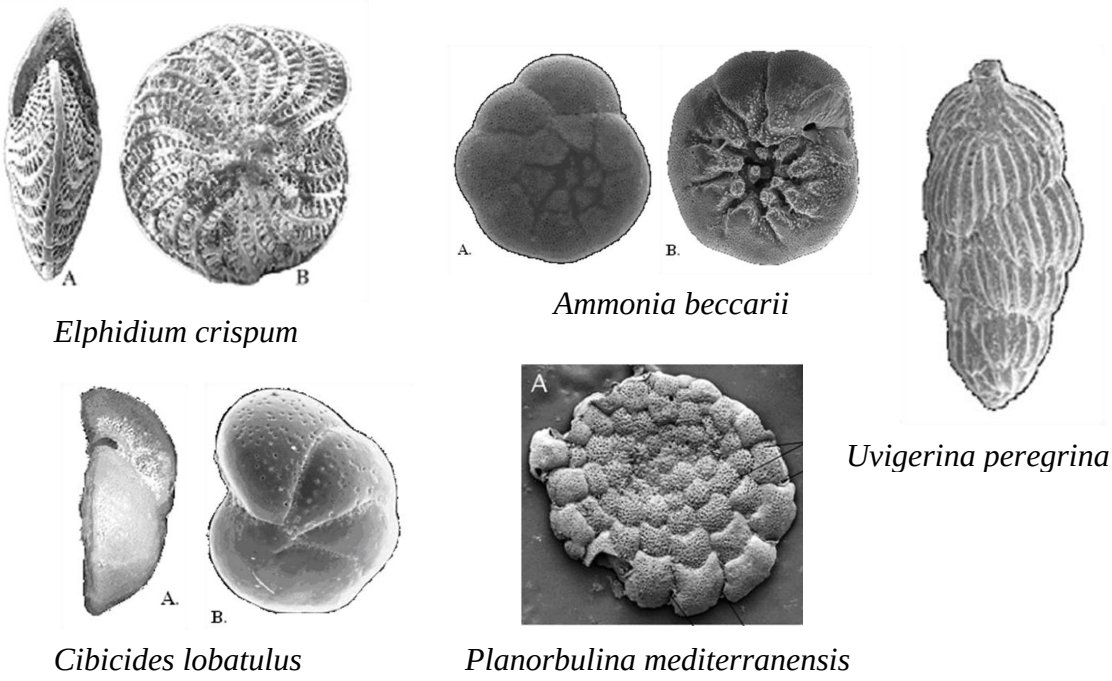

Figure 3-1 Images of five foraminifera used in study (not to scale).

3.1.1 Processing of specimens

Twenty specimens of each species were picked from sediment that had been sieved at 250 μm and placed in individual sinks on a slide. When studying sedimentary environments Tanner (1991) states that 20 samples generally makes a stable suite for correlation analysis and in many instances 12-15 may be enough to be verified statistically for sand and silt sized particles. A variety of sizes of each taxon were picked to investigate impact of growth (Fig3-2).

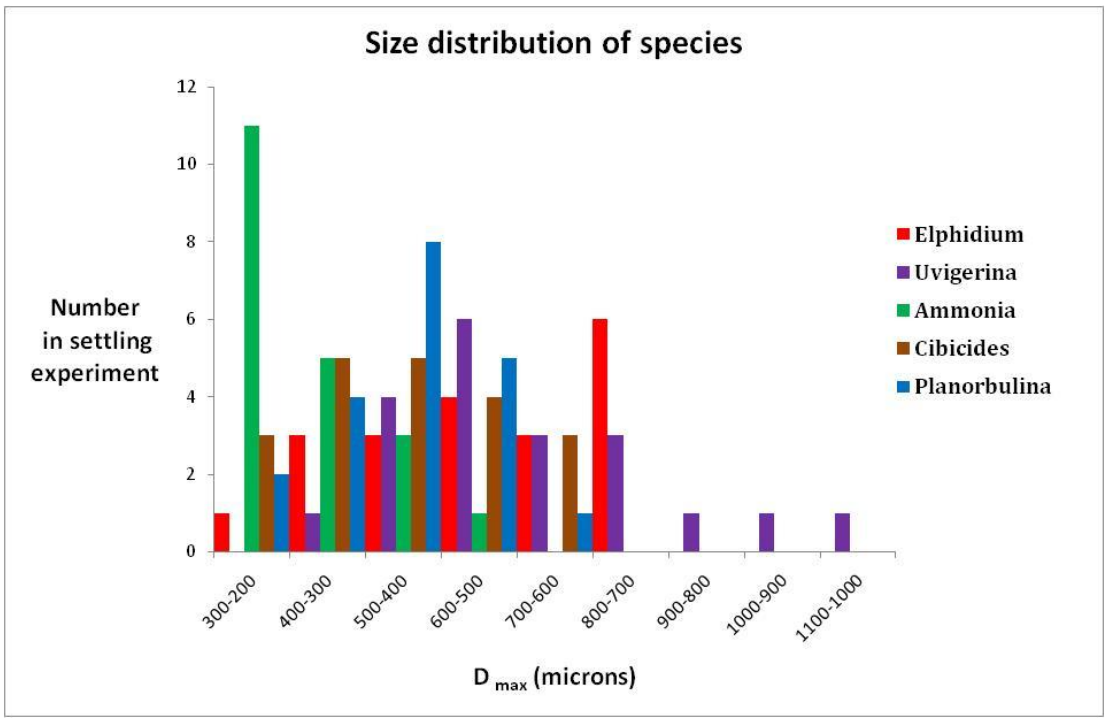

Figure 3-2 Size distribution of foraminifera used in settling velocity experiment. The majority of samples lay within the size range of 300-800µm with the average being 500µm.

Individuals chosen were those with the least signs of abrasion, alteration and deterioration. All specimens were cleaned with distilled water to remove surface dust and dried in a cool oven at 50ºC for an hour. The main three dimensions (a, b and c) were then measured using a micron gradational scale under a binocular SZ60 Olympus microscope.

3.1.2 Measuring volume, mass and density

Test volume was measured using an ‘Alicona infinite focusing microscope’. The Alicona microscope takes 3D measurements in the micro and nano range and this data is then manipulated using 'Rapidform software'. This enables a high-resolution, full image of the specimen to be resolved from which the volume of the test is presented in the software computation.

The foraminifera were smaller than other fossils commonly used under the Alicona microscope so a device was manufactured to hold them in place under the lens. A rotating arm was devised so images of the forams could be taken every 60° to be

downloaded to the software (Fig.3-3). A chuck held a pin on which the forams were glued, so they were held in suspension beneath the microscope. Six scans per specimen enabled a full view of the foram at all angles.

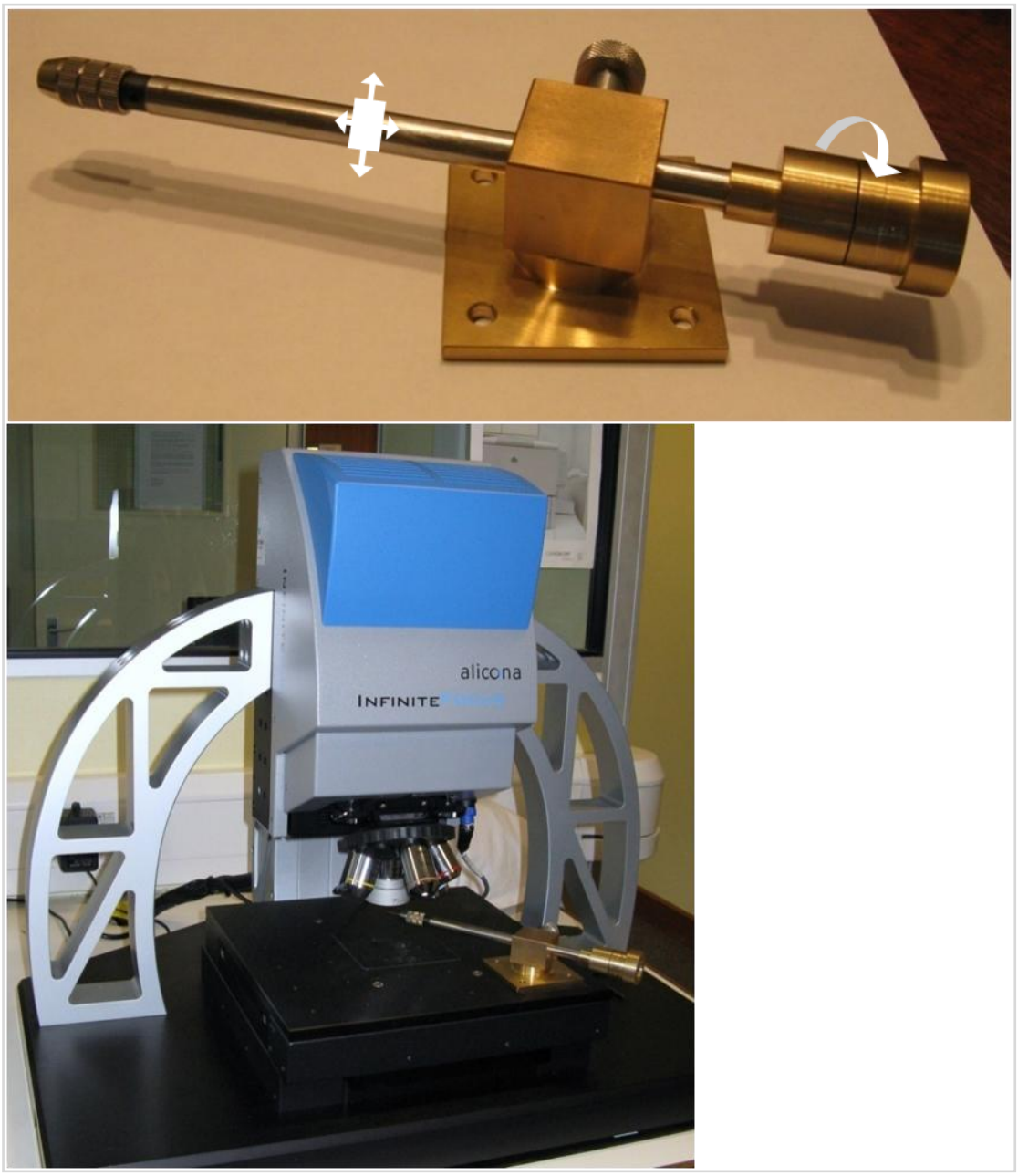

Figure 3-3Upper image: Rotational arm. Pin chuck holds specimen (on left), arrows indicate movement, with arm being moveable in and out and left to right to enable positioning under microscope. Rotational movement for 60° views (on right). Lower image: Alicona microscope with rotational arm in place.

When attaching the test to the pin end various glues were tried; more viscous types left a trail of glue and covered too much of the specimens. Thick glues did not retain the glue at the end of the pin due to surface tension and formed a circle of glue a distance from the tip of the pin. This was less pronounced on less viscous forms. Low viscosity glue did not form a large enough surface area on the pin tip to retain the specimen for any length of time. To overcome this problem each pin was filed down so the tip was flattened to 200 µm. This resulted in a coarse, flat surface area which retained the glue and enabled the foram to be securely placed, without too much loss of information on surface morphology of the foram. A low viscosity Superglue provided the best strength over the smallest surface area.

A full field of vision permitted X10 magnification for large forams and X20 for smaller ones. Lighting was adjusted for exposure, gamma, gain, light source and ring light to capture a good image. For each scan the upper and lower region was measured to produce a complete 3D image (Fig.3-4).

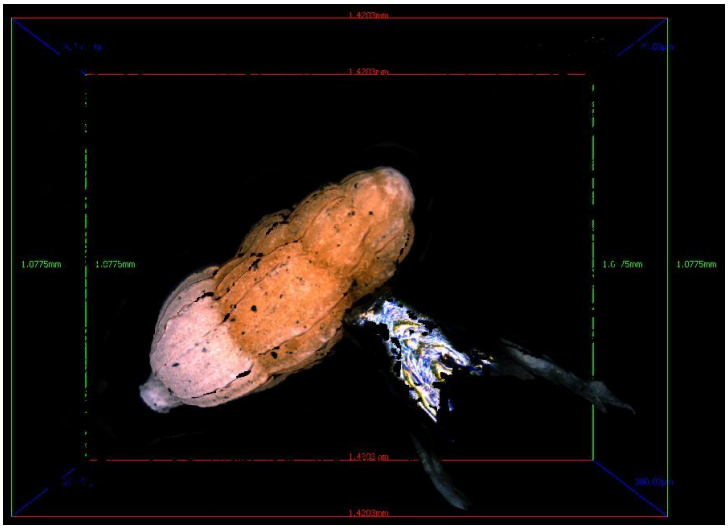

Figure 3-4 Example of *Uvigerina peregrina* scan on pin.

The scans were then imported to software Rapidform 2006 (Inus Technology, Inc.) to process a 3D image of the forams. Each image had to be manipulated so the foram was the only feature in the picture, removing the background noise and pin (Fig.3-5). The console enabled the foram to be rotated, moved around and zoomed in and out to remove all unnecessary features. All holes and spikes within the image were removed. Bridging holes with ‘curvature’ kept the entire shape of the test.

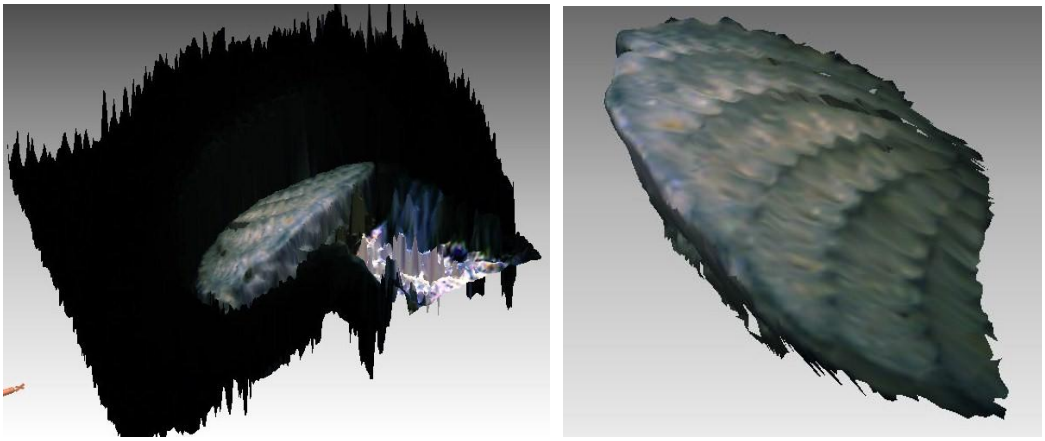

Figure 3-5 Before and after cleaning of *Elphidium crispum* image.

Each scanned image was merged individually with the next rotation (Fig.3-6). Registration was accomplished by identifying at least three features on the two datasets. The application calculated the position of one foram with respect to the other using these common geometric features between them. The first scan was then moved to the second scan and the foram merged by aligning these registration points and overlapping the regions.

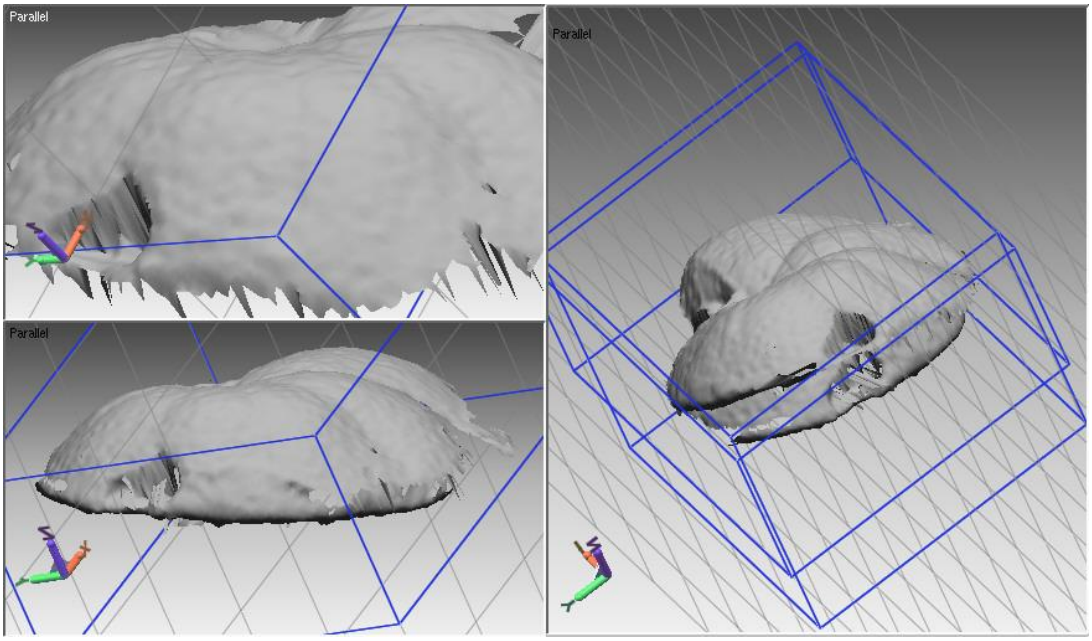

Figure 3-6 Merging of two scans towards building a full image of *Cibicides lobatulus*. The two scans on the left are merged together as shown on the right.

A final 3D image was built from the six scans enabling measurements to be taken from the software (Fig.3-7). Volume calculation was provided in the model information list.

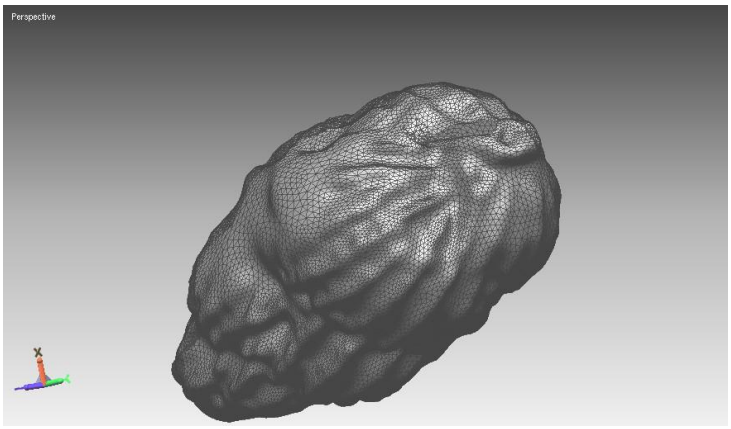

Figure 3-7 Final 3D built model of *Uvigerina peregrina.*

Due to time constraints not all 100 foraminiferal specimens were constructed to calculate volume using this software. Axial dimensions were taken from specimens where volume had been established using Rapidform software and compared to the rest of the specimens where axial dimensions had been taken using a GXCAM-5 imaging camera with a binocular SZ60 Olympus microscope. A full data set of volume values was resolved by proportioning the Rapidform values to dimensional data (see Appendix 9.2).

The mass of the specimens were measured using a Mettler MT5 mass balance scale with sensitivity to 0.001 mg (1µg). Each specimen was measured individually three times and an average taken.

The density of each specimen in air was calculated from the volume and mass data. To calculate the density in water, calcite density of the foraminifera is required. Yordanova & Hohenegger (2007) estimated calcite density of hyaline foraminifera to 2.216 mg/mm. Calculations were based on the fact that the foraminiferal test wall does not consist of solid material throughout (calcite density = 2.710 mg/mm) but is reduced by the proportion of pore space. Microscopic examination enabled the proportion of pore space to be calculated and hence the density of hyaline test walls.

The proportion of test which is calcite is calculated using the equation:

$$\frac{\rho_f}{\rho_c} X\ 100 = \%C \quad (3.1)$$

where ρ_f is the density of the foraminifera in air (mass/volume) and ρ_c in the density of the test of calcite (2.216). The percentage which is not calcite is replaced with water and the density is calculated using the formula:

$$\frac{\rho_w}{100} X\ \%W = \rho_{w1} \quad (3.2)$$

where ρ_w is the density of water and $\%W$ is the percentage of foraminifera space which is filled with water. Foraminifera density in water is calculated by adding ρ_f and $\rho_{w1.}$

The record of volume, mass and density for all specimens are given in Appendix 9.2.

3.2 Equipment and procedure for settling experiment

A 1.4 m long clear perspex pipe with an internal diameter of 194 mm was mounted on a stage, which is similar to the design used in the classic settling experiments by Gibbs *et al.*, (1971; 1972). To measure fall distance, lines were marked around the tube every 15 cm to eliminate parallax when looking through the cylinder. The settling velocity of each test was measured from the fall time between the marked lines. The cylinder was filled with de-ionised water as it is homogenous, and is thus of precisely known density and did not vary between experiments because of evaporation. Moreover, this also enabled comparison with other settling velocity literature. The water was allowed to equilibrate with room temperature for several days prior to use. Temperature was measured using a Thermamite 5 gauge at the beginning and end of daily trials. Temperature was found to be consistent throughout the tube and throughout the period of experimentation at 21°C, so viscosity changes were negligible.

A circular internal capture net slightly smaller than tube diameter with mesh size 35µm was fitted into tube and suspended by four lengths of fishing line tied to the net edge (Fig.3-8). This was connected to an outer collar which was pulled up without tilting after each experiment. This allowed the test to be recovered from the capture net and the settling velocity to be measured three times for each test. A stopwatch with a split timer was used to record the time taken to transit through every 15cm interval, which is a similar approach to that taken by previous authors (Maiklem, 1968; Gibbs *et al.*, 1971; Fok-Pun & Komar, 1983; Yordanova & Hohenegger, 2007). Wall effects were minimal due to the large inner diameter of the tube in comparison to the test diameter, but on the rare occasions that a foraminifera spent time near the cylinder wall or hit it, these were excluded from the subsequent analysis.

Figure 3-8 Settling tube showing capture net and retrieval collar which was lowered to raise net after each experiment.

Before trials the forams were placed in a very dilute detergent for 48 hrs. Detergents promote wetting by reducing the meniscus force, enabling air bubbles to escape from the foram chambers. Each individual test was settled three times and a mean and standard deviation were recorded. Tests were introduced to the centre of the tube by use of an artist's brush (size 00) and released into the water by dabbing the brush through the water surface. After each trial, time was allowed for the water column to return to a static state before the next experiment, to eliminate fluid turbulence within the settling column. Between trials, samples were kept in water so they did not dry out.

To understand if there are significant differences between species and therefore a likelihood that taxa will fractionate during post mortem transport an ANOVA (analysis of variance) test was carried out. The sample number for each species was n=20 and at a significant level of 0.05. This determines whether there is more variation between taxa, than within taxa.

3.3 Design, equipment and procedure for flume experiments

3.3.1 Introduction

The concept of designing a laboratory experiment which will in some way replicate what occurs in the natural environment has inherent difficulties, especially for experiments concerning phenomena that are rarely observed, such as oceanic turbidity currents. As oceanic currents vary greatly in size and duration a laboratory experiment can only represent a very small fraction of what occurs under natural conditions. Kneller & Buckee (2000) state that experiments are useful for visualising patterns of behaviour even though there are considerable problems in comparing experiments directly with individual natural turbidity currents. Therefore modelling involves substantial simplification, requiring compromises in some parameters to achieve adequate scaling of the parameters of most interest (Kneller & Buckee, 2000). The degree to which this laboratory scaled experiment can be accurately up-scaled to predict the behaviour of foraminiferal distribution in the sea can be related

to the scaling laws using the non-dimensional Froude, Reynolds and Richardson numbers (Alexander & Mulder, 2002).

3.3.2 Overview of field prototype for experiment

The field prototype we are attempting to model is that of a turbidity current within a submarine canyon system as shown in Fig 3-9.

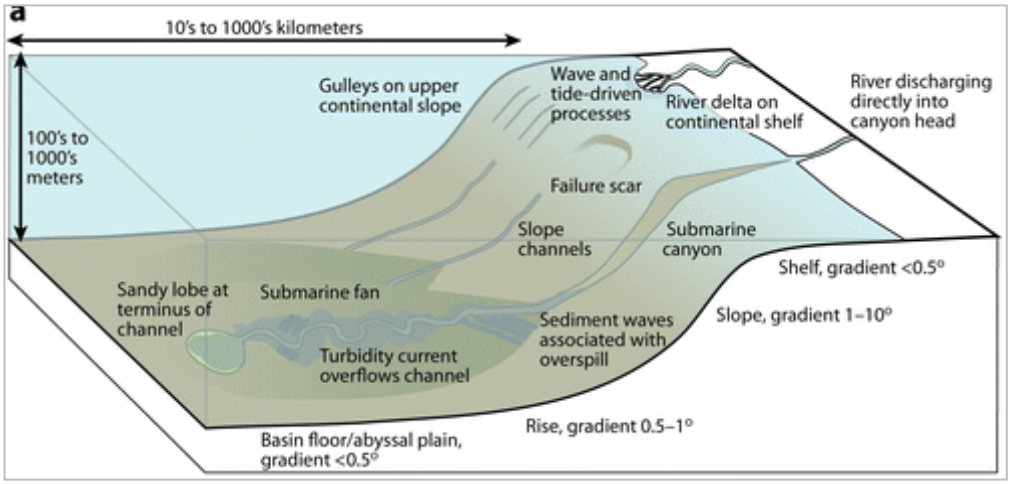

Figure 3-9 Example of a depositional setting for a turbidite channel and fan system (adapted from Meiburg & Kneller, 2010).

For the experiment only a narrowly defined set of parameters are of interest to study the transport and deposition of foraminifera. The fundamental properties of this dimensional analysis include velocity (distance and time), discharge (volume and time), density difference (between the ambient and current flow), viscosity of the flow and gravitational forces. Velocity, density and bed conditions are all constraints that are considered within the flume experiment. The character of the turbidity current is defined by the relative density between the current and ambient water and the velocity of the flow (including slope angle) for deposition of the forams.

In the ocean foraminifera are found within sandy and muddy sediment, so to emulate the conditions in which these sediments are laid down requires an understanding of velocities at which this deposition occurs. Post mortem transport occurs when the foraminifera are picked up from the sea floor during the early stages of the turbidite

typified by erosion and acceleration at the shelf break. Deposition occurs as the turbidite begins to wane as the current reaches the sea floor and starts to slowly lose its energy as gravity is no longer a driving factor (Allen, 1977). At this stage velocities are < 2 ms^{-1}, declining on average with distance (Drago, 2002). In previous flume experiments rapid deposition of sand (density 2330-2448 kg m^{-3}) has been shown to begin at a near-bed fluid velocity of 1.6–1.7 ms^{-1} (Sumner *et al.*, 2008) while fine sands, silts and clays are deposited at velocities < 0.1 ms^{-1} (Bearman, 2002; Pirmez & Imran, 2003). Foraminifera are much lighter than sand grains and experiments have shown that 'large' benthic foraminifera are entrained at velocities < 0.2 ms^{1} (Yordanova & Hohenegger, 2007) while smaller benthics are entrained at 0.1-0.04 ms^{-1} (Snyder *et al.*, 1990; Wallbridge, 1998). To reproduce the distal stages of a turbidite, velocities in the laboratory < 2 ms^{-1} will ensure entrainment and transport of the foraminifera within the turbidite system.

In the experiments described in this thesis, saline solutions were used to produce a density current. Saline solutions are in many aspects a good substitute for low-density, sediment-bearing gravity currents as dissolved salt serves as a surrogate for fine mud in suspension (Stacy & Bowen, 1988; Best *et al.*, 2001; Sequeiros *et al.*, 2010a). It also enables the microscopic foraminifera to be picked out without other particles being in the water. A turbidity current has the characteristics of a Newtonian fluid but with a density higher than the ambient water, up to 1200 kg m^{-3} (Drago, 2002). In the ocean, density is around 1031 kg m^{-3}, making a maximum difference of 169 kg m^{-3} between seawater and the turbidity current. The densities of currents are often described using the concentration of sediment by volume, with a maximum of 9% for turbidity currents, based on grain densities of 2000–2500 kg^{-3} (Völker *et al.*, 2008). A typical vertically averaged excess density for turbidity currents is a $\Delta\rho_{tc}$ of 50 kg m^{-3} (volume concentration of 3%) (Pirmez & Imran, 2003). This information is useful when modelling turbidite behaviour as a saline density current can replicate the density of a turbidity current.

The slope and bottom conditions have a large impact on sedimentary deposition in the ocean (Talling *et al.* 2007) and in laboratory conditions these can be greatly amplified due to the small size of the flume tank. Most turbidity current slopes

average < 1°, being around 0.7-0.8° (Nof, 1996; Pirmez & Imran, 2003; Talling *et al*., 2007; Salles *et al.,* 2008). The gradient is therefore required to be continuous with no breaks in slope as this produces hydraulic jumps and flow separation which enhances deposition (Garcia & Parsons, 1989). When studying submarine flows Talling *et al.* (2007) noted that even a small change in gradient from 0.05° to 0.01° triggered deposition.

Experimental measurements of laboratory turbidity currents are often presented within confined channels where there is some initial lateral spread before the current is confined by the tank walls (Kubo & Nakajima, 2002; Alexander & Mulder, 2002; Mohrig & Marr, 2003; Felix *et al*., 2005). The 30cm wide tank used in the experiment can be seen as analogous to a confined flow which occurs down submarine channels previously eroded on the seafloor.

To maintain suspension of the forams for as long as possible to enable differences between species to be examined, good vertical transport within the flow was required. A smooth bed leads to less turbulence near the bed while greater roughness and high turbulence at the bed compared to other shear stresses within the flow will lead to deposition. Increased resistance at the boundary lowers flow velocity, which in turn may enhance deposition (Middleton & Southard, 1984). In oceanic settings unconfined turbidity current friction factors are in the range of 3×10^{-3} to 7×10^{-3} (Price & O'Neil Baringer, 1994: Ercilla *et al*., 2002; Kubo & Nakajima, 2002; Pirmez & Imran, 2003). The problem with scaling the surface roughness from the prototype to the model is that the model roughness becomes impractically small. When investigating deposition from turbidity currents in laboratory flumes, beds consisting of metal, glass, perspex or plastic surfaces for slope construction ensure minimal surface roughness (Kubo & Nakajima, 2002; Hosseini *et al.,* 2006; Alexander *et al.,* 2008). These smooth, flat surfaces reduce friction factors in the scaled down experiments so they are comparable to oceanic conditions.

3.3.3 Waning flow experiment

A small flume experiment was initially set up to understand the basic parameters of foraminifera transport and deposition during a unidirectional, non-uniform flow downslope. This initial pilot experiment consists of a lock-exchange method where a fixed volume of fluid is released by opening a valve into the flume tank. The flume consisted of a 2.5 m long, 0.23 m wide and 0.42 m high tank containing 236 litres of tapwater[1]. Within this a narrow open channel, 2 m long pipe with a 0.17 m diameter was submerged in the water. On a slope greater than 9° some *Uvigerina* rolled downslope when deposited at right angles to the flow, so all experiments were run with gradient < 9º. A header tank and release valve were placed at the top end of the channel (Fig.3-10). The flow from the header tank was controlled by a valve.

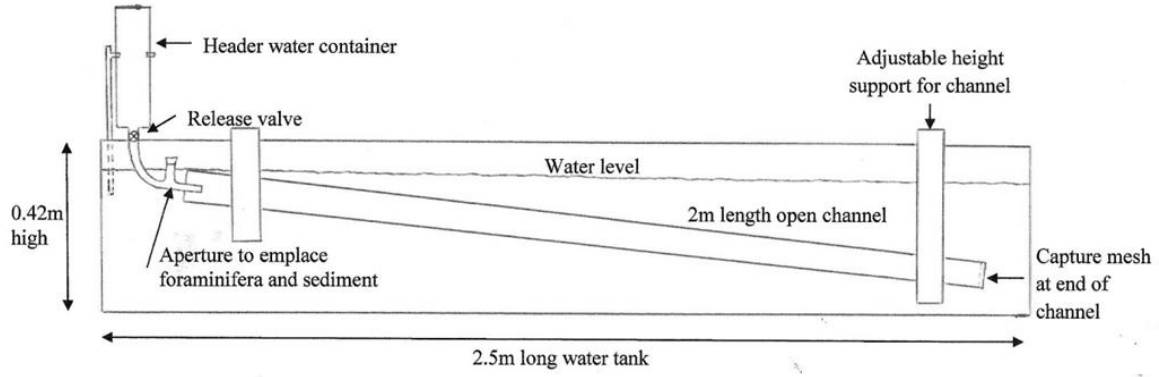

Figure 3-10 Schematic diagram of flume profile, not drawn to scale.

The dispensing header tank consisted of a graded measuring cylinder enabling exact repeatability of flow dynamics. Volumes of up to 500 ml were expelled from the header tank through a circular pipe outlet with a 0.013 m diameter. This pipe contained the foraminifera which were placed via an aperture which was then sealed with a cork. Dense brine[2] within the header tank was drained into the pipe and expelled the foraminifera into the narrow open channel. The injection of brine into

[1] Unlike distilled water tapwater contains trace minerals which may have a negligible effect on the density of the water in the flume experiment. Water is sourced from groundwater where key mineral parameters are 107.6 mg kg^{-1} calcium, 0.71 mg kg^{-1} fluoride and 78.7 mg kg^{-1} chloride (http://waterquality.anglianwater.com/map.aspx)

[2] The brine consisted of a 20% salt solution which was dissolved in warm water and then cooled to 5ºC to maintain a constant density for the experiments

the main tank produced a high density flow that descended within the smooth hemicylindrical channel as the velocity waned downslope. The brine flow had a density of 1159 kg m^{-3}, a density difference of 159 kg m^{-3} between the flow and the ambient water which was sufficient for the flow to remain within the open channel. Due to the difference in refractive index between the water masses, the flow could be monitored visually as an oily wave descending the channel.

Preparation of foraminifera was the same as for the settling velocity experiment. Fastened at the end of the channel was a 35 μm mesh to capture any drifting tests. Once the foraminifera settled within the channel the water was very slowly drained from the tank to ensure the tests were not disturbed.

Once dry, the channel was gently lifted at the lower end and placed on a platform for horizontal inspection, enabling examination without disturbance. To aid collection of data the channel was marked every 10 cm and foraminifera were collected using a strong light and a x10 eyepiece. The distance travelled for approximately 100 specimens of each taxon was recorded before placing them into a slide for further experiments. If in doubt, specimens were checked under the microscope to confirm which species of foraminifera it was. The mesh at the end of the channel was inspected for any stray taxa and the number of missing tests from each run was recorded. Flow rate at the leading head of the wave was documented using a stopwatch as it progressed downslope.

3.3.4 Considerations leading to final experiment

The initial pilot study highlighted several obstacles which need to be addressed. The main issue which needed to be tackled was the large hydraulic jump which occurred when the current entered the ambient water, resulting in high deposition. To ensure continuous entrainment of foraminifera it was necessary to reduce the Froude number in the proximal region. This was be achieved by having greater control on the flow rate as it entered the flume. Rather than using a lock-exchange release method, a separate input tank from the main flume allowed the current to be controlled by valves. This experimental set-up resulted in a ‘continuous quasi-steady

flow' rather than a 'surge type flow'. The quasi-steady flow has continuous momentum on entering the flume, rather than an initially static, short burst followed by rapid deceleration, with the volume of the external input tank relative to the main flume tank determining the flow type (Peakall *et al.* 2001). The initial experiments have shown that much lower velocities than 2 ms^{-1} can be applied, and this will reduce the Froude number on entering the open channel. By using a larger tank, reducing initial velocities and using a quasi-steady flow it is possible to monitor and analyze each run ensuring repeatability.

3.3.5 Continuous Current Experiment

For these experiments, several thousand foraminifera were picked from core top samples from the Gulf of Cadiz (SE Spain). Too few individuals of *Ammonia beccarii* were available from this material, so a sample was taken from the Humber estuary where this taxon is extremely common (Brasier, 1981; M. Rogerson, unpublished data). A range of sizes were selected in order to investigate the impact of ontogeny (Fig.3-11).

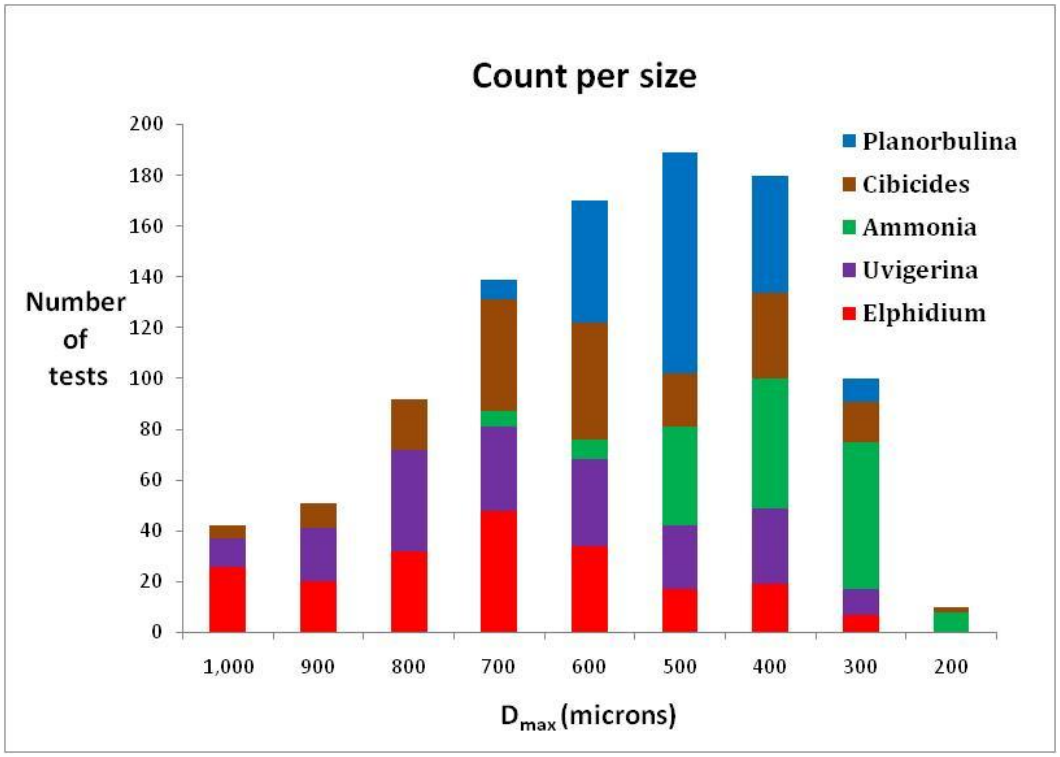

Figure 3-11 Final sizes and number of tests picked from the flume experiment.

The flume for continuous current experiments was 7.5 m long, 0.3 m wide and 0.54 m deep and contained a static tapwater body[3] into which a brine turbidity current flowed (Fig. 3-12)

.

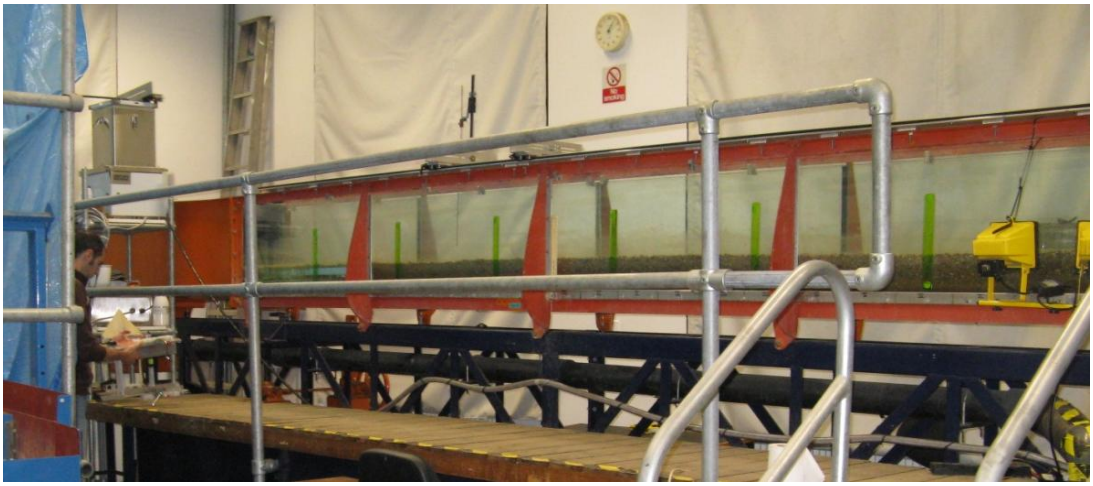

Figure 3-12 Laboratory flume.

The flume was set to a slope of 1/1000. The input tank containing the brine for the turbidity current was positioned on the top of the flume, see Fig.3-13. A salinity of 10%, equating to a density 1084 kg m^{-3} at 14°C[4], and a slope gradient of 1° were used. This was fed by a reservoir tank with a pump which enabled constant hydraulic head and continuous flow from the input tank.

[3] Water is borehole/river derived where key mineral parameters are 137.9 mg/l calcium, 0.12 mg/l fluoride and 39.6 mg/l chloride (http://www.yorkshirewater.com/extra-services/in-your-area.aspx?loc=hu6&section=water-quality)

[4] Density was calculated using the Levitus & Isayev (1992) approximation for the equation of state for seawater.

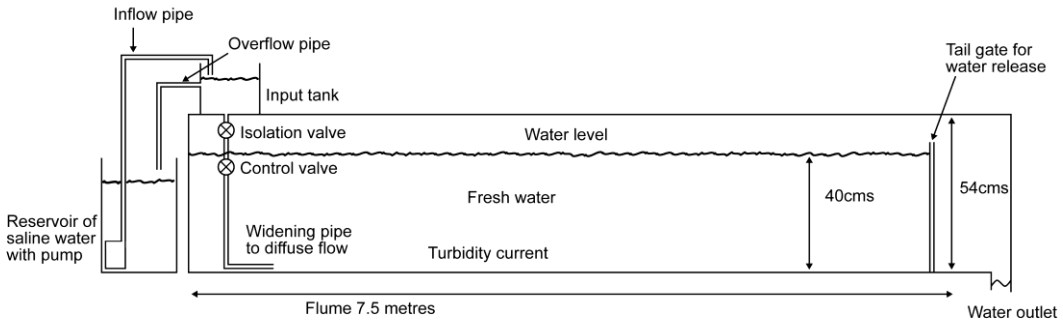

Figure 3-13 Schematic diagram of flume profile, not drawn to scale.

Water was released by the isolation valve which entered a down pipe. The ambient water level was filled to the height of the control valve giving a head of half a metre.

The pipe outlet had a bore diameter of 15 mm, which was too narrow to achieve flow conditions suitable for our experiments. Therefore a larger pipe was fitted at right angles to the pipe outlet to reduce the initial Froude number and ensure continuous entrainment of the forams. The expansion pipe was 20 cm in length and had a diameter of 27 mm (Fig.3-14). This contains an aperture via which the user could emplace the forams into the tube so they were entrained into the flow before it was discharged into the flume.

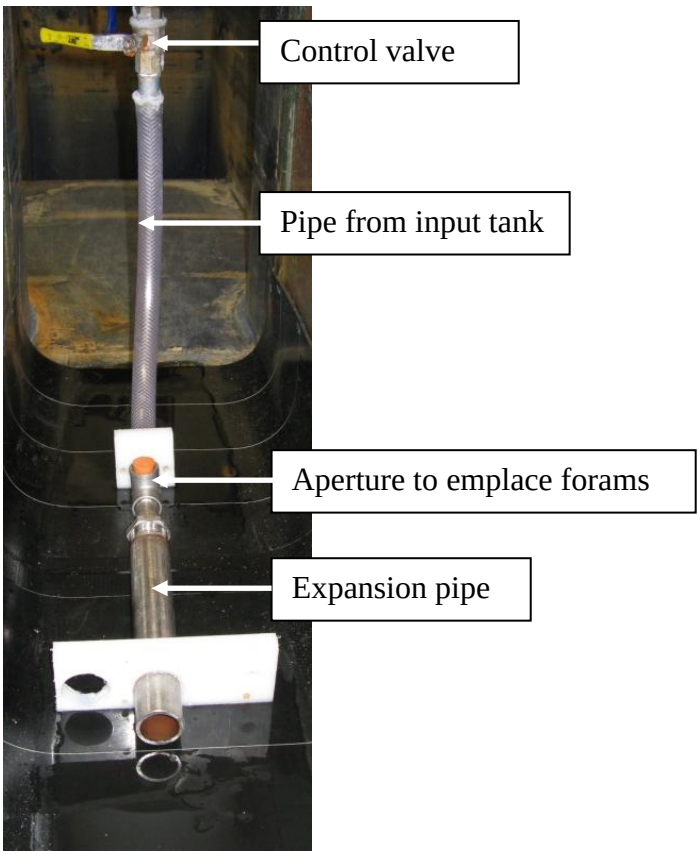

Figure 3-14 Pipe configuration with emplacement of forams within the duct.

On opening the control valve the water flowed under gravity and produced an initial surge followed by a period of steady flow. Flow velocity reduced down flume as the water mixed and lost its momentum. Each experiment was run for 60 seconds, which was sufficient for the leading edge of the flow to reach the end of the flume. The transport distance was measured for each foraminiferal test in each experiment. Once retrieved from the flume floor each test was measured for its longest diameter (D_{max}) using a GXCAM-5 imaging camera with a binocular Pyser SGI (X80) microscope.

To ensure that all foraminifera were entrained as they entered the flume, flow velocities close to the bed were 0.28 ms^{-1} at the upstream end of the flume, and decreased in distance to around 0.1-0.15 ms^{-1}. A density of 1084 kg m^{-3} was used producing a density difference of 84 kg m^{-3} between the ambient water and the turbidity current. This is well within Drago's (2002) maximum value. A black rubber mat was placed along the length of the flume floor and flume walls, ensuring the surface roughness was the same for both floor and walls. The matting allowed the

white microscopic tests to be identified and ensured that the forams were retained and available for further experiments.

3.3.6 Direct measurement of flow properties

Flow measurements were taken using Acoustic-Doppler Velocimeters (ADV)'s. This is a sensor system based on the Acoustic Doppler principle and is suitable for high-resolution measurements of three-dimensional velocities at a rate of 25 Hz (Sarker, 1998). An ADV operates by emitting a burst of sound waves with known duration and frequency from a source transducer and using three receiving transducers to measure the backscatter waves (Fig.3-15). Since the backscatter wave frequency is shifted by moving particles available in the target area, the magnitude of this frequency shift (also known as 'Doppler shift') is proportional to the flow velocities. For this reason, ADV can measure flow velocities without calibration. Owing to a high temporal resolution by the fast response, it is suitable to measure instantaneous velocities of turbulent flow (Ha *et al.*, 2009).

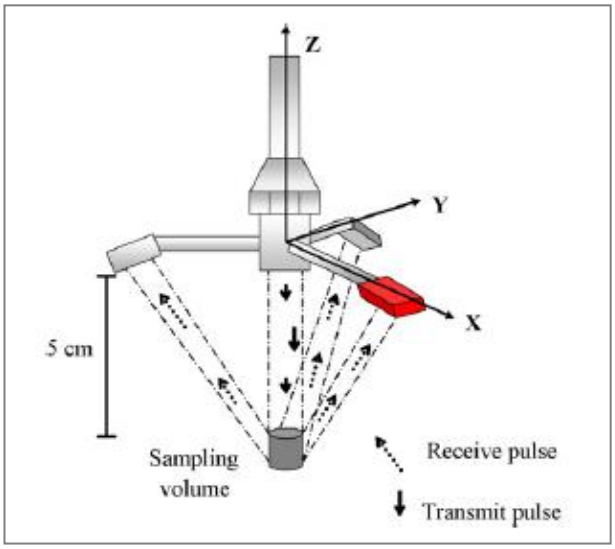

Figure 3-15 Velocity sensors (Masalo *et al.*, 2008) Turbulent velocities are measured 5 cm from the tip of the transmitter with a sampling volume height of 9 mm and diameter of 7 mm. A brine flow results in a strong acoustic reflection enabling the ADV measurement of fluid movement.

Up to five Acoustic Doppler Velocity meters were set up along the flume to measure the velocity of the flow. These were mounted to a gantry railing and operated

simultaneously using a computer controlled data acquisition system. All probes were orientated with the downstream flow component (x) parallel to the channel centreline. Data was processed using software WinADV32 (developed by T. L. Wahl, U.S. Bureau of Reclamation. Available at: http://www.usbr.gov/pmts/hydraulics_lab/twahl/winadv/winadvdownload.html), a post-processing freeware package designed specifically for the analysis of ADV files. Data was filtered to remove spikes, measurements with low correlations (<60%) and/or low signal-to-noise ratio (<5 dB) (McLelland & Nicholas, 2000; Alexander *et al.*, 2008).

3.3.7 Scaling Parameters

The transport of foraminifera in the flow can be related to scaling laws so the behaviour may be related to the behaviour in much larger, natural systems. The properties of the flow can be defined in terms of the following equations:

Reynolds values are calculated using the equation:

$$\mathrm{Re} = D\mathrm{W_S}/\nu \tag{3.3}$$

where D is the diameter of the particle, W_S is the settling velocity and ν the kinematic viscosity of the fluid. The densimetric Froude number was calculated using the formula:

$$Fr = U / \sqrt{(g' d)} \tag{3.4}$$

where U is the velocity, g' is the reduced gravity ($g' = g(\Delta\rho/\rho_a)$ and g is the acceleration due to gravity, $\Delta\rho$ is the density difference between the current and ambient fluid and ρ_a is the ambient fluid) and d is the depth of the flow (Middleton, 1993). Fluid entrainment is calculated using the Richardson number defined by the formula:

$$Ri = {}^{g'd}/_{U^2} \tag{3.5}$$

For the flume experiment, Froude numbers were analogous to canyon fan systems where flows are supercritical in proximal regions, becoming subcritical once the slope comes close to horizontal (Allen, 1977). Estimated Froude numbers for submarine systems have been calculated by Pirmez & Imran (2003) to range from ~1.4 upstream to ~0.3 downstream while Sequeiros *et al.* (2010) calculated values between 2.2 to 0.4. Froude scale models are appropriate for turbidity currents where the model is fully turbulent i.e. *Re* >2000 (Kneller & Buckee, 2000). The Richardson number was used to assess the stability of the flow boundaries (Parker *et al.*, 1986: Salles *et al.*, 2008). Entrainment with the ambient water becomes significant when the Richardson number is below 1; Price & O'Neil Baringer (1994) state this is only likely to occur when there is a change in topography such as at the shelf-slope break (i.e. in the proximal area of the turbidite). In the experiment the Richardson number was only below 1 in the very proximal region as the flow entered the flume. Downstream turbulence was dampened as a quasi-equilibrium condition was reached. Parameters for the flume experiment are shown in Table 3-1.

Table 3-1 Scaling parameters of flume experiment

	Exit point (proximal)	0.5 m downstream	2.5 m downstream (distal)
Velocity (ms^{-1})[1]	0.23	0.14	0.15
Froude	1.53	0.69	0.61
Reynolds	5,009	5,658	8,459
Richardson	0.43	3.01	2.12

[1]All velocities are taken from ADV measurements at a distance of 1 cm from bed.

3.3.8 Statistical Analysis

To see whether there is a significant difference between distances travelled between species in the flume experiment ANCOVA is carried out. It is clear from the settling velocity analysis that size affects deposition so we need to take account of size when determining if there are any significant differences in the deposition between species. ANalysis of COVariance, (ANCOVA), includes a supplementary variable (covariate) into the model. Here, size is treated as the covariate (a quantitative variable which is free to vary and the researcher simply records its value). If the covariate chosen is responsible for some of the variation in the dependent variable,

use of analysis of covariance will remove this variation from the error or random variance. The result is improved sensitivity of the tests for treatment effects and increase in the statistical power.

The test of covariance is intended to cover two types of analyses; (1) the analysis of adjusted treatment means and (2) the test of homogeneity of slopes (test of parallelism). The latter is a testable assumption of the first. By using linear regression we can look at distance (the dependent/response variable) against size (covariate or independent/ explanatory variable) for the five species. On this analysis it should noted that the factor 'species' is not randomly assigned to the foraminifera and in effect this is therefore a non-randomized study (Dunn & Clark, 1987).

The underlying model H_1 is that there are five separate regressions. This is tested against H_0, where all the species data is combined to obtain a single regression coefficient by using the sample sum of squares across products. H_1 states that 'there is a significant difference in transport distance between species' and this is tested against H_0, the null hypothesis where 'there is no difference in transport distance between species and all species have a common slope'.

The Kolmogorov-Smirnov (K-S) test is used to compare two data sets. This is a nonparametric test which compares the empirical distribution function between two samples (Sprent, 1989). This is a suitable statistic where the sample sets have an unequal number of data. A two-tailed test is used to compare the sample distribution function, the test statistic being the difference of greatest magnitude between the two functions. The null hypothesis states that the two samples have the same distribution while the alternative hypothesis is that they are significantly different. Critical values for various samples sizes are given via tables where at a nominal 5% level the null hypothesis cannot be rejected.

3.3.9 Conclusion

The flume experiment was set up to replicate possible oceanic conditions as closely as possible. The experiment adheres to the scaling laws and can be related to the

oceanic environment by the Froude, Reynolds and Richardson numbers. These non-dimensional values compare favourably with other studies where models have been used to evaluate the oceanic conditions of turbidity currents. Velocities, density and bed constrains all fall within realistic parameters permitting the deposition of foraminifera within the flow to be critically analysed and assessed.

4 Characteristics of settling velocity for hyaline benthic foraminifera

4.1 Abstract

Knowledge of the behaviour of solid particles settling through fluids is one of the key variables in the study of sediment transport and deposition. However, despite microfossil tests being largely of silt-sand size, very little progress has been made in understanding their post-mortem transportation behaviour. This study presents new constraints on the transportation potential of five taxa of hyaline benthic foraminifera from laboratory controlled settling velocities studies in static water focussing on the impact of test size, shape and density. It is demonstrated that a quantitative similarity in the behaviour of these tests to falling spheres occurs due to the controlling intra-specific changes in settling velocity. However, test morphology is the dominant control on inter-specific differences in transport and deposition. Due to size, shape and density differences inducing different settling velocities, it is possible to demonstrate that different species of foraminifera are likely to significantly fractionate within non-planar flows with heavier, larger taxa becoming deposited within relatively short distances of their sources while lighter, smaller species are transported much greater distances. This result is significant, as it means that the assemblage of tests deposited by a current may not well reflect the composition of the assemblage entrained into it. As the settling behaviour of the taxa investigated in this study suggest a hydraulic equivalence to quartz sand in the 50-600 μm size range, this means that hydraulic sorting of tests must be considered an important contributor to assemblage composition in all but the lowest energy settings.

4.2 Introduction

Palaeoenvironmental reconstruction using foraminifera relies on the assumption that assemblages reflect the ecological conditions at the time of deposition (Murray, 2006). However, the distribution of taxa can be greatly affected by transport and reworking of tests which is particularly important in high energy environments such

as submarine canyon and fan systems (Mullenbach *et al.,* 2004). Due to post mortem processes, reconstruction of these major pathways of sediment from the continental shelf to the abyssal plain can be difficult, but it is possible that assemblages contain useful hydraulic information (Rogerson *et al*., 2006). Experiments that investigate movement of foraminifera in off-shore environments will enable assessments to be made as to the degree to which assemblages are modified by post-mortem transport and of the processes that modified them.

Empirical observations and measurements under specific settling conditions on empty tests in static water are used here to determine differences in settling between species to establish which are most buoyant and likely to remain in suspension longest. Hyaline foraminifera are selected for experimentation, as they are the most abundant tests found in shelf and upper-slope environments (Armstrong & Brasier, 2005).

4.3 Methods

Foraminifera were sourced and sized as detailed in the Methods, section 3.1.1 using a gradational scale and microscope. This enabled analysis into shape as described in this Chapter, section 4.4.1. To find the density of foraminifera the volume and mass was determined as described in Methods, section 3.1.2. Mass was determined using a balance scale. The volume was determined using the Alicona microscope which entailed constructing a detailed scan of the test surface enabling software calculation of the volume. All settling velocity measurements were determined using the procedure described in Methods, section 3.2.

4.4 Results

4.4.1 Shape

Dimensional analysis was carried out on twenty specimens for each of the five species to understand the diversity of shape (*Elphidium crispum, Ammonia beccarii, Uvigerina peregrina, Cibicides lobatulus* and *Planorbulina mediterranensis*). The

main three dimensions (a, b and c) were measured using a micron gradational scale representing the long, intermediate and short orthogonal axes of each particle respectively. The geometric data is related to triangular diagrams which are used extensively in sedimentary environments to present primary particle shape data (Graham & Midgley, 2000; Benn & Ballantyne, 1993). As shown in Fig.4-1 the taxa vary significantly in shape.

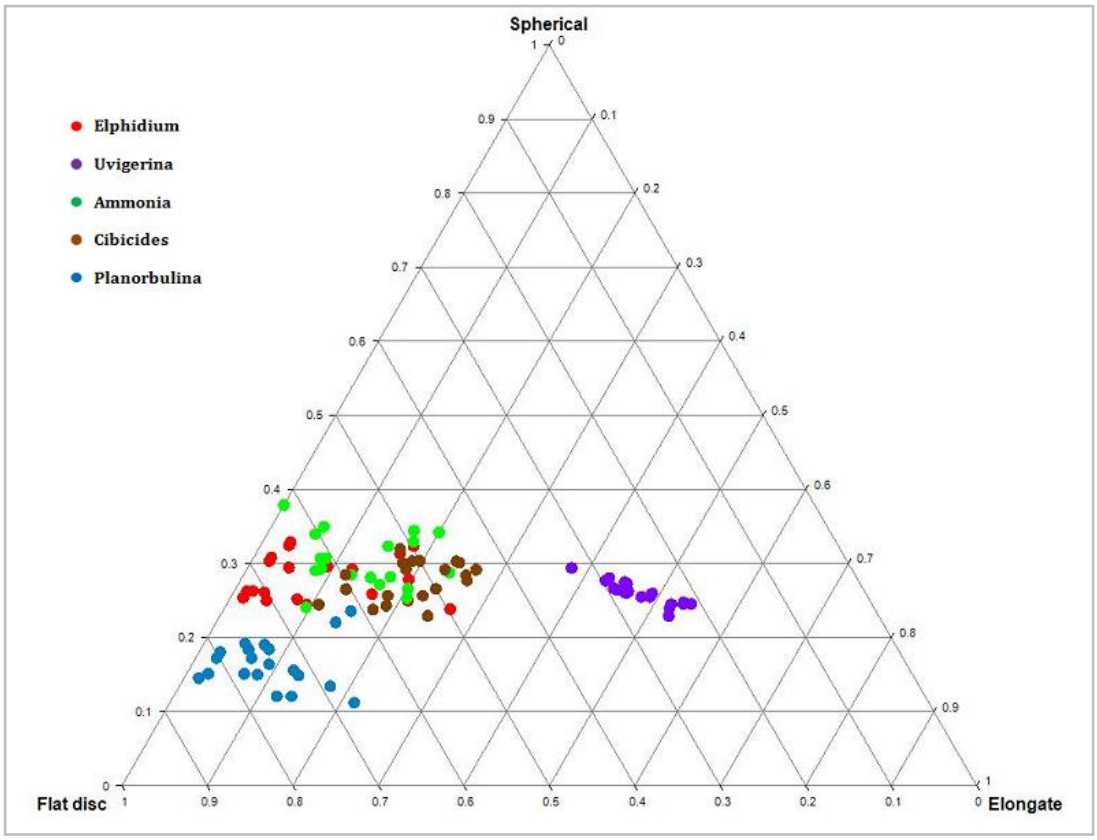

Figure 4-1 Triangular diagram to illustrate differences in shape of foraminifera taxa. The orthogonal axis analyzes the three dimensions of shape; a (long), b (intermediate) and c (short). Flat disc to spherical represents the relationship between c:a. Spherical to elongate b:a and elongate to flat disc (a-b)-(a-c) (Sneed & Folk, 1958).

The most extreme shapes are *Planorbulina mediterranensis*, which resembles a flat disc, and *Uvigerina peregrina*, which is relatively elongate. Other taxa approximate to spheroids, and vary mainly in terms of the ratio between their *a* (width of test) and *c* (height of test) dimension, which effectively differentiates between *Elphidium crispum*, *Ammonia beccarii.* and *Cibicides lobatulus.* Fig.4-2 shows the changes in aspect ratio with ontogeny, with major increases in the deviation from a sphere for *E. crispum*, *C. lobatulus* and *A. beccarii* differences with regards to size for each species, although *Ammonia* (oval in shape) always remains more spherical.

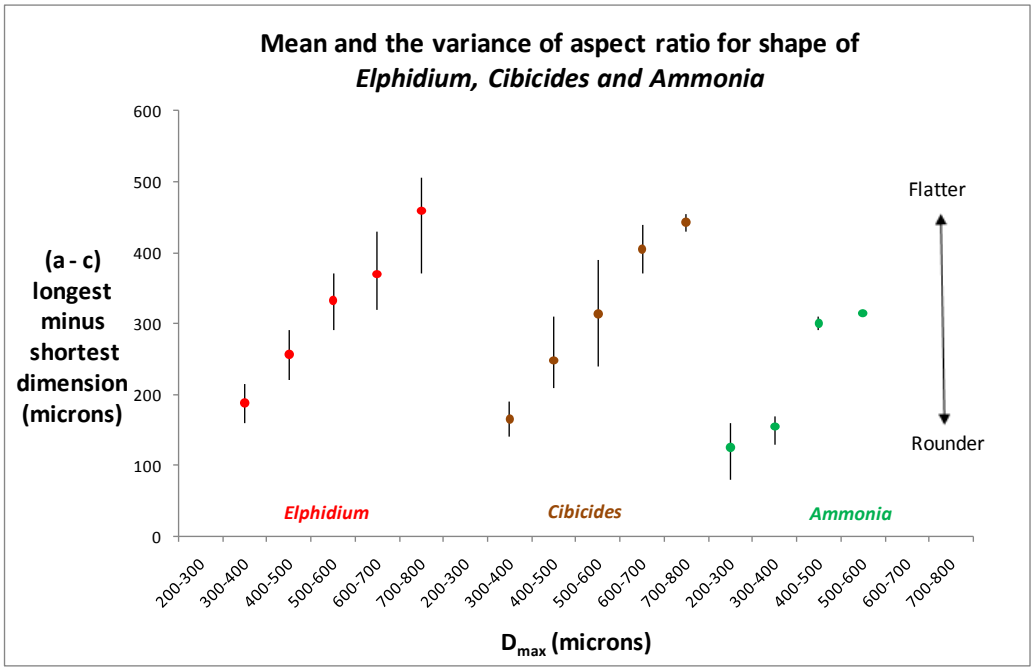

Figure 4-2 Dimensional analysis of *Elphidium, Cibicides* and *Ammonia* in relation to length and width in association to size with error bars showing relative variability.

4.4.2 Density

Density of the tests differs between species and also changes within species during growth (Fig.4-3).

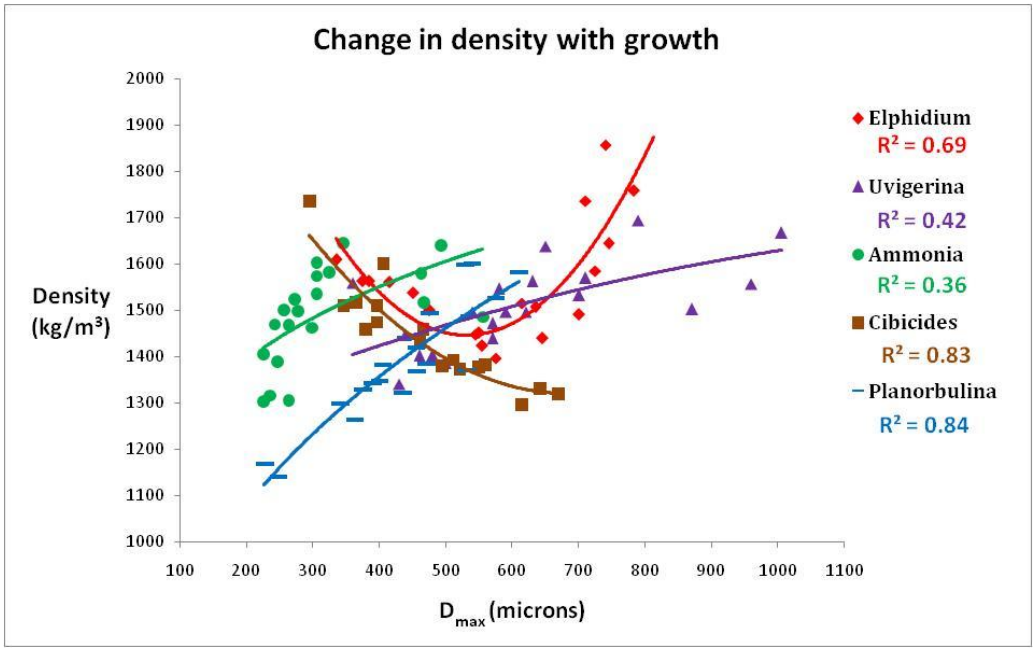

Figure 4-3 Change in density with growth for five different benthic taxa in relation to size. Best fit trend lines for *Elphidium, Uvigerina* and *Cibicides* are curved. *Ammonia* and *Planorbulina* show a power trend line.

Generally, there is an increase in density with growth, but *Cibicides* shows the opposite trend. The R^2 values show there is a large scatter in the data due to varying growth patterns. To understand if there are significant differences in density between species ANOVA was carried out. The foraminifera have a calculated F value of 0.22 (with a critical table value of 2.47), meaning that the there is not a significant difference between species (there is more variation within taxa, than between taxa).

Differences in density between species are presented in Table 4-1.

Table 4-1 Statistical analyses of densities of foraminifera, all values are in kg m^{-3}. Densities of other foraminifera are from the study by Yordanova & Hohenegger (2007).

Species	Mean	Median	5^{th} percentile	95^{th} percentile
Elphidium	1573	1549	1509	1637
Uvigerina	1511	1500	1468	1555
Ammonia	1491	1500	1442	1540
Cibicides	1468	1549	1407	1529
Planorbulina	1394	1377	1333	1454
Densities of other foraminifera				
Soritids & Denritina	1200-1300	These are very light porcellaneous taxa		
Amphisteginids &Nummulids	1780 - 1850	These are very heavy, large robust taxa		

4.4.3 Settling Velocity

Settling velocity was carried out as described in Chapter 3, section 2. Throughout experiments the first time measurement was taken at 15 cms down the tube, by which time all taxa had reached constant terminal settling velocities. The total range of settling velocities identified within the results of the experiments was > 0.01 to 0.06 m sec^{-1} (Fig.4-4).

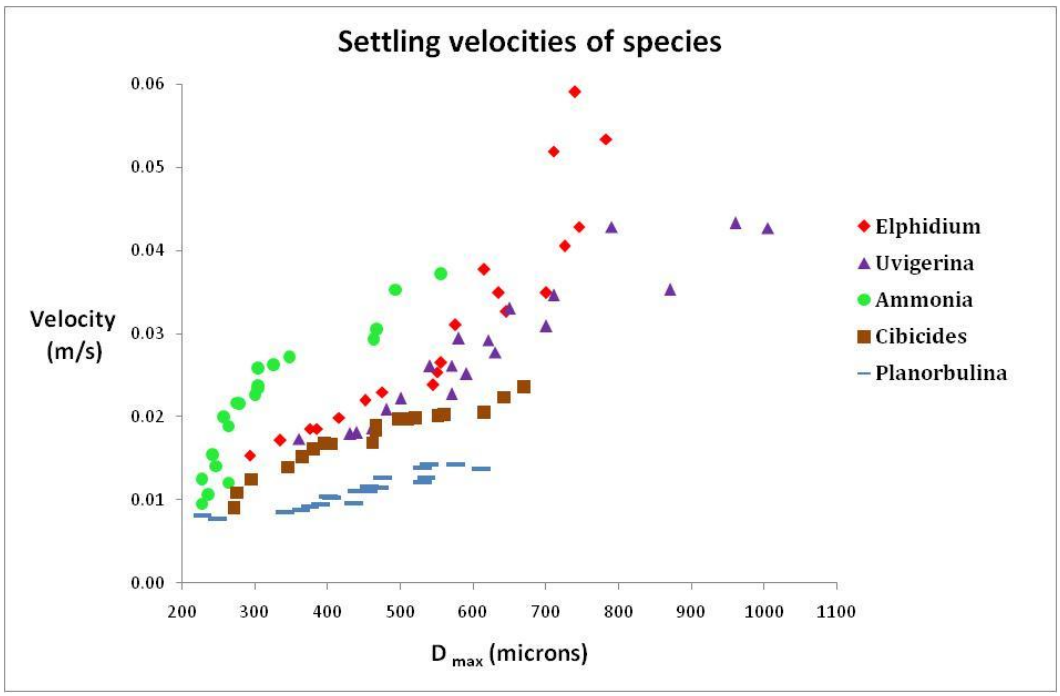

Figure 4-4 Settling velocities of five different benthic taxa in relation to size. D_{max} is the longest dimension; this is an important measurable parameter due to the fact that during settling all foraminifera fall horizontal to the flow.

Highest velocities were exhibited by *Elphidium crispum* in the size range 300-800 µm and the lowest velocities by *Planorbulina mediterranensis* in the size range 200-600 µm with larger specimens falling faster than smaller ones. The relative variability within settling velocities of a species shows the faster settling species such as *Elphidium crispum* show more scatter than the slower settling ones such as *Planorbulina mediterranensis* (Fig.4-5).

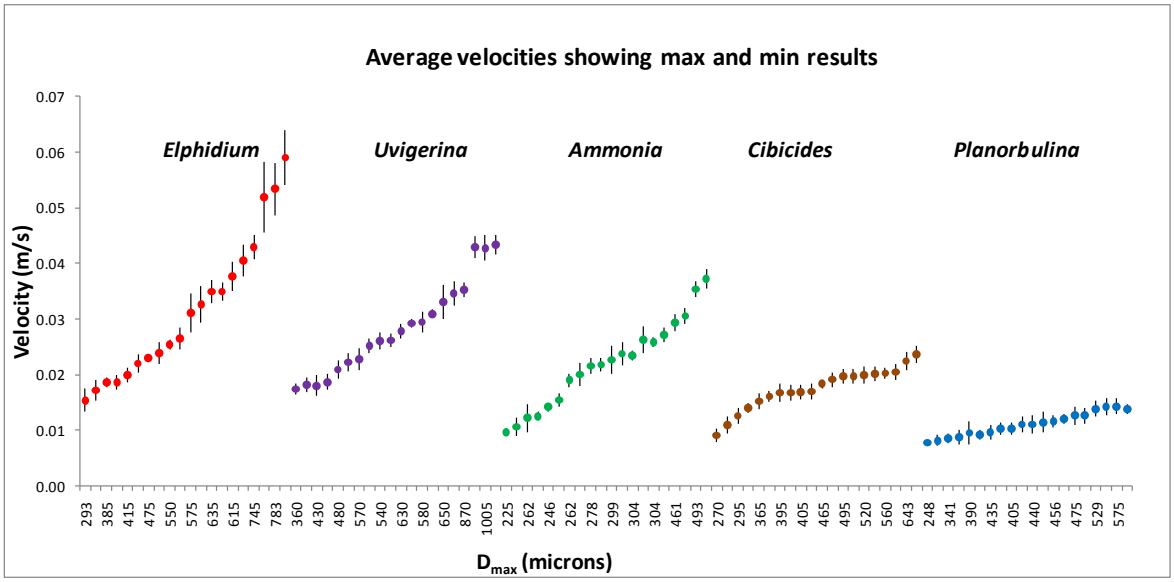

Figure 4-5 Settling velocities of five different benthic foraminifera with error bars showing relative variability. Each species shows smallest to largest in size on horizontal axis from left to right.

Due to the great diversity in morphology and test size, settling velocity is not homogenous and there is considerable variation in settling velocity between species. To understand if there are significant differences between species and therefore a likelihood that taxa will fractionate during post mortem transport ANOVA was carried out. The foraminifera have a calculated F value of 19.01, making them significantly different (there is more variation between taxa, than within taxa).

4.5 Discussion

4.5.1 Size and shape

Inter-species differences in settling velocity may arise from differences in size, shape and density. Pearson Correlation analysis of settling velocity against size provides a correlation coefficient of 0.73 showing that this is an important variable with larger (i.e. the D_{max}) specimens falling faster than smaller ones, but other factors such as shape and density are also important.

The controls on settling velocity behaviour can be explored by examining the particle Reynolds number and form drag. The Reynolds number is the fundamental representation of the particles hydraulic behaviour as shown in equation 4.1

$$Re = DW_S/v \quad (4.1)$$

where D is the diameter of the particle, W_S is the settling velocity and v the kinematic viscosity of the fluid. Within the size ranges of 200 μm to 1100 μm Reynolds numbers varies as shown in Fig.4-6.

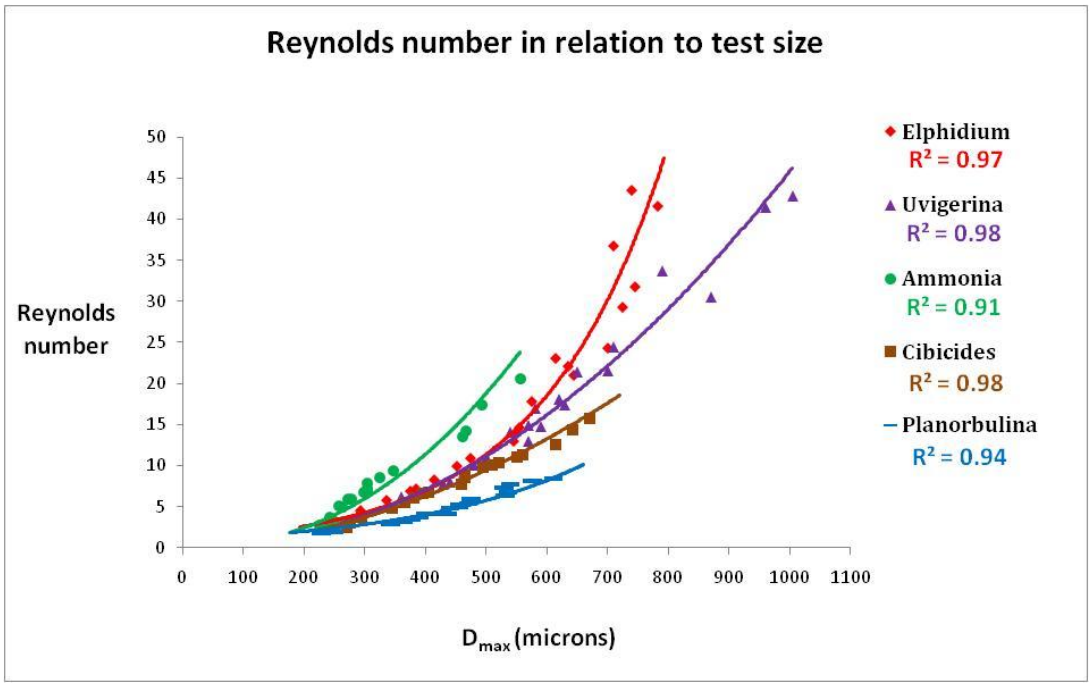

Figure 4-6 Reynolds number for five different benthic taxa in relation to size. Best fit trend lines for *Elphidium* and *Planorbulina* are exponential. *Uvigerina*, *Cibicides* and *Ammonia* show a power trend line.

The dimensionless Re number characterizes the nature of the flow regime around the foraminifera and the drag that the falling tests induce. Drag coefficients for spheres are related to Reynolds where:

Stokes flow $C_D = 24/Re$ (4.2)

Allen flow $C_D = \frac{4(\rho s - \rho)gD}{3\rho W_{s2}}$ (4.3)

Newton flow $C_D = constant\ 0.44$ (4.4)

Flow characteristics are separated by Re numbers such that Stokes flow = Re<0.2, Allen flow = 0.2<Re>500 and Newton flow = 500<Re>10^5 (Munson *et al.* 2006). Fig. 4-6 shows that foraminifera fall within the scope of Allen's flow, where flow around foraminifera creates some turbulence, but is neither fully laminar nor fully turbulent.

A secondary control on settling velocity is the shape of the foraminifera which influences the drag, affecting flow separation in the wake of the test. Smaller (in terms of D_{max}) tests have low Re numbers and high drag. Buoyancy is high and the foraminifera fall slowly through the water column. Fig.4-6 shows that species such as flat disc *Planorbulina mediterranensis* which has the greatest deviation in shape from a sphere has low Re number (related to large drag) while oval shaped *Ammonia beccarii* which is closest to a sphere has a higher Re number (and low drag) for the same sized test.

4.5.2 Density

A tertiary control which affects settling velocity is the density of the foraminifera. All taxa alter their density during ontogeny, which can be explained by the change in chamber size and architecture during growth. Density affects the settling velocity in that the heavier species such as *Elphidium* and *Uvigerina* fall faster than lighter species such as *Cibicides* and *Planorbulina*. ANOVA testing suggest that there is no statistical difference between species in terms of density, but test density is sufficiently variable (Fig.4-3) that it would be expected to have an influence on the particle hydraulics of individual tests. When the Reynolds number (which is closely associated with size and shape, Fig.4-6) is plotted against density per species there is an average R^2 of 0.74, suggesting that density is closely linked to the hydraulic behaviour and drag of foraminifera. It is therefore useful to understand the inter-species differences during ontogeny.

The majority of foraminifera increase in density as they grow as during addition of a new chamber a new layer of shell material is secreted, covering the exposed earlier part of the shell which leads to an increase in thickness from later to earlier chambers and an overall increase in density with growth. This does not occur with *Cibicides lobatulus* which shows a decrease in density with growth. This taxa only has a few chambers in the final whorl (usually around 6-8) compared to the other taxa which are many-chambered. As *Cibicides lobatulus* grows, each new chamber is much larger than the previous one, meaning there is greater volume of space (chamber cavity) to test wall (which does not alter in thickness) and hence a reduction in density as it develops.

Elphidium shows a decrease in density then an increase as it matures. This may be due to the development of proportionally large new chambers as a juvenile then the development of the umbilical plug which forms a dense calcite structure in the central boss as the foraminifera grows. (See Appendix 9.1 for a detailed taxonomy). *Elphidium* and *Ammonia* are from the same Superfamily Rotaliacea, *Ammonia* also develops an umbilical plug but has much fewer chambers and may grow in a more homogenous manner. *Uvigerina* comes from the Superfamily Buliminacea which has small triserial chambers, becoming biserial as the chambers increase in size with ontogeny. *Cibicides* and *Planorbulina* both come from the Superfamily Planorbulinacea where the test is more delicate; *Cibicides* grows few chambers compared to the multichambered *Planorbulina.*

4.5.3 Implications for sedimentary behaviour of benthic foraminiferal test populations

Particle size analysis is universally used to measure the characteristics of a particle in relation to the depositional process. One such measure is the ‘sedimentation diameter’ of the particle. This is defined as the as the diameter of a sphere which has the same density and settling velocity as the given particle and in a given media. Determination of the sedimentation diameter of a particle requires knowledge of the relationship between a spheres diameter and its settling velocity.

Using Gibbs *et al.,* (1971) formulae for settling velocities of quartz spheres in water, the settling characteristics of foraminifera can be compared to quartz grains of identical diameter, therefore depicting the sedimentary regime in which foraminifera may be found. Equivalent settling velocity diameter (or sedimentary diameter) is calculated using the formulae:

$$R_{sed} = \frac{0.55804W_s^2\rho + \sqrt{0.003114W_s^4\rho^2 + [g(\rho_S - \rho)]\,[4.5\mu W_S + 0.008705W_s^2\rho_S]}}{g(\rho_S - \rho)} \quad (4.5)$$

where R_{sed} is the sedimentary radius in cm, W_s is the settling velocity in cm s^{-1}, ρ is the density of the fluid in g cm^{-3}, ρ_s is the density of the forams in g cm^{-3}, g is the acceleration due to gravity in cm s^{-2} and μ is the dynamic viscosity of the fluid in poise (g cm^{-1} s^{-1}).

Fig.4-7 shows that the foraminifera assessed during this work have hydraulic equivalence to quartz spheres in the range of very fine to coarse sand. Equivalence is again controlled largely by inter-species differences, with the largest *Elphidium crispum* being equivalent to coarse sand, small *E. crispum* and the majority of other taxa behaving equivalently with fine - medium sand. *Planorbulina mediterranensis* and the smallest (albeit >300 μm) *Cibicides lobatulus* fall within the range of very fine sand.

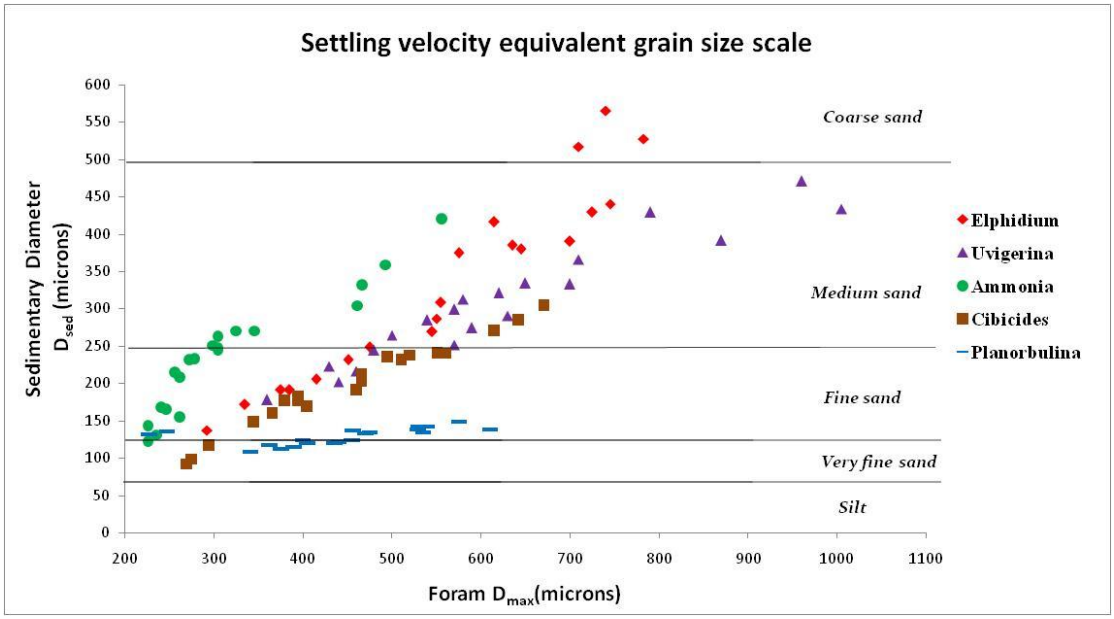

Figure 4-7 Settling velocity of foraminifera in relation to equivalent sedimentary diameter. Horizontal categories define the sedimentary environment in which foraminifera are likely to be deposited.

All settling velocities are lower than for quartz grains with an identical diameter, reflecting the lighter equivalent mass of foraminifera and therefore slower settling characteristics. The data reflects the varying mass and shape of the different taxa, with the lighter, less spherical forams having the largest sedimentation diameters. The most spherically shaped (and heavier taxa) *Ammonia* have sedimentary diameters that are systematically higher than other taxa. The most non-spherical shapes are found in *Planorbulina mediterranensis*, which does not behave like the other taxa. This very light species only marginally increases its sedimentary diameter with increasing size. When foraminifera are hydraulically sorted this may result in fractionation of assemblages, reflecting equivalent settling velocities of sediment grains.

4.5.4 Towards a suitable equation to describe settling velocity of benthic foraminifera:

Do forams behave like spheres?

It would be convenient for future research if foraminiferal test behaviour could be approximated via standard particle hydraulic equations, and the data presented here

allows the first test of whether this approach is valid. To estimate a suitable settling velocity formula, a comparison can be made to see if foraminifera behave like spheres. Allen flow equation (4.3) from Munson *et al.,* 2006 described in section 4.5.1 can be used to calculate a suitable drag coefficient

Allen flow $$C_D = \frac{4(\rho s - \rho)gD}{3\rho W_{s^2}} \quad (4.3)$$

To test the validity of the Allen equation the observed settling velocity (W_s^2) for each species is plotted against $4(\rho s - \rho)gD/3\rho$ giving a gradient of $1/C_D$. The drag coefficient is determined by forcing the regression line through the origin. The gradient of the relationship $1/C_D$ should be close to $y = x$ and R^2 should be ~1 if the Allen approximation is an effective means of describing foraminifera behaviour. This will reveal whether the settling velocities increase linearly with D and ρ, and whether foraminifera do act like spheres. Results are shown in Table 4-2.

Table 4-2 Graph summary of regression for individual species in a comparison of settling velocity against diameter and density. Generic settling equation $y = m\left(\frac{4(\rho s - \rho)gD}{3\rho}\right) + c$.

Species	R^2 through origin	Gradient through origin	$1/C_D$
Elphidium	0.76	0.3037	3.29
Uvigerina	0.89	0.2099	4.76
Ammonia	0.85	0.2730	3.66
Cibicides	0.11	0.3612	2.77
Planorbulina	0.83	0.0490	20.41

From this it can be seen that Allen's flow holds reasonably well for all taxa except *Cibicides.* Using linear regression to see how diameter relates to density, *Cibicides* shows that density decreases in a consistent and linear fashion with diameter, (R^2 = 0.79) which is not in line with the results found for the other species of foraminifera, and nor with equation (4.3). This is because *Cibicides* reduces in density with growth, whereas all other taxa in the study increase in density with growth (see section 4.4.2). Allen's flow therefore does not hold for *Cibicides* but by using a negative regression with the same form as Allen's flow and changing the equation of $4(\rho s - \rho)gD/3\rho$ to $-4(-\rho s - \rho)gD/3\rho$ this now raises the correlation coefficient towards values typical of other taxa (R^2 = 0.80), with the same gradient and drag

coefficient as shown in Table 4-2. This analysis indicates that individually the taxa can indeed be approximated as spheres. For each species shape does not change significantly with size, so the main elements of Allen's flow (size and density) hold when plotted individually.

The C_D values arising from this analysis can be used to calculate a settling velocity for each of the species by rearranging equation 4.3 to:

$$Ws = \sqrt{\frac{4gD(\rho s - \rho)}{3\rho C_D}} \tag{4.6}$$

A comparison between the observed and the calculated settling velocities is shown in Fig.4-8.

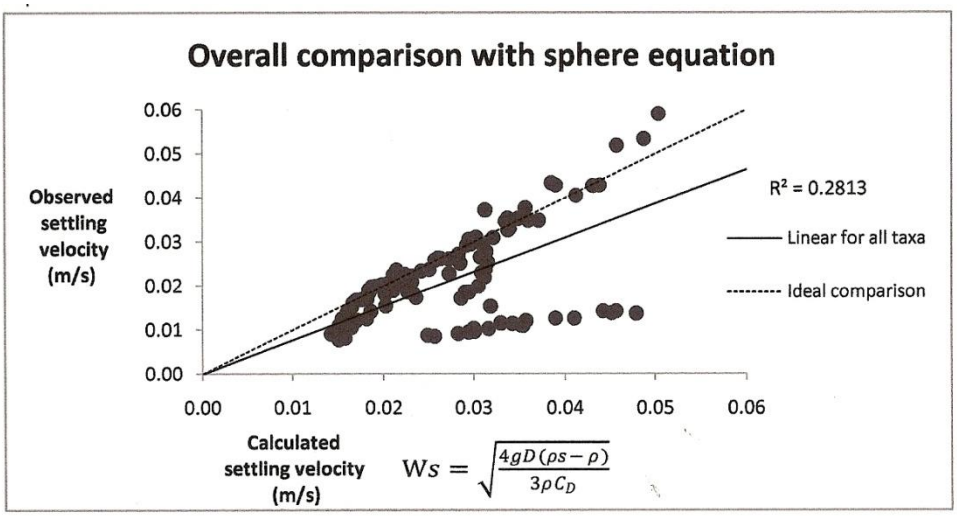

Figure 4-8 Comparison of observed and calculated settling velocities.

Fig.4-8 shows that when all taxa are considered together, the shape differences become apparent and the settling equation for spheres is no longer suitable as an overall equation. The settling equation for spheres, on average, over-estimates velocities. This is especially true for *Planorbulina* (flat disc) whose shape differs most from a sphere. Differences arise due to shape and the fact that settling velocities for species do not precisely increase linearly with size. So in response to the question "Do foraminifera behave like spheres?" the analysis has shown that

there is a good correlation when species are considered in isolation, but when analyzed as an assemblage this proposal does not hold true.

Do forams behave like larger shells?

Allen (1984) and Yordanova & Hohenegger (2007) incorporated volume and area into the equation in an attempt to account for shape differences. The following equation was used to yield different settling velocities for bivalve shells and ellipsoid and lenticular shaped larger foraminiferal tests:

$$Ws = \sqrt{\frac{2g\ M(\rho_{test} - \rho)}{C_D \rho\ \ A\,\rho_{test}}} \qquad (4.7)$$

where g is the gravitational force, ρ the density of the test and water, M/ρ_{test} indicates test volume, A the test area being in horizontal position during sinking and C_D the drag coefficient (Allen, 1984).

To see if this yields a more accurate settling velocity equation for small benthic foraminifera, the observed settling velocity W_s^2 (y axis) was plotted against $2gM(\rho_{test} - \rho)/\rho A\,\rho_{test}$ (x axis), giving a gradient of $1/C_D$. C_D values can then be used to calculate settling velocity using equation 4.7. Results are shown in Table 4-3.

Table 4-3 Graph summary of regression for individual species in a comparison of settling velocity against volume and area. Generic settling equation $y = m\left(\frac{2gM(\rho test - \rho)}{\rho A \rho test}\right) + c$.

Species	R^2 through origin	Gradient through origin	$1/C_D$
Elphidium	0.79	0.6641	1.55
Uvigerina	0.91	0.3354	2.98
Ammonia	0.68	0.5899	1.70
Cibicides	-0.94	0.3812	2.62
Planorbulina	0.60	0.2933	3.41

When compared to spheres, Table 4-4 shows that Allen's equation yields a slightly better result for *Elphidium, Uvigerina* and *Cibicides* but not for *Ammonia* and *Planorbulina*. This indicates that when looking at individual species, either equation is equally appropriate in describing the settling velocity of foraminifera.

Table 4-4 Regression comparison of Allen's settling velocity equation against that of spheres.

Species	R^2 (Allen, 1984)	R^2 (spheres)
Elphidium	0.79	0.76
Uvigerina	0.91	0.89
Ammonia	0.68	0.85
Cibicides	-0.94	0.80
Planorbulina	0.60	0.83

A comparison between the observed and the calculated settling velocities using Allen's equation is shown in Fig.4-9.

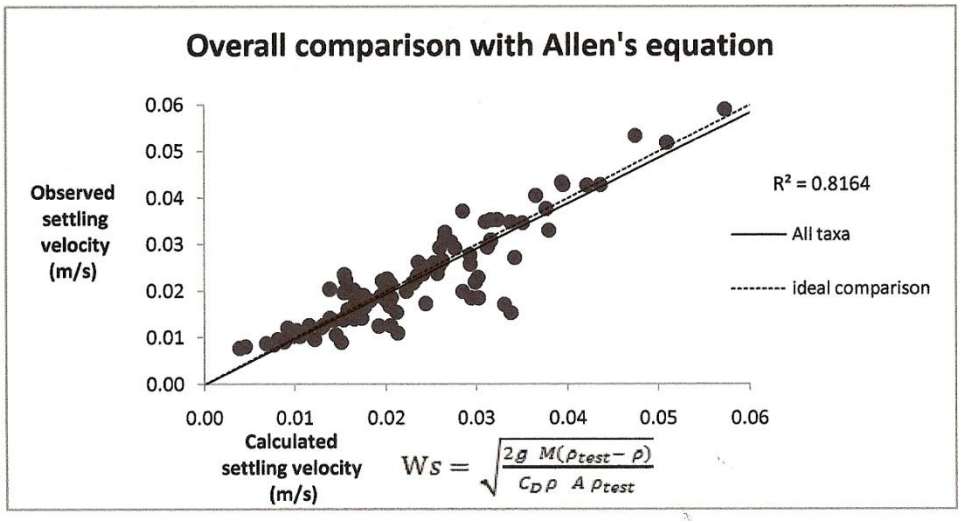

Figure 4-9 Comparison of observed and calculated settling velocities using Allen's equation.

Fig.4-9 shows a marked improvement from Fig.4-8 when comparing the full assemblage of all foraminiferal taxa (Fig.4-9, $R^2 = 0.82$) compared to the analysis for spheres (Fig.4-8, $R^2 = 0.28$). This is again related to the degree of shape difference. There are larger shape differences between different species and therefore differences in settling velocity are more closely related to the specimens *A* and *M*/ ρ_{test}.

This analysis shows that shape is an important parameter when considering the settling behaviour of an assemblage of foraminiferal tests, but not when considering a species in isolation. In this latter case it is valid to predict their settling velocity using an equation derived for spheres, and fractionation of the specimens during deposition will be largely driven by differences in diameter and density. The

influence of shape can be constrained by using mass and the area of the specimen horizontal to the flow rather than diameter.

In the Gibbs *et al.,* (1971) formulae for equivalent quartz grain size, D_{sed} (sedimentary diameter) all flow characteristics are incorporated. To include this as the size parameter rather than the true *D*, the settling equation is improved confirming the validity of Gibb's equation for these particles. Analysis of all the taxa together shows an $R^2 = 0.93$. This means that a single coefficient value cannot accurately explain overall settling velocity behaviour for all the foraminifera investigated in this experiment. However, even when all flow characteristics are incorporated using D_{sed} there is still a slight unpredictability as foraminifera do not increase linearly with size.

4.5.5 Effects of sedimentary fill on individual tests

Taphonomic processes after death can affect the hydrodynamic properties of foraminifera by the inclusion of sand and silts into the test once chambers become damaged. The effects of sand infill on settling behaviour can be calculated by substituting a volume of sediment for the volume of seawater within the test. In calculating the density of foraminifera in water, the percentage of test consisting of calcite wall was determined and the remaining space within the test was understood to be water (See Chapter 3 Methods, section 3.1.2). By substituting quartz (density 2634 kg m^{-3}) for water we are assuming all spaces are replaced with sediment infill. Although it is rare for a test to be filled with pure quartz, we argue that this case represents a midpoint evaluation of the impact of test filling as a test may be infilled with mud (density ~1730 kg m^{-3}) or the test may be subject to pyritic alteration (density ~ 4000 kg m^{-3}) in which case the test would become much heavier.

This new density is then used in Gibbs *et al.* (1971) equation to calculate the equivalent settling velocity diameter (or sedimentary diameter). On calculating the D_{sed}, the most effective settling velocity equation is considered using the formulae:

$$Ws = \sqrt{\frac{4g\ D_{sed}(\rho_s - \rho)}{3\rho C_D}} \qquad (4.8)$$

The increase in settling velocity per species is shown in Fig.4-10.

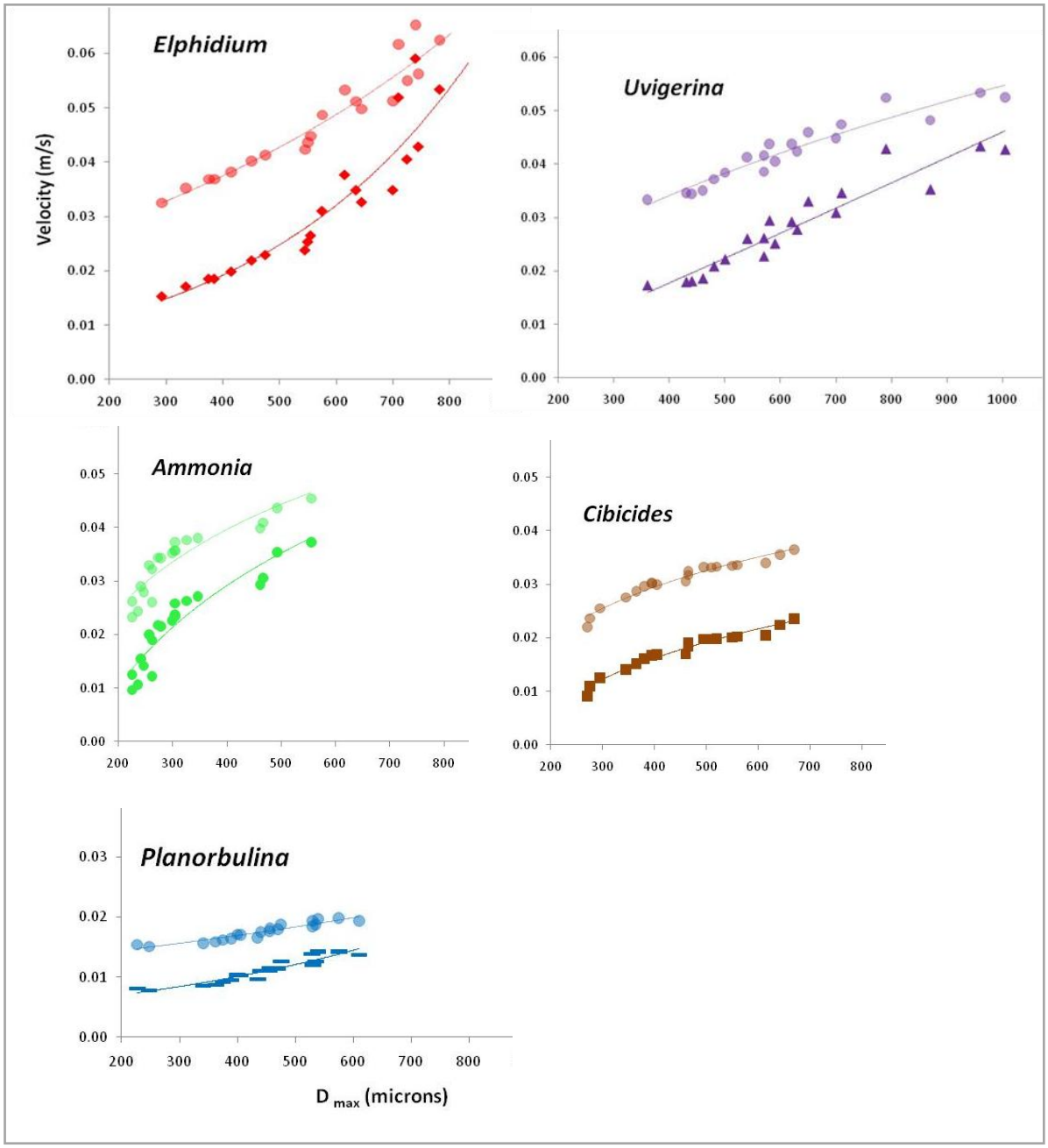

Figure 4-10 Change in velocity with an infilling of quartz for five benthic species. Lines for each graph show comparison between those filled with water and those filled with sand. Lighter spherical symbols represent quartz filled tests while darker symbols represent water filled tests.

The settling behaviour for each species results in a different pattern of change with size when they become infilled with sediment. Some taxa increase in terms of settling velocity more than others, which is a simple reflection of their internal

chamber volume. Fig.4-11 gives an overall picture of changes during ontogeny for each species. In general, there is a greater change in velocity when the tests are smaller; this shows that more juvenile tests have a larger amount of internal space compared to architecture of chamber walls. Apart from *Cibicides*, which changes very little, smaller tests will become heavier and fall faster, whereas larger ones are less affected.

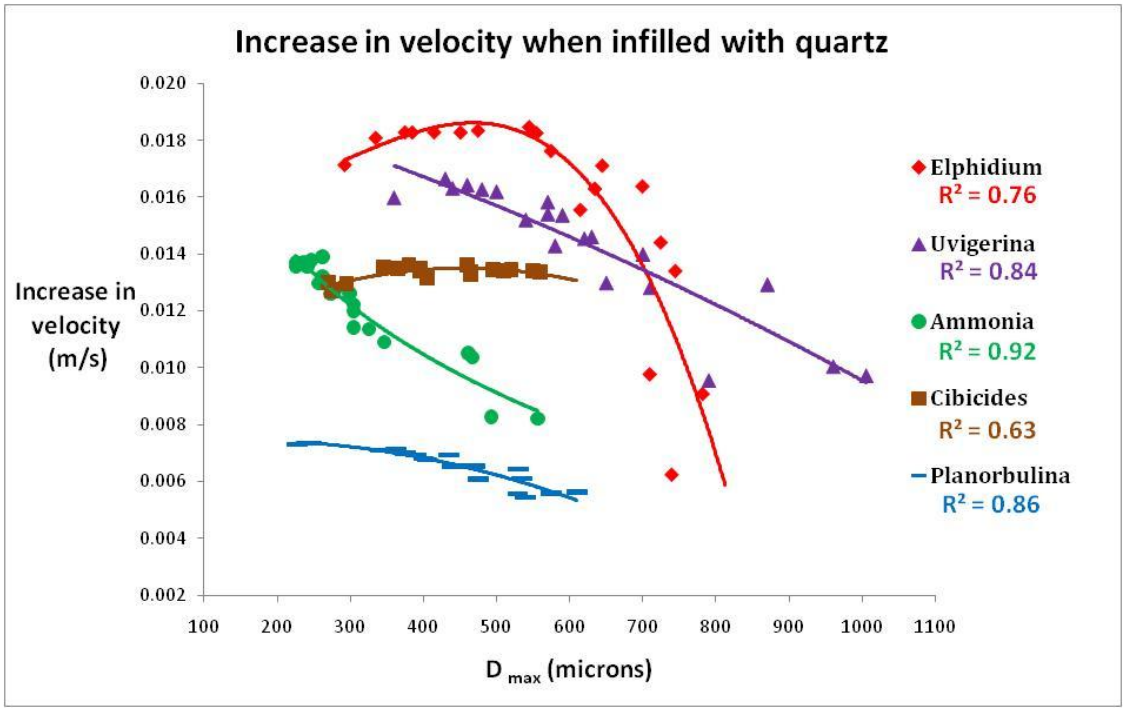

Figure 4-11 Increase in settling velocity when tests infilled with quartz for five different benthic taxa in relation to size. Best fit trend lines for *Elphidium, Uvigerina, Cibicides* and *Planorbulina* are curved. *Ammonia* show a logarithmic trend line.

Elphidium shows little change in the amount of sediment that can enter the test when small, then a decrease once it develops beyond 500 μm. This may represent the development of the central boss, taking up more space in proportion to the new chambers as it begins to mature. *Ammonia* also shows a decrease in the amount of sediment that can enter the test as it grows. Again this taxon has a central boss and a complex canal system, all of which take up more proportional space as the test grows. For *Uvigerina* there is almost a linear decrease in the amount of sediment that can enter the test as it grows reflecting the steady increase in density during ontogeny shown in Figure 4-3. The impact of sedimentary infilling is relatively small for the lighter species *Cibicides* and *Planorbulina. Cibicides* overall density when

filled with water decreases as it grows due to addition of larger chambers which is reflected by a very slight increase in sediment infill with size. *Planorbulina* shows a slight decrease in sediment fill as it grows, which reflects its multichambered architecture and that the proportion of chamber space to test wall changes little as it grows.

Although it is not possible to gauge how much sediment may fill a test during post mortem transport, this analysis shows how sediment infill can change the settling behaviour of individuals and populations. As the foraminifera grows and matures, differences arising from the architecture of the test become more significant as each species develops its own characteristics. Conversely, there is generally a reduction in the difference between a water filled test and a sediment filled test with an increase in size, making sediment infilling less significant as it grows. This suggests that the signal of fractionation may not be drowned out by the "noise" produced by sediment addition to tests, which does not lead to random inter-species differences. ANOVA analysis of inter-species differences in the change of settling velocity arising from infilling provides an F value of 13.85, making species significantly different but not as different as water filled tests F value of 19.01.

4.6 Conclusion

Settling tube analysis of several foraminiferal species has shown that velocities are significantly different between taxa, meaning that assemblages are likely to fractionate according to species during transportation. Inter-species differences are related to the variation in size, shape and density between taxa. The primary control is size, as larger specimens fall faster than smaller ones. Shape differences are a secondary control, arising from differences in Reynolds number and form drag; i.e. the dynamics of the flow around a falling test. The Re number shows foraminifera characteristics become increasingly different with growth, as the Re number increases. We find that Allen's flow is applicable to describe the drag experienced by foraminifera, and show that tests with greater deviation from sphericity result in greater drag. These tests have greater buoyancy and therefore fall more slowly through the water column. Density also varies between species due to varying

growth patterns in test architecture during ontogeny. Denser species are heavier and therefore fall faster than lighter ones.

Investigation into the equivalent settling velocity and the subsequent recognition of the D_{sed} (sedimentary diameter) has revealed an important association between foraminifera and the depositional setting. As shown above, benthic foraminifera are likely to fractionate on species lines during transport, providing opportunities for hydraulically sorted assemblages to be identified by their common 'equivalent diameter'. By characterizing foraminifera and comparing them to other grains in the oceanic environment, an understanding of the hydraulics of post mortem transport can be considered. When an assemblage has similar settling velocities to the surrounding sediments it is likely to have experienced the same energy regime and transport processes, with fractionation of grains and foraminifera occurring simultaneously before final deposition on the sea floor.

Comparison in settling velocity of foraminifera to spheres reveals that - individually - taxa can be modelled reasonably well as spheres, where settling is controlled by diameter and density. This is because individual species do not change shape significantly with size. However, when comparison is made with an assemblage of different species, they do not behave like a population of spheres; the shape differences between taxa are simply too large. Settling velocity of an assemblage of foraminifera can be better described by using mass and the surface area of the specimen rather than diameter. By using Allen's (1984) equation (4.7), shape differences between taxa can be accounted for.

The effect of sand infill on tests is different for each species due to varying test architecture. Size is an important parameter with smaller tests having a greater relative increase in settling velocity due to sediment fill. Effects reduce as the foraminifera grow and test architecture becomes more pronounced, meaning that sediment infilling becomes less significant with size in determining inter-species differences. It can be inferred that during post mortem transport smaller tests may be found in conjunction with larger tests of the same species when a substantial amount of sediment infilling has occurred. Settling velocities are still significantly different

between taxa even when infilling of tests is considered, showing that fractionation of species is likely to take place whether the foraminifera are filled with sea water or with sediment.

5 Hydraulic sorting of empty foraminiferal tests

5.1 Abstract

Experiments with steady and waning flows demonstrate that foraminifera fractionate spatially according to size and shape. Suitable scaling of the model allows further examination of the specific particle hydraulic behaviour of foraminifera, and reveals that it is not related to velocity in a simple manner but is more closely associated to the turbulent kinetic energy, (TKE) within the flow. The vertical transport and suspension of foraminifera are influenced by the level of turbulent energy which has a significant influence on the depositional sequence of tests. Turbulent intensity in the flow reduces downstream, and as a consequence heavier large taxa become deposited within relatively short distances of their source while smaller, lighter individuals are transported greater distances.

The experiments show that there are significant statistical differences in settling velocity of different foraminiferal taxa and this is likely to result in significantly different transport distances between species in natural settings. To further constrain this potential, a simple analytical model of oceanic turbidite behaviour is employed in conjunction with settling velocity data to examine the potential for fractionation of species downslope on realistic scales.

5.2 Introduction

The assemblage of microfossils within a sedimentary deposit can be greatly affected by transport and reworking of tests due to turbulence and currents before final deposition and accumulation on the sea floor (Murray, 2006). Post-mortem transport of foraminifera from the continental shelf to the deep sea make palaeoenvironmental reconstruction particularly difficult in off-shore locations where hydrocarbons are often found (Murray, 2006; Talling *et al.,* 2007). This issue is complicated by the lack of basic knowledge about the specific particle hydraulic behaviour of

foraminiferal tests globally and for specific taxa. This Chapter describes a series of experiments aimed at providing the basic physical characterization of foraminiferal transport that subsequent Chapters will apply to "real-life" case studies. In the process, it provides the foundations on which a physics-based understanding of how benthic foraminiferal assemblages are modified by post-mortem transport and of the processes that modified them. The experiments were conducted using a spatially waning turbid current forced by a saline density flow, and the hydrodynamics of the foraminifera were examined in relation to both downstream and vertical changes in the flow itself. To provide insights into foraminiferal particle hydraulic behaviour on open-ocean scales, the constraints drawn from the empirical experiments and established empirical formulae are used to simulate a turbidite-like waning flow.

5.3 Methods

Experiment design is fully described in Methods, Chapter 3, section 3.3.

5.4 Experimental Results

5.4.1 Experiments 1-3; results of the waning flow experiment.

Preliminary experiments involved inducing a surge-type waning flow which lasted a few seconds from release to reaching the end of the channel, and investigated the impact on foraminiferal test transport. A range of velocities were used to examine deposition downslope over 2 m (Table 5-1).

Table 5-1 Velocities down flume in ms^{-1} with initial Froude in waning flow experiment.

Experiment	Proximal Froude	Proximal velocity	velocity at 0.5 m	velocity at 1m	velocity at 1.5 m	velocity at 2 m	Average Velocity
1	4.8	1.70	0.17	0.10	0.11	0.12	0.44
2	6.3	2.24	0.21	0.12	0.12	0.11	0.56
3	7.1	2.54	0.25	0.14	0.13	0.11	0.64

In these experiments, declining velocity downslope occurred following an exponential decay pattern, with the greatest decrease occurring in the region proximal to the inlet pipe, and the distal velocity being quasi-constant regardless of

initial velocity. Nevertheless, in all experiments the faster the initial flow the further the travelling distances for all species (Fig.5-1). This replicates other sedimentary studies where the higher the velocity of the flow, the longer the horizontal component of settling trajectory (Alexander & Mulder, 2002; Pirmez & Imran, 2003).

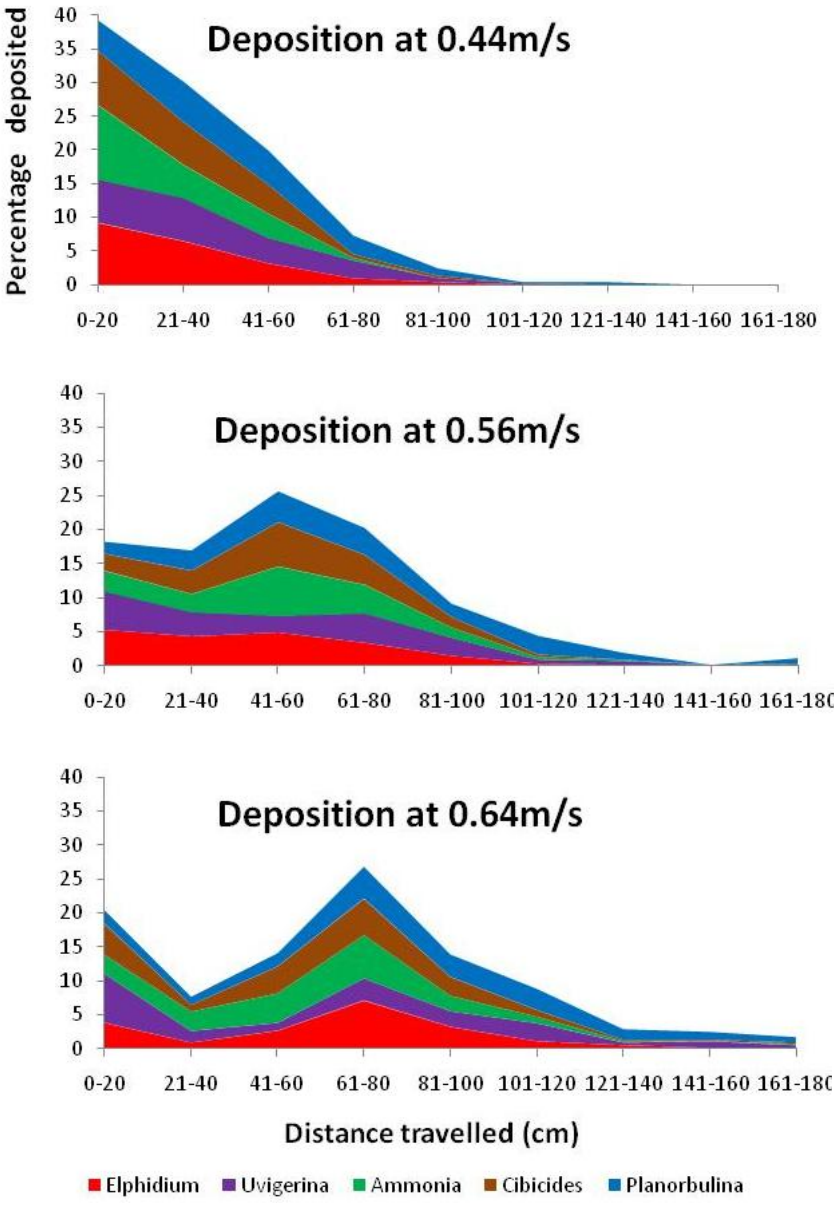

Figure 5-1 Proportional deposition of foraminifera species downslope with various average flow velocities. Deposition from pipe outlet.

Overall heavier taxa such as *Elphidium crispum, Uvigerina peregrina* and *Ammonia beccarii* settled out first while lighter taxa *Cibicides lobatulus* and *Planorbulina mediterranensis* settled the furthest down the channel (Fig. 5-1). The results show some fractionation by species, but depositional distributions are affected by the large drop in energy at the pipe exit, especially in the high setting of energy experiment 3. As the flow leaves the pipe and expands within the channel it changes from super- to sub-critical resulting a hydraulic jump (forming a cylindrical standing wave) which causes a large proportion of foraminifera to be deposited out. This affect becomes greater with increasing initial velocity. To reduce the effect of the hydraulic jump on foraminifera, tests were placed 20 cm from the pipe. This increased the observed fractionation of species with an increase in the deposition of lighter, smaller tests downslope (Fig.5-2).

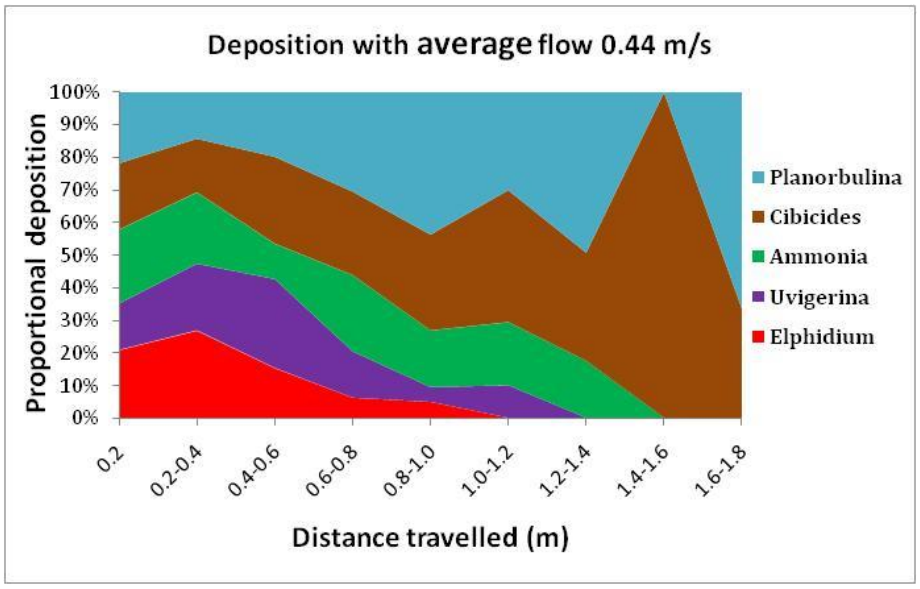

Figure 5-2 Proportional deposition downslope when foraminifera are placed 0.2 m from pipe exit.

The large drop in energy and flow recirculation within the standing wave at the pipe exit results in a high proportion of all foraminifera being deposited; when this proximal effect is reduced differing transport distances for the remaining taxa can be detected. From the initial trials fractionation of species can therefore be identified in principle, but information from these experiments highlighted the need for adequate

control of the hydraulic jump and a steady flow down flume to enable a more detailed study of the depositional patterns of foraminifera to be undertaken.

5.4.2 Experiment 4; results from continuous flow

5.4.3 Flow characteristics

A ‘continuous quasi-steady flow’ rather than a ‘surge type flow’ was used in experiment 4 to allow much greater control of flow dynamics. Considerations leading to this experiment and methods are described in Methods, Chapter 3, section 3.3.4 and 3.3.5. The sustained or quasi-steady flow in the larger tank enabled accurate measurement of the velocity and Froude number down the flume. Velocity measurements for the full length of the flume were recorded at ~1 cm above the bed. The flow had an initial velocity of 0.23 ms^{-1} and a densiometric Froude number of 1.5 (Fig.5-3 & 5-4).

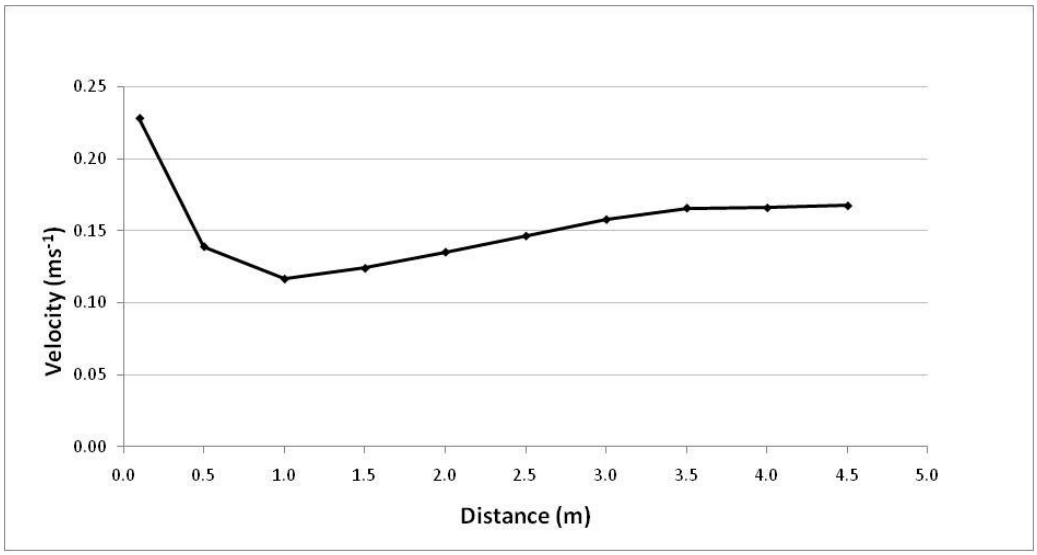

Figure 5-3 Velocity of turbidity current in flume approximately 1 cm above the bed.

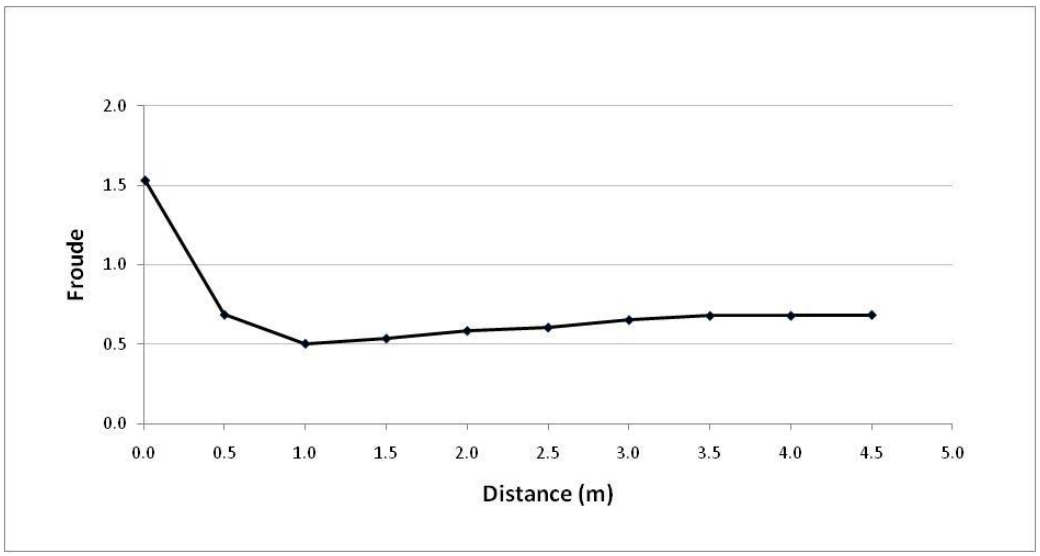

Figure 5-4 Turbidity current changes in densiometric Froude number down flume.

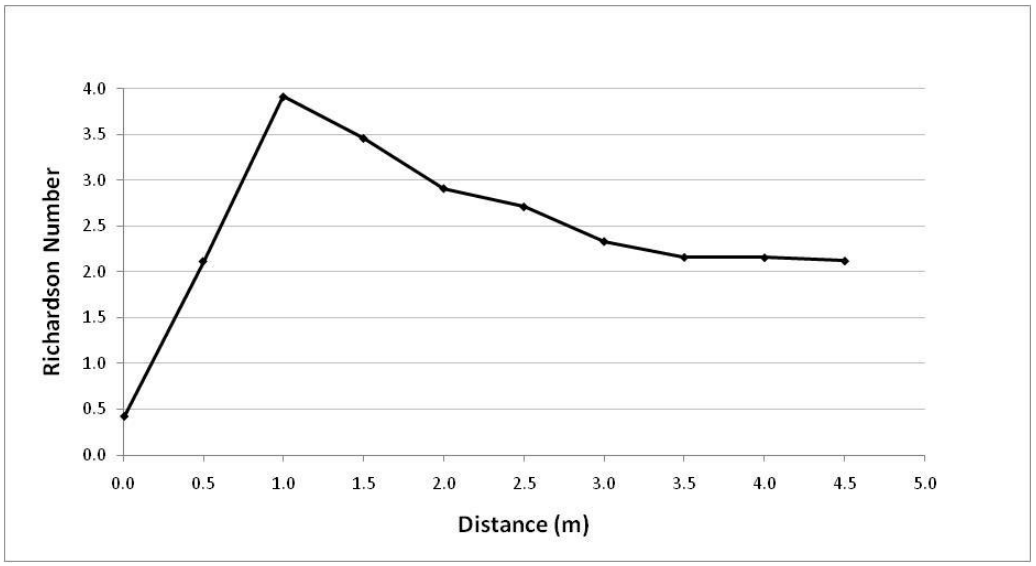

Figure 5-5 Changes in Richardson number down flume.

The flow transition to subcritical where F<1 begins around 0.4 m down flume. This initial drop in densiometric Froude number is associated with entrainment of the ambient water and deceleration as the current spreads laterally from the pipe to the full width of the tank. The Richardson number is below 1 only in the first 0.2 m (Fig.5-5) indicating intense entrainment and mixing at the beginning of the flow when the Froude is supercritical, which is similar to the behaviour of turbulent dense-water flows in the ocean (Price & O'Neil-Baringer, 1994) and also reflects oceanic settings where the angle of slope decreases causing a change from a supercritical to subcritical flow (Komar, 1977). After the first metre the Richardson

number begins to fall, moving towards a quasi-constant value, showing little entrainment as the flow expands very slowly downslope.

Both vertical and horizontal dynamics may be important in understanding how the foraminifera are transported in the flow so a more detailed picture is shown in Fig.5-6 showing how the flow geometry changes with depth and velocity downslope. Measurements were taken up to 3.5 m downstream by which time all foraminifera had deposited out. ADV probes were located at 0.25, 0.5, 0.75, 1.0, 1.5, 2.0, 2.5 and 3.5 m down flume. At each location measurements were taken at 0.005, 0.015, 0.02, 0.03, 0.04, 0.05, 0.06 and 0.07 metres above the bed.

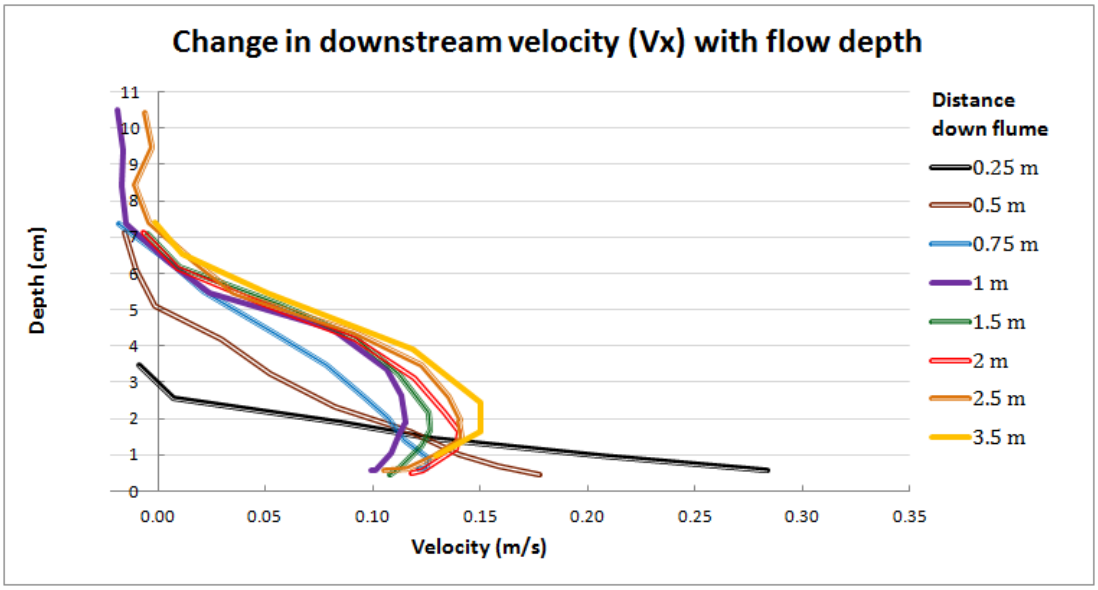

Figure 5-6 Vertical downstream velocity changes from the boundary (0 depth) to the top of the flow as the flow migrates down flume.

The top of the density current is understood to be when the velocity reaches zero on the *x* axis. i.e. where ambient flow is present and is not influenced by the flow released at the top end of the flume. Fig.5-6 shows that the downstream velocity is fastest close to the pipe exit when the flow is at its shallowest. At this location (0.25 m downstream) the velocity reaches 0.28 ms^{-1} close to the bed (supercritical condition). At a distance of around 0.5 m the flow begins to thicken and velocity decreases with distance becoming more persistent around 0.1-0.15 ms^{-1} as the flow continues downstream (subcritical condition).

Beyond 0.5 m downstream the effect of the shear stresses at the bottom and upper interface can be seen. The velocity maximum is around 2-3 cm above the boundary; this is where velocity achieves a maximum and the average shear stress falls (Middleton & Southard, 1984). This change in velocity gradient (inflection point) signifies the existence of a distinct shear layer. The level of velocity maximum is controlled by the ratio of the friction forces at the lower and upper boundaries; the bed and the water-turbidite interface (Middleton, 1993). High levels of friction at the upper boundary tends to lower the level of velocity maximum, while high lower boundary friction will raise the level of the velocity maximum (Buckee *et al.*, 2001). At a distance of 0.5 m the velocity maximum is close to the bed because the upper boundary friction is dominant. As the flow migrates downstream the drag in the upper flow reduces and friction at the bed becomes more dominant, raising the velocity maximum to around 2-3 cms above the bed. Below this height of 2-3 cm the bottom shear stress is determined by the roughness of the bottom which slows the velocity towards the bed. The velocity distribution below the level of maximum velocity is logarithmic (Fig.5-6). Above the velocity maximum shear stresses are mainly due to the resistance at the boundary between the flow and ambient water. This is mainly due to mixing across the boundary which results in an exchange of momentum between the two fluids and entrainment of the ambient water in the direction of the flow. The resistance depends on the degree of turbulent mixing across the interface, and this in turn depends on the density contrast across the interface and on the velocity and scale of the current. By ~1m from the pipe outlet the Froude number has become nearly constant with distance and an established velocity profile for a turbidity current has developed.

5.4.4 Underlying physics of turbulent kinetic energy

To understand the dynamics of the flow an analysis of turbulence is described using turbulent kinetic energy. The turbulent kinetic energy (TKE) per unit mass represents the energy extracted from the mean flow by turbulent eddies (Robert, 2003). The passage of eddies manifests itself as instantaneous fluctuations in velocity; the magnitude of the fluctuations being a measure of the intensity of turbulence (Buckee

et al., 2001). The RMS expresses the average magnitude of velocity fluctuations (Versteeg & Malalasekera, 2007) and turbulence intensities are estimated from turbulent fluctuations using the formulae:

$$TKE = 0.5\rho(\overline{u'^2} + \overline{v'^2} + \overline{w'^2}) \quad (5.1)$$

Where ρ is the fluid density and u', v' and w' are the streamwise, spanwise and vertical velocity fluctuations. Fig.5-7 shows the changes in TKE downstream from where the foraminifera begin to deposit out at 0.5m onwards.

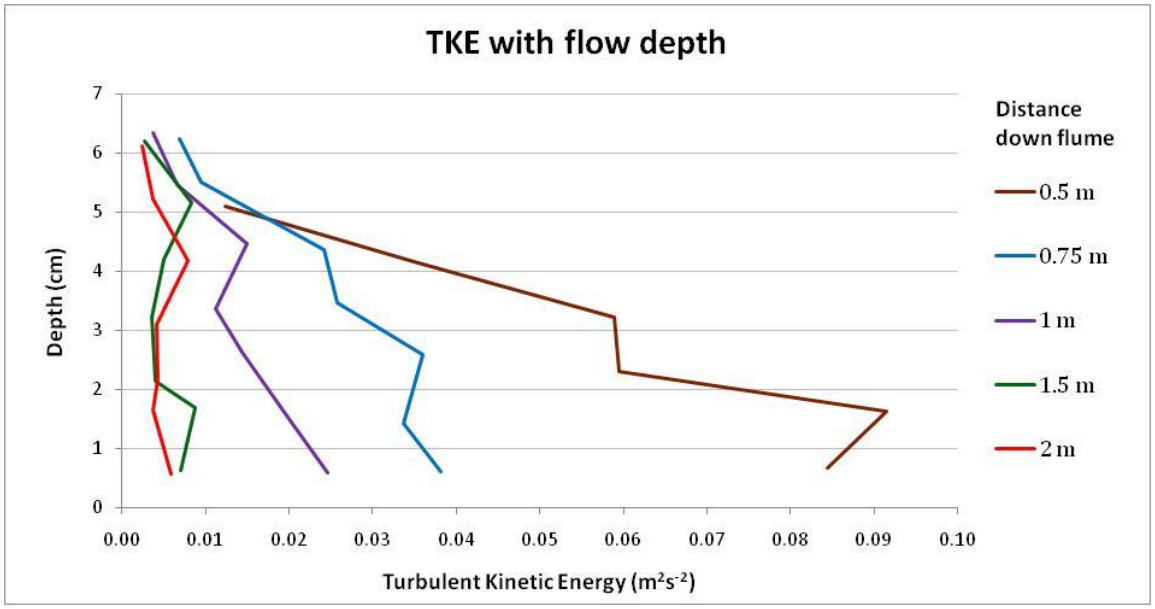

Figure 5-7 Turbulent kinetic energy of flow from the bed (0 cms) to the top of the turbidity current. Each line depicts a distance down flume.

The largest TKE values are found in the region proximal to the pipe outlet where the mean velocity gradient is largest. Values then diminish downstream, rapidly reducing once the flow becomes more stable. The results are similar to the turbulent energy distribution from saline gravity currents found by Kneller *et al*. (1999) and Buckee *et al.* (2001) where maximum values occurred towards the base of the flow. As the TKE drops below 0.10 m^2s^{-2} and turbulent fluctuations reduce the foraminifera start depositing, while at greater turbulent velocities they are kept in suspension by strong turbulent momentum.

5.4.5 Foraminiferal deposition

All foraminifera moved downslope, with the majority of deposition occurring around 0.5 – 1.0 metres as shown in Fig.5-8a. As the flow enters the flume the foraminifera are fully entrained and only limited deposition occurs nearer the pipe exit. During this supercritical stage there is therefore sufficient kinetic energy to keep the foraminifera in suspension. Deposition begins to increase as the velocity drops rapidly and the flow becomes subcritical.

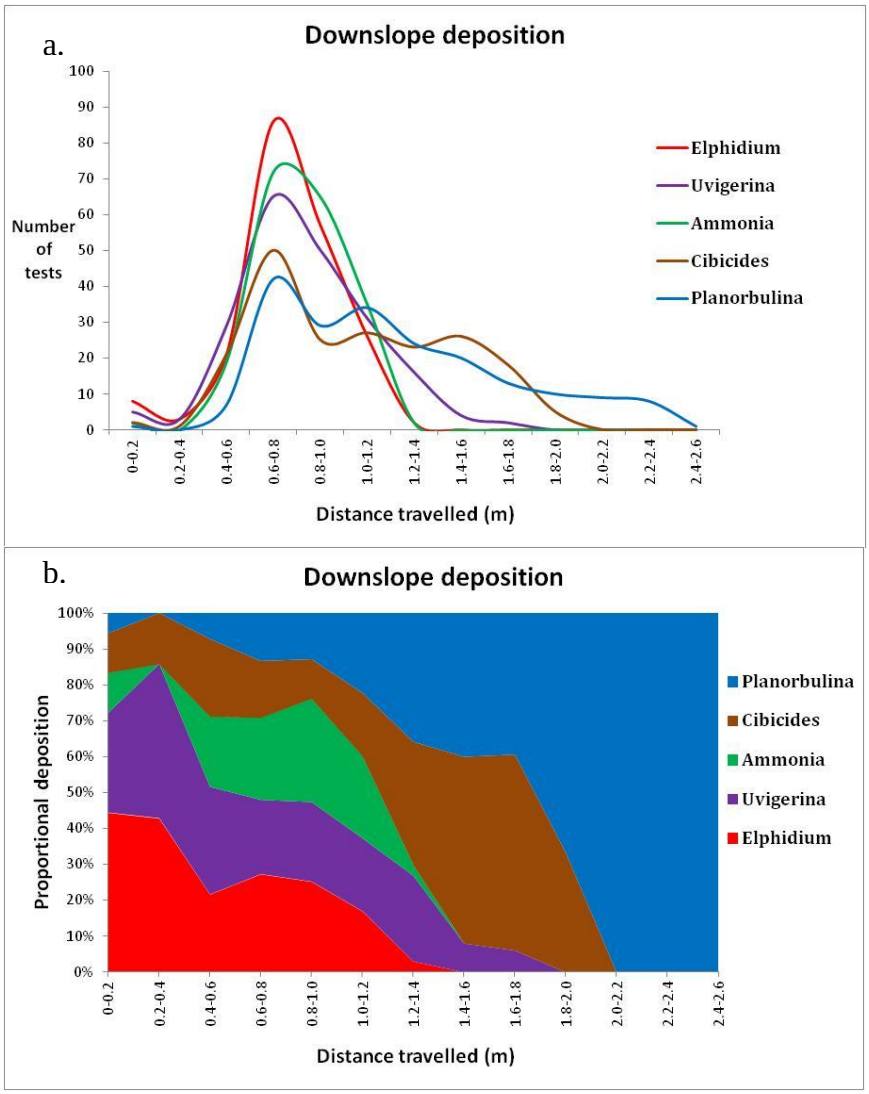

Figure 5-8 (a) Number of foraminifera deposited downslope (b) Proportion of foraminifera downslope.

Figures 5.8a & b show there is a clear sedimentation pattern as deposition wanes down slope, with separation of taxa as the foraminifera travel down the flume. Fig.5-

9 shows a drop in velocity in the first metre, and then an increase where only the smallest and lightest foraminifera continue to be carried in the flow with exclusively *Planorbulina mediterranensis* remaining in suspension for up to 2.5 m.

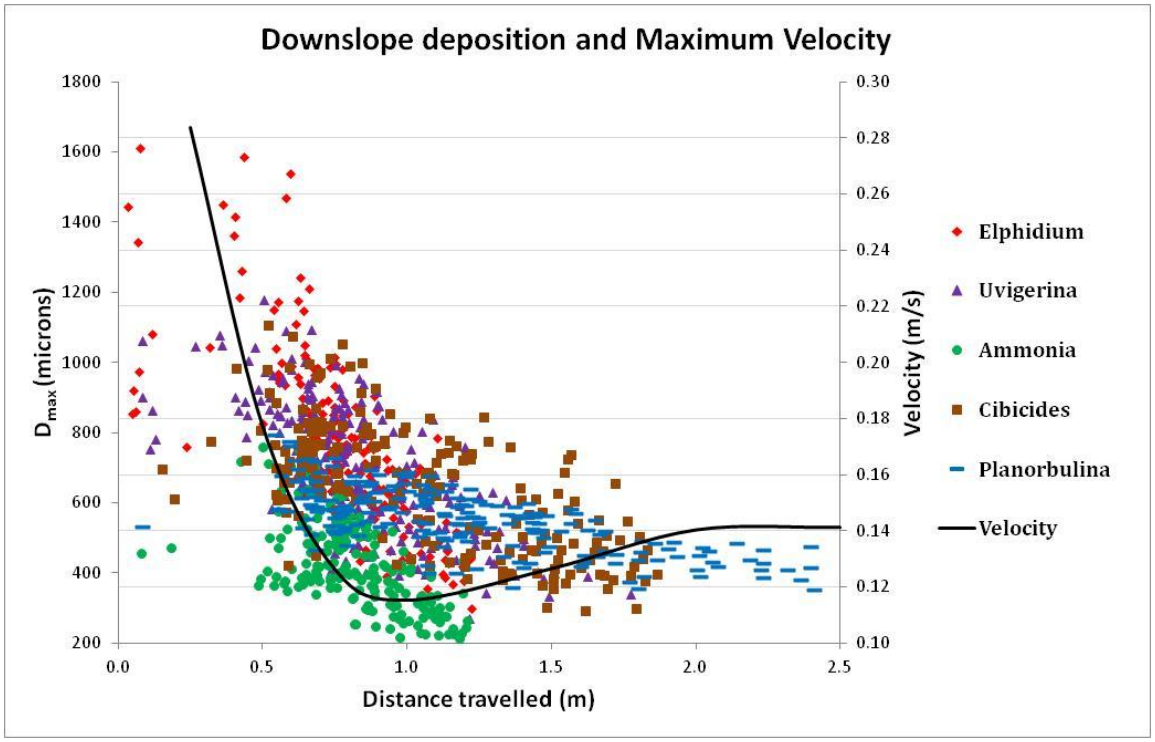

Figure 5-9 Deposition of foraminifera in relation to maximum velocity.

To see whether there is a significant difference between distances travelled between species an ANCOVA (carried out as described in Methods, Chapter 3, section 3.3.8) test was carried out. It produced an *F* value of 59.1 and a critical value of 4.7, at the 95% confidence level, confirming that there is more variation between taxa than within taxa.

5.4.6 Foraminiferal deposition and distance travelled

Settling velocity measurements in Chapter 4, section 4.3.3 have shown that there are significant statistical differences in settling velocity of foraminifera and the flume experiments show statistically significant differentiation in transport distances between species in a density current. A greater proportion of the most robust, heavy species such as *Elphidium crispum* with faster settling velocities travel shorter

distances than the lighter, more slowly settling taxa such as *Planorbulina mediterranensis*, Fig.5-10. The correlation between settling velocity (W_s) and distance travelled in the laboratory is shown in Table.5-2

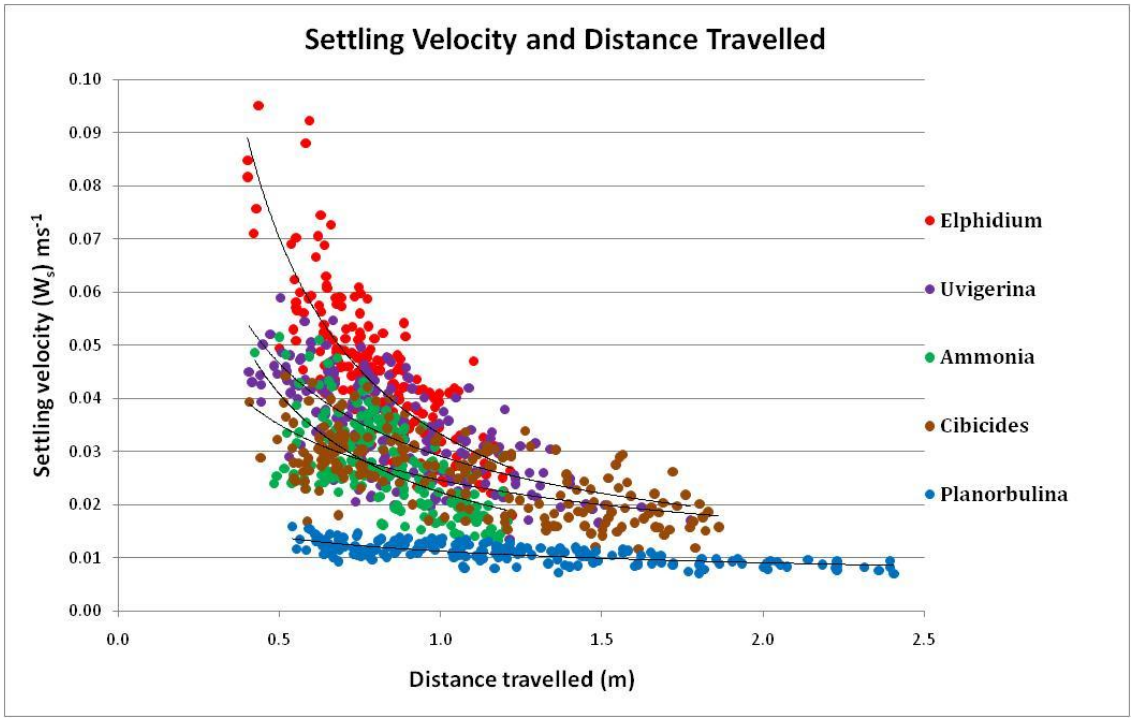

Figure 5-10 Distance travelled for each foraminifera based on settling velocity.

Table 5-2 Graph summary of regression for W_s against distance travelled. Gradients relate to power distribution of the data.

Species	R^2	Best fit line
Elphidium	0.65	$y = 0.03x^{-1.08}$
Uvigerina	0.48	$y = 0.03x^{-0.68}$
Ammonia	0.39	$y = 0.02x^{-0.82}$
Cibicides	0.46	$y = 0.02x^{-0.51}$
Planorbulina	0.50	$y = 0.01x^{-0.31}$

For the lightest foraminifera there is a non-linear increase in distances travelled with reduced settling velocity, resulting in a power distribution in the deposited populations. Differences occur between species, with *Elphidium* individuals tending to behave like each other while *Ammonia* are less predictable. The relationship between the settling velocity and distance travelled is proportional to the power law, which agrees with other studies on the vertical dynamics of sediments in a flow

where particles with slow settling velocities travel much further than those with fast settling velocities (Shi *et al.*, 2003; Sanchez, 2006).

5.5 Discussion

5.5.1 Scaling of the flow to the field

Experiment 4 resembles natural turbidites where the initial slope declines and the current reaches gently sloping parts of the sea bed. At the fan apex or toe of the continental slope gravity action decreases and deceleration of the current begins as the current gradually loses power with increasing distance and time (Allen 1977). During the initial deceleration there is a change from a supercritical to subcritical flow. This change occurred in the experiment in first 0.5 m of the flow when the depth more than doubled (changes from 0.027 m to 0.05 m); the velocity halved (changed from 0.26 to 0.14 ms^{-1}) and the density anomaly reduced from Δρ 0.084 to 0.061 kg m^{-3}. The initial changes occur as the flow adjusts from a narrow to a wide flow resulting in a rapid change in flow thickness, velocity and density during the hydraulic jump. For the average canyon-channel system, the flow thickness more than doubles during the hydraulic jump (h_1 to h_2), its velocity is halved (U_1 to U_2) and the entrainment of water through the interface of the flow during the jump is significant in reducing the density (ρ_{f1} to ρ_{f2}) of the flow (Komar, 1977). Fig.5-11 depicts this condition. In experiments 4 the hydraulic jump completed in the first metre while in the ocean the hydraulic jump completes itself within the order of 1 km channel length (Komar, 1977).

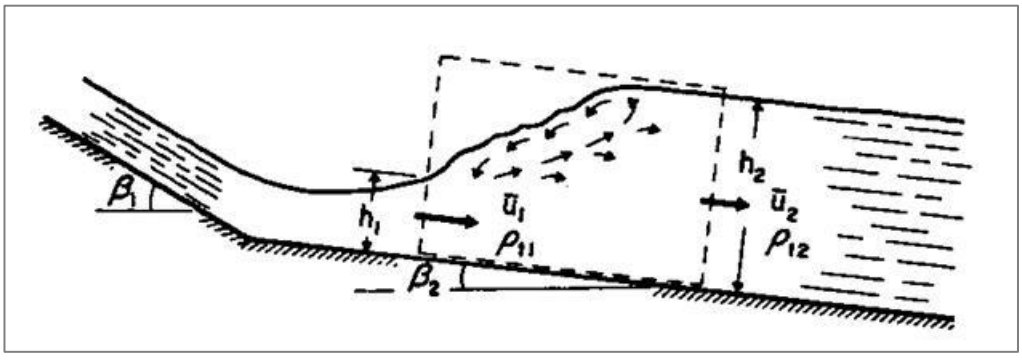

Figure 5-11 Hydraulic jump of a turbidity current where the flow passes from supercritical (Fr >1) to subcritical (Fr < 1) (Komar, 1971).

Beyond 1 metre in the experimental flow there was then a phase of minimal increase in depth and then a slight overall increase in velocity before the flow became quasi-constant. Downstream the flow became essentially uniform in that the velocity, density and thickness become almost invariable with distance in the direction of flow. This transition can be seen in the velocity profile in Fig.5-6 as the turbidite matures and velocity is related to shear stresses within the flow.

The experiment shows that deposition occurs when the velocity drops as well as when there is a slight increase in velocity. As in the ocean, deposition in the flume is clearly not related in a simple manner to mean velocity, but might be better related to the turbulent structure of the flow. From here-on in the objective is to gain an understanding of how variables within the flow change downstream and infer which of these variables cause the foraminifera to remain in suspension or settle out.

5.5.2 Relation of turbulent kinetic energy and velocity to deposition in the flow

Fig.5-12a shows the changes between the TKE (at the top, middle and bottom of the flow) and foraminifera deposition, while Fig. 5-12b shows the changes between the velocity within the flow and foraminifera deposition.

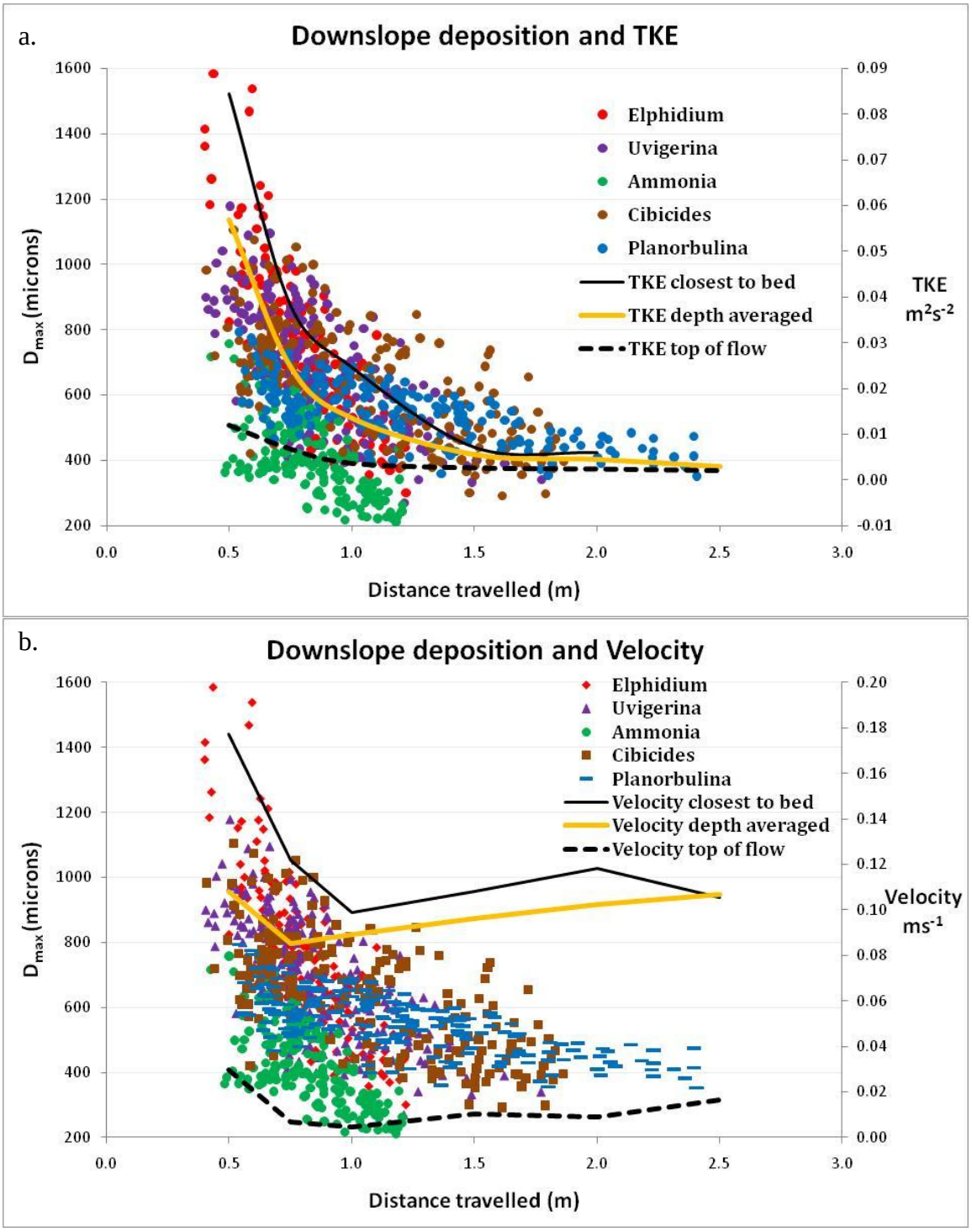

Figure 5-12 (a) Downslope changes in TKE and foraminifera deposition and (b) downslope changes in velocity and foraminifera deposition.

Fig.5-12a shows a comparison between the TKE, velocity downslope and deposition, indicating a better correlation between deposition and TKE. TKE shows a relatively straightforward picture with turbulence intensity reducing downstream (with the

greatest values at the base of the flow reducing to the top of the flow) while velocity shows a decrease then increase with distance. The longitudinal change in depth averaged TKE and velocity can be correlated to the longitudinal change in travelling distance by using the 'best-fit' lines for each foraminifera taxa as shown in Fig.5-13.

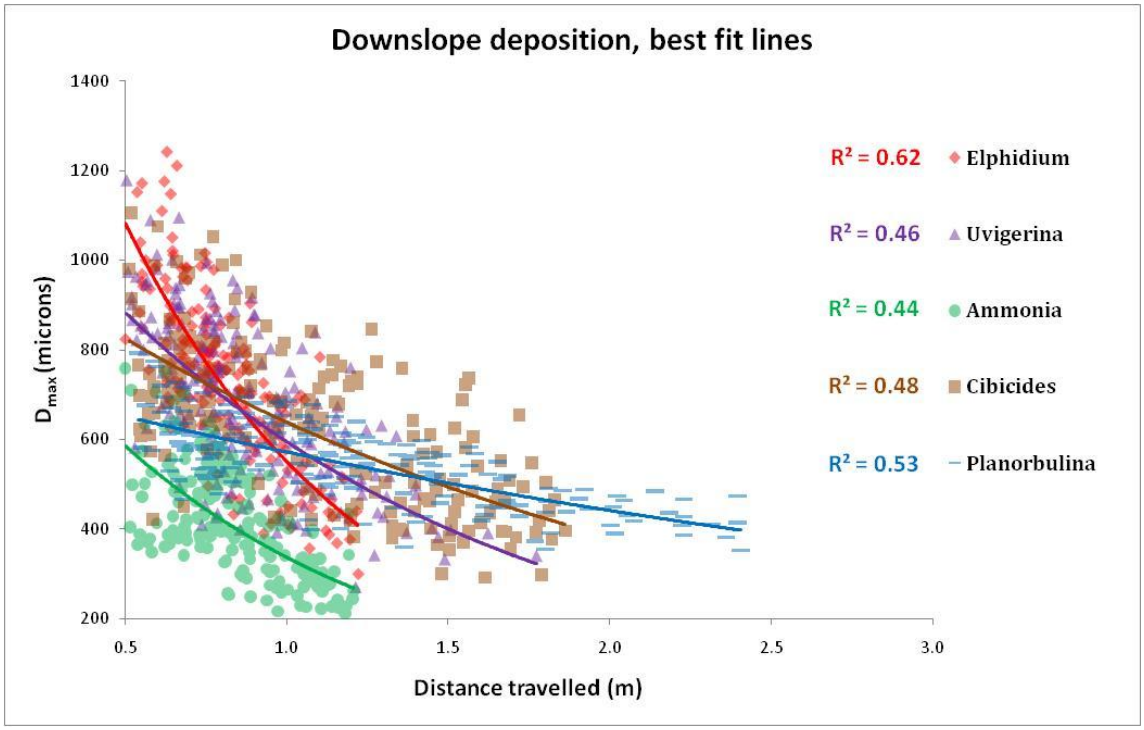

Figure 5-13 Best fit lines for taxa, showing exponential deposition downslope in the flume experiment.

From Fig.5-13 it can be seen that on average only 50% of the variance within species is explained by the regression lines. Taking this into account and accepting this level of error an analysis is carried out to reveal if there is any correlation between the 'best fit' lines and depth average velocity and TKE for each foraminifera species (Table 5-3).

Table 5-3 Pearson correlation to 'best fit' line between foraminifera deposition, depth average TKE and depth average velocity values.

Species	TKE	Velocity
Elphidium	0.96	0.76
Uvigerina	0.91	0.33
Ammonia	0.95	0.74
Cibicides	0.90	0.29
Planorbulina	0.85	-0.38

The greater correlation occurs with the TKE confirming the suggestion that it is the amount of turbulent energy in the flow that plays a crucial role in the deposition of foraminifera rather than velocity. Greater correlation also occurs with the heavier taxa such as *Elphidium crispum* and *Ammonia beccarii* indicating these foraminifera may be more responsive to changes in the turbulent structure of the flow while lighter taxa such as *Planorbulina mediterranensis* have a relaxation or lag time before responding to a change in turbulent structure. As a consequence of their small size and mass there is less settling force available to respond to changes in the flow, therefore creating a slightly longer response time than larger more robust species.

5.5.3 Analytical model of oceanic turbidite behaviour

The analysis above (section 5.5.2) has shown that turbulent kinetic energy has a strong correlation to foraminifera deposition (with an average Pearson correlation of 0.96 between the 'best-fit' line of distance travelled and the depth averaged TKE downstream – Table 5-3); unfortunately, a description of the turbulence of turbidites is not yet available, meaning there is no statistical method to parameterize the experimental laboratory data to observational field data. Process-orientated studies should be based on both observations and models but turbidity currents are difficult to study in the field (Fukushima *et al.,* 1985; Parker *et al.,* 1986). To measure turbulence, the relevant fluctuating physical properties must be recorded in a highly-resolved, four-dimensional domain (three space and one time dimension) and the measurements must be of sufficient intensity and duration to yield robust statistical properties (Burchard *et al*., 2008). In the ocean however, such observations are generally not possible; turbulence is highly intermittent, so spatial or temporal under-sampling is always an issue (Burchard *et al.*, 2008).

Detailed TKE profiles of turbidity currents have not been available as they occur infrequently, can be destructive - so measuring instruments do not survive these violent events (Inman *et al.,* 1976; Prior *et al.,* 1987; Paull *et al.,* 2003; Xu *et al.,* 2004), or instruments are placed too high above the sea floor for reasons of safety (Xu *et al.,* 2002). Problems arise if the instrument alignment is not normal to the

seabed, as the instrument tilt will bias the stress estimate, although the bias is small provided the tilt angles < 6° (e.g. Lu & Lueck, 1999; Rippeth *et al.*, 2003). In tidal flow a potentially bigger problem is the presence of surface waves, which significantly bias the stress estimates even for small (~2°) misalignments in the instrument mounting (Rippeth *et al.*, 2003). Recent years have seen advances in mechanical, acoustic and optical observational techniques which will yield deeper insight into turbulent phenomena but at present much research is limited by the cost of the instrumentation and its handling (Gargett, 1999; Gemmrich & Farmer, 1999; Prandke *et al.*, 2000; Lueck *et al.*, 2002; Wolk *et al.*, 2002; Rippeth *et al.*, 2002; Thorpe *et al.*, 2003; Lorke & Wuest, 2005; Wiles *et al.*, 2006; Luznik *et al.*, 2007; Nimmo Smith *et al.*, 2002, 2004, 2005, 2008).

The other parameter that is related to foraminifera deposition is velocity. Single point velocity measurements in submarine environments have been available since the 1970's with the result that the behaviour of turbidites in relation to velocity is much better understood (Osborn, 1974; You, 1994; Lueck *et al.*, 2002). A formula is available describing turbidite behaviour in relation to velocity which has been developed from oceanic research (Middleton, 1966; Allen, 1977; Mitchell, 2005; Salles *et al*., 2008). Therefore, by using velocity it is statistically possible to parameterize the experimental laboratory data to observational field data.

The velocity of turbidites is calculated using the formulae developed by Middleton (1966), Allen (1977), Mitchell (2005) and Salles *et al* (2008):

$$U_{tc} = \sqrt{\left(\frac{8g\prime\phi}{f(1+a)}\right)}\,hS \qquad (5.2)$$

where U_{tc} represents the mean flow velocity, ϕ sediment volume concentration, h is the flow height, S bottom slope, f the Darcy–Weisbach friction coefficient (~0.04), and a an empirical coefficient (~0.43 as Ri~1). The turbidity current velocity U_{tc} is predictable from the balance of gravitational body force and flow resistance based on the classical Chezy formula since, given the large flow distances, the currents should have reached steady flow conditions (Mitchell, 2005). This formula, analogous to

that found in Daly (1936) for river flows, is obtained simply by writing the balance between the apparent weight, $g'\phi hS$ and the steady friction resistance $f/8(1+a)U^2$ (Salles *et al*., 2008).

The height of the current can be calculated by rearranging equation 5.2 to:

$$h = {U_{tc}^2}\Big/{S\left(\frac{8g'\phi}{f(1+a)}\right)} \qquad (5.3)$$

Knowing the height of the flow at any given turbidite velocity means the distance the foraminifera travel can be calculated if it is assumed all foraminifera begin their transport from the top of the flow. Using the data base of the distribution of settling velocity for each species calculations can be made for how far each specimen will travel from the top of the turbidite to the bed at a given velocity. Settling velocity data is taken for the experimental records of the 100 specimens (20 of each 5 taxa). Sizes of foraminifera are between 200-1100 µm and settling velocities vary from 0.06 ms^{-1} to > 0.01 ms^{-1}. Based on their settling velocity and knowing the height of the flow, the time it takes to settle through the turbidite will reveal the distance they are likely to travel before deposition on the sea floor.

To undertake realistic estimates an understanding of turbidite velocities in an oceanic environment is required. Maximum velocities reached by turbidity currents have been estimated to reach 10–15 ms^{-1} and 16.6-27.7 ms^{-1} in extreme conditions (Mulder *et al.,* 1997; Drago, 2002; Fine *et al*., 2005) while current heights have been estimated to 280-450 m above the sea floor (Pirmez & Imran, 2003; Volker *et al.*, 2008). For the majority of time, turbidite systems remain much more quiescent as shown in Table 5-4

Table 5-4 Results of turbidite velocity measurements within submarine channel systems, proximal velocities reduce downstream terminating within the fan system.

Observed/ estimated	Velocity ms^{-1}	Author
Observed	0.5-0.25	Shepard *et al.* 1979
Observed	0.15-0.25	van Weering *et al.*, 2002
Observed	1.21-0.03	Khripounoff *et al.* 2003

Estimated	0.8-0.3	Ercilla *et al*., 2002 & 2002a
Estimated	4-0.5	Pirmez & Imran, 2003
Estimated	4-1	Salles *et al*., 2008

Calculations and figures for this study are based on velocities declining from $4ms^{-1}$as this encompasses normal conditions.

The formulae shows that the faster the velocity, the thicker the flow, therefore the further the foraminifera will travel. (Fig.5-14).

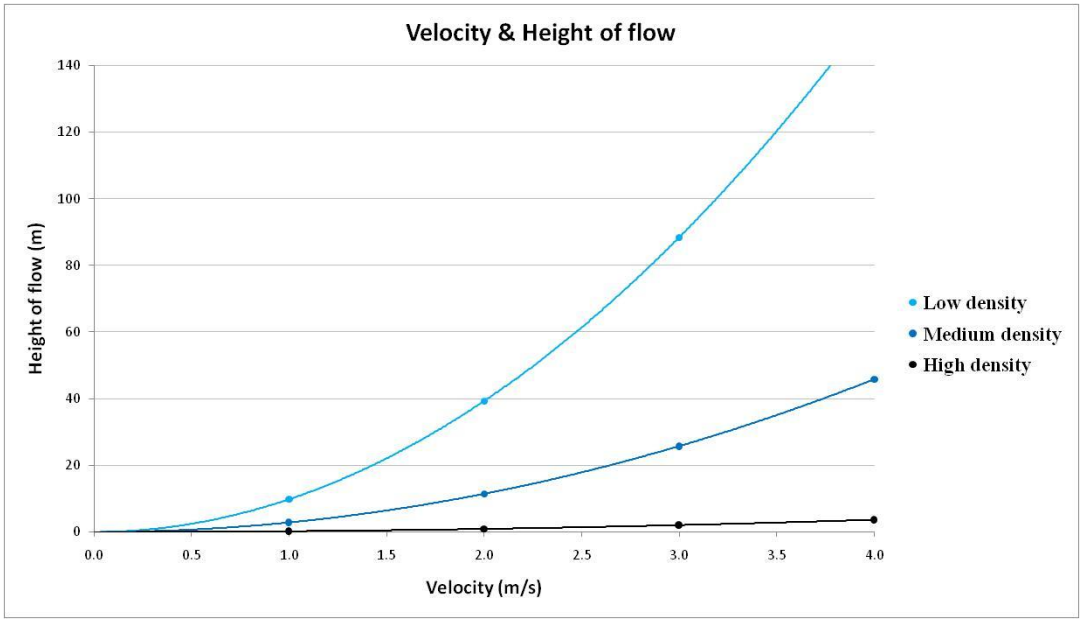

Figure 5-14 Salles *et al*, (2008) turbidite height based on velocity and density. High density is 100 kg m^{-3}, medium density is 50 kg m^{-3} and low turbidite density is 17 kg m^{-3}.

Distribution of foraminifera are dependent on the density as well as velocity of the turbidite, with higher velocities and less dense flows being associated with prolonged travelling distances. An example of how far foraminifera may travel is shown in Fig.5-15 where a typical vertically averaged turbidite density of 50 kg m^{-3} is applied (Pirmez & Imran, 2003). Modelling histogram distribution the deposition distances in kilometers of the five foraminifera taxa are shown for three different turbidite velocities.

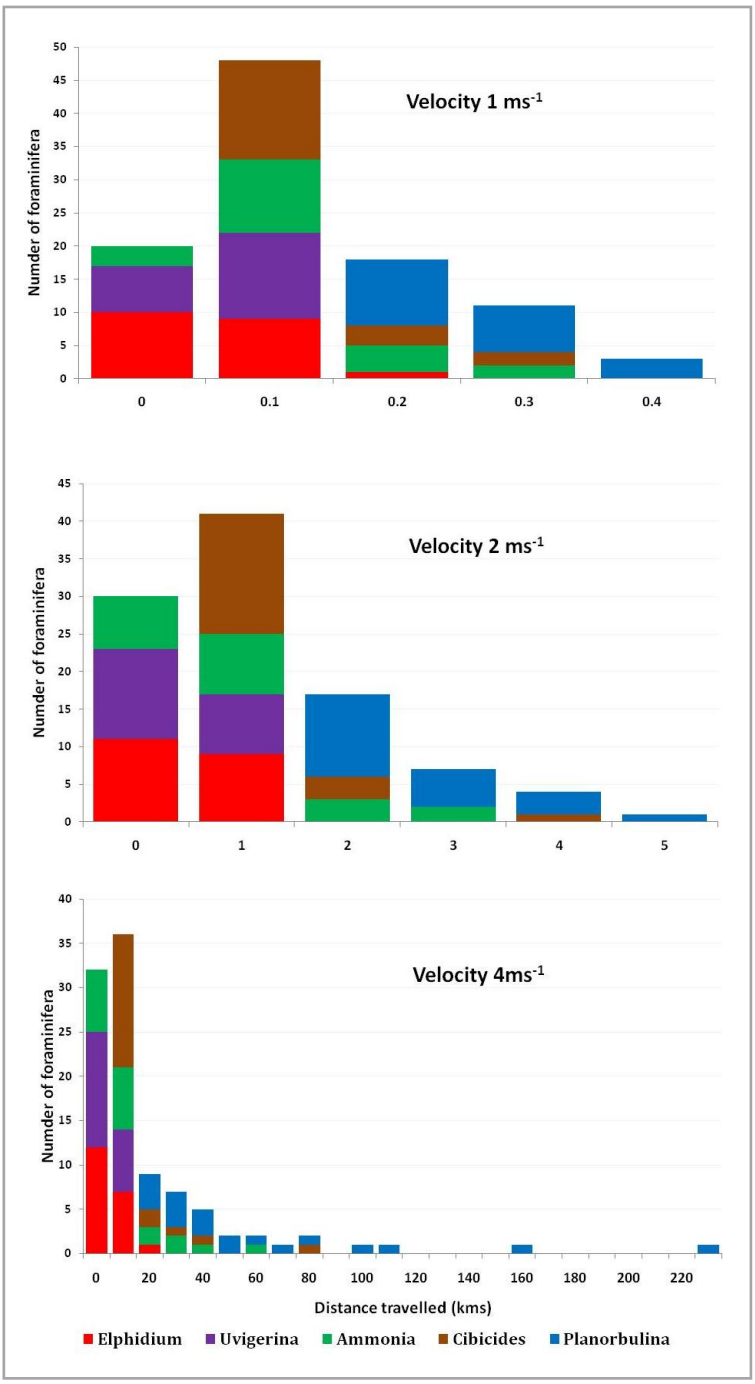

Figure 5-15 Histogram of distances travelled (km) for five foraminifera taxa at different turbidite velocities. Sizes of foraminifera are between 200-1100µm and settling velocities vary from 0.06 ms^{-1} to > 0.01 ms^{-1}. Each graph depicts distribution under turbidite velocity shown. Medium turbidite density 50 kg m^{-3}, sediment volume 3%, slope 0.1°.

Results showed that there was a distinct pattern of distribution of foraminifera where the travelling distances increase the longer they are in the water column. To relate the model to the experimental data the results are presented as proportional fractionation of species downslope (Fig.5-16). The *x*-axis is scaled by division of the

maximum distance as the pattern of distribution remains the same whatever velocity and density values are applied, i.e. distribution is extended at greater velocities but the basic fractionation pattern remains the same.

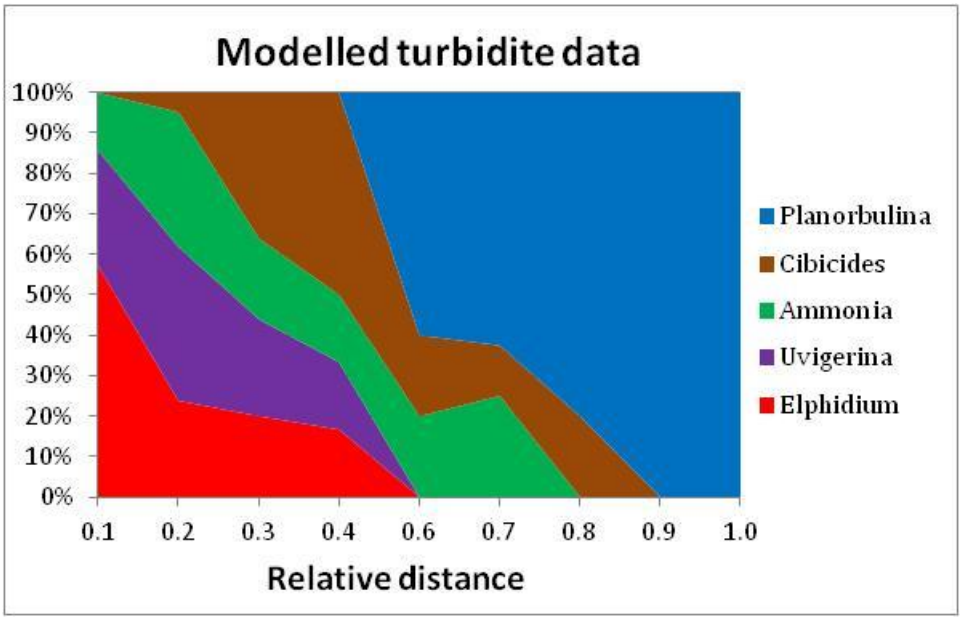

Figure 5-16 Fractionation of species downslope when deposition is calculated via velocity of flow and depth of turbidite .Data includes settling velocity of 100 specimens.

This analysis shows that when using velocity of a turbidite as a model for deposition of foraminifera, fractionation of species is likely to occur, with heavier taxa being deposited out in proximal areas and lighter, smaller species depositing out in the more proximal fan area of a turbidite.

The turbidite model can be compared to the flume data to see if similar distribution occurs. Fig.5-17 shows the fractionation from the laboratory experiments.

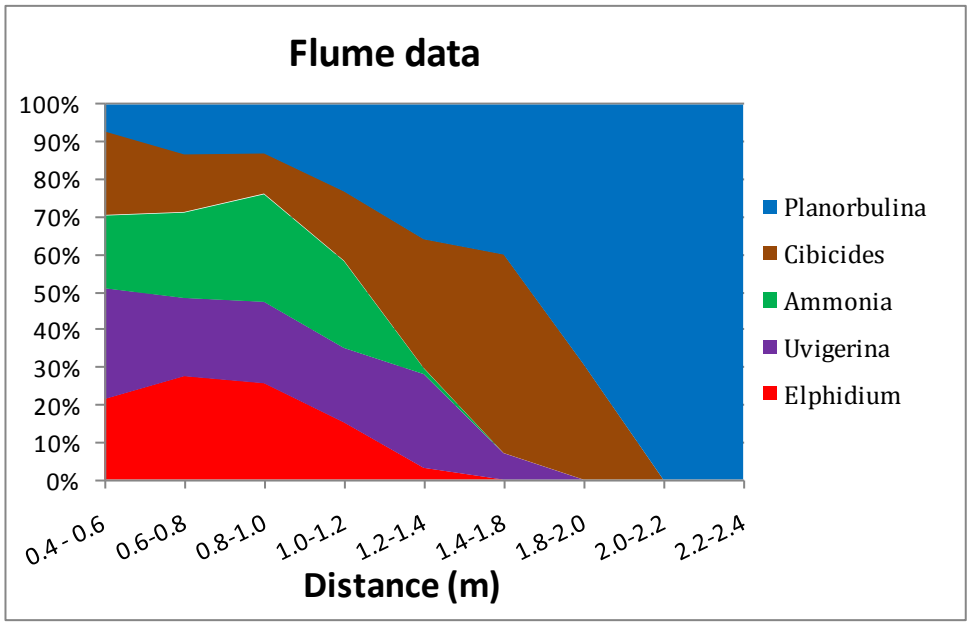

Figure 5-17 Fractionation of species downslope in the laboratory flume, experiment 4.

The flume data shows a similar pattern, with a Pearson correlation of 80%. To understand how the flume data is different to the modelled output data the calculation is applied for the height of the flow in the flume with settling velocity of foraminifera. When applying the model formula to the flume foraminifera Fig.5-18, shows a similar sequence.

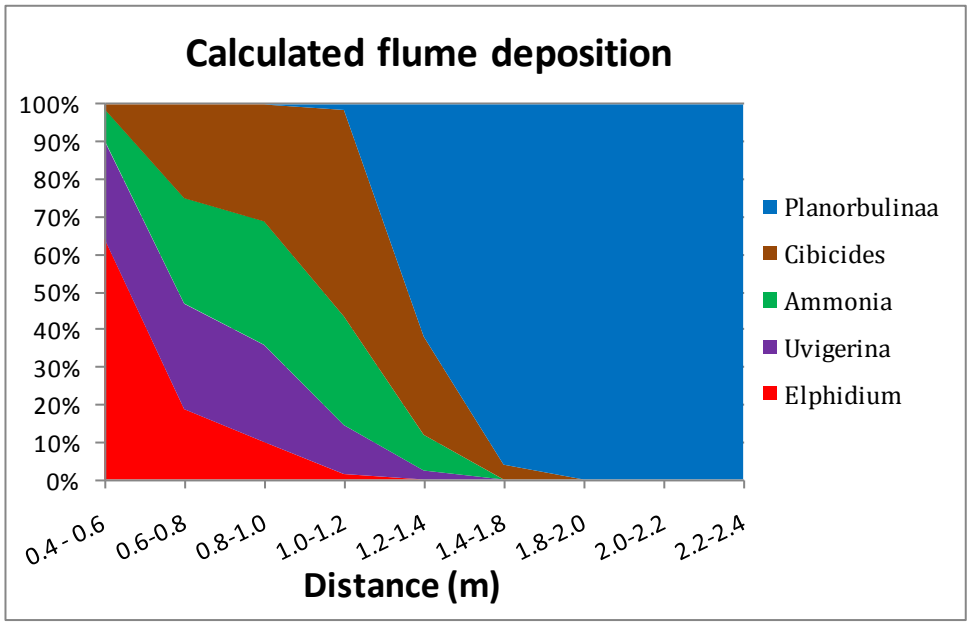

Figure 5-18 Fractionation of species when deposition is calculated on velocity and depth of flow.

The distribution also shows an 80% correlation between calculated and real flume data. To test whether they are significantly different a Kolmogorov-Smirnov test is undertaken as described in Methods Chapter, section 3.3.8. At a 95% confidence level, the maximum difference between the cumulative distributions, $D = 0.222$, which is greater than the critical probability value, $P = 0.189$ suggesting that the two distributions are significantly different from each other.

In the real flume data there is a proportion of all species of foraminifera that settle out at the beginning of the flow due to the change to subcritical condition during the hydraulic jump. In the modelled data, both for the flume and the turbidite, only the heaviest foraminifera settle out at the beginning, leaving a larger proportion of lighter species down flume. Using Salles *et al*. (2008) calculation in this way skews the proportion of heavier species upstream and ligher species downstream. This model data does not take into account the turbulent dynamics of the flow which prior analysis has shown to have a greater correlation than velocity. Using settling velocity in this straight-forward manner as a measure for foraminifera hydrodynamic behaviour gives a similar overall qualitative, sequential pattern of fractionation to the experimental data, but quantitatively is inadequate as an indicator of possible deposition distances in a turbidite environment.

5.6 Conclusion

Analysis has shown that there are significant differences between depositional distances for foraminifera according to species within a laboratory flume. In both the pilot study and the final experiment the pattern of deposition shows the same trend with heavier species depositing out before less robust species. Deposition is not related to velocity in a simple manner but is more closely associated with the turbulent activity (TKE) in the flow. The observed depositional pattern of the foraminifera can be related to the longitudinal turbulent structure down flume. The large drop in velocity and TKE at the beginning of the flow results in high deposition as the flow changes to a subcritical condition. Only the smaller, lighter foraminifera are transported downstream as the TKE intensity reduces downstream.

Using Salle's *et al.* (2008) formula for turbidite velocity in the ocean the deposition of foraminifera is modelled by means of probability density function with settling velocity information. With an assumption that foraminifera are transported to the top of the flow due to turbulence, this study shows that species are likely to fractionate during post mortem transport. Attempts to scale the transported distance per species cannot be represented in the model as it relies on velocity of the turbidite as the main variable, while the experimental data has shown it being the TKE rather than velocity which has greater influence on depositional sequence.

6 Hydraulic control on benthic foraminiferal assemblages: Case study from the Gulf of Cadiz contourite

6.1 Abstract

Micropalaeontological studies generally neglect to consider the role of transport and sorting. Only where these processes are truly impossible to overlook, such as in canyon and fan systems, are they explicitly considered. This usually results in these environments being excluded from analyses. This study explicitly considers the transport problem via a case study of a specific contourite system with the aim of applying new physical understanding of post mortem foraminiferal transport, derived from laboratory work to a naturally occurring system. Here we present results of a comparative micropalaeontological study on benthic foraminifera from surface sediments from the Gulf of Cadiz from the shelf to the lower slopes. Comparisons are made between quiescent conditions away from submarine channels and two channels with different energy regimes. Analysis shows that a greater signal of fractionation is revealed in the largest channel where downslope processes predominate. In the smaller channel where along slope processes are as important as downslope processes the lighter species are transported laterally rather than down channel, revealing an atypical downslope sedimentary regime. In both cases, post mortem transport of foraminifera results in a marked difference from the quiescent autochthonous assemblages.

6.2 Introduction

6.2.1 Foraminifera in Submarine Channels and fans

An overview of transport of foraminifera in different oceanic environments is given in Chapter 2, section 2.1 and 2.5.2, which also reviews the state of knowledge about the effects of disturbance and post mortem transport of foraminifera in submarine

channels and fans. Active submarine canyons are major sedimentary conduits between the coastal zone and the deep oceanic province, influencing the sedimentary cover and ecology of the adjacent shelf and slope (Guerreiro *et al.,* 2009) and are therefore sites of post mortem foraminifera transport. Defaunation due to physical disturbance and recolonisation and evolution of foraminifera communities has been studied within submarine canyon systems and turbidite muds (Rogerson *et al.,* 2006; Koho *et al.*, 2007; Fontanier *et al.,* 2008; Schröder-Adams *et al.,* 2008; Drinia & Dermitzakis, 2010; Ortiz *et al*.,2011, Jones, 2011). Post mortem transport of foraminifera within submarine channels has been inferred when studying downslope changes (Stanley *et al.,* 1986; Lin *et al.,* 2005; Jones *et al.,* 2005; Rogerson *et al.,* 2006; Kender, 2007; Schröder-Adams *et al.,* 2008; Guerreiro *et al.,* 2009). Guerreiro *et al.* (2009) noted that light and delicate foraminifera were practically absent within the submarine channels of the Nazaré Canyon off the Portuguese margin, reflecting a post-mortem effect of the canyon's enhanced hydrodynamic activity on the settling and preservation of these more fragile foraminifera. Kender's (2007) study of the Congo Fan noted that channel deposits were either barren or dominated by single species, inferred to be as a result of high energy and the winnowing effect of currents, while levee components contained high abundance of re-deposited planktonic and benthic foraminifera where there was reduced energy and generally lower sand content. It was also noted that the shift from channel to levee deposition could be detected only on the basis of micropalaeontological content, and was not marked by any change in the gamma log.

The examination of assemblage changes within turbidite muds has also been noted (Brunner & Ledbetter, 1987; Drinia & Dermitzakis, 2010) where considerable differences in diversity, community organization, feeding and habitat preferences have been detected among benthic foraminiferal assemblages below, across and above turbiditic episodes (Drinia & Dermitzakis, 2010). In a study of an early Tortonian succession in the Gavdos Island of Greece, the enhanced supply of organic matter by transport was reflected in species that could keep pace with high sedimentation. In the upper part of the turbiditic sequence, opportunistic fauna entirely composed of an infaunal *Bolivina spathulata* assemblage was observed, indicating a nutrient-rich but largely unpopulated substrate. The reduction in the

dominance of *Bolivina* spp. and the reappearance of both infaunal and epifaunal taxa reflected the recovery of the benthic ecosystem. Brunner & Ledbetter (1987) studies the changes in the composition of foraminifera in transported muds. They compared the difference between turbidite muds and hemipelagic muds and found that fossil assemblages in turbidite muds were hydraulically sorted and subtly altered. Hemipelagic muds contained benthic tests that were large and variable in size, whereas turbiditic muds and silts contained specimens that were small and similar in size. The sorting subtly altered the relative species frequencies in turbiditic assemblages compared to those in hemipelagic muds.

To build upon this existing knowledge, a case study of a region is required where post mortem transport of foraminifera are likely to occur and fractionation of species can be observed. To understand the role played by submarine channels' energy regime and the spatial distribution of benthic foraminifera an area where strong hydraulic process occur is required as well as areas unaffected by channelisation processes. Such a region is the Gulf of Cadiz where a signal of fractionation may arise from different energy regimes within the contourite environment off the Iberian Peninsula (Schonfeld 2002 & 2002a; Rogerson *et al.*, 2011). The Gulf of Cadiz is an area of exceptionally high energy as waters flow in both an eastward and westward direction through the narrow Strait of Gibraltar where the Mediterranean Sea connects with the Atlantic Ocean (Nelson *et al.*, 1993 & 1999; Hernandez-Molina *et al.*, 2003 & 2006; Ferreira *et al.*, 2008). A study of foraminifera transport in this area will enable comparison between more quiescent areas where the outflow is less strong and areas where hydrodynamic activity of fauna is greatly affected by the change in energy as water masses move through the restricted waterway and down into the Atlantic Ocean.

6.2.2 The Gulf of Cadiz Contourite

Sediments deposited on the slope of the Gulf of Cadiz form one of the most fully studied and best understood contourite deposits in the world (Faugeres *et al.*, 1984; Stow *et al.*, 2002; Mulder *et al.*, 2002; Hernandez-Molina *et al.*, 2003 & 2006). They comprise fine sand, silt and muds transported and deposited along and downslope by

the action of the near-geostrophic Mediterranean Outflow (MO) current system between 400 and 1800 m and by the compensating Atlantic Inflow (AI) current above 300m (Nelson *et al.,* 1993 & 1999). The MO is a warm (13ºC) and saline (38‰) dense tongue of water formed by outflow of Mediterranean water through the Strait of Gibraltar and traveling northwestward (Bryden & Stommel, 1982). Bottom current speeds typically range from ~2.5 ms^{-1} at the Strait of Gibraltar to speeds of about 0.1 to 0.3 ms^{-1} near Cape St. Vincent (Ferreira *et al.,* 2008). Sediment is supplied to the upper slope via reworking of shelf sediments, primarily as a consequence of the activity of the AI (Nelson *et al.,* 1999). This current flows in the reverse direction of the MO, and tends to transport sediment southeastwards (Rodero *et al.,* 1999; Llave *et al.,* 2001). This results in the sedimentary lobes of rivers debouching from Iberia (the Rio's Gaudiana, Guadalquivir and Tinto / Odiel amongst others) being asymmetric, extending nearly twice as far from the estuary to the east as they do to the west (Rodero *et al.,* 1999; Lobo *et al.,* 2004).

Once transported beyond the shelf edge, sediment dynamics are generally controlled by the activity of the Mediterranean Outflow (Bryden & Stommel, 1982; Nelson *et al.,* 1993; Habgood *et al.,* 2003; Hernandez-Molina *et al.,* 2003 & 2006; Ferreira *et al.,* 2008). Strong geostrophic flow results in the occurrence of downslope-oriented channels on the margin being relatively rare, with along slope processes dominating over downslope processes (Habgood *et al,* 2003). However, from a water depth of around 1200m the contourite system is abruptly limited seaward by downslope submarine valleys which reflects the dominance of downslope processes towards the lower slope and abyssal plains (Habgood *et al.,* 2003, Hernandez-Molina *et al.,* 2003). Two important examples of downslope-oriented channels are the Gil Eanes Channel and the Cadiz Channel (Hernandez-Molina *et al.,* 2006).

6.2.3 Approach

Foraminifera of core top data from the Gulf of Cadiz were available from the study carried out by Rogerson *et al.* (2011) on the palaeohydrography in the Gulf of Cadiz. The foraminiferal assemblages comprised of the fauna living at the time of sampling and the dead fauna in core tops (Rogerson *et al.,* 2011). From this data base,

information for five species of foraminifera were extracted to continue the study of the taxa where information has already been accrued from previous settling and flume work. Specimens of the five species *Elphidium crispum, Ammonia beccarii, Uvigerina peregrina, Cibicides lobatulus* and *Planorbulina mediterranensis* analysed in previous chapters herein were already picked and presented on slides. Abundance records at twenty-nine locations were available, enabling quantitative analysis of spatial distribution across the area. Samples were taken from locations were these species were present enabling comparison between low energy sites and areas of strong transportation processes within submarine canyon systems where fractionation of species could be observed.

Post mortem processes are recognized by a shift from an autochthonous assemblage to an allochthonous assemblage which is marked by foraminifera being transported away from their ecological niche (Murray, 1991a). Downslope transport of relatively shallow water-derived material includes foraminifera and it is therefore essential to understand life habits and water depth preferences of species. Previous benthic foraminiferal distribution data from the region has been compiled by Mendes *et al*. (2004 & 2010a) and Schonfeld (2002 & 2002a). *Elphidium crispum, Ammonia beccarii* and *Planorbulina mediterranensis* all have life habits in the inner shelf (0-100 m) being shallow marine species and can therefore be expected to be reworked from the shelf (Murray, 1991; Rogerson *et al.,* 2011). *E. crispum* and *A. beccarii* are associated with muddy sand while *P. mediterranensis* are found in sediments of sand and silt content. Mendes (2004 & 2010) found these three shallow marine species were most abundant down to 30m depth, while Schonfeld (2002a) found the highest proportion of *A. beccarii* at depths above 272m on the shelf and uppermost slope.

Uvigerina peregrina and *Cibicides lobatulus* live from the inner shelf to the bathyal zone (Murray, 1991). *U. peregrina* is an infaunal species which lives in muddy sediments while *C. lobatulus* is an attached epibenthic species and feeds where nutrients are carried in the current so is closely linked to near-bottom currents for its nutritional needs (Altenbach *et al.,* 1999; Schonfeld 1997, 2002, 2002a). In the Gulf of Cadiz *C. lobatulus* is found at various depths within the slope environment reflecting a filter feeder specialised for environments with strong bottom currents,

such as the core of the Mediterranean Outflow plume (Schonfeld 2002 & 2002a; Mendes *et al.*, 2004). Schonfeld (2002a) found *C. lobatulus* was associated with current-swept passages and deep, high-energy environments on the outer shelf and upper slope. In the Gulf of Cadiz Mendes *et al.*, (2004) found *U. peregrina* is common in muds in depths below 95 m, living in soft sedimentary substrates. Due to the slope environment of these two species it may be more difficult to detect transported specimens. As *C. lobatulus* is associated with the presence of strong bottom currents, its presence may be related to reworked and sorted populations.

6.3 Methods

Assemblage data was taken from core tops from the study of Rogerson *et al.* (2011) in the area shown in Fig.6-1 where the Mediterranean Sea enters the Atlantic Ocean into the Gulf of Cadiz.

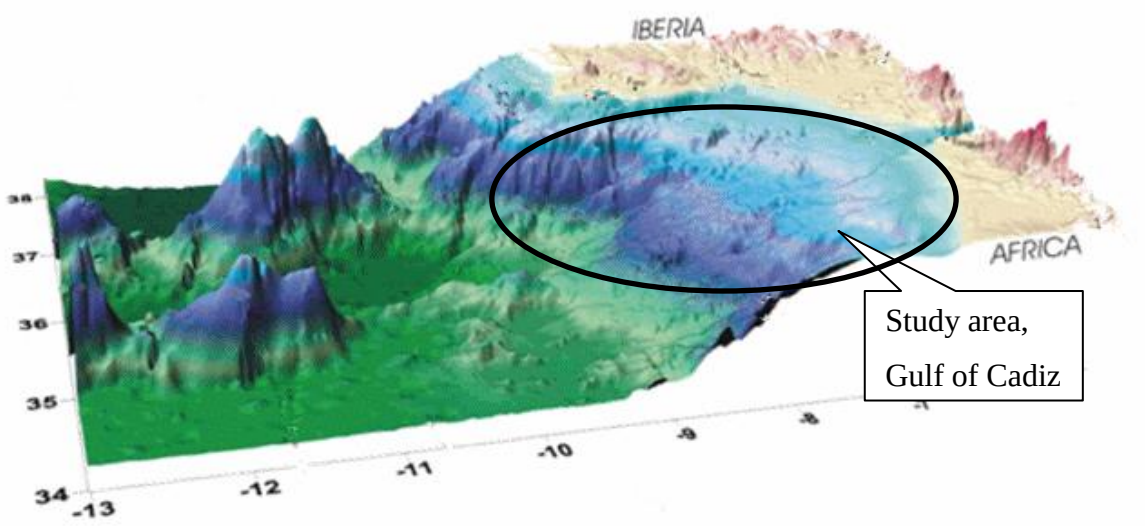

Figure 6-1 Study area of post mortem transport adapted from Hernandez-Molina *et al.* (2006).

The criteria for analysis included locations where transport processes occur in submarine channels and locations outside of these enhanced transport areas to allow comparison of assemblages between quiescent and high energy environments.

Locations away from submarine channels are used as a baseline where transport is expected to be minimal and autochthonous taxa will dominate. Within submarine channels where post mortem transport processes are more likely to occur it may be that assemblages are dominated by more allochthonous taxa. Submarine channels studied here are the Gil Eanes Channel and the Cadiz Channel. The Gil Eanes channel is relatively small, between 0.8-1.7 km wide and 50 km long with steep walls flanked by significant drift sediments due to the MO (Garcia, 2002). The Cadiz channel is a much larger channel, extending to 110km with a width of 2.4 – 8 km (Hernandez-Molina et al., 2006). Location of core top samples are shown in Fig.6-2.

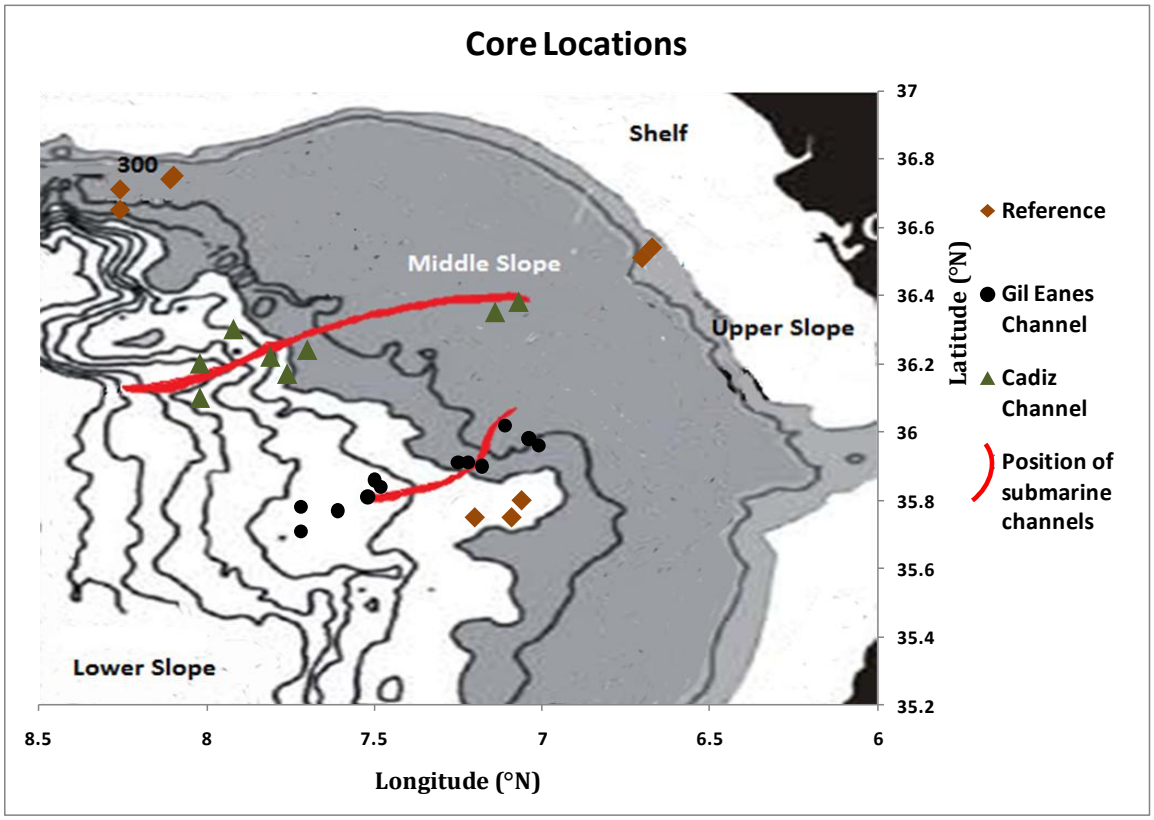

Figure 6-2 Position of Reference locations, Gil Eanes and Cadiz submarine channels in the Gulf of Cadiz. Cores positions within upper slope and mid slope within grey area, lower slope in white. Adapted from Hernandez-Molina *et al.*(2006).

Here, core top locations are grouped into three areas (Reference, Gil Eanes and Cadiz Channels) which are then further sub-divided in terms of depth; the upper slope being above 300 m, midslope is between 300-1100 m and lower slope is below 1100 m. The only 'upper slope' samples are within the Reference sample group close to the shelf edge. Due to the varying bathymetry, areas available 'away from

channel' (reference locations) are to the north of Cadiz Channel for midslope analysis. Here the location is distal from the Straits of Gibraltar where the momentum of the MO is reduced and the contourite system has decelerated resulting in a relatively low energy environment (Ferreira *et al.*, 2008). The lower slope location is nearer to the Straits of Gibraltar but at depths where low energy prevails due limited downward penetration of the MO on this part of the slope (Habgood *et al*, 2003). Table 6-1 over page is presented detailing the core data and grouping system. All core data is from of Rogerson *et al.* (2011). Bedform and location data is from Hernandez-Molina *et al.* (2006).

Table 6-1 Core data used in Gulf of Cadiz foraminifera analysis.

Area	Depth	Long	Lat	Grain Size (µm)					Bedform	Location	Grouping
Reference	(m)	(°N)	(°N)	< 63	63-125	125-150	150-250	> 250			
M39005-3	118	6.74	36.54	46	40	6	6	1	Smooth erosive surface	Near shelf break	R-up
M39006-1	214	6.77	36.51	35	43	9	10	2	Smooth erosive surface	Near shelf break	R-up
M39022-1	668	8.26	36.71	74	18	2	3	2	Sheeted drift	Midslope	R-mid
M39020-1	726	8.11	36.74	61	17	5	12	4	Sheeted drift	Midslope	R-mid
M39019-2	730	8.1	36.75	38	10	7	25	20	Sheeted drift	Midslope	R-mid
M39021-5	901	8.26	36.61	21	23	16	23	17	Sheeted drift	Midslope	R-mid
D13689	1128	7.06	35.77	90	4	1	2	3	Sedimentary lobe	Lower slope	R-low
D13687	1232	7.2	35.72	93	3	1	2	2	Sedimentary lobe	Lower slope	R-low
D13688	1237	7.09	35.72	91	6	1	1	2	Sedimentary lobe	Lower slope	R-low
Gil Eanes											
D13695	853	7.01	35.96	24	60	9	3	3	Sedimentary lobe, levee	Midslope	G-mid
D13697	891	7.04	35.98	0	2	3	51	44	Sedimentary lobe	Midslope	G-mid
D13696	885	7.11	36.02	7	9	6	30	48	Sedimentary lobe	Midslope	G-mid
D13679	952	7.25	35.86	31	57	7	3	2	Sedimentary lobe, close axis	Midslope	G-mid
D13686	956	7.18	35.85	10	83	4	2	1	Sedimentary lobe, close axis	Midslope	G-mid
D13680	1010	7.22	35.86	0	25	5	6	64	Channel axis	Midslope	G-mid
D13683	1163	7.5	35.86	89	6	1	2	2	Muddy mini basin	Lower slope	G-low
D13682	1458	7.61	35.77	9	44	29	16	1	Muddy mini basin	Lower slope	G-low
D13899	1179	7.48	35.84	90	8	0	0	1	Muddy mini basin	Lower slope	G-low
D13900	1297	7.52	35.81	79	9	2	5	4	Muddy mini basin	Lower slope	G-low
D13892	1497	7.72	35.78	95	2	0	1	2	Muddy mini basin	Lower slope	G-low
D13893	1442	7.72	35.71	93	3	1	2	2	Muddy mini basin	Lower slope	G-low
Cadiz											
M39008-4	577	7.07	36.38	50	35	4	5	6	Deformed sheeted drift	Midslope	C-mid
M39009-1	681	7.14	36.35	1	12	24	46	18	Deformed sheeted drift	Midslope	C-mid
M39004	966	7.73	36.24	85	12	1	1	0	Deformed sheeted drift	Midslope	C-mid
D13700	1191	7.92	36.32	6	59	28	6	1	Drift	Lower slope	C-low
D13701	1061	7.81	36.22	45	27	22	4	1	Smooth sea floor	Lower slope	C-low
D13703	1161	7.76	36.06	25	58	11	5	1	Muddy mini basin	Lower slope	C-low
D13707	1533	8.02	36.2	63	28	5	3	1	Muddy mini basin	Lower slope	C-low
D13706	1946	8.02	36.1	3	18	31	45	3	Muddy mini basin	Lower slope	C-low

1132 foraminifera of the five species specified in section 6.2.3 were found within the core top samples and were used for further analysis. Foraminiferal tests studied were all >250 μm in size to maintain comparability with the laboratory studies. All foraminifera used for analysis described here were measured for the longest diameter (D_{max}) using a GXCAM-5 imaging camera with a binocular Pyser SGI (X80) microscope. The equivalent grain size (D_{sed}) was then established using the modified approach of Gibbs (*et al.,* 1971) developed in Chapter 4, section 4.5.3. Although the use of the >250 μm size range neglects the ecologically important size ranges below 250 μm, we are motivated by the need to generate a tool that is directly useful to both academic and industrial micropalaeontologists. Within the hydrocarbon industry micropalaeontologists typically analyse only the fraction 250 μm, as larger sizes enable quick identification of taxa. Although sometimes the 150-250 μm fraction is used, it is only rarely the 90-150 μm size is looked at (personal communication Dr. N. Holmes 14/5/09). Within the extremely fine fraction foraminiferal characteristics become increasingly similar meaning taxa are more difficult to identify to species level, but perhaps more importantly they are less likely to differ in terms of their hydrodynamics (See Chapter 4, section 4.5.1) and so the approach taken here is not likely feasible for individuals of this small size.

6.4 Results

6.4.1 Autochthonous dominated, low energy environment

The proportion of foraminifera at each depth for the reference locations is shown in Fig.6-3.

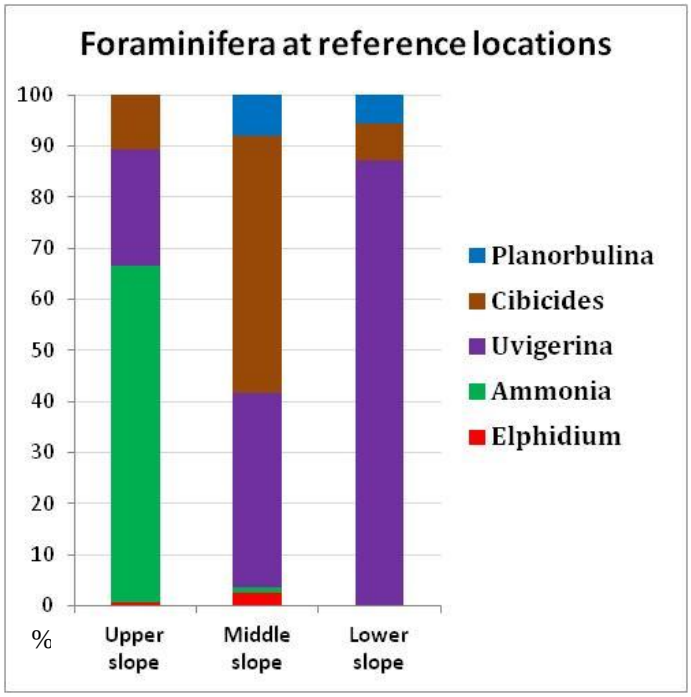

Figure 6-3 Proportion of species at each depth for reference locations.

In these low energy environments away from the submarine channels the population is dominated by *Uvigerina, which* contributes of 44% of the total number of tests. *Ammonia* contributes 29% and *Cibicides* 20%. *Elphidium* and *Planorbulina* contribute only 2% and 5% respectively. At the upper slope there are no obviously transported species with the dominant species being shelf dwelling *Ammonia* and a few *Elphidium*. *Uvigerina* and *Cibicides,* which inhabit all depths, are also present. At the midslope a small proportion of *Planorbulina*, *Ammonia* and *Elphidium* have been transported downslope, while only a few of the lightest taxon (*Planorbulina*) have reached the lower slope. *Uvigerina* becomes increasing dominant downslope indicative of its preference for muddy sediments. *Cibicides* which is associated with near bottom currents dominates the midshelf where the sediment surface experiences some flow from the Mediterranean Outflow (Schonfeld 2002 & 2002a; Mendes *et al.*, 2004).

To investigate whether sedimentary grains and foraminifera both show the same hydrodynamic signature, Figure 6-4 shows comparison of sediment grain size and equivalent foraminifera size for each depth interval. Equivalent foraminifera size is the sedimentary diameter (D_{sed}) as explained in Chapter 4, Section 4.5.3.

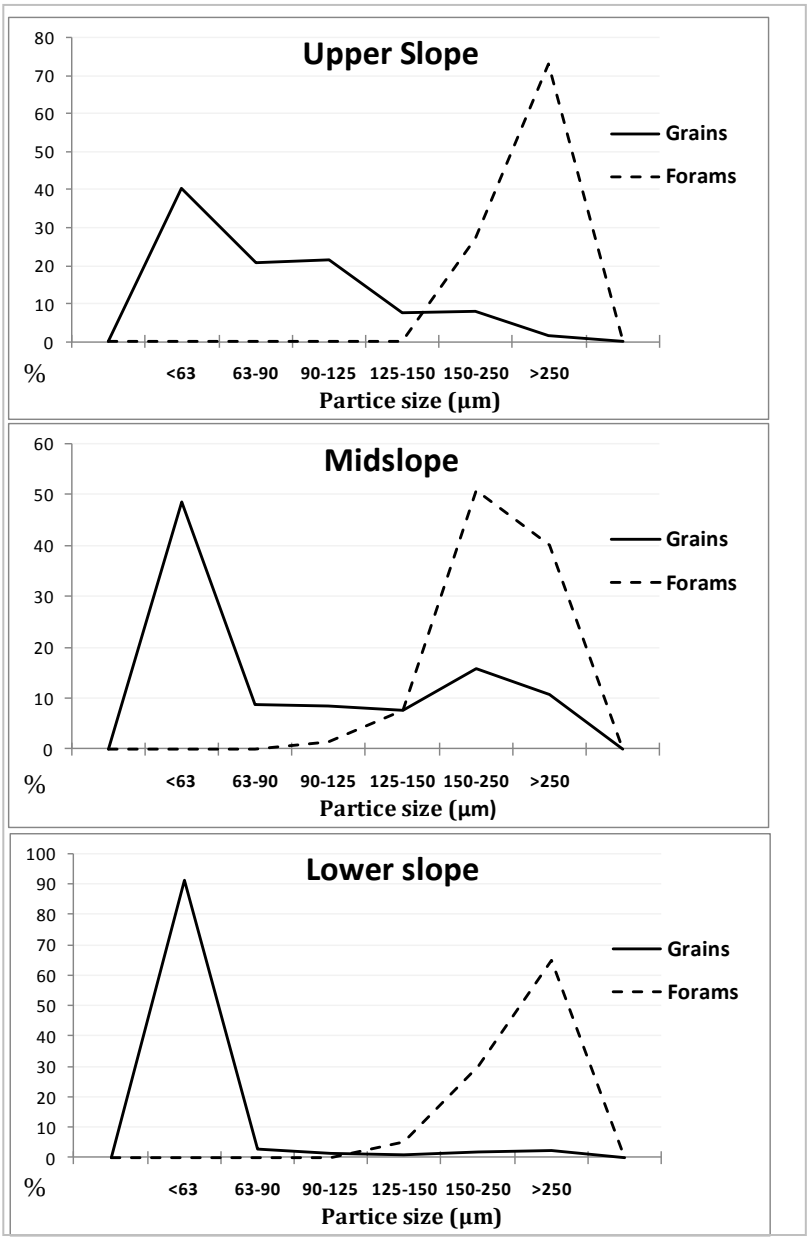

Figure 6-4 Grain size proportion and equivalent foraminifera size (D_{sed}) for each depth for reference locations.

In the upper slope, the highest proportion of grain size is < 63 µm, gradually decreasing in proportion with increasing size. At this depth the foraminiferal equivalent sizes are mostly > 250 µm with a smaller proportion between 150-250 µm. In the midslope the greatest proportion of grain size is again < 63 µm, with a minor secondary peak at 150-250 µm. Foraminiferal equivalent size falls between 150-250 µm and > 250 µm. In the lower slope nearly all the grain size is < 63 µm while the foraminiferal equivalent sizes fall between 150-250 µm and > 250 µm.

There is no significant correlation between foraminifera and grain size suggesting that transport is minimal and no significant allochthonous assemblage is present.

6.4.2 Gil Eanes Channel

The proportion of foraminifera at each depth for the Gil Eanes Channel is shown in Fig.6-5

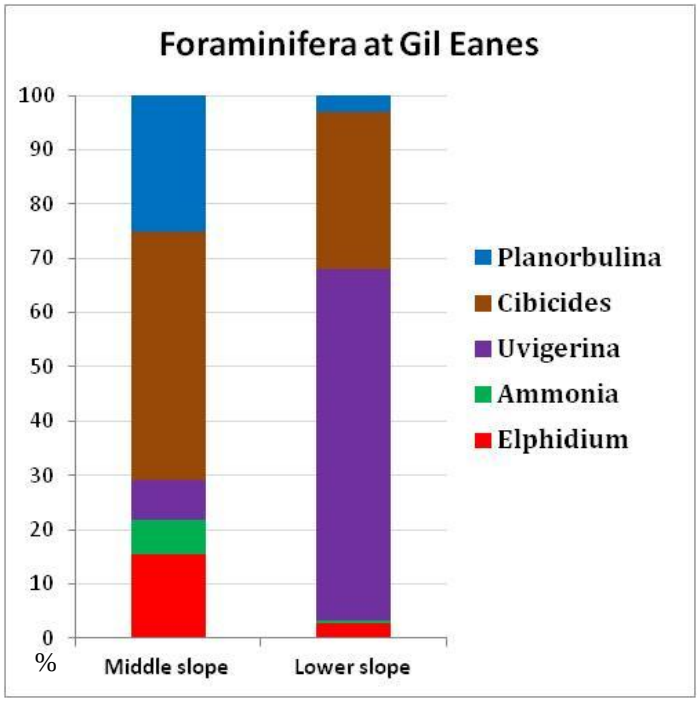

Figure 6-5 proportion of species at mid and lower slope for Gil Eanes Channel.

In the Gil Eanes channel the population is dominated by *Cibicides* contributing 43%, with *Uvigerina* 17%, *Ammonia* 16%, *Elphidium* 14% and *Planorbulina* contributing 10% respectively. The midslope assemblage differs considerably from the reference midslope with 47% of foraminifera being transported from the shelf (*Elphidium*, *Ammonia* and *Planorbulina*). There are significantly fewer *Uvigerina* in the midslope with most taxa in the lower slope. The lower slope is similar to the reference locations where both *Uvigerina* and *Cibicides* predominate suggesting a return to more autochthonous conditions.

A comparison between grain size and equivalent foraminifera size is shown in Fig6-6 for each depth.

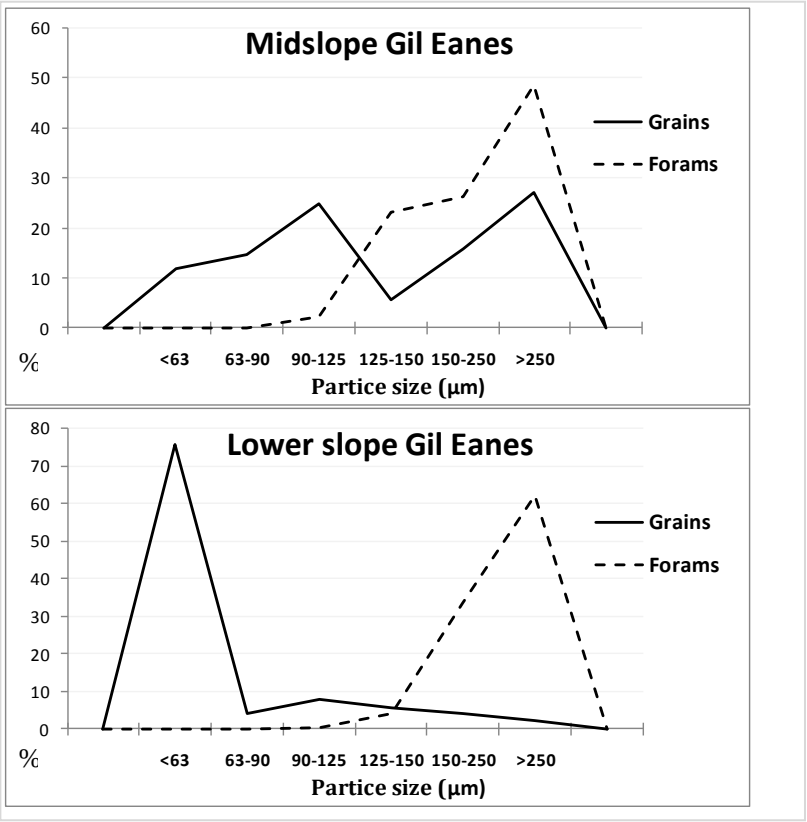

Figure 6-6 Grain size proportion and equivalent foraminifera size (D_{sed}) for each midslope and lowerslope in the Gill Eanes Channel.

In the midslope the proportion of sediment grain size is bimodal, with the highest proportions at 90-125 µm and >250 µm. Foraminiferal equivalent size compares very well with the coarser mode of the siliciclastic sediment, with maximum numbers at 250 µm, gradually decreasing to 90-125 µm. Note that it would not be possible to resolve the finer mode in the foraminiferal equivalent sizes regardless of whether it was present, as this would require expanding our foraminiferal analysis to tests < 250 µm. In the lower slope, nearly all the sediment is < 63 µm while the foraminiferal equivalent sizes fall between 150-250 µm and > 250 µm.

6.4.3 Cadiz Channel

The proportion of foraminifera at each depth for the Cadiz Channel is shown in Fig.6-7.

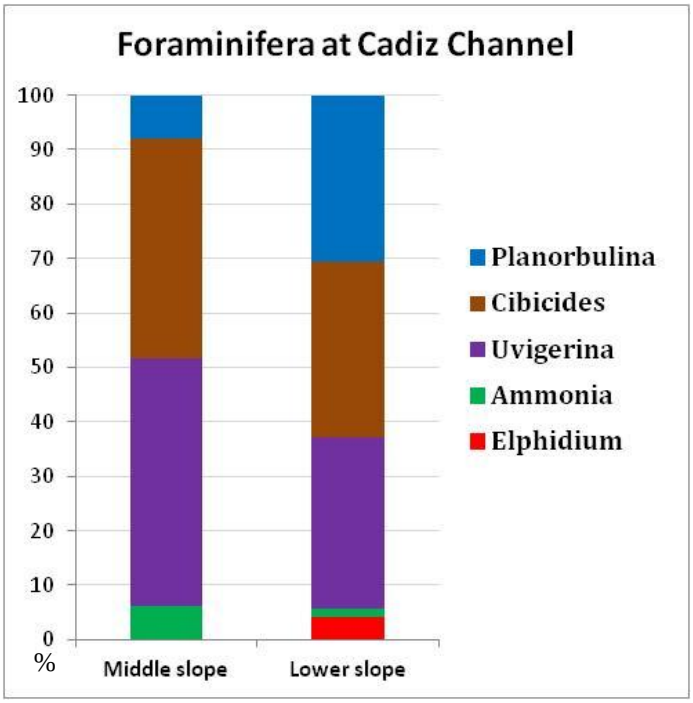

Figure 6-7 Proportion of species at mid and lower slope for Cadiz Channel.

In the Cadiz Channel the population is dominated by *Cibicides*, contributing 40% of all tests, *Planorbulina* 26%, *Ammonia* 17%, *Uvigerina* 14% and *Elphidium* 4%. The midslope is dominated by *Cibicides* and *Uvigerina* with 14% of the population transported from the upper shelf (*Ammonia* and *Planorbulina*). The lower slope shows the greatest amount of transported tests with 48% of species being transported. This suggests taxa are bypassing the midslope to the lower slope and being deposited as the flow wanes in the fan area downslope.

A comparison between grain size and equivalent foraminifera size is shown in Fig6-8 for each depth.

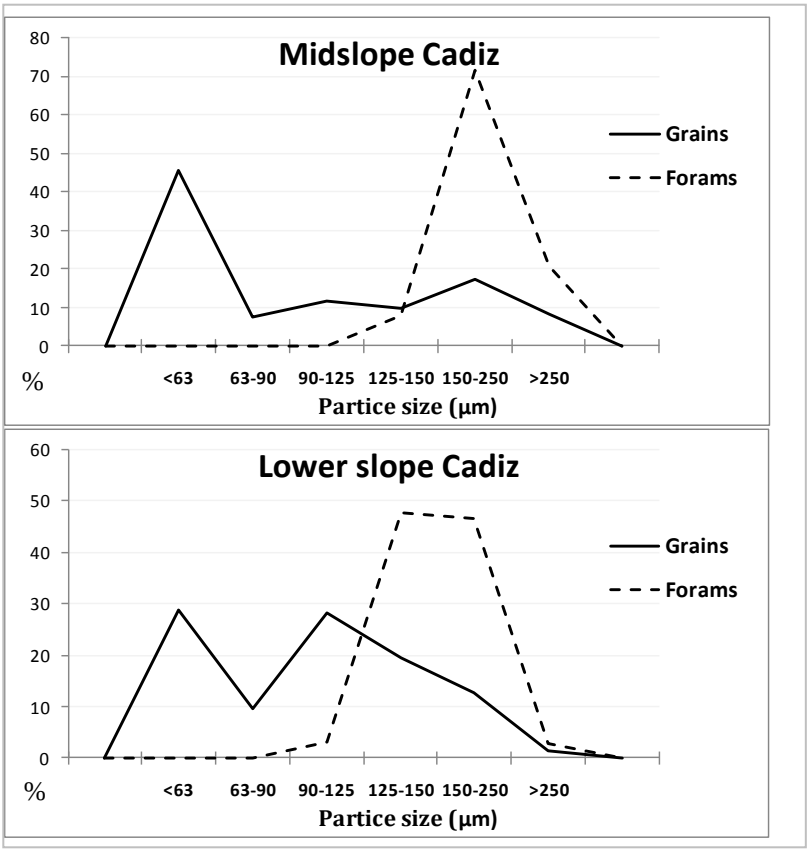

Figure 6-8 Grain size proportion and equivalent foraminifera size (D_{sed}) for each midslope and lowerslope in the cadiz Channel.

In the midslope the highest proportion of grain size is < 63 µm while foraminiferal equivalent size is greatest at 150-250 µm. However, as with the Gil Eanes channel there is a bimodal distribution to the sedimentary grain size data, and again the foraminiferal equivalent size distributions match the shape of the coarser mode. In the lower slope the grain size is variable, being greatest at <63 µm and 90-125 µm. The foraminiferal equivalent sizes have the highest proportion at 125-150 µm and 150-250 µm, again comparing well with the coarser mode of the sedimentary data. Particularly important is the fact that the upper limit of sizes in both sedimentary and foraminiferal equivalent sizes correspond extremely well. As this limit is constrained by neither selection of foraminiferal tests or by the sediment grain size measurements, this can be considered a critically important indicator of hydraulic equivalence between these populations.

6.5 Discussion

6.5.1 Transport and deposition of foraminifera in the vicinity of submarine channels

The results have highlighted two areas where transportation of shelf species has occurred within the submarine channels. The first one is the Gil Eanes channel at midslope where the assemblage is dominated by transported shelf species (*Elphidium*, *Ammonia* and *Planorbulina*). *Cibicides* is also present which is associated with strong bottom currents and reworked populations while the infaunal taxon *Uvigerina* is absent, possibly due to other environmental factors such as changes in oxygen and/or organic carbon content of sediment (Loubere & Fariduddin, 2002; Bernhard & Sen Gupta, 2002; Sweetman *et al*., 2009). The second location is the lower slope of the Cadiz channel. Here the assemblage is dominated by the transported *Planorbulina*. *Elphidium*, *Ammonia* and *Cibicides* are also present, also with reduced numbers of *Uvigerina.* A comparison of populations transported from the shelf are shown in Fig.6-9, highlighting the difference between the reference location and the two channels where transport has occurred midslope at the Gil Eanes and lowerslope at the Cadiz channel.

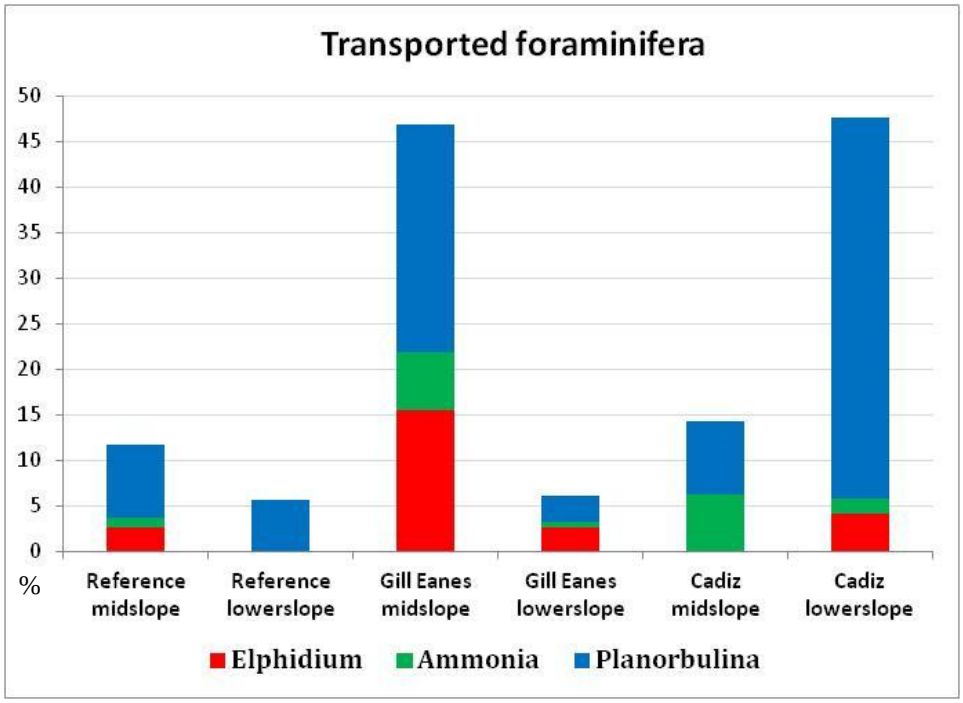

Figure 6-9 Proportion of transported foraminifera for Reference location, Gil Eanes Channel and Cadiz Channel.

6.5.2 Particle size analysis at the Gil Eanes Channel

There is a greater correlation between grain size and equivalent foraminiferal size in the midslope, suggesting a similar behaviour of all particles and therefore evidence of post mortem transport. The lower slope is very similar to the reference location showing no correlation to grain size, suggesting little post mortem transport. In more detail, differences in grain size can be made between the coarse and fine sediment, Table 6-2

Table 6-2 Division of cores into coarse and fine sediment for midslope Gil Eanes.

Core	Depth (m)	Highest % grain size (μm)	
D13697	891	150-250	Coarse
D13696	885	> 250	Coarse
D13680	1010	> 250	Coarse
D13695	853	63 - 125	Fine
D13679	952	63 - 125	Fine
D13686	956	63 - 125	Fine

Fig.6-10 shows foraminifera equivalent size in relation to the coarse and fine grain size and the taxa present.

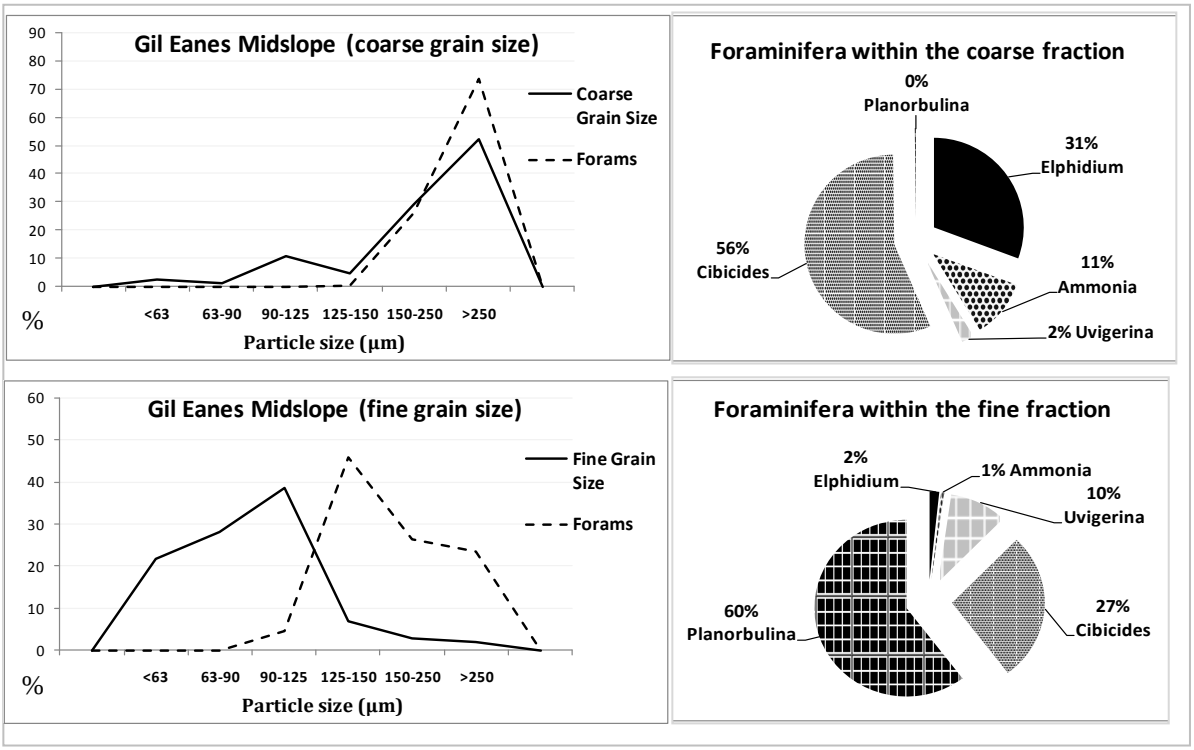

Figure 6-10 Coarse and fine grain size proportion and equivalent foraminifera size (D_{sed}) to the left and proportion of foraminifera on the right for Gill Eanes midslope.

Fig.6-10 shows a very close relationship between particles at the coarse grained locations. This coarse grain size may be associated with higher energy, possibly at the channel axis (Habgood *et al.,* 2003). Within these cores the transported foraminifera from the shelf are mostly the heavier species *Elphidium* and *Ammonia* (42%) with none of the lighter *Planorbulina* present. A high proportion of *Cibicides* and very few *Uvigerina* are present indicating strong bottom currents.

Foraminifera in the fine sediment locations show a distinct translation towards finer equivalent grain size. This finer grain size may be associated with lower energy, as this location represents drift sediment at the side of the channel. From swath bathymetry surveys of the region Garcia (2002) affirms that the Gil Eanes channel is relatively small with steep walls flanked by significant drift sediments due to the Mediterranean Outflow. Within these cores 87% of the transported foraminifera are the lighter species *Planorbulina* and *Cibicides.* There are very few of the heavier *Ammonia* and *Elphidium.* There is a slight increase in *Uvigerina* indicating possible recolonisation in this quieter environment.

The more transported assemblage at the midslope is associated with along slope processes driven by the Mediterranean Outflow. Within the channel there is preferential deposition of coarser sediments from the basal flow and transportation of finer sediments into the water column and away from the depositional site to lower energy locations. In this case the Gil Eanes sedimentary lobe area is affected by cross-currents from the Mediterranean Outflow and the lighter *Planorbulina* are being transported laterally rather than further downslope. In the lower slope there are much fewer transported species with the predominant species being *Uvigerina* (an indigenous taxa within its niche habitat), indicating down slope transport processes are less significant than along slope processes in this smaller submarine channel.

6.5.3 Particle size analysis at the Cadiz channel

Grain size at the lower slope of the Cadiz Channel is slightly more varied between cores and can be divided into a coarse, intermediate and fine. Table 6-3 shows differentiation between grains.

Table 6-3 Division of cores into coarse, intermediate and fine sediment for lower slope Cadiz.

Core	Depth (m)	Highest % grain size (μm)	
D13706	1946	150-250	Coarse
D13700	1191	63 - 125	Intermediate
D13703	1161	63 - 125	Intermediate
D13701	1061	< 63	Fine
D13707	1533	< 63	Fine

Fig.6-11 shows foraminifera equivalent size in relation to the coarse, intermediate and fine grain sediment and the taxa present.

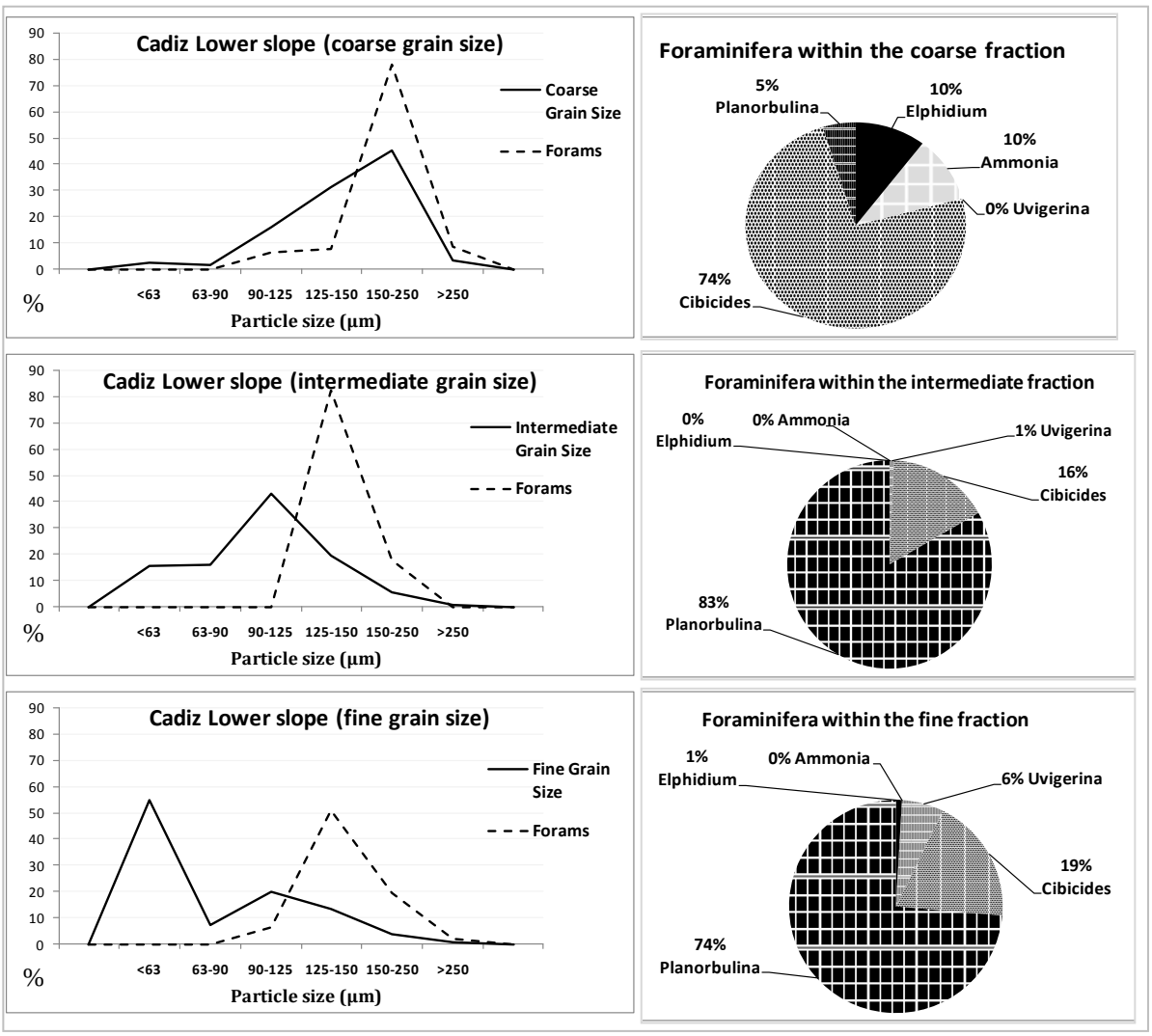

Figure 6-11 Coarse, intermediate and fine grain size proportion and equivalent foraminifera size (D_{sed}) to the left and proportion of foraminifera on the right for Cadiz lower slope.

Fig.6-11 shows an increasing translation towards smaller foraminifera equivalent size as the sedimentary grain size at the location becomes finer. However, although the peaks match in the coarser sites, these peaks become more separated as the sedimentary grain size becomes finer. Within the coarse sediment 20% of the transported foraminifera consist of the heavier species *Ammonia* and *Elphidium*. A high proportion of *Cibicides* and no *Uvigerina* again indicates strong bottom currents. In the intermediate and fine grain sediment *Planorbulina* dominates while the heavier species *Ammonia* and *Elphidium* are absent. In the fine sediment there is a slight increase in *Uvigerina* again indicating possible recolonisation in this quieter environment.

In the Cadiz channel area *Planorbulina* shows a clear transported assemblage downslope with numbers dramatically increasing to the lower slope (Fig.6-9). The Cadiz channel is a much larger channel than the Gil Eanes, with a higher energy regime resulting in a greater proportion of foraminifera being transported through the midslope to the lower slopes. It is also further northwest in a position where the effects of the MO are reduced, facilitating the influence of down slope rather than along slope processes.

6.5.4 Further analysis of the Cadiz Channel

The Cadiz channel has shown a change in assemblage down slope as foraminifera are transported from the shelf and deposited in the muddy basin on the sea floor, (section 6.4.3 and 6.5.1). Analysis in section 6.5.3 has shown a relationship between grain size and foraminiferal equivalent size where transport processes are dominant resulting in the two populations of particles becoming increasingly similar in depositional size. The relationship between grain and foraminiferal equivalent size indicates that a transported mud can be recognized from a pelagic mud by analysis of foraminiferal equivalent particle size, as previously speculated by Brunner & Ledbetter (1987). To confirm the relationship between foraminiferal equivalent and grain size is not a consequence of careful selection of taxa for investigation, all the benthic foraminifera species that represent least 5% of the population in all the Cadiz Channel samples were studied, and equivalent sizes estimated via comparison of test shape and density with the five species where transport behaviour is understood. This included assessment of family and test architecture to access density and shape of each species as shown in table 6-4.

Table 6-4 List of species used for expanded population with similar characteristics to experimental taxa.

Species	**Superfamily**	**Family**	**Shape**	**Architecture**	**Density**
Species similar to *Uvigerina peregrina*					
U.peregrina	Buliminacea	Buliminellidea	conical	triserial, bilamellar	
U.mediterranea	Buliminacea	Buliminellidea	conical	triserial, bilammellar	same
Bulimina costata	Buliminacea	Buliminidae	conical	triserial, bilalmellar	same

Globobulimina	Buliminacea	Buliminidae	plum	triserial	lighter
Amphycoryna	Nodosariacea	Vaginulinidae	conical	multichambered monolamellar	lighter
Species similar to *Cibicides lobatulus*					
C.lobatulus	Planorbulinacea	Cibicidae	hemispherical	low trochospiral	
Cibicidoides dutemplei	Planorbulinacea	Cibicidae	hemispherical	low trochospiral	same
Cibicidoides kullenbergi	Planorbulinacea	Cibicidae	hemispherical	low trochospiral	same
Rosalina glutinata	Discorbacea	Rosalinidae	hemispherical	low trochospiral	same
Rosalina sp.	Discorbacea	Rosalinidae	hemispherical	low trochospiral	same
Species similar to *Ammonia beccarii*					
A.beccarii	Rotaliacea	Rotaliidae	oval	low trochospiral	
Gyroidina spp.	Chilostomellacea	Gavelinellidae	oval	low trochospiral	lighter
Nonion barleeanum	Nonionacea	Nonionidae	oval	planispiral	lighter
Nonion soldanii	Nonionacea	Nonionidae	oval	planispiral	lighter
Species similar to *Elphidium crispum*					
E.crispum	Rotaliacea	Elphidiidae	lenticular	multichambered	
Hoeglundia elegans	Ceratobuliminacea	Epistominidae	lenticular	multichambered	lighter
Lenticulina spp.	Nodosariacea	Vaginulinidae	lenticular	multichambered	lighter
Species similar to *Planorbulina mediterranensis*					
P.mediterranensis	Planorbulinacea	Planorbulinidae	flat disc	planispiral	
Planulina ariminensis	Planorbulinacea	Planulinidae	flat disc	trochoispiral	heavier
Hyalinea balthica	Planorbulinacea	Planulinidae	flat disc	trochoispiral	heavier[5]

The size and abundance data was then incorporated into the particle dataset, the results of which are shown in Fig.6-12. The initial population comprises of the five experimental species which accounts for 20% of the assemblage. The expanded population comprises of twenty species which accounts for 50% of the total assemblage.

[5] The D_{max} and D_{sed} is known for the five experimental species. These were plotted against each other for each species and an equation for each species was extrapolated from the best fit trend lines. Each foraminifera from the expanded population was categorized to the equivalent experimental species and the D_{sed} was calculated using the trendline equation. If lighter or heavier characteristics were inferred then the trendline (and equation) was shifted slightly to account for differences in density.

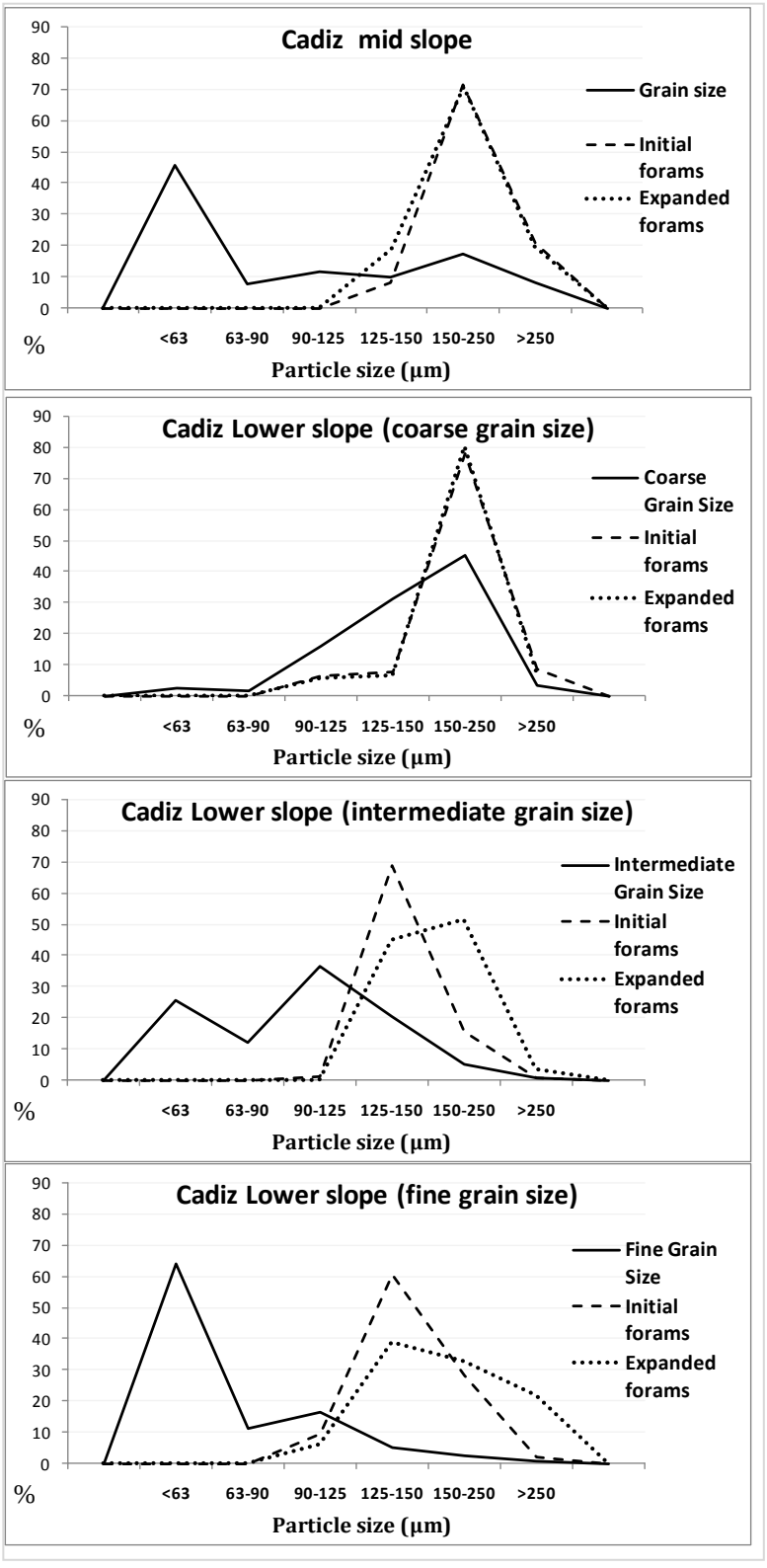

Figure 6-12 Proportional grain size data with equivalent foraminifera size where the initial and expanded populations are included in the analysis.

Fig.6-12 shows almost identical outcome for the midslope whether the initial or expanded populations of foraminifera data is analysed. In the lowerslope where

transport processes are recognized the coarse grained data shows a similar trend. In the high energy environment where coarse grains are deposited, only transported species are present, meaning that particle analysis will remain the same whether a small or large data set is examined.

The intermediate and fine particle data is slightly skewed to the coarser sediment when a larger dataset of foraminifera are used. This is more evident in the fine grain size when the proportional predominance of the very light *Planorbulina* is reduced. This indicates there are some autochthonous individuals in the fine grained samples as this low energy environment is more favorable to colonization by bathyal species. There is still a definite shift towards similar particle size when comparing the midslope to lowerslope, confirming the theory that a transported mud can be detected by micropalaeontological composition alone.

6.6 Conclusion

The Gulf of Cadiz is a complex depositional system due to the strong contourite regime as well as submarine channels. Even so, the signal of fractionation of species downslope can clearly be seen when the foraminifera's ecological niches are taken into consideration. The effect of post mortem transport within the submarine channels clearly shows the same trend as the experimental work, with lighter species being carried further into more quiescent conditions.

Analysis has shown that there is a marked difference in assemblages where post mortem transport occurred in the channel areas. Reference cores reveal mainly 'in situ' assemblages emerging under quiescent conditions. In the reference locations there was a gradual fining of grains down slope but the foraminifera size did not reflect this change, indicating an autochthonous assemblage was present at all depths.

In the Gil Eanes channel transport processes are most prevalent in the midslope where there is a change to an allochthonous assemblage. Here, the transported assemblage is associated with along slope processes driven by the Mediterranean

Outflow with more transportable species being transported laterally rather than further downslope. Although the grains fined downslope the foraminifera size only correlated to the midslope grain size indicating less significant transport process to the lower slope as foraminifera had already been transported laterally away from the channel area.

In the larger Cadiz channel transport processes occur down to the lower slopes as downslope processes dominate. There is a marked change in assemblage composition with a high proportion of the lightest taxa transported downslope, eventually depositing in the more quiescent fan area. Within this there is a great variety of grain sizes indicating deposition in the fan where microchannels and levees have developed over many depositional occurrences within the muddy basin. The correlation between grain size and equivalent foraminiferal size can be related to individual cores indicating a significant detailed relationship between the two particle types where transport processes have occurred. Study of a larger data set in the Cadiz lower slope revealed particle similarity in the coarse grained sediment indicating an allochthonous assemblage while the fine grained sediment some autochthonous species were present in this lower energy environment.

The contourite oceanic environment has shown the same effect as the laboratory conditions but to a much greater extent. Over time the foraminifera get picked up and deposited many times over considerable time spans and spatial distances, resulting in a much greater signal of fractionation than shown in a few seconds in the laboratory flume.

7 Extracting the signal of post mortem transport from standard core data in an active exploration / development context; a case study from the Hibiscus and Poinsettia fields, Trinidad

7.1 Abstract

Investigation into core data from the Hibiscus and Poinsettia fields, Trinidad, shows that a biostratigraphical summary of logs can be used to decipher palaeoenvironmental differentiation between sediments in time and space. Using foraminiferal data, post mortem transport can be identified in turbidite muds where fractionation of different species occurs due to differing settling velocities. Transported muds are established using two newly proposed indices; TDI (Transport Dominance Index) which shows the variance in settling velocities between individual tests in an assemblage and TPI (Transport / Pelagic Index) which looks at the character of the energy regime. Within assemblages that have been entirely transported, the differentiation between different energy regimes can be quantified in terms of the settling velocity of the population of tests. Using these two indices together it can be determined whether muds have been laid down under quiescent pelagic conditions or from a submarine fan which is important in understanding the lateral extent of cap rocks.

7.2 Introduction

This chapter considers how the experimental work described in previous chapters can be applied to understand the origin of assemblages of foraminifera from an actively producing petroleum field. The case study area is the eastern Venezuelan basin of Trinidad and Venezuela. The petroleum geology of this region is most recently affected by the collision during the Oligocene between the South America and the Caribbean plates. Foreland sedimentation dominates the latter part of the

Oligocene to the present and the area remains extremely tectonically active (Jones, 2011). The foreland basin phase is represented by a range of sediments varying from alluvial and fluvial conglomerates and sandstones through peri-deltaic sandstones and coals and prodeltaic shales to turbiditic sandstones and basinal shales (Jones, 2011). Source rocks for hydrocarbons are of Middle Cretaceous age from the Querecual of eastern Venezuela and Naparima Hill of Trinidad (Jones, 2011). The most important reservoirs onshore and offshore Trinidad constitute marginal to shallow marine and, locally, deep marine clastics of Neogene and Pleistocene age (Wood, 2000). Caprocks to this sequence are intraformational (locally deposited) mudstones.

This Chapter examines drilling records from offshore Trinidad on the coast of Venezuela to see whether a signal of fractionation during transport can be identified and if useful assemblage transportation data can be extracted to interpret the depositional environment. Ichron Ltd supplied a biostratigraphical summary of a 2004 drilling campaign for analysis. Five summary logs from core data are examined, the geographical position of which is shown in Fig.7-1 & 7-2.

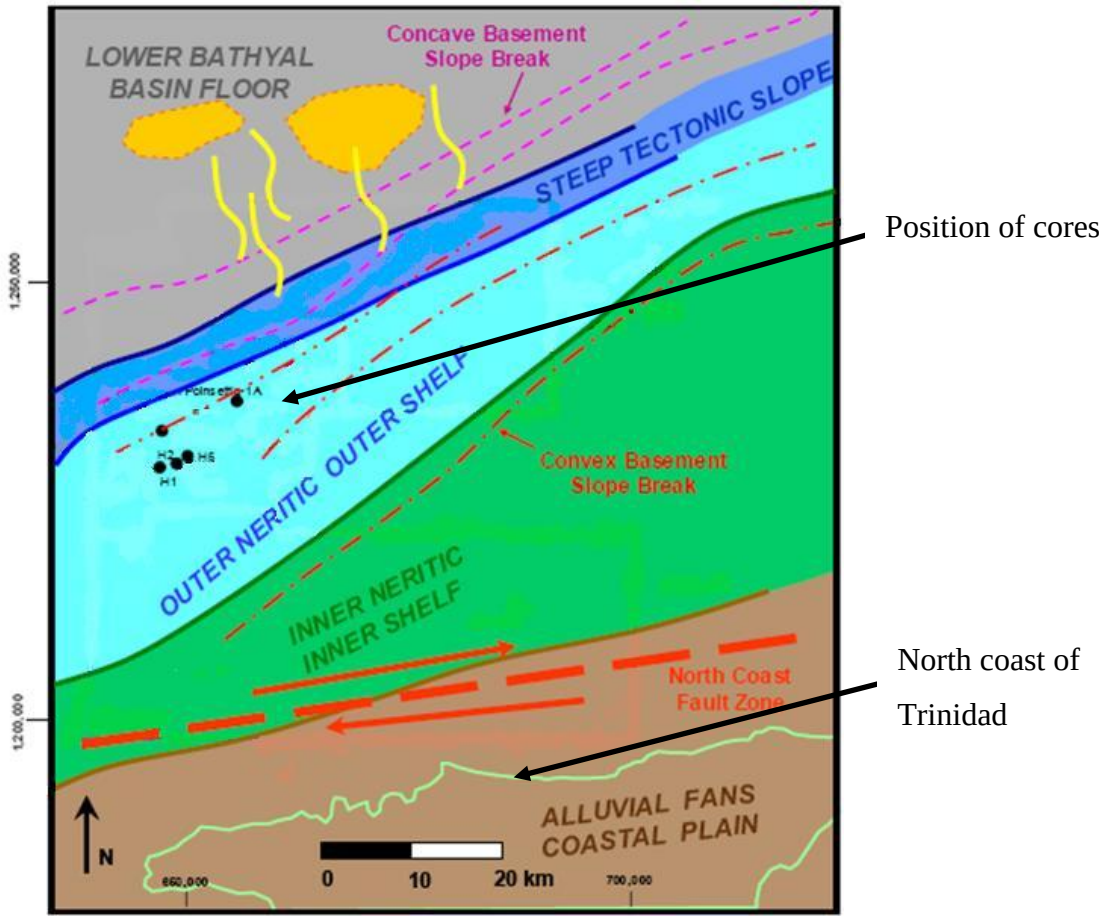

Figure 7-1 Position of cores superposed on a palaeogeographic map in relation to coast of Trinidad (adapted from Ichron, 2009).

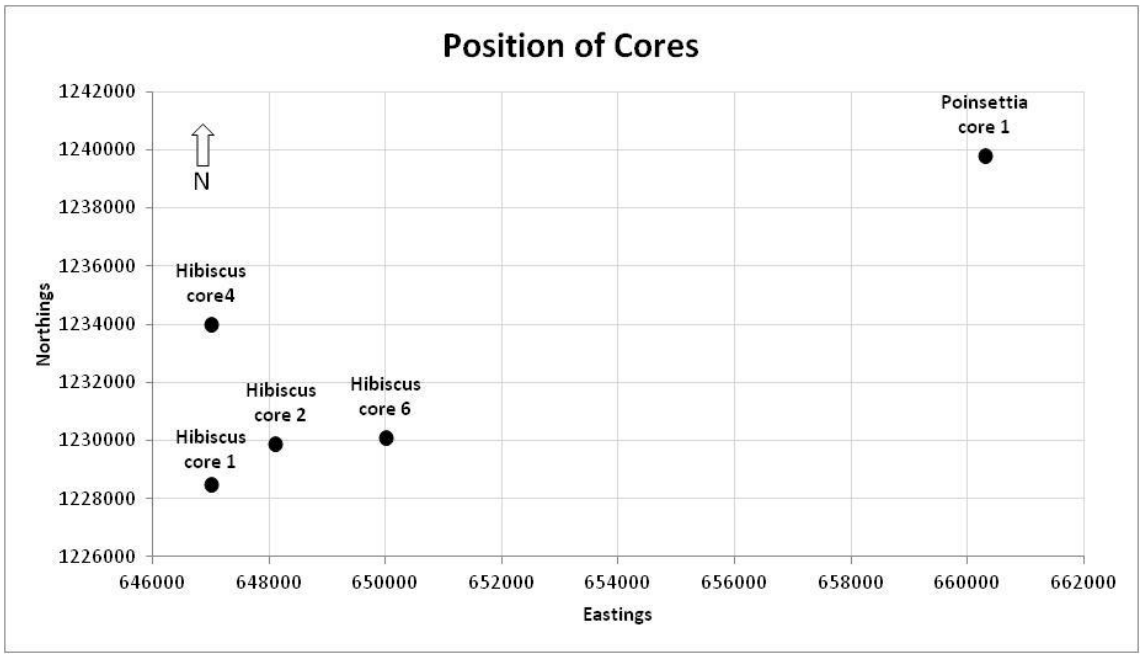

Figure 7-2 Detailed position of cores (the coast of Trinidad presently lies approximately 20 miles to the south).

The Hibiscus and Poinsettia fields are part of an offshore development encompassing six gas fields: Hibiscus, Poinsettia, Chaconia, Ixora, Heliconia and Bougainvillea. This NCMA (North Coast Marine Area) is situated off the north coast of Trinidad in roughly 500 feet (152 meters) of water depth in the Caribbean Sea. Both the Hibiscus and Poinsettia fields are operated by BG with the Hibiscus platform producing since 2003 (production capacity of 400 MMcf/d[6]) and the Poinsettia from 2009 (production capacity 350 MMcf/d), (SubSeaIQ, 2011).

The biostratigraphical summary logs examined comprise of distribution lists recording the number of different species present at each horizon. This Palaeoenvironmental interpretation is shown in Fig.7-3 where the thirteen zones identified are biofacies or ecozones as opposed to chronozones.

[6]MMcf/d - Millions of cubic feet per day (of gas)

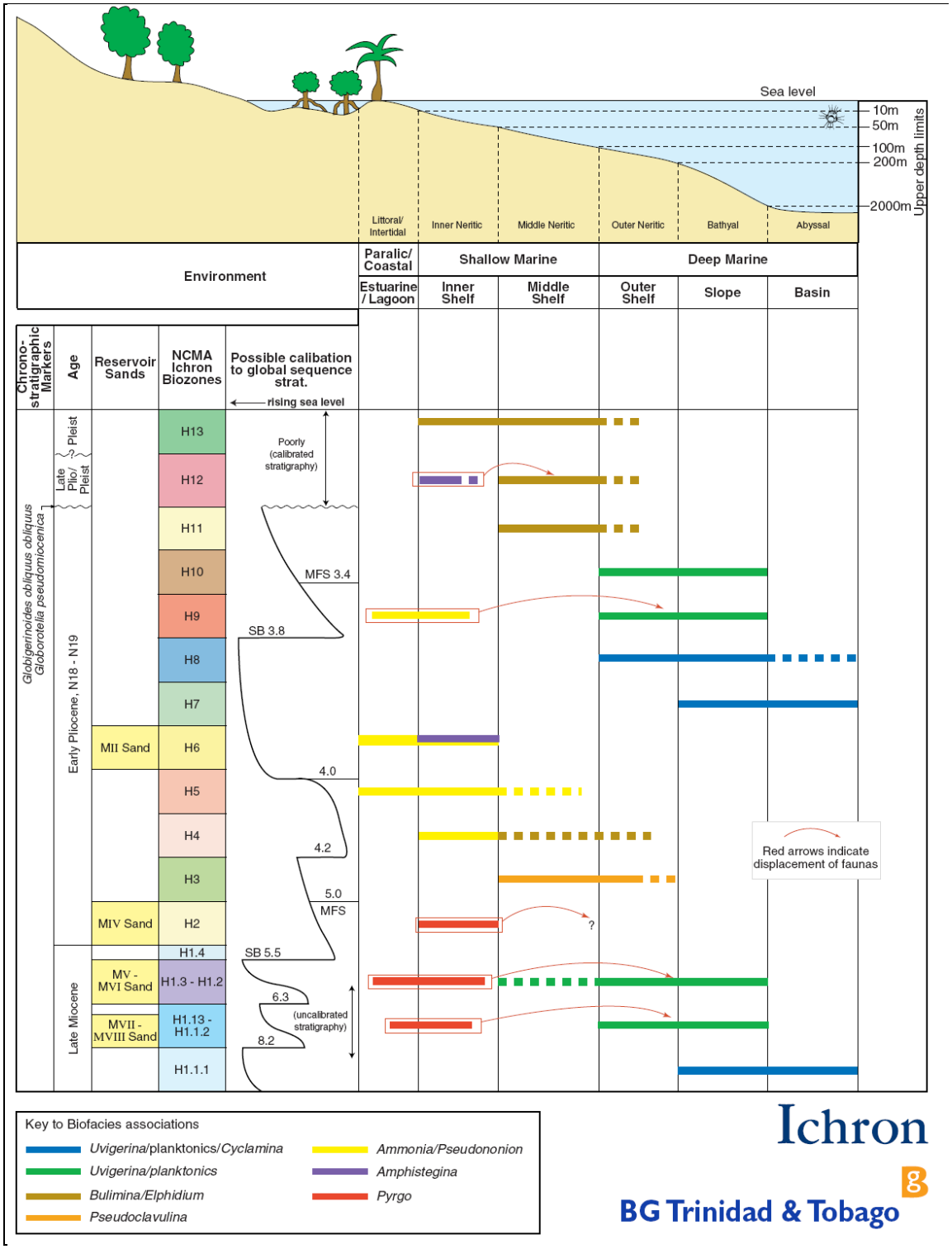

Figure 7-3 Palaeoenvironmental interpretation of the micropalaeontological biozones.

The implied calibration of the various bio-events against global eustatic sequence statigraphy is based on Haq *et al.* (1988). On the basis of cycle counting, the biofacies zones are calibrated against sea-level cycles, sequence boundaries and maximum flooding surfaces but calibration is tentative (Ayress *et al.*, 2004).

Unfavourable environmental conditions meant that standard biostratigraphic techniques (i.e. the use of open ocean planktonic foraminiferal or calcareous nannoplankton assemblages in global standard biozonations) for dating provided limited resolution. High sedimentation rates caused dilution of foraminifera numbers and increased scarcity of key marker species. Only two planktonic foraminiferal chronozones are potentially available for confirmation of the chronostratigraphy, which are Pleistocene markers *Globorotalia truncatulinoides* and *Pulleniatina obliquiloculata* (Spencer-Cervato & Thierstein, 1997). Data was mainly obtained from cuttings during drilling operations, so cavings during the drilling process have also lowered the resolution of depth stratigraphy (Ayress *et al.*, 2004).

Consequently biostratigraphy is based on benthonic foraminiferal "biozone" characterization. Biozones are intervals of geological strata that are defined on the basis of their characteristic fossil taxa. In this region benthic foraminifera are the principle group of use in palaeobathymetic interpretation (Jones, 2011). They are of particular use in the discrimination of sedimentary sub-environments in marginal marine to shallow marine, peri-deltaic and also in deep marine, submarine fan and reservoirs (Jones & Simmons, 1999). Accurate interpretation of environments of deposition in marine sequences is aided by an understanding of the environmental preferences of these foraminifera which are also critical to the interpretation of water depth. The biostratigraphical zones employed are defined on down-hole occurrence of key marker taxa (for time and depth) and also influxes and changes in assemblage composition. The regional biostratigraphical zonation for the north coast marine area, Trinidad is shown in Appendix 9.3

The five cores chosen for analysis contain the greatest number of foraminifera, due to muddy horizons being present, and encompass all biozones identified. Fig.7-3 shows that it is likely that some down slope transportation of faunas has occurred within certain zones (arrows on diagram).

7.3 Method

7.3.1 Foraminiferal analysis

Distribution charts from the Hibiscus and Poinsettia fields record one hundred and thirty-five calcareous benthic foraminifera species. To allow this data to be considered from the perspective of postmortem transportation, each taxon was listed within family order, grouped by test architecture and shape. This information was used to identify the probable density of these taxa forams from the understanding of the control of this parameter from wall layering and chamber architecture drawn from the same method of analyses as in Chapter 6, section 6.5.4. An indicative size was determined for each species from publications by Cushman (1948), Murray (1971), Loeblich & Tappan (1988; 1988a), Bolli *et al.*, (1994) and Robertson (1998). (A list of species characteristics is given in Appendix 9.4). If these standard taxonomic sources provided strongly differing indicative sizes, the average of the available sizes is used in further analyses. The living depth of taxa were also taken (i.e. shelf, bathyal or abyssal) from Murray (1991). The settling velocity for each species was then calculated using the formulae described in Chapter 4, section 4.5.4, i.e.:

$$Ws = \sqrt{\frac{4gDsed(\rho s - \rho)}{3\rho C_D}} \qquad (7.1)$$

7.3.2 Developing an index of post mortem transport

To interpret the depositional environment and comprehend the magnitude of post mortem transport processes which may have occurred, an understanding of the energy regime at the time of deposition is required. To differentiate between an autochthonous assemblage which contains a taxa in-situ and under normal lifetime conditions and an allochthonous assemblage which either contains taxa brought in from other areas or is missing taxa exported from the life assemblage, the signal of fractionation has to be identified. The signal of fractionation has previously been identified in the experimental studies described in Chapters 3 to 5 and in the case study area of the modern Gulf of Cadiz (Chapter 6). In this previous work, it was demonstrated that in high energy environments such as submarine channels, there

was a marked increase in transported taxa from the high energy channel axis into more quiescent areas, resulting in more transportable taxa (i.e. those with the lowest settling velocity) being deposited in low energy areas. This resulted in a distinct change in assemblage characteristics compared to autochthonous assemblages, in which a greater variety of foraminifera sizes are observed to occur. In high energy environments only the least transportable taxa are present while under moderate energy conditions only the most transportable taxa are present.

Here, two new settling velocity-sensitive indices are presented for application to calcareous benthic foraminiferal populations which provide semi-quantitative analyses of transportation for the first time. To test whether an assemblage has a significant transported component, the "TDI" (Transport Dominance Index) is employed which is a parameter summarising the variance between settling velocities of individual tests in the assemblage. This is calculated using the formula:

$$\mathrm{TDI} = \sigma(P_s W_s) \tag{7.2}$$

where σ is the standard deviation of the proportion of species and their settling velocity within a horizon. P_s is the proportion of species ($P_s = \frac{S_n}{\sum S_n} x\ 100$), S_n is number of a certain species; $\sum S_n$ is the sum of all species. The proportion of each species is then multiplied by the settling velocity (W_s).

Within assemblages that have been entirely transported, the differentiation between different energy regimes can be quantified in terms of the settling velocity of the population of tests, which is represent here as the "TPI" (Transport/Pelagic Index). This TPI index can be simply computed for each sample in which a representative population of foraminifera are available using the formula:

$$\mathrm{TPI} = \frac{\sum P_s W_s}{\overline{W_s}} \tag{7.3}$$

Where P_s is the proportion of species ($P_s = \frac{S_n}{\sum S_n} x\ 100$), S_n is number of a certain species; $\sum S_n$ is the sum of all species, W_s, is the settling velocity and $\overline{W_s}$ is the mean

of settling velocities for all the foraminifera in all samples from the five cores under analysis. As this is presented as a relative index of bottom energy, and it primarily reflects foraminiferal settling velocities; implying a scalar meaning for the "real world" would be misleading, so this index is presented as a dimensionless number[7]. Where transport has been identified, values above 1 indicate a high energy environment while those below 1 indicate a low energy environment.

Analysis is undertaken using the TDI (Transport Dominance Index) and the TPI (Transport/Pelagic Index) to see if a distinction can be made between an autochthonous and a transported assemblage. The TDI confirms whether the assemblage has been transported while the TPI looks at the character of the energy regime. Several scenarios are possible:

a) A high TDI will always indicate an autochthonous assemblage (taxa have a variety of settling velocities)
b) A low TDI value may indicate a transported assemblage (taxa have similar settling velocities) where some sorting has taken place **or** an assemblage with foraminifera of a similar taxonomy (e.g. the upper to middle slope sub-environments are characterised by buliminides (Jones, 2006)).

If transport is demonstrated then the TPI can be an indicator of the energy regime and the following scenarios are possible:

c) A high TPI may indicate a high energy environment (less transportable taxa) which may be the result of transportation processes **or** it may indicate an assemblage of large foraminifera with high settling velocities (e.g. a shallow water environments where there is an abundance of taxa such as *Amphistegina* spp.)
d) A low TPI may indicate a low energy environment (more transportable taxa) which may be the result of transportation processes **or** it may indicate an assemblage of mostly small or juvenile foraminifera

[7] Dimensionless numbers are of key importance in parametric analysis of scientific problems. They are useful in understanding the similarity among problems belonging to the same broad class and allows the task of data reduction of similar problems.

To decipher the different scenarios a clearer interpretation can be made when evaluating the TDI and TPI together.

The effect of b) can be deciphered:

1. "Low TDI & High TPI" (transported, high energy) fractionation (sorting) has taken place, proximal sandy turbidites or high energy currents
2. "Low TDI & Low TPI" (autochtohonous, low energy) not transported but foraminifera have similar characteristics

The effect of c) can be deciphered:

3. "High TPI & Low TDI" (high energy, transported) fractionation (sorting) has taken place, turbidites or high energy currents (same as 1 above)
4. "High TPI & High TDI" (high energy, autochthonous) climax assemblage, where most foraminifera are robust have grown to large size and are able to live in a relatively high energy environment

The effect of d) can be deciphered:

5. "Low TPI & High TDI" (low energy, autochthonous) colonisation assemblage, ‘a good place to live’, large variation in settling velocities
6. "Low TPI & Low TDI" (low energy, transported) more transportable taxa have been deposited in a distal environment, muddy turbidites or low energy currents. This scenario has the same indices as 2 (above), therefore it may be necessary to look at the species ecological niche to decide whether it is in its ‘in-situ’ or if it has been transported downslope.

It must also be noted that if the sediment is unsorted such as in a debris flow, then the foraminifera will also be unsorted, meaning it will not be possible to distinguish between a transported and non-transported assemblage.

7.4 Results and discussion

7.4.1 Overview of cores

Fig.7-4 shows the trends of TPI and TDI analysis for each of the five cores.

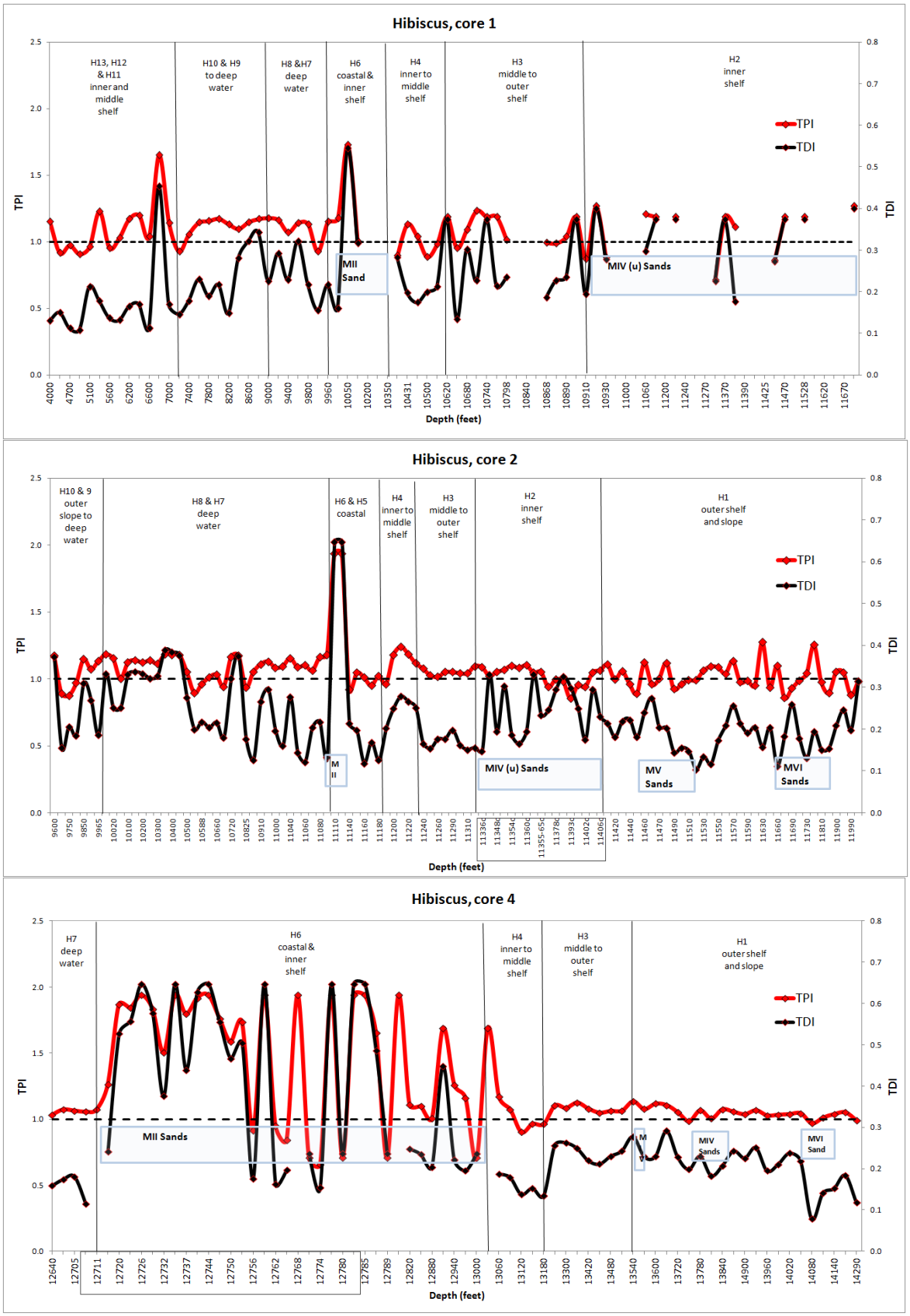
Hibiscus, core 1
H13, H12 & H11 inner and middle shelf
H10 & H9 to deep water
H8 &H7 deep water
H6 coastal & inner shelf
H4 inner to middle shelf
H3 middle to outer shelf
H2 inner shelf
TPI
TDI
MII Sand
MIV (u) Sands
Depth (feet)
Hibiscus, core 2
H10 & 9 outer slope to deep water
H8 & H7 deep water
H6 & H5 coastal
H4 inner to middle shelf
H3 middle to outer shelf
H2 inner shelf
H1 outer shelf and slope
MII
MIV (u) Sands
MV Sands
MVI Sands
Depth (feet)
Hibiscus, core 4
H7 deep water
H6 coastal & inner shelf
H4 inner to middle shelf
H3 middle to outer shelf
H1 outer shelf and slope
MII Sands
MIV Sands
MVI Sand
Depth (feet)

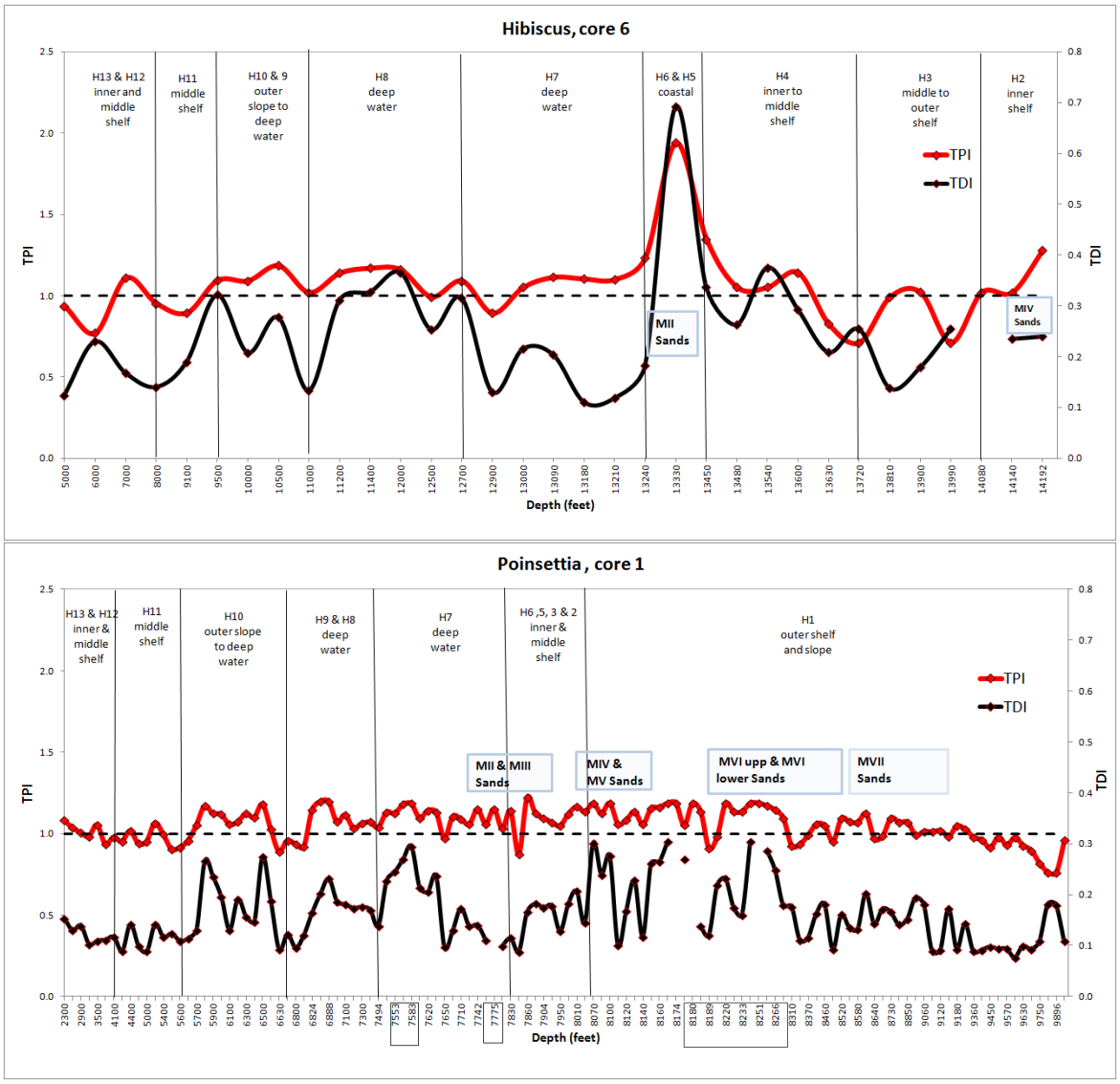

Figure 7-4 TPI and TDI for logs from Hibiscus 1, 2, 4, 6 and Poinsettia 1, boxed depths show core data rather than cuttings. Missing data is where no taxa are present. Single point calculations for all horizons.

The graphs show a very diverse regime with generally a much greater variance of indices within the sands compared to muds. Typically in MII sands there are high TDI values with a positive correlation to high TPI values. The combination of high TPI and high TDI can be interpreted as Scenario 4:

4. "High TPI & High TDI" (high energy, autochthonous) climax assemblage, where most foraminifera are robust have grown to large size and are able to live in relatively high energy environment

The high TPI is due to the presence of *Amphistegina lessoni*, a large robust shelf species with a high settling velocity. A high proportion of this species does not

indicate a transported assemblage but an assemblage which is able to inhabit these high energy sands. This confirms Ayress *et al.* (2004) interpretation where MII sands are progradational shoreface deposits occurring during high stand, laid down under a high energy wave-dominated regime.

MIV, MV, MVI and MVII sands record a different relationship. In general the TDI values are very low while the TPI values are less extreme than in MII sands (there is no correlation between indices as seen in MII sands).
Most of the time the TPI is above 1 indicating Scenario 1:

1. "Low TDI & High TPI" (transported, high energy) fractionation (sorting) has taken place, proximal sandy turbidites or high energy currents

When the TPI is below 1 this indicates Scenario 2 or 6:

2. "Low TDI & Low TPI" (autochtohonous, low energy) not transported but foraminifera have similar characteristics
6. "Low TPI & Low TDI" (low energy, transported) more transportable taxa have been deposited in a distal environment, muddy turbidites or low energy currents.

An investigation into the species in these sands showed that a variety of taxa are present from different families, dismissing scenario 2, that foraminifera have similar characteristics. The TPI waxes and wanes while the TDI remains low indicating transported turbidite sands. This shows variable energy and hence a movement between the "fine", "intermediate" and "coarse" environments (similar to the Cadiz lower slope – Chapter 6, section 6.5.3).

This analysis shows that by evaluating the TDI with the TPI a distinction can be made between an autochthonous and a transported assemblage. MII sands in biozone H6 indicate a more autochthonous assemblage with both high TDI and TPI values. On the other hand the older sands in biozones H1 and H2 show the waxing and waning of energy with sorting of taxa during transport with low TDI values where the signal of fractionation indicates a transported assemblage.

Differences in energy regime can also be observed laterally across cores. It can be seen that biozone H6 clearly represents the highest energy level where MII sands are laid down. During the early Pliocene during high-stand the more south western logs (Hibiscus 1, 2, 4 & 6) show clinoforms which prograde towards the west, consistent with the shoreface orientation (Ayress *et al.*, 2004). It can be seen in the Poinsettia location further north-east did not experience the same high energy regime during this time.

7.4.2 Exploring the signal of fractionation in muds

Cap rocks which constrain the reservoir consist of muds and silts where foraminifera are found in the geological record. An understanding of whether muds are laid down under quiescent pelagic conditions or from a submarine fan is important in understanding the lateral extent of the cap rock. This section therefore analyses the muddy horizons to understand the energy regime in which these sediments are laid down.

Two regions of biozones are compared; those above the MII sands, consisting of biozones H7 to H10 (described as MII muds) and those above the MIV sands, consisting of biozones H3 to H5 (described as MIV muds). Both stages were laid down during the early Pliocene. Any differences between these sections will highlight changes in the hydrodynamic energy regime under which these muds were laid down. The TDI and TPI values are shown in Fig.7-5 for both regions.

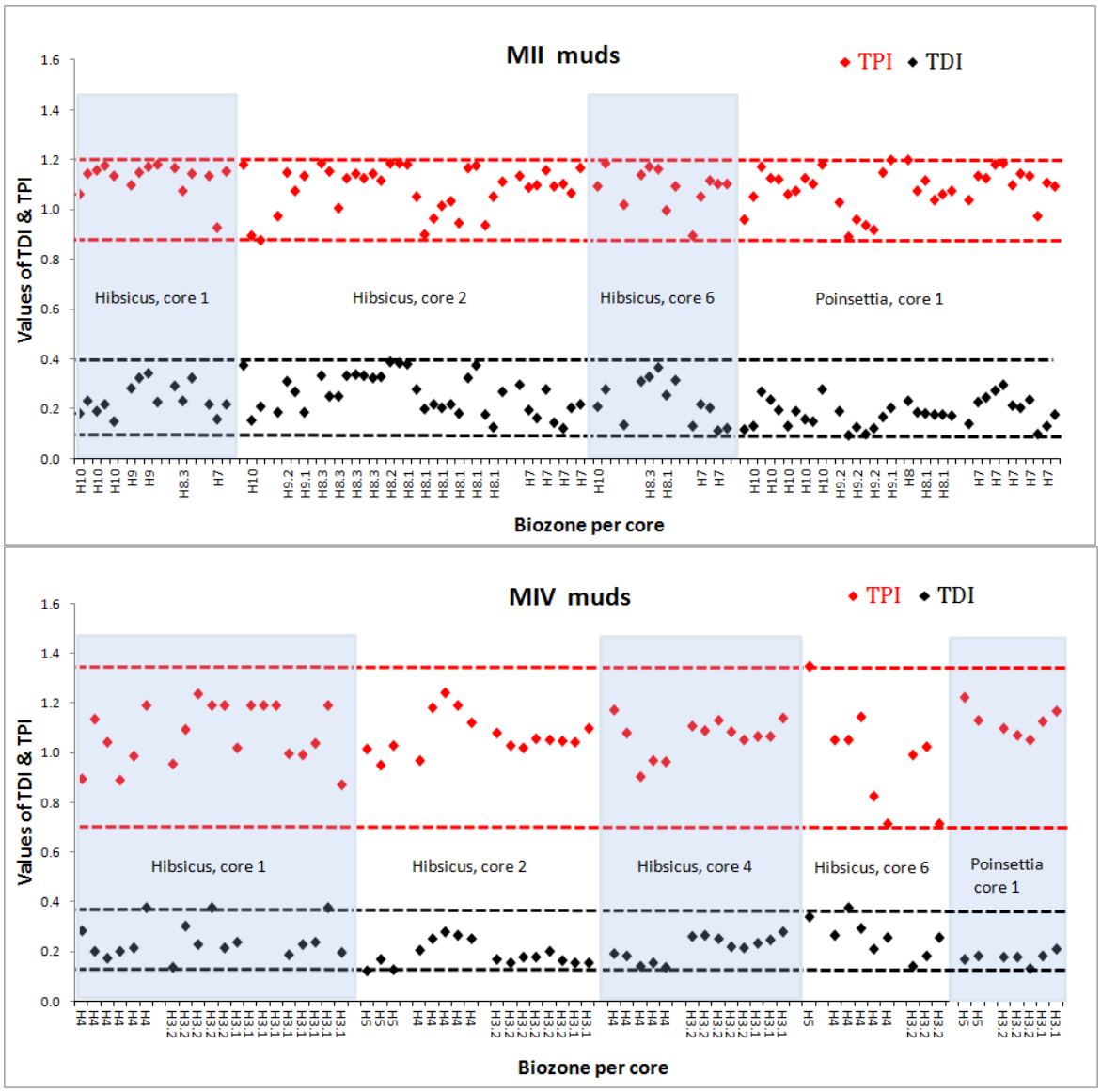

Figure 7-5 TPI (Transport/Pelagic index) and TDI (Transport Dominance Index) values within MII and MIV muds. Broken red horizontal lines depict minimum and maximum values for TPI. Broken black horizontal lines depict minimum and maximum values for TDI.

When looking at the muds a different scenario takes place compared to the higher energy sands. The differences are much subtler here where the muddy environment show less variation in TPI and consistently lower TDI values.

MII muds vary between TDI values of 0.39 and 0.09 while in the MIV muds have slightly less variability, between 0.38 and 0.12. These low TDI values indicate either Scenario 1, 2 or 6:

1. "Low TDI & High TPI" (transported, high energy) fractionation (sorting) has taken place, proximal turbidites or high energy currents

2. "Low TDI & Low TPI" (autochtohonous, low energy) not transported but foraminifera have similar characteristics
6. "Low TDI & Low TPI" (transported, low energy) more transportable taxa have been deposited in a distal environment, muddy turbidites or low energy currents.

An examination of these biozones within the five cores shows that the key species within these muds is *Uvigerina peregrina*, an infaunal species living in marine environments from the shelf to the abyssal. In MII muds 70% of the population is *U. peregrina* while in MIV muds *U. peregrina* is 53% of the total population. This key species and other similar Buliminacea within the muds have similar settling velocities. When examining TDI as the main variable this indicates that Scenario 2 is quite likely as foraminifera have similar characteristics. Therefore an assessment of TPI is needed.

The TPI in Fig.7-5 are distinctly different for MII and MIV muds. The MII muds show little variation in TPI (with values between 1.20 – 0.88) indicating more consistent conditions. The MIV muds show a more dynamic environment, where the TPI is more varied (with values between 1.35 – 0.71). The differences between the TPI can be used to infer whether one mud is more transported than the other. It is possible that the more consistent lower TPI values of MII muds indicate Scenario 2:

2. "Low TDI & Low TPI" (autochtohonous, low energy) not transported but foraminifera have similar characteristics

While the more dynamic and higher and lower TPI values in MIV muds can be interpreted as Scenario 1 and 6:

1. "Low TDI & High TPI" (transported, high energy) fractionation (sorting) has taken place, proximal turbidites or high energy currents
6. "Low TDI & Low TPI" (transported, low energy) more transportable taxa have been deposited in a distal environment, muddy turbidites or low energy currents.

It must be borne in mind that these biozones contain all the individuals living and being transported over hundreds of years, there is no ‘steady state’ and all

environments are dynamic. MII muds may have experienced more quiescent conditions with occasional muddy turbidites while MIV has a more dynamic history. The similarity between TDI values indicates that there is much mixing going on. Turbidites bring in many sorted tests and drive the TDI down while there are also sufficient quiescent periods for climax faunas to periodically establish which increases the TDI. Both muds may have experienced both turbidite and quiet periods but the two may have been bioturbated together into a mixture containing both types of sediment and both types of foraminifera. The greater proportion of the key species in MII muds indicates more quiescent conditions as the more dynamic environment of MIV muds may make it more difficult for infaunal species to colonize.

Further analysis of these biozones enhances this interpretation as only 2% of the population in MII muds are foraminifera transported from the shelf, while MIV muds contain 5% of transported shelf species, indicating MIV muds are more turbiditic. Finally, taking into account that there are 33% more horizons recorded in MII muds compared to MIV muds, MIV only contain 6.5% of the foraminifera numbers. This suggests that in the MII muds more complex optimal communities have developed in more quiescent conditions.

To test whether the muds are significantly different a Kolmogorov-Smirnov test was undertaken as described in Methods Chapter, section 3.3.8. At a 95% confidence level, the maximum difference between the cumulative distributions, $D = 0.303$, which is greater than the critical probability value, $P = 0.02$ suggesting that the two distributions are significantly different from each other. Cumulative distribution is shown in Fig.7-6.

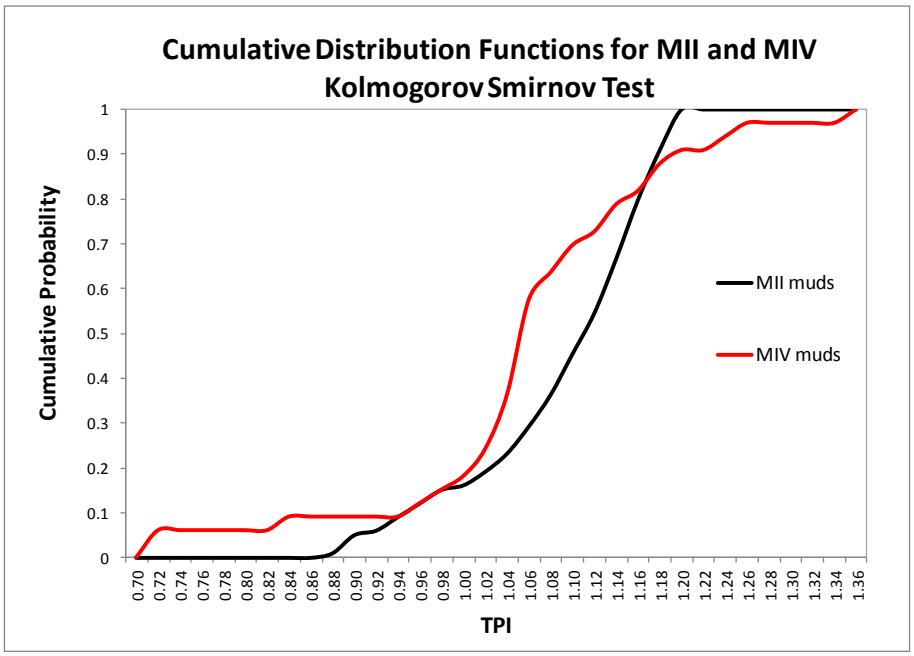

Figure 7-6 Cumulative distribution for MII and MIV muds.

Fig.7-6 shows a much greater variation in energy regime for MIV muds confirming MII and MVI muds are significantly different. A comparison of the two regions of biozones indicates that biozones H7, H8, H9 & H10 above MII sands have experienced more quiescent conditions with occasional turbidite events while biozones H3, H4 & H5 above MIV have a more dynamic history with more extensive periods of turbidite activity.

7.5 Conclusion

Investigation into the Trinidad cores has shown that it is possible to decipher a signal of fractionation within sands and turbidite muds using foraminiferal data. A biostratigraphical summary of cores across a region does enable sedimentological differentiation to be found during time spans within an Epoch. Spatial variations between and within logs presents a different scale than investigating changes down a single submarine canyon, documenting changes in the depositional environment through time and space.

The TDI (Transport Dominant Index) depicts if transportation processes are taking place and a distinction can be made between an autochthonous and a transported

assemblage. The TPI (Transport/Pelagic Index) looks at the character of the energy regime and depicts changes in detail in the sedimentological record. Analysis of these two indices enables separation between and autochthonous and allochthonous assemblage and the energy regime in which they exist.

Fine grained muds are important as cap rocks in hydrocarbon exploration and depositional analysis is particularly difficult due to the consistent nature of the sediment. These indices are able to differentiate between turbiditic and more quiescent conditions that gamma ray logs may not be able to highlight. Using the indices subtle differences in the TPI and TDI signify changes within community populations varying through time. Two muddy biostratigraphical horizons over different time periods have been shown to be statistically different. Muds above MII sands show relatively consistent TPI readings across the region and down log. This indicates quiescent conditions and the possibility of an extensive cap rock constraining the reservoir within MII sands. The muds above MIV sands show a much more dynamic regime with TPI readings reaching more extreme high and low values. These can be interpreted as turbidite muds fed from the shelf during low-stand. These shelf slope muds may be much more impersistant, resulting in a less enduring cap rock to the reservoir within MIV sands.

8 Conclusion and future work

8.1 Conclusion

Static water experiments have shown that settling velocities are significantly different between taxa, meaning that assemblages are likely to fractionate according to species as well as according to size during transportation. Inter-species differences are related to the variations in shape and density between taxa. Investigation into the equivalent settling velocity and the subsequent recognition of the D_{sed} (sedimentary diameter) has revealed an important association between foraminifera and the depositional setting providing real scope for hydraulically sorted assemblages to be identified by their common 'equivalent diameter'. Settling velocities are still significantly different between taxa even when infilling of tests is considered, showing that fractionation of species is likely to take place whether the foraminifera are filled with sea water or with sediment according to roughly the same spatial patterns.

The occurrence of spatial separation of taxa within a single flow has been directly tested using a flume model of a turbidity current simulated by a saline density flow. Results show that the slowly settling tests such as *Planorbulina mediterranensis* and *Cibicides lobatulus* remain suspended in the current for longer, and are thus transported further than more rapidly settling taxa such as *Elphidium crispum* and *Ammonia beccarii.* Deposition is not related to velocity in a simple manner but is more closely associated with the turbulent activity (TKE) in the flow. This experimental data has been related to open-ocean turbidite and contourite environments to confirm fractionation of species in high energy environments. Fractionation can be observed associated with submarine channels in recent sediments (Gulf of Cadiz) and also in older (Neogene) data (Trinidad cores). In the Gulf of Cadiz the effect of post mortem transport was clearly seen within the submarine channels where there was a marked change in assemblage composition. A high proportion of the lightest taxa were transported away from the high energy environment in the channel axis to more quiescent areas in the levees and fan areas.

Away from channels an autochthonous community existed, showing a more diverse assemblage of settling velocities within a sample.

The Trinidad core data was studied to understand the changing energy regime within muddy environments and whether it is possible to decipher a signal of fractionation within turbidite muds using foraminiferal data. A hydraulic signature was developed using the TDI (transport dominant index) and TPI (transport/pelagic index) based on settling velocity of taxa. Analysis revealed that it is possible to differentiate between an autochthonous pelagic mud and a transported assemblage within turbidite mud using this method. This information is important when investigating the extent of cap rocks to hydrocarbon fields during drilling campaigns. These results also have implications for palaeoenvironmental interpretations and help towards understanding the energy regime under which sediments are laid down. This palaeohydraulic micropalaeontology provides new insights into processes of oceanic sediment transportation and past ocean-bottom current activity.

8.2 Future work

An association has been found between the deposition of different foraminiferal taxa and distances travelled along the declining flow of a turbidity current. This has shed significant light into the processes of transportation and deposition but requires further investigation to fully understand the degree to which assemblages are modified. Suggestions for future work are as follows:

8.2.1 Settling velocities

More settling velocity experiments should be carried out on various shaped foraminifera, such as the blade shaped taxa of *Brizalina*, elongate taxa of *Siphonodosaria* and *Nodosaria* and more unusual shaped taxa such as the curling *Vaginulinopsis*. This could consolidate the data base of foraminiferal differences due to density and shape. Settling velocities can also be investigated for other calcareous groups such as microgranular and porcellaneous *Fusulinina* and *Miliolina*.

8.2.2 Volumetric calculations

More recently a more efficient way of measuring morphometric parameters has been developed in collaboration between the Natural History Museum in Basel (NMB), the University of Applied Sciences Northwestern Switzerland (FHNW), and the Geological-Paleontological Institute (GPI) of the University of Basel. AMOR (**A**utomated **M**easurement system for shell m**OR**phology) uses digital imaging and has been specifically designed for microfossils such as foraminifera (Knappertsbusch *et al.,* 2009). A greater use of this in benthic foraminiferal studies will enable more accurate calculations of size, shape and density of foraminifera.

8.2.3 Flume experiment

The behaviour of foraminiferal transport during turbidite flow has been studied using brine as a density current. Using mud rather than brine would more closely replicate the oceanic natural environment. Flocculation may occur with some shaped taxa which would be reflected in changes to an expected depositional sequence. In this study only non-cohesive particles have been considered. Cohesive-less sediments avoid the formation of flocs which could play a major role in sediment transport. Indeed the aggregation of the fine particles will increase their settling velocities and thus will decrease their transport distance within the turbidity current (Mulder *et al.*, 1997).

It has been suggested (Baas & Best, 2002) that the presence of a small clay fraction can suppress turbulence and so cause waning–collapse to occur earlier, but Baas & Best (2002) note that this also remains to be tested in large-scale flows. This means that the deposit laid down following the collapse of turbulence may only represent a small fraction of the total amount of sediment transported by the current. The TKE may affect flocculation and fragmentation processes of suspended particulate matter. Flocculation processes are very complex due to suspended particulate matter rates and organic content which may change down the canyon and fan. High turbulence within the canyon is likely to cause fragmentation while in the fan flocculation is more likely to occur.

An experiment which involves the use of mud would need to be carried out in a much larger flume such as one used by Alexander *et al.* (2008). This study utilized a flume 10 m long and 6 m wide with an input tank, pump and control valves. A volume of around 30 gallons of mud would be required with thousands of different foraminifera mixed to a Newtonian fluid before releasing into the flume. A quasi-steady flow would run for a few minutes allowing the density current to decrease in velocity downslope. The mud would then be allowed to settle before slowly draining the tank. Once empty 1 inch cores could be taken at varying distances from the exit point. These can then be individually dried and the foraminifera examined for identification and size. Heavier taxa settling out before lighter ones would reinforce previous experimental work. This would increase our understanding of the hydrodynamic behaviour of foraminifera and the possible extent to which assemblages can be modified by post mortem transport.

8.2.4 Analysis of core data

Further statistical analysis could be carried out on core data similar to that from Trinidad where turbidites are common and compared to a seafloor setting which is known to be more quiescent. Foraminifera from cores could be examined in more detail from different lateral and vertical parts of a sea floor such as a submarine channel axis, levees and fans as well as away from turbidite activity to compare hydraulic behaviour and deposition between the different energy regimes within the same oceanic basin. The signal of fractionation can be studied in more detail i.e. within centimetres rather than metres as in the Trinidad study here. It is expected that shorter time scales will reiterate the degree to which assemblages are modified by post mortem transport.

Biostratigraphic core data could be analysed in more detail encompassing sediment grain size and foraminifera to 150 μm in size. It is inferred from this study that it is examination of the fine fraction that is particularly revealing for transported assemblages. By comparing the particle size with the D_{sed} of foraminifera a greater correlation indicates turbidite activity with sorting and deposition of tests occurring in conjunction with the sediment. This would be further confirmation that the greater

the distance and time that sediment grains and foraminifera are transported, the greater the degree of sorting in the deposits that form, other conditions being equal.

8.2.5 In-situ turbidite measurements

More research is required to understand sedimentation and how it is affected by turbulence. It was stated in Chapter 5, section 5.5.3 that TKE measurements in turbidites are difficult to acquire in the field. The problem of obtaining field observations is being addressed and advancements are taking place in deployment of devices and development of instrumentation. This has led to trials with Acoustic Doppler Current Profilers (ADCPs)[8] and particle image velocimetry (PIV)[9]. The availability of higher-frequency, broad-band ADCP has enabled the estimation of turbulence parameters. Gargett (1999) developed a method for estimating the rate of dissipation of TKE from measurements of larger-scale turbulent structures using an ADCP with one beam oriented in the vertical. PIV instruments have a submersible component which is mounted on a stable seabed platform which can take measurements up to 9.75m above the sea bed. As yet this has only been deployed on shelf seas (Nimmo Smith *et al.*, 2002, 2005), so there is a need for deployment in deeper settings. Other seabed instrumentation includes STABLE (Sediment Transport And Boundary Layer Equipment). It is a tripod standing about 2.5m high and the feet occupy a circle about 3.5m in diameter: it weighs about 2,500kg and measures the interactions between turbulent currents and sediments at the sea-bed. It has been used for shelf edge and slope locations to understand sediment mobilization

[8] The ADCP exploits the Doppler effect by transmitting sound at a fixed frequency and listening to echoes returning from sound scatterers in the water column. The along-beam velocity of the scatterers (which are assumed to move with the water) is calculated from the Doppler shift of the echo. An ADCP normally has four beams inclined at 20° or 30° to the vertical. The Cartesian velocity components (u, v, w) are then calculated from the along-beam velocities.

[9] Particle image velocimetry (PIV) is a technique capable of mapping two components of the instantaneous velocity distribution within a section of a flow field. PIV is achieved by seeding the flow with microscopic tracer particles and illuminating a thin 2D plane with a laser sheet. Pulsing the laser more than once, with a known interval between pulses, while recording an image of the 2D plane leaves multiple traces of each particle on the image. A velocity distribution is then extracted from each image by measuring the mean displacement of particles within small sub-windows of the image using an autocorrelation routine.

but can be prone to toppling in storm conditions (Huthnance *et al*., 2002: Williams & Rose, 2001).

The development of new observational methods and modelling techniques has yielded deeper insight into turbulent phenomena, especially in coastal seas (Gemmrich & Farmer, 1999; Thorpe *et al.,* 2003; Umlauf & Burchard, 2005), but the consequences for mean transports of mass and suspended matter and the interaction with the sediment remain partially unresolved (Burchard *et al.,* 2008). Much more research is required to understand the processes which underlie mobilisation and sedimentation events occurring within turbidity currents. As demand for more robust equipment increases, so hopefully will the cost of equipment as technology advances.

9 Appendix

9.1 Detail of foraminifera in study

9.1.1 Foraminiferal architecture

The density of taxa varies between species due to test architecture and also structure of the bilamellar walls. Bilamellar walls are where each chamber wall is composed of two distinct lamellae of calcite on either side of a tectin membrane (a primary organic sheet), of which only the outer lamella coats previous chambers (Armstrong & Brasier, 2005; Hottinger, 2006). Wall structure consists of layering of test walls due to superposition of consecutive deposited outer lamella on exposed outer surfaces as shown in Fig.9-1. As a new chamber is added one new layer of shell material is secreted, covering the exposed earlier part of the shell (Goldstein, 2002).

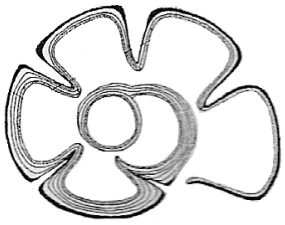

Figure 9-1 Lamination in perforate foraminifera and the construction of a supplemental skeleton by successive outer lamella (Hottinger, 2000).

This outer lamella may only cover the two previous chambers or any number of chambers depending on the morphology of the test (Sen Gupta, 2002). The thickness of each lamella may be only a few microns or less than a micron. This leads to an increase in thickness from later to earlier chambers (Hansen, 2002), which has the advantage of increasing the strength of the test wall with growth (Armstrong & Brasier, 2005).

In *Rotaliida* the amount of layering on previous chambers varies between genera altering the thickness of tests. Simple forms are where the inner lining stops at the

junction with the previous chamber, while the outer lamella continues over the exposed parts of the earlier chambers to form a secondary lamella. These are termed as ‘primary doubled-layered’ while more complex forms are termed as ‘secondary doubled-layered’ (Murray, 1971). In more intricate forms the inner lining does not stop at the junction with the previous apertural face but continues as a calcareous layer deposited onto the penultimate septum (former apertural face), leading to a three-layered septum. The ultimate septum is two-layered while the penultimate and earlier septa are three-layered. The calcareous layer covering the penultimate septum is termed the ‘septal flap’ together with a space called a rotaliid canal (Hansen, 2002). Such canal systems provide for the rapid extrusion of cytoplasm during chamber construction and reproduction (Armstrong & Brasier, 2005)

9.1.2 *Uvigerina peregrina* (Cushman 1923)

Uvigerina peregrina is from the Superfamily Buliminacea with a bilamellar wall structure (Sen Gupta, 2002). The test is conical in shape, with the chambers low, weakly inflated; surface with longitudinal costae, high and depressed with the upper margin blunt and usually serrate, changing into rows of spines on the later chambers, which are interrupted at sutures, very distinct except in the basal portion; intercostate areas and extremities of test covered with small granules and spines; aperture terminal on a short neck with a coarse lib provided with a internal hemicylindrical toothplate; wall perforated with pores of 0.3-0.6 microns (Guimerans & Currado, 1999). Average length 0.8mm (Murray, 1971) (Glossary of terms shown in Appendix 9.1.7).

Figure 9-2 SEM photograph of *Uvigerina peregrina* (Palaeo-Electronica, 2002a).

Note: *Uvigerina peregrina* is mainly infaunal living in marine environments from the shelf to the abyssal. It is mostly found in muddy sediments where there is high organic matter (Murray, 2006). Hottinger (2000) noted that the finer-grained their encasing sediment, the more longitudinal and flow-related the ornament. *U. Peregrina* has costae that flow from the aperture, down the elongated body, covering the whole shell. This suggests a kind of burrowing motility in apertural direction within a rhizopodial sheath enveloping the shell on all sides (Hottinger, 2000).

9.1.3 *Cibicides lobatulus* (Walker & Jacob 1798)

Cibicides lobatulus is from the Superfamily Planorbulinacea where the septa are primarily double-layered (Murray, 1971; Sen Gupta, 2002). The test is low trochospirally coiled with the spiral side flat or irregular and the umbilical side convex. Shape is hemispherical and often influenced by the ultimate chamber which is inflated and larger than other chambers. This epifaunal species attaches and grows around substratum, which can result in morphological variation with increased growth. Aperture is an interiomarginal arch, with a lip extending along the spiral suture on the spiral side beneath a flap. Average diameter is 0.8mm (Murray, 1971).

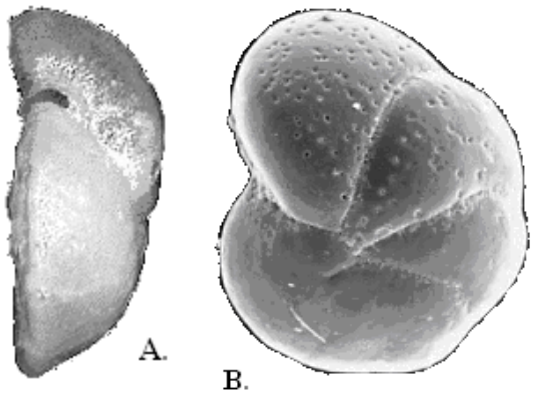

Figure 9-3 A. *Cibicides lobatulus* edge view with flattened spiral side (Palaeo-Electronica, 2001) B. Bioconvex, umbilical side with shallow umbilicus (Palaeo-Electronica, 2002) Sutures are slightly depressed on both sides. The periphery is angular and has an imperforate keel (Murray, 1971).

9.1.4 *Planorbulina mediterranensis* (d'Orbigny 1826)

Planorbulina mediterranensis is from the Superfamily Planorbulinacea where the septa are primarily double-layered (Murray, 1971; Sen Gupta, 2002). The early part of the test is trochospirally coiled but later chambers are added in a cyclical pattern (Murray, 1971). The umbilical side is slightly convex with a flat spiral side. The test is typically quadrate in outline with depressed sutures forming a flat circular shape. Each chamber has two or more lipped apertures which remain open on the spiral side after the addition of new chambers. Average diameter is 0.5 mm (Murray, 1971).

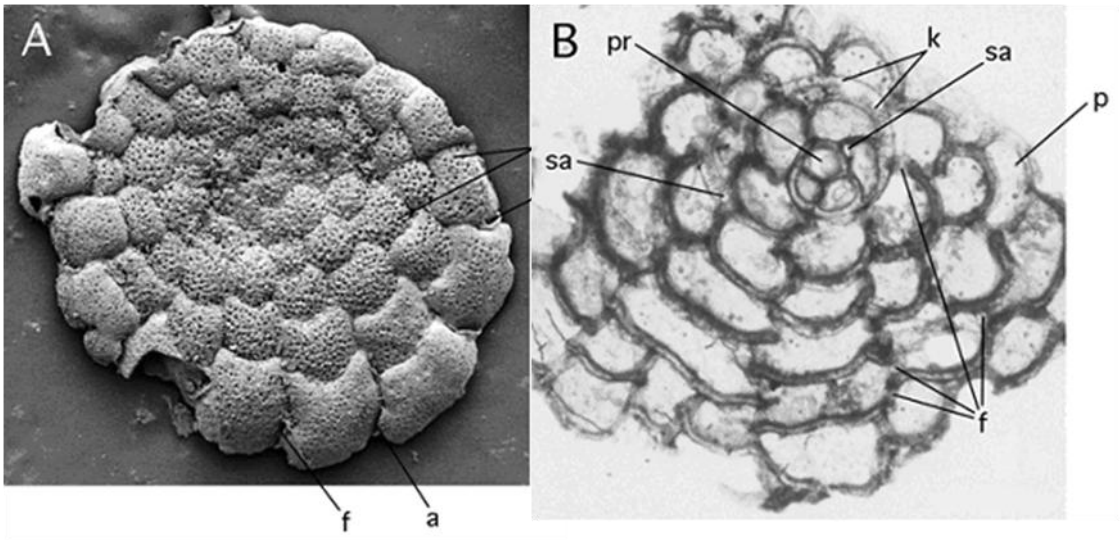

Figure 9-4 A. SEM photograph of *Planorbulina mediterranensis*, umbilical side (Hottinger, 2006). B. Transmitted light micrograph of *Planorbulina mediterranensis*. Equatorial section showing the nepionic, keeled spiral chambers followed by early chamberlet cycles with their oblique foramina and supplementary apertures where the section passes immediately below or within the attached chamber walls. **a:** aperture; **f:** foramen; **p:** pore; **pr:** proloculus; **k:** keel of the nepiont **sa:** supplementary aperture (Hottinger, 2006).

Note: *Cibicides lobatulus* and *Planorbulina mediterranensis* are both primarily double-layered but *C. lobatulus* has a few large chambers while *P. mediterranensis* has many small chambers. *P. mediterranensis* has an early growth stage similar to *C. lobatulus*, but develops into a planispiral chamber arrangement (Armstrong & Brasier, 2005). Both species are epifaunal, living mostly in shelf environments, either mobile or attached by their spiral side to seagrass and hard substrates (Murray, 2006). Attachment to irregular surfaces results in deposition of organic glues (glycoglue) fixing the shell to the substrate (Murray, 2006). Both species collect food by developing pseudopodial 'tunnels' on blades of marine grass *Poisidonia* (Arnold, 1974).

9.1.5 *Ammonia beccarii* (Linnaeus 1758)

Ammonia beccarii is from the Superfamily Rotaliacea where the septa are secondarily double-layered. The test is low trochospiral with numerous chambers forming a bioconvex ellipsoid circular in shape. On the spiral side later sutures become more deeply depressed while on the umbilical side they support tubercular growths. The central umbilicus has a calcite boss. The aperture is an interiomarginal slit. The average diameter being 0.4mm (Murray, 1971)

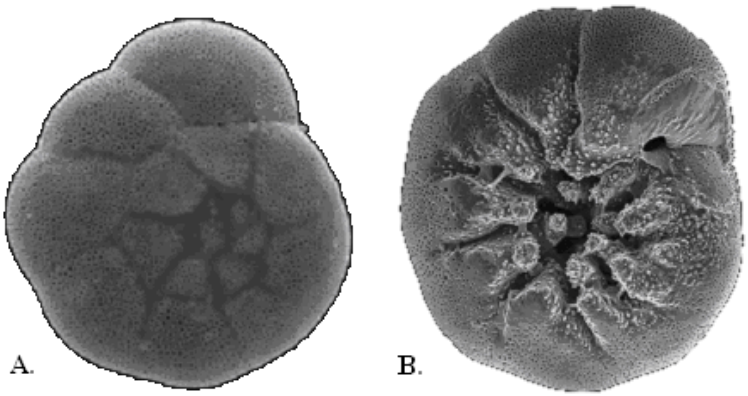

Figure 9-5 A. *Ammonia beccarii* spiral view (USGS, 2000). B. *Ammonia beccarii* umbilical side with umbilical boss or plug (USGS, 2000).

Fig.9-6 shows a diagram of a Rotaliid spiral shell similar to *Ammonia* illustrating the internal structural details and umbilical plug.

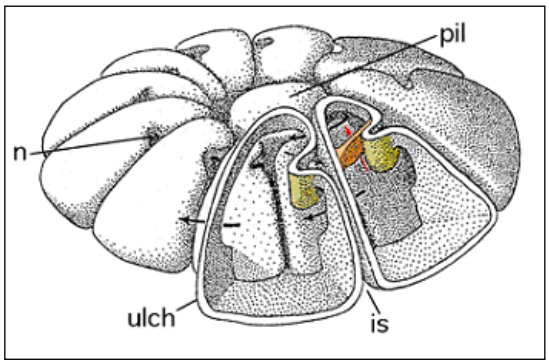

Figure 9-6 Oblique-ventral view of model showing position of cover plates and communications (not to scale, ornamentation of chamber walls omitted). **n:** notch; **pil:** umbilical plug; **ulch:** ultimate chamber; **is:** interlocular (intrasepal) space (Hottinger, 2000).

9.1.6 *Elphidium crispum* (Linnaeus 1758)

Elphidium crispum is from the Superfamily Rotaliacea where the septa are secondarily double-layered (Murray, 1971). The test is planispiral forming a lenticular bioconvex shape. The outer whorl has many narrow chambers spanned with retral processes which occupy about two thirds of the chamber width (Murray, 1971). These retral processes are posterior extensions attached to the exterior-most part of the preceding apertural face when a new chamber is added. This leads to the formation of a well-anchored final chamber with little chance of mechanical damage, in spite of the presence of deep interlocular spaces, resulting in a very strong test (Hansen, 2002). It has a central calcite boss and keeled periphery with an average diameter of 0.8mm (Murray, 1971).

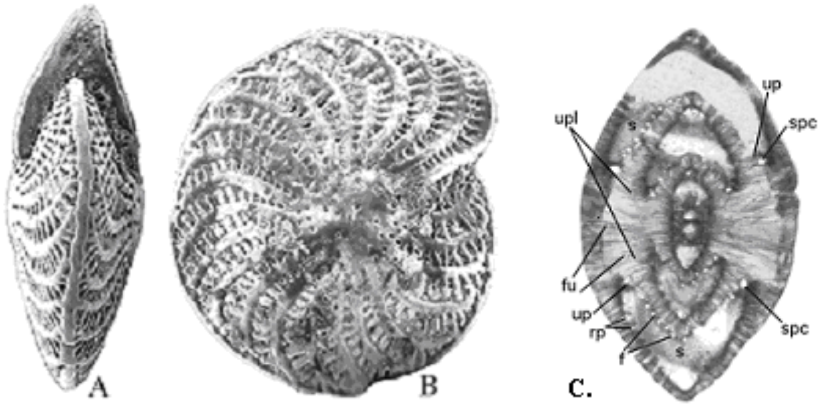

Figure 9-7 A. Side view of *Elphidium crispum* (Palaeo-Electronica, 1998). B. General view (Palaeo-Electronica, 1998). C. Transmitted light micrograph, axial section of *Elphidium craticulatum* (Fichtel et Moll), showing similar chamber arrangement to that of *Elphidium*

crispum. Note the foramina at the base of the chamber and the retral processes in the chamber roof (Hottinger, 2006). Umbilical plates vary in size within *Elphidium*; *E. craticulatum* has a broad umbilical plate with funnels, it is likely that *E. crispum's* umbilical plate is similar. **f:** foramen; **rp:** retral process; **s:** septum; **spc:** spiral canal; **up:** umbilical plate; **fu:** funnel; **upl:** umbilical plug (Hottinger, 2006).

Note: *Ammonia beccarii* and *Elphidium crispum* are both secondary double-layered forming very strong robust tests with a central boss. The central boss can produce considerable weight to the test which may enhance stability of the shell (Hottinger, 2000). Both are widespread and live in inner shelf, marginal marine environments. *A. beccarii* is infaunal found in sandy substrates while *E. crispum* is epifaunal (Murray, 2006).

9.1.7 Glossay of terms

aperture – the primary opening of the foraminiferal shell cavity towards the ambient environment

chamber lumen – a shell cavity filled with protoplasm (usually of an endoplasmic nature except in newly formed chambers), coated by an organic lining, the primary cell envelope. The term 'chamber lumen' is used in particular to distinguish between the inside and outside of a shell, ie, between intra- and interlocular spaces.

fistulose chamberlet – in agglutinated foraminifera the space produced through separation either peripherally or laterally of part of the chamber from the main chamber-lumen by a paraporous partition

foramen – plural foramina, the opening or openings that allow communication between the lumina of consecutive chambers and provide passage for functional endoplasm

funnel – a tubular (interlocular) space more or less normal to the test surface produced by secondary lamination over several whorls. Funnels originate from the margins of sutural canals or fossettes, or of foliar apertures communicating with a spiral-umbilical canal.

interlocular (intrasepal) space – a space formed as a consequence of a deeply sunken suture between consecutive chamber walls or between consecutive coils.

keel of the nepiont – a keel is a peripheral thickening of the shell and nepiont is the growth stage following the embryonic stage and different in architecture from the adult stage

notch – a single indentation of the proximal chamber wall in a sutural position. It marks the limit between a spiral main chamber and its folium and may extend into an internal infold.

pore – a minute tubular perforation traversing a lamellar chamber wall, coated internally by an organic sheathe

proloculus – the initial chamber of the foraminiferal test without nepionic differentiation. Usually a proloculus has a spherical outline and a single aperture.

retral process – finger-like proximally directed extensions of the chamber lumen covered by ponticuli present at the margins of an intraseptal interlocular space (ponticuli is a bridge of lateral wall spanning an intraseptal interlocular space)

septum – a wall separating two consecutive main chamber lumina, ie. the portion of the free chamber wall that is covered by subsequent chambers and thus incorporated in the architecture of the shell as a partition between successive main chamber lumina.

spiral canal – a more or less tubular or flattened space between the umbilical plates and the wall of the preceding coil or between plates, folia and the preceding foil; or between toothplates and the preceding coil.

supplementary aperture – primarily formed openings either in the apertural face or in a sutural position, always in addition to a main cameral aperture.

umbilical plate – a more or less contorted plate-like test element, extending between distal and proximal chamber walls and joined by both, attached to the intercameral foramen and to the main aperture, but not protruding into the latter. Separates the main chamber lumen from a primary umbilical-spiral canal. Between the plate and the adjacent coil or within the plate itself and opening provides connection between chamber and foliar chamberlet, whenever present.

umbilical plug – a pile of lamellae forming a solid, more or less free standing plug in the centre of the umbilicus, often separated from foliar tips by a spiral fissure

ultimate chamber – the last chamber formed in an individual.

9.2 Measurement data

Species	Settling velocity (m/s)	Diameter/ length (mm)	Mass (mg)	Volume (mm^3)	Density in water (kg/m^3)	Reynolds	Drag
Elphidium	0.0591	0.740	0.240	0.153	1857.6	43.5	2.4
crispum	0.0534	0.783	0.197	0.142	1759.5	41.6	2.7
	0.0519	0.710	0.190	0.141	1737.2	36.7	2.6
	0.0429	0.745	0.136	0.116	1644.9	31.8	3.4
	0.0405	0.725	0.117	0.109	1585.6	29.3	3.4
	0.0377	0.615	0.097	0.103	1515.7	23.1	2.9
	0.0349	0.700	0.088	0.098	1491.1	24.3	3.7
	0.0349	0.635	0.084	0.090	1508.7	22.1	3.5
	0.0327	0.645	0.059	0.073	1440.4	21.0	3.5
	0.0311	0.575	0.050	0.069	1397.2	17.8	3.1
	0.0265	0.555	0.044	0.057	1424.3	14.7	4.4
	0.0254	0.550	0.040	0.048	1451.8	13.9	5.1
	0.0238	0.545	0.039	0.048	1448.6	12.9	5.7
	0.0230	0.475	0.038	0.042	1500.6	10.9	5.9
	0.0220	0.451	0.032	0.033	1537.9	9.9	6.6
	0.0199	0.415	0.024	0.023	1560.6	8.2	7.7
	0.0186	0.375	0.022	0.021	1563.2	6.9	8.0
	0.0186	0.385	0.022	0.021	1564.0	7.1	8.3
	0.0172	0.335	0.020	0.018	1609.6	5.7	9.1
	0.0154	0.293	0.013	0.008	1867.2	4.5	14.1
Uvigerina	0.0434	0.960	0.177	0.174	1557.7	41.5	3.7
peregrina	0.0427	1.005	0.161	0.132	1668.5	42.8	4.8
	0.0429	0.790	0.134	0.106	1695.4	33.7	3.9
	0.0353	0.870	0.083	0.090	1503.7	30.6	4.6
	0.0346	0.710	0.078	0.075	1571.1	24.5	4.4
	0.0330	0.650	0.077	0.066	1639.2	21.4	5.0
	0.0309	0.700	0.060	0.062	1533.3	21.6	5.1
	0.0295	0.580	0.044	0.044	1547.6	17.0	4.8
	0.0292	0.620	0.036	0.040	1497.6	18.1	4.7
	0.0278	0.630	0.034	0.033	1564.2	17.4	6.1
	0.0262	0.570	0.023	0.029	1440.0	14.9	4.8
	0.0261	0.540	0.022	0.024	1497.6	14.0	5.2
	0.0252	0.590	0.020	0.022	1497.6	14.8	6.1
	0.0228	0.570	0.019	0.022	1472.6	12.9	6.8
	0.0222	0.500	0.014	0.020	1386.6	11.1	5.2
	0.0209	0.480	0.013	0.018	1403.9	10.0	5.8
	0.0187	0.460	0.013	0.018	1403.9	8.5	7.0
	0.0180	0.430	0.011	0.018	1341.5	7.7	6.0
	0.0181	0.440	0.009	0.011	1447.6	7.9	7.9
	0.0174	0.360	0.009	0.009	1560.1	6.2	8.8

Species	**Settling velocity (m/s)**	**Diameter/ length (mm)**	**Mass (mg)**	**Volume (mm^3)**	**Density in water (kg/m^3)**	**Reynolds**	**Drag**
Ammonia	0.0372	0.556	0.047	0.053	1488.0	20.6	2.6
beccarii	0.0354	0.493	0.040	0.034	1640.7	17.4	3.3
	0.0305	0.467	0.029	0.031	1517.2	14.2	3.4
	0.0293	0.461	0.024	0.023	1579.3	13.5	4.1
	0.0272	0.346	0.022	0.019	1644.9	9.4	4.0
	0.0258	0.304	0.013	0.012	1603.6	7.8	3.6
	0.0263	0.325	0.012	0.011	1582.9	8.5	3.6
	0.0234	0.304	0.009	0.009	1535.1	7.1	3.9
	0.0237	0.304	0.009	0.009	1576.5	7.2	4.1
	0.0226	0.299	0.007	0.008	1464.6	6.7	3.6
	0.0218	0.273	0.007	0.007	1524.1	5.9	4.0
	0.0216	0.278	0.006	0.007	1499.3	6.0	3.9
	0.0200	0.257	0.006	0.007	1501.0	5.1	4.2
	0.0190	0.262	0.005	0.006	1468.9	5.0	4.5
	0.0154	0.241	0.005	0.006	1471.8	3.7	6.3
	0.0142	0.246	0.004	0.006	1389.2	3.5	6.3
	0.0125	0.225	0.004	0.005	1404.9	2.8	7.7
	0.0122	0.262	0.003	0.005	1306.2	3.2	7.1
	0.0106	0.236	0.003	0.005	1318.1	2.5	8.8
	0.0096	0.225	0.002	0.004	1303.1	2.2	9.7
Cibicides	0.0236	0.670	0.046	0.079	1320.0	15.7	5.1
lobatulus	0.0224	0.643	0.042	0.069	1331.4	14.3	5.6
	0.0205	0.615	0.033	0.061	1296.7	12.5	5.7
	0.0202	0.560	0.032	0.046	1381.6	11.3	6.9
	0.0201	0.550	0.030	0.043	1377.6	11.0	6.8
	0.0199	0.520	0.025	0.037	1372.3	10.3	6.5
	0.0197	0.510	0.025	0.035	1394.8	10.0	6.8
	0.0197	0.495	0.022	0.032	1379.9	9.7	6.4
	0.0191	0.465	0.022	0.026	1458.7	8.8	7.7
	0.0183	0.465	0.022	0.026	1458.7	8.5	8.3
	0.0169	0.460	0.020	0.025	1430.6	7.8	9.1
	0.0169	0.405	0.019	0.017	1600.2	6.8	11.3
	0.0168	0.395	0.015	0.016	1510.5	6.6	9.4
	0.0167	0.395	0.014	0.016	1476.3	6.6	8.8
	0.0161	0.380	0.012	0.014	1458.5	6.1	8.9
	0.0152	0.365	0.012	0.013	1517.6	5.5	10.8
	0.0140	0.345	0.010	0.011	1510.8	4.8	11.8
	0.0126	0.295	0.009	0.007	1736.2	3.7	18.1
	0.0110	0.275	0.008	0.005	1808.0	3.0	24.2
	0.0091	0.270	0.005	0.005	1532.9	2.4	23.1

Species	**Settling velocity (m/s)**	**Diameter/ length (mm)**	**Mass (mg)**	**Volume (mm^3)**	**Density in water (kg/m^3)**	**Reynolds**	**Drag**
Planorbulina	0.0137	0.610	0.028	0.026	1583.4	24.8	0.15
mediterranensis	0.0142	0.575	0.025	0.026	1527.4	19.7	0.17
	0.0142	0.539	0.025	0.023	1600.5	21.0	0.19
	0.0138	0.529	0.024	0.022	1598.4	21.7	0.19
	0.0126	0.535	0.016	0.018	1487.2	21.6	0.15
	0.0126	0.475	0.016	0.018	1494.5	19.4	0.21
	0.0121	0.530	0.012	0.018	1371.8	17.9	0.15
	0.0115	0.456	0.011	0.016	1368.3	16.6	0.22
	0.0114	0.470	0.011	0.016	1385.3	18.3	0.19
	0.0110	0.440	0.011	0.014	1440.0	21.0	0.20
	0.0111	0.455	0.010	0.013	1420.7	20.6	0.18
	0.0103	0.405	0.009	0.013	1382.1	19.2	0.25
	0.0103	0.400	0.008	0.013	1348.0	17.2	0.25
	0.0096	0.435	0.007	0.012	1321.7	19.9	0.18
	0.0092	0.375	0.006	0.010	1329.9	19.4	0.24
	0.0095	0.390	0.006	0.010	1344.1	19.7	0.21
	0.0088	0.363	0.004	0.008	1264.3	16.5	0.22
	0.0085	0.341	0.004	0.007	1299.0	18.6	0.23
	0.0081	0.227	0.001	0.003	1167.8	7.7	0.35
	0.0078	0.248	0.001	0.004	1140.8	7.7	0.32

9.3 Regional Biostratigraphic zonation for NCMA, Trinidad

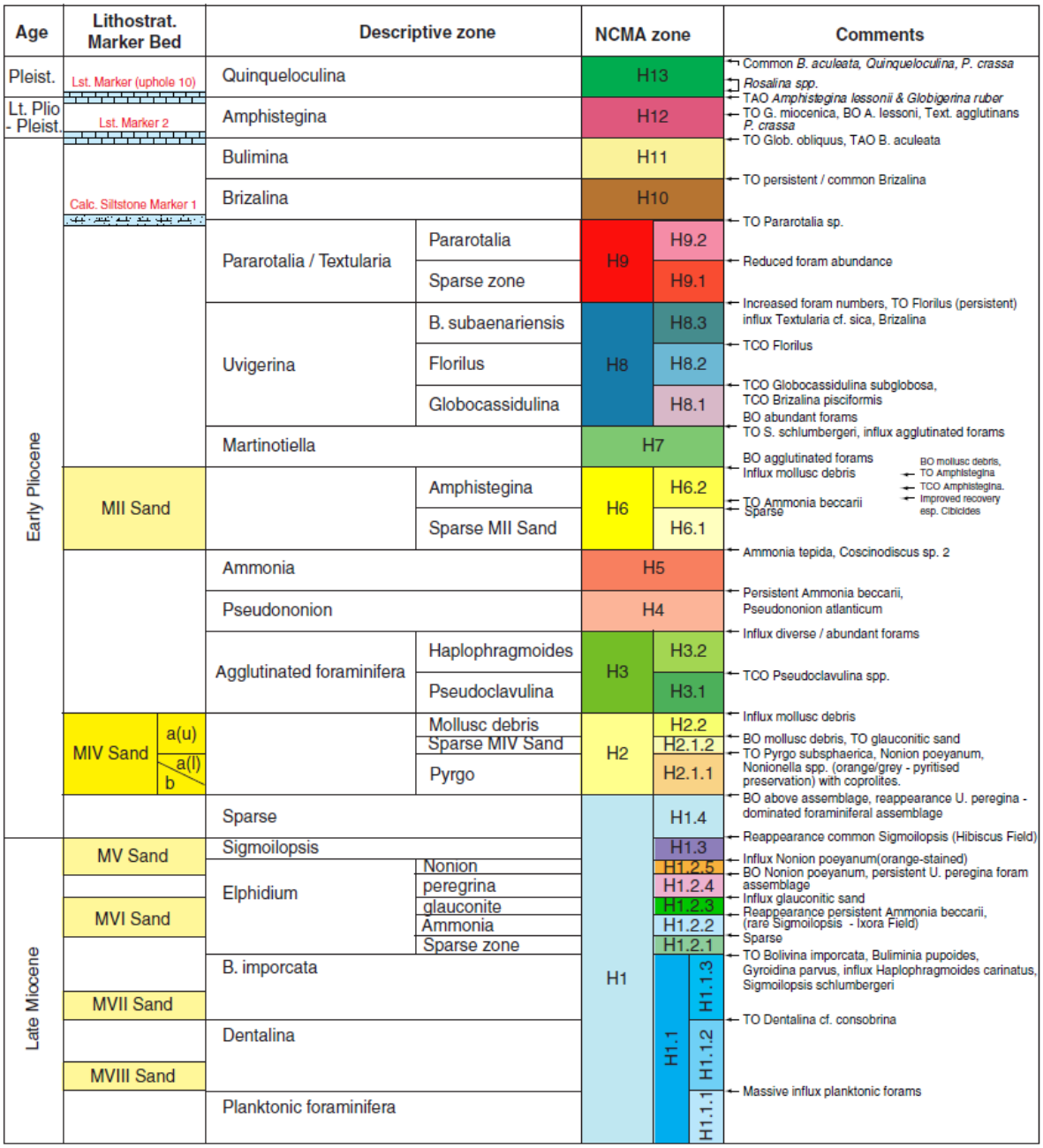

9.4 Trinidad taxa characteristics

Species	Superfamily	Family	Shape	Architecture	D_{sed} (μm)	Ws (cm/s)
Ammonia beccarii	Rotaliacea	Rotaliidae	oval	low trochospiral	303	2.63
Ammonia tepida	Rotaliacea	Rotaliidae	oval	low trochospiral	303	2.63
Amphistegina lessoni	Asterigerinacea	Amphisteginidae	lenticular	trochospiral	1031	4.85
Amphistegina spp.	Asterigerinacea	Amphisteginidae	lenticular	trochospiral	719	4.05
Angulogerina spp.	Buliminacea	Uvigerinidae	conical	high trochospiral	202	2.15
Anomalinoides flintii	Chilostomellacea	Gavelinellidae	oval	low trochospiral	377	2.79
Anomalinoides spp.	Chilostomellacea	Gavelinellidae	oval	low trochospiral	346	2.81
Anomalinoides trinitatensis	Chilostomellacea	Gavelinellidae	oval	low trochospiral	341	2.65
Archaias angulatus	Soritacea	Soritidae	oval	planispiral	1144	5.11
Articulina atlantica	Miliolacea	Tubinellidae	plum	coiled	105	1.47
Asterigerina spp.	Asterigerinacea	Asterigerinidae	oval	trochospiral	179	2.02
Bolivina imporcata	Bolivinacea	Bolivinidae	conical	biserial	249	2.38
Bolivina isidroensis	Bolivinacea	Bolivinidae	conical	biserial	249	2.38
Bolivina lohmani	Bolivinacea	Bolivinidae	conical	biserial	155	1.88
Bolivina suteri	Bolivinacea	Bolivinidae	conical	biserial	202	2.15
Bolivina floridana	Bolivinacea	Bolivinidae	conical	biserial	212	2.20
Brizalina alata	Bolivinacea	Bolivinidae	conical	biserial	296	2.60
Brizalina barbata	Bolivinacea	Bolivinidae	concial	biserial	202	2.15
Brizalina lanceolata	Bolivinacea	Bolivinidae	conical	biserial	202	2.15
Brizalina pisciformis	Bolivinacea	Bolivinidae	conical	biserial	249	2.38
Brizalina spp.	Bolivinacea	Bolivinidae	conical	biserial	202	2.15
Brizalina striatula	Bolivinacea	Bolivinidae	conical	biserial	202	2.15
Brizalina subaenariensis gp.	Bolivinacea	Bolivinidae	conical	biserial	387	2.97

Brizalina subaenariensis mexicana	Bolivinacea	Bolivinidae	conical	biserial	387	2.97
Brizalina subaenariensis westermanni	Bolivinacea	Bolivinidae	conical	biserial	387	2.97
Brizalina lohmani	Bolivinacea	Bolivinidae	conical	biserial	273	2.50
Bulimina aculeata	Buliminacea	Buliminidae	conical	triserial	158	1.80
Bulimina marginata	Buliminacea	Buliminidae	plum	triserial	235	2.20
Bulimina pupoides	Buliminacea	Buliminidae	plum	triserial	168	1.86
Bulimina striata	Buliminacea	Buliminidae	conical	triserial	179	1.92
Bulimina spp.	Buliminacea	Buliminidae	plum	triserial	185	1.95
Buliminella cf. picaensis	Buliminacea	Buliminellidae	plum	high trochospiral	136	1.67
Buliminella spp.	Buliminacea	Buliminellidae	plum	high trochospiral	105	1.47
Bulininella picaensis	Buliminacea	Buliminellidae	plum	high trochospiral	136	1.67
Cancris auriculus	Discorbadea	Bagginidae	lenticular	low trochospiral	446	3.03
Cancris sagrai.	Discorbadea	Bagginidae	lenticular	low trochospiral	446	3.03
Cancris spp.	Discorbadea	Bagginidae	lenticular	low trochospiral	446	3.03
Cassidulina laevigata	Cassidulinacea	Cassidulinidae	lenticular	planispiral	125	1.23
Cassidulina spp.	Cassidulinacea	Cassidulinidae	lenticular	planispiral	74	1.60
Ceratobulimina spp.	Ceratobuliminacea	Ceratobuliminidae	oval	trochospiral	235	2.20
Chilostomella ovoidea	Chilostomellacea	Chilostomellidae	plum	low trochospiral	222	2.02
Chilostomelloides spp.	Chilostomellacea	Chilostomellidae	plum	low trochospiral	390	2.68
Cibicides pachyderma	Planorbulinacea	Cibicididae	hemispherical	low trochospiral	276	2.26
Cibicides pseudoungerianus	Planorbulinacea	Cibicididae	hemsipherical	low trochospiral	276	2.26
Cibicides spp.	Planorbulinacea	Cibicididae	hemispherical	low trochospiral	170	1.77
Cibicidoides mantaensis	Planorbulinacea	Cibicididae	hemispherical	low trochospiral	304	2.37
Cibicidoides spp	Planorbulinacea	Cibicididae	hemispherical	low trochospiral	222	2.02
Dentalina cf. consobrina	Nodosariacea	Nodosariidae	elongate	uniserial	189	1.87
Dentalina spp.	Nodosariacea	Nodosariidae	elongate	uniserial	176	1.80

Discorbis spp.	Discorbacea	Discorbidae	hemispherical	low trochospiral	222	2.02
Elphidium discoidale	Rotaliacea	Elphidiidae	Oval	planispiral	479	3.30
Elphidium spp.	Rotaliacea	Elphidiidae	lenticular	planispiral	137	1.77
Epistominella spp.	Discorbinellacea	Pseudoparrellidae	oval	low trochospiral	47	0.98
Eponides parantillarum	Discorbacea	Eponididae	oval	low trochospiral	305	2.51
Eponides praecinctus	Discorbacea	Eponididae	hemispherical	low trochospiral	341	2.65
Eponides repandus	Discorbacea	Eponididae	lenticular	low trochospiral	446	3.03
Eponides spp.	Discorbacea	Eponididae	lenticular	low trochospiral	340	2.65
Fissurina spp.	Polymorphinacea	Ellipsolagenidae	oval	single chamber	144	1.63
Florilus triangulare	Nonionacea	Nonionidae	oval	planispiral	303	2.63
Frondicularia spp.	Nodosariacea	Nodosariidae	conical/flat	biserial	164	1.74
Fursenkoina pontoni	Fursenkoinacea	Fursenkoinidae	elongate	twisted biserial	290	2.45
Fursenkoina spp.	Fursenkoinacea	Fursenkoinidae	elongate	twisted biserial	275	2.38
Fursenkoina sp.1	Fursenkoinacea	Fursenkoinidae	elongate	twisted biserial	300	2.49
Globobulimina pacifica	Buliminacea	Buliminidae	plum	triserial	414	2.92
Globocassidulina subglobosa	Cassidulinacea	Cassidulinidae	round	planispiral	47	0.98
Gypsina? spp.	Acervulinacea	Acervulinidae	round	spiral	332	2.47
Gyroidina neosoldanii	Chilostomellacea	Gavelinellidae	oval	high trochospiral	390	2.98
Gyroidina spp.	Chilostomellacea	Gavelinellidae	oval	trochospiral	390	2.98
Gyroidinoides byramensis	Chilostomellacea	Gavelinellidae	hemispherical	trochospiral	947	4.65
Gyroidinoides parvus	Chilostomellacea	Gavelinellidae	hemispherical	trochospiral	139	1.78
Gyroidinoides venezuelanus	Chilostomellacea	Gavelinellidae	hemispherical	trochospiral	179	2.02
Hanzawaia americana	Chilostomellacea	Gavelinellidae	oval	low trochospiral	332	2.47
Hanzawaia concentrica	Chilostomellacea	Gavelinellidae	oval	low trochospiral	390	2.68
Hanzawaia spp.	Chilostomellacea	Gavelinellidae	oval	low trochospiral	527	3.30
Haynesina germanica	Nonionacea	Nonionidae	oval	planispiral	346	2.81
Hoeglundina elegans	Ceratobuliminacea	Epistominidae	lenticular	trochospiral	307	2.51

Lagena spp.	Nodosariacea	Lagenidae	elongate	single chamber	123	1.51
Lagena sulcata	Nodosariacea	Lagenidae	phial	single chamber	140	1.70
Lenticulina americana	Nodosariacea	Vaginulinidae	lenticular	planispiral	520	3.42
Lenticulina atlantica	Nodosariacea	Vaginulinidae	lenticular	planispiral	375	2.78
Lenticulina calcar	Nodosariacea	Vaginulinidae	lenticular	planispiral	440	3.17
Lenticulina cf. americana grandis	Nodosariacea	Vaginulinidae	lenticular	planispiral	819	4.32
Lenticulina occidentalis	Nodosariacea	Vaginulinidae	lenticular	planispiral	966	4.46
Lenticulina 'pauciloculata'	Nodosariacea	Vaginulinidae	lenticular	planispiral	356	2.85
Lenticulina peregrina	Nodosariacea	Vaginulinidae	lenticualr	planispiral	440	3.17
Lenticulina spp.	Nodosariacea	Vaginulinidae	lenticular	planispiral	440	3.17
Lingulina spp.	Nodosariacea	Nodosariidae	conical	uniserial	522	3.45
Marginulina spp.	Nodosariacea	Vaginulinidae	elongate	serial, coiled	200	2.03
Nodosaria ewaldi	Nodosariacea	Nodosariidae	elongate	uniserial	176	1.80
Nodosaria spp.	Nodosariacea	Nodosariidae	elongate	uniserial	164	1.74
Nodosaria vertebralis	Nodosariacea	Nodosariidae	elongate	uniserial	183	1.83
Nonion poeyanum	Nonionacea	Nonionidae	oval	planispiral	261	2.44
Nonionella spp.	Nonionacea	Nonionidae	oval	planispiral	219	2.24
Oridosalis umbonatus	Chilostomellacea	Oridorsalidae	lenticular	low trochospiral	152	1.77
Pararotalia spp.	Rotaliacea	Rotaliidae	oval	low trochospiral	204	2.16
Planulina crassa	Planorbulinacea	Planulinidae	flat disc	low trochospiral to planispiral	126	1.53
Planulina mantaensis	Planorbulinacea	Planulinidae	flat disc	low trochospiral to planispiral	356	2.56
Planulina sp.1	Planorbulinacea	Planulinidae	flat disc	low trochospiral to planispiral	440	2.85
Pseudononion atlanticum	Nonionacea	Nonionidae	oval	planispiral	139	1.78
Pullenia spp.	Nonionacea	Nonionidae	round	planispiral	261	2.44
Pyramidulina stainforthi	Nodosariacea	Nodosariidae	elongate	uniserial	322	2.58

Pyrgo denticulata	Miliolacea	Hauerinidae	oval	round initial chamber	276	2.26
Pyrgo spp.	Miliolacea	Hauerinidae	oval	round initial chamber	276	2.26
Pyrgo subsphaerica	Miliolacea	Hauerinidae	oval	round initial chamber	332	2.47
Quinqueloculina lamarkiana	Miliolacea	Hauerinidae	oval	overlapping chambers	305	2.51
Quinqueloculina seminula	Miliolacea	Hauerinidae	oval	overlapping chambers	168	1.86
Quinqueloculina spp.	Miliolacea	Hauerinidae	oval	overlapping chambers	235	2.20
Reussella atlantica	Buliminacea	Reussellidae	conical	triserial	342	2.79
Reussella spp.	Buliminacea	Reussellidae	conical	triserial	226	2.27
Rosalina spp.	Discorbacae	Rosalinidae	hemispherical	low trochospiral	222	2.02
Sigmoilopsis schlumbergeri	Miliolacea	Hauerinidae	oval	round initial chamber	305	2.51
Siphogenerina senni	Buliminacea	Siphogenerinoididae	elongate	biserial	320	2.70
Siphogenerina spp.	Buliminacea	Siphogenerinoididae	elongate	triserial/ biserial	320	2.70
Siphonina pulchra	Siphoninacea	Siphoninidae	lenticular	low trochospiral	211	2.09
Siphonina spp.	Siphoninacea	Siphoninidae	lenticular	low trochospiral	211	2.09
Siphonodosaria spp.	Stilostomellacea	Stilostomellidae	elongate	uniserial	164	1.74
Sphaeroidina bulloides	Discorbacea	Sphaeroidinidae	round	overlapping chambers	222	2.02
Sphaeroidina bulloides (large forms)	Discorbacea	Sphaeroidinidae	round	overlapping chambers	332	2.47
Spiroloculina spp.	Miliolacea	Spiroloculinidae	flat disc	coiled tubular	410	2.91
Triloculina gracilis	Miliolacea	Hauerinidae	oval	overlapping chambers	305	2.51
Triloculina linneiana	Miliolacea	Hauerinidae	oval	overlapping chambers	683	3.75
Triloculina spp.	Miliolacea	Hauerinidae	oval	overlapping chambers	683	3.75
Uvigerina isidroensis	Buliminacea	Uvigerinidae	conical	triserial	226	2.27
Uvigerina peregrina	Buliminacea	Uvigerinidae	conical	triserial	387	2.97
Uvigerina rugosa	Buliminacea	Uvigerinidae	conical	triserial	296	2.60
Uvigerina rustica	Buliminacea	Uvigerinidae	conical	triserial	342	2.79
Uvigerina rutila	Buliminacea	Uvigerinidae	conical	triserial	296	2.60
Uvigerina spp.	Buliminacea	Uvigerinidae	conical	triserial	342	2.79

Vaginulinopsis subaculeata glabrata	Nodosariacea	Vaginulinidae	oval	coiled multichambered	763	3.97
Vaginulinopsis superbus	Nodosariacea	Vaginulinidae	elongate	coiled multichambered	927	4.37
Vaginulinopsis spp.	Nodosariacea	Vaginulinidae	oval	coiled multichambered	845	4.17
Valvulineria venezuelana	Discorbacea	Bagginidae	oval	low trochospiral	377	2.79

9.5 Laboratory experiments which did not work

9.5.1 Measurement of density

Several methods were attempted to measure density. Individual foraminifera were too small and light to use the traditional hydrometer where water volume is displaced by an object of known mass. A high density separating fluid was tried to see if distinct tests settled out at different fluid densities. The idea was that the foraminifera would initially remain at the top of the fluid, then the density of the fluid would gradually be diluted until the foraminifera sunk to the bottom of the beaker. Sodium polytungstate [$Na_6(H_2W_{12}O_{40})H_2O$] is a non-toxic, high density (1·0–3·1 g/cm^3) separating compound which generates an almost neutral solution (pH 6) of relatively low viscosity (Madella *et al.*, 1998). Using this SPT did not work as the tests attached to the surface meniscus and would not fall unless turbulence was introduced. Problems also arose when adding water with a pipette to the beaker to gradually dilute the solution as this resulted in varying densities within the fluid.

A gas pycnomter was also tried; this uses helium displacement to determine absolute density of particles. The pycnometer determines volume and density by measuring the pressure change of helium in a calibrated volume. The AccuPyc 1330 pycnomter was used which has a cylinder size of 1 cm^3 with a capacity to reduce this to a smaller chamber of 0.25 cm^3. This was trialed with various foraminiferal species but their volume not large enough to displace enough gas to register on the report.

9.5.2 Settling velocity trials

Five samples of each species were initially selected to find the best method for observing and capturing the falling tests. Two methods were undertaken to find the most effective way to observe the falling foraminifera and recapturing them for retrial. As the capture net was white the foraminifera were dyed to increase visibility when retrieving after settling. Initially foraminifera were stained with Alizarin Red by immersing in the dye for a minute before conducting tests. Alizarin Red is a

solute in 1½% HCl and it was noted that with delicate tests such as *Planorbulina* and *Cibicides*, the chambers showed some evidence of dissolution once dyed. Therefore Methylene Blue stain was used. This is a heterocyclic aromatic chemical compound that is a solid, odorless, dark green powder, yielding a blue solution when dissolved in water or a weak solution of ethanol. The calcite tests took up enough stain to turn them dark; making observation easier. The stain remained where there was organic matter which was most easily seen in the pores. This is because most empty foraminiferal tests result from asexual or sexual reproduction leaving behind a few organic substances (especially in the test walls) (Yordanova & Hohenegger, 2007). Settling trials were conducted on specimens without the stain and repeated when stained. No difference in settling times where found. Observation was improved by placing a white card behind the settling tube and using a strong light directed towards the cylinder.

The second method was to dye the capture net rather than the foraminifera. The white mesh of the capture net is nylon and therefore non-porous and would not easily dye. The best result was obtained by using a black permanent marker pen. The tests were most easily observed when a bright light and black paper were placed behind the tube. The 'sparkle' of the foraminifera was observed as they fell through the water column. Therefore experiments were carried out without staining the tests and by staining the capture net black.

9.5.3 Flume trials for Experiment 4

Trials were carried out using a diffuser box at the pipe exit enabling a subcritical flow to be produced straight from the exit point. (The diffuser unit was attached to the pipe exit, being 20 cms high, 20 cms long and 3 cms wide containing gravel constrained by fine wire to promote alignment of flow from the unit). The foraminifera were placed in front of the wire and became entrained into the flow as it entered the flume. The subcritical flow eliminated the hydraulic jump where an initial velocity of 0.14 ms^{-1} was more than enough to entrain the foraminifera; but this system did not produce a forward motion of tests. Some of the foraminifera

deposited to the side with the lighter ones being more affected by turbulence. The foraminifera were therefore placed at various distances from the exit in an attempt to generate forward motion of all taxa. Several runs were carried out with entrainment of all species occurring 10cms from the exit where initial velocities were 0.08ms^{1} (which was still high enough to entrain the foraminifera).

None of the forams travelled very far, with deposition occurring within the first 50 cms towards the sides of the flume. This behaviour was more marked with the lighter species which tended to deposit out first towards the sides of the flume. This can be attributed to the buoyancy associated with the fluid motion near the head of the gravity current, see Fig.9-8.

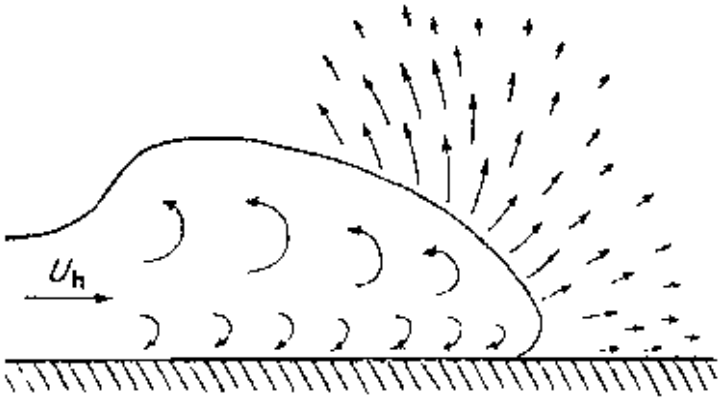

Figure 9-8 Fluid motion in and near the head of a gravity current. Motion relative to the ground. The current vectors shown in the ambient medium are to be compared with the vector for *Uh* (velocity of the head) (Allen, 1977).

The lighter foraminifera have neutral buoyancy and were merely displaced away from the bed as the saline density flow arrived. Being of greater density in comparison to the freshwater in the flume, a strong shear but little associated turbulence developed at the base of the displaced flume water. This displaced water had non forward velocity and low turbulence. Therefore, the displaced foraminifera could not enter the higher density gravity flow even in the slower flowing tail region. Consequently, they remained in the displaced water mass and finally settle back to the bed once the gravity flow has passed by. The heavier taxa become entrained into

the turbulent zone at the rear of the head where large, rapidly circulating vortices occur, enabling them to be carried in the flow. Consequently they were therefore transported forward and travelled greater distances before depositing out as the velocity waned. This resulted in a reverse signal of deposition with the lighter taxa depositing out before the heavier taxa.

A similar scenario has been noted by Pritchard & Gladstone (2009) where 'lofting' of fine grained sediment in turbidity currents has been suggested. In thinly bedded turbidites there is a tendency for fine sediment to be carried higher in the current while heavier sediment is carried in the lower part of the current. A rising buoyant cloud is enhanced which leads to preferential dumping of coarser fractions from the basal flow and transportation of the fines into the water column by the cloud and away from the depositional site by cross-currents. This can lead to the rhythmic layering of fine sand and mud, which is often characteristic of thinly-bedded turbidites and may be the result of deposition from lofting turbidity currents. The fine sand represents deposition from the ground-hugging component and the mud the rainout from the non-stripped cloud (Prichard & Gladstone, 2009).

From these results it was apparent that the foraminifera needed to be within the turbidity current at these low initial velocities, before the flow entered the ambient water. Therefore in the final experiment all taxa were entrained within the density current reducing the likelihood of 'lofting' of lighter foraminifera. The short distances travelled also indicated a relatively high density flow was required to retain the velocity and travelling distances down the flume.

10 References

Ahrens, J.P. 2000. The fall-velocity equation. **Journal of Waterway, Port, Coastal and Ocean engineering 126 (2),** 99-102

Allen, J.R.L. 1977. *Physical Processes of Sedimentation*. 4th impression with revised readings. George Allen and Unwin Ltd., London

Allen, J.R.L. 1984. Experiments on the settling, overturning and entrainment of bivalve shells and related models. **Sedimentology 31**, 227–250

Alexander, J., McLelland, S.J., Gray, T.E., Vincent, C.E., Leeder, M.R. & Ellett, S. 2008. Laboratory sustained turbidity currents form elongate ridges at channel mouths. **Sedimentology 55,** 845-868

Alexander, J. & Mulder, T. 2002. Experimental quasi-steady density currents. **Marine Geology 186,** 195-210

Altenbach, A.V., Pflaumann, U., Schiebel, R., Thies, A., Timm, S. & Trauth, M., 1999. Scaling percentages and distributional patterns of benthic foraminifera with flux rates of
organic carbon. **Journal of Foraminiferal Research 29**, 173–185.

Alve, E. 1995. Benthic foraminiferal responses to estuarine pollution, a review. **Journal of Foraminiferal Research 25,** 190–203

Amy, L., Talling, P., Edmonds, V., Sumner, E. & Lesueur, A. 2006. An experimental investigation on sand–mud suspension settling behaviour: implications for bimodal mud contents of submarine flow deposits**. Sedimentology 53**, 1411–1435

Armstrong, H.A. & Brasier, M.D. 2005. Foraminifera. In: *Microfossils*. 2nd Edition. Blackwell Publishing, Oxford, UK, pp142-187

Arnold, Z.M. 1974. Field and laboratory techniques for the study of living foraminifera. In: Hedley, R.H. & Adams, C.G. (Eds) *Foraminifera: Volume 1*. Academic Press, London

Ayress, M., Holmes, N. & Cater, J. 2004. *A Biostratigraphical and Sedimentological
summary of the NCMA drilling campaign, focusing on the Early Pliocene MII and MIV Sand reservoir intervals.* Prepared for British Gas Trinidad & Tobago Ltd. Ichron Ltd., March 2004, Ref: 03/666/B/S

Baas, J.H. 2004. Conditions of formation of massive turbiditic sandstones by primary depositional processes: **Sedimentary Geology 166**, 293–310

Baas, J.H. & Best, J.L. 2002. Turbulence modulation in clay-rich sediment-laden flows and some implications for sediment deposition. **Journal of Sedimentary Research 72 (3),** 336–340

Baas, J.H., McCaffrey, W.D., Haughton, P.D.W. & Choux, C. 2005. Coupling between suspended sediment distribution and turbulence structure in laboratory turbidity current. **Journal of Geophysical Research 110**, C11, CitelD C11015, doi:10.1029/ 2004JC002668.

Baas, J.H., Van Dam, R. & Storms, J. 2000. Duration of deposition from decelerating high-density turbidity currents. **Sedimentary Geology 136**, 71–88

Baba, J. & Komar, P.D. 1981. Measurements and analysis of settling velocities of natural sand grains. **Journal of Sedimentary Petrology 51**, 631–640

Babinneau, N., Savoye, B., Cremer, M. & Klein, B. 2002. Morphology and architecture of the present canyon and channel system of the Zaire deep-sea fan. **Marine and Petroleum Geology 19,** 445-467

Bandy, O.L. 1964. Foraminiferal trends associated with deep water sands, San Pedro and Santa Monica basins, California. **Journal of Paleontology 38**, 138-148

Barbieri, R. 2001. Taphonomic implications of foraminiferal composition and abundance
in intertidal mudflats, Colorado River Delta (Mexico). **Micropaleontology 47,** 73–86

Bearman, G. (Ed). 1999. *Seawater: its composition, properties and behaviour*. Butterworth Heinemann, Open University Press, Milton Keynes

Bearman, G. (Ed). 2002. W*aves, tides and shallow water processes*. Butterworth Heinemann, Open University Press, Milton Keynes

Benn, D.I. & Ballantyne, C.K. 1993. The description and representation of particle shape. **Earth Surface processes and landforms 18 (7),** 665-672

Berkeley, A., Perry, C.T. & Smithers, S.G. 2009. Taphonomic signatures and patterns of test degradation on tropical, intertidal benthic foraminifera. **Marine Micropaleontology 73,** 148–163

Berner, R.A., Berner, E.K. & Keir, R.S. 1976. Aragonite dissolution on Bermuda pedestal — its depth and geochemical significance. **Earth and Planetary Science Letters 30 (2),** 169–178

Bernhard, J.M. & Sen Gupta, B.K. 2002. Foraminifera of oxygen-depleted environments. In: Sen Gupta, B.K. (Ed) *Modern Foraminifera*. Kluwer Academic Publishers, Dordrecht, pp.217-235

Best, J.L., Kirkbride, A.D. & Peakall, J. 2001. Mean flow and turbulence structure of sediment-laden gravity currents: new insights using ultrasonic Doppler velocity profiling. **Special Publication of the International Association of Sedimentologists 31**, 159-172

Bock, W.D. 1970. *Thalassina testudinum*, a habitat and means of dispersal for shallow water benthonic foraminifera. **Transactions of the Gulf Coast Association of Geological Societies 19,** 337-340

Bolli, H.M., Beckmann, J-P & Saunders, J.B. 1994. *Benthic foraminiferal biostratigraphy of the Southern Caribbean region.* Cambridge University Press, Cambridge, pp 65-166

Boltovskoy, E. & Lena, H. 1969. Les epibiontes de 'Macrocystis' flotante como indicadores hidrologicos. **Neotropica 15,** 135-137

Boltovskoy, E., Scott, D. & Medioli, F. 1991. Morphological variations of benthic foraminiferal tests in response to changing ecological parameters: a review. **Journal of Paleontology 65 (2),** 175-185

Booth, J.R., Dean, M.C., DuVernay, III,A.E. & Styzen, M.J. 2003. Paleo-bathymetric controls on stratigraphic architecture and reservoir development of confined fans in the auger Basin: central Gulf of Mexico slope. **Marine and Petroleum Geology 20**, 563-586

Borah, A. & Chhabra, R.P. 2005. Drag on freely falling cones in Newtonian and Power Law Fluids. **The Canadian Journal of Chemical Engineering 83 (3),** 559-565

Boucot, A.J. 1953. Life and dead assemblages among fossils. **American Journal of Science 251,** 25-40

Brasier, M.D. 1981. Microfossil transport in the tidal Humber basin. In: Neale, J.W. & Brasier, M.D. *Microfossils from recent and fossil shelf seas*. Ellis Horwood, Chichester/Halsted Press, New York.pp314-322

Brasier, M.D. 1982. Architecture and evolution of the foraminiferid test – a theoretic approach. In: Banner, F.T. & Lord, A.R. (eds) *Aspects of Micropalaeontology*. George Allen & Unwin, London, pp1-41

Bridge, J.S. 2003. Fundamentals of water flow. In: Bridge, J.S. *Rivers and floodplains, forms processes and sedimentary record.* Blackwell Publishing, Oxford, pp17-43

Bridge, J.S. 2003a. Fundamentals of sediment transport. In: Bridge, J.S. *Rivers and floodplains, forms processes and sedimentary record.* Blackwell Publishing, Oxford, pp. 44-77

Briggs, L., McCulloch, D. & Moser, F. 1962. The hydraulic shape of sand particles. **Journal of Sedimentary Petrology 32**, 645-656

Briguglio, A. & Hohenegger, J. 2009. Nummulitids hydrodynamics: an example using *Nummulites globules* Leymerie, 1846. **Bollettino della Società Paleontologica Italiana, 48 (2),** 105-111

Brunner, C.A. & Ledbetter, M.T. 1987. Sedimentological and micropaleontological detection of turbidite muds in hemipelagic sequences: an example from the Late Pleistocene level of Monterey Fan, central California continental margin. **Marine Micropaleontology 12,** 233-239

Bryden, H.L. & Stommel, H.M. 1982. Origins of the Mediterranean outflow. **Journal of Marine Research 40,** 55–71

Buckee, C., Kneller, B. & Peakall, J. 2001. Turbulence structure in steady, solute-driven gravity currents. **Special Publication of the International Association of Sedimentologists 31**, 173-187

Burchard, H., Craig, P.D., Gemmrich, J.R., van Haren, H., Mathieu, P-P., Meier, H.E.M., Alex, W., M. Smith, M.N., Prandke, H., Rippeth, T.P., Skyllingstad, E.D., Smyth, W.D., Welsh, D.J.S. & Wijesekera, H.W. 2008. Observational and numerical modeling methods for quantifying coastal ocean turbulence and mixing. **Progress In Oceanography 76 (4),** 399-442

Buzas, M.A., Culver, S.J. & Jorissen, F.J. 1993. A statistical evaluation of the microhabitats of living (stained) infaunal benthic foraminifera. **Marine Micropaleontology 20,** 311-320

Buzas-Stephens, P. & Buzas, M.A. 2005. Population dynamics and dissolution of foraminifera in Nueces Bay. Texas. **Journal of Foraminiferal Research 35,** 248–258

Camenen, B. 2007. Simple and general formula for the settling velocity of particles. **Journal**

Cearreta, A. 1988. Population dynamics of benthic foraminifera in the Santona estuary, Spain. **Revue de paleobiologie, volume special, 2,** 721-724

Chhabra, R.P., Agarwal, L. & Sinha, N.K. 1999. Drag on non-spherical particles: An evaluation of available methods. **Powder Technology 101**, 288-295

Cheng, N.S. 1997. Simplified settling velocity formulae for sediment particle. **Journal of Hydraulic Engineering 123 (2),** 149-152

Collins, M. & Rigler, J. 1982. The use of settling velocity in defining the initiation of motion of heavy mineral grains under unidirectional flow. **Sedimentology 29**, 419-426

Corliss, B.H. 1985. Microhabitats of benthic foraminifera with deep-sea sediments. **Nature 314**, 435-438

Corliss, B.H. & Chen, C. 1988. Morphotype patterns of Norwegian Sea deep-sea benthic foraminifera and ecological implications. **Geology 16**, 716-719

Corey, A.T. 1949. *Influence of shape on the fall velocity of sand grains*. MS Thesis, Colorado A & M College, Fort Collins, Colorado

Cottey, T.L. & Hallock, P. 1988. Test surface degradation in *Archaias angulatus*. **Journal of Foraminiferal Research 18,** 187–202

Culver, S.J. & Banner, F.T. 1978. Foraminiferal assemblages as Flandrian palaeoenvironmental indicators. **Palaeogeography, Palaeoclimatology, Palaeoecology 24,** 53-72

Cushman, J.A. 1948. *Foraminifera: Their Classification and Economic Use,* 4th Edition, Harvard University Press, Cambridge

Daly, R.A. 1936. Origin of the submarine canyons. **American Journal of Science 31**, 401–420

Darling, K.F. & Wade, C.M. 2008. The genetic diversity of planktic foraminifera and the global distribution of ribosomal RNS genotypes. **Marine Micropalaeontology 67,** 216-238

De Stigter, H.C., Jorissen, F.J. & van der Zwaan, G.J., 1998. Bathymetric distribution and microhabitat partitioning of live (Rose Bengal stained) foraminifera along a shelf to bathyal transect in the southern Adriatic Sea. **Journal of Foraminiferal Research 28,** 40–65

Dietrich, W. E. 1982. Settling velocity of natural particles. **Water resources Research 18,** 1615-1626

Douglas, J.F., Gasiorek, J.M., Swaffield, J.A. & Jack, L.B. 2005. *Fluid Mechanics*. 5th edition. Pearson, Prentice Hall, Harlow, England

Doyle, P. 2004. *Understanding Fossils. An introduction to Invertebrate Palaeontology.* John Wiley & Sons, Chichester

Drago, M. 2002. A coupled debris flow-turbidity current model. **Ocean Engineering 29,** 1769-1780

Drinia, H. & Dermitzakis, M.D. 2010. The response of benthic foraminifera to palaeoenvironmental disturbance; A quantitative approach in turbidite successions. **Neues Jahbush Fur Geologie Und Palaontologie Abhandlungen 258 (3),** 325-338

Dunn, O.J & Clark, V.A. 1987. *Applied Statistics: Analysis of Variance and Regression*. Wiley, New York

Ercilla, G., Wynn, R.B., Alonso, B. & Baraza, J. 2002. Initiation and evolution of turbidity current sediment waves in the Magdalena turbidite system. **Marine Geology 192,** 153-169

Ercilla, G., Alonso, B., Wynn, R.B & Baraza, J. 2002a. Turbidity current sediment waves on irregular slopes: observations from the Orinoco sediment-wave field. **Marine Geology 192,** 171-187

Faugeres, J.-C., Mezerais, M.-L. & Stow, D.A.V. 1993. Contourite drift types and their distribution in the North and South Atlantic Ocean basins. **Sedimentary Geology 82,** 189–203

Faugeres, J. C., Gonthier, E. & Stow, D.A.V. 1984, Contourite drift remolded by deep Mediterranean outflow. **Geology 12**, 296-300

Felix, M., Sturton, S. & Peakall, J. 2005. Combined measurements of velocity and concentration in experimental turbidity currents. **Sedimentary Geology 179**, 31-47

Ferreira, J., M. Cacha, M. & Gonzalez, R. 2008. Reworked calcareous nannofossils as ocean dynamic tracers: The Guadiana shelf case study (SW Iberia). **Estuarine, Coastal and Shelf Science 79,** 59–70

Fine, I.V., Rabinovich, A.B., Bornhold, B.D., Thomson, R.E. & Kulikov, E.A. 2005. The Grand Banks landslide-generated tsunami of November 18, 1929: preliminary analysis and numerical modeling. **Marine Geology 215 (1–2),** 45–57

Fok-Pun, L. & Komar, P.D. 1983. Settling velocities of planktonic foraminifera: density variations and shape effects. **Journal of Foraminiferal Research 13**, 60-68

Fontanier, C., Jorissen, F.J., Chaillou, G., Anschutz, P., Gremare, A. & Griveaud, C. 2005. Live foraminiferal faunas from a 2800m deep lower canyon station from the Bay of Biscay: faunal response focusing of refractory organic matter. **Deep Sea Research I, 52,** 1189-1227

Fontanier, C., Jorissen, F., Geslin, E., Zaragosi, S., Duchemin, G, Laversin, M. & Gaultier, M. 2008. Live and dead foraminiferal faunas from Saint-Tropez canyon (Bay of Frejus): Observations based on in situ and incubated cores. **Journal of Foraminiferal Research 38 (2),** 137-156

Fukushima, Y., Parker, G. & Pantin, H.M. 1985. Prediction of ignitive turbidity currents in Scripps Submarine Canyon. **Journal of Marine Geology 67**, 55-81

Ganguly, U.P. 1990. On the prediction of terminal settling velocity of solids in-solid systems. **International Journal of Mineral Processing 29** (3/4), 235-247

Gao, S. & Collins, M. 1995. Net sand transport directions in a tidal inlet, using foraminiferal tests as natural tracers. **Estuarine, Coastal & Shelf Science 40**, 681-697

Garcia, M. 2002. *Caracterizacion morfologica del sistema de canals y valles submarinos del talud medio del Golfo de Cadiz (SO de la Peninsula Iberica): Implicaciones oceanograficas.* Tesis de Licenciatura, Facultad de Ciencias del Mar, University of Cadiz, pp114

Garcia, M.H. & Parker, G. 1989. Experiments on hydraulic jumps in turbidity currents near a canyon-fan transition. **Science 245**, 393-396

Gargett, A.E., 1999. Velcro measurement of turbulent kinetic energy dissipation rate**. Journal of Atmospheric and Oceanic Technology 16**, 1973–1993

Gemmrich, J.R., Farmer, D.M. 1999. Near surface turbulence and thermal structure in a wind driven sea. **Journal of Physical Oceanography 29**, 480–499

Gibbs, R.J. 1972. The accuracy of particle size analysis utilizing settling tubes**. Journal of Sedimentary Petrology 42**, 141-145

Gibbs, R.J., Mathews, M.D. & Link, D.A. 1971. The relationship between sphere size and settling velocity. **Journal of Sedimentary Petrology 44(1),** 7-18

Goldstein, S. T. 2002. Foraminifera: a biological overview. In: Sen Gupta, B.K. (Ed). *Modern Foraminifera*. Kluwer, Dordrecht, pp.37-55

Gooday. A.J., Levin, L.A., Linke, P. & Heeger, T. 1992. The role of benthic foraminifera in deep-sea food webs and carbon cycling. In: Rowe, G.T. & Pariente, V. (Eds), *Deep-Sea Food Chains and the Global Carbon Cycle.* Kluwer, Dordrecht. pp.63-91

Goudie, A.S. & Sperling, C.H.B. 1977. Long distance transport of foraminiferal tests by wind in the Thar Desert, northwest India**. Journal of Sedimentary Petrology 47**, 630-633

Gradstein, F.M. & Berggren, W.A. 1981. Flysch-type agglutinated foraminifera and the Maestrichtian to Paleogene history of the Labrador and North Seas. **Marine Micropaleontology 6,** 211-268

Graham, D.J. & Midgley, N.G. 2000. Graphical representation of particle shape using triangular diagrams: an Excel spreadsheet method. **Earth surface processes and landforms 25 (13),** 1473-1477

Guerreiro, C., Rosa, F., Oliveira, A., Cachão, M., Fatela, F. & Rodrigues A. 2009. *Calcareous nannoplankton and benthic foraminiferal assemblages from the Nazaré Canyon (Portuguese continental margin): preliminary results*. IOP Conf. Series: Earth and Environmental Science 5 (2009) 012004. doi:10.1088/1755-1307/5/1/012004

Guimerans, P.V. & Currado, J.L.C. 1999. The recent uvigerinids (benthic foraminifera) in the northeastern Gulf of Cadiz. **Boletin del Instituto Espanol de Oceanografia 15 (1-4),** 191-202

Guo, J. 2002. Logarithmic matching and its applications in computational hydraulics and sediment transport. **Journal of Hydraulic Resources 40 (5),** 555-565

Ha, H.K., Hsu, W.-Y., Maa, J.P.-Y., Shao, Y.Y. & Holland, C.W. 2009. Using ADV backscatter strength for measuring suspended cohesive sediment concentration. **Continental Shelf Research 29,** 1310–1316

Habgood, E.L., Kenyon, N.H., Masson, D.G., Akhmetzhanov, A., Weaver, P.P.E., Gardner, J. & Mulder, T. 2003. Deepwater sediment wave fields, bottom current sand channels and gravity flow channel-lobe system: Gulf of Cadiz, NE Atlantic. **Sedimentology 50,** 483–510

Hallock, P. 1979. Trends in test shape with depth in large, symbiont- bearing foraminifera. **Journal of Foraminiferal Research 9,** 61–69

Hallock, P. 1980. The application of ecologic studies of living, algal symbiont-bearing foraminifera to paleoecologic interpretation. **American Association of Petroleum Geologists Bulletin 47,** 716–717

Hallock, P. 1983. Larger foraminifera as depth indicators in carbonate depositional environments. **American Association of Petroleum Geologists Bulletin 67**, 477–478

Hansen, H.J. 2002. Shell construction in Modern Calcareous Foraminifera. In: Sen Gupta, B.K. (Ed) *Modern Foraminifera*. Kluwer Academic Publishers, Dordrecht

Haq, B.U. Hardenbol, J. & Vail, P.R. 1988. Mesozoic and Cenozoic chronostratigraphy and eustatic cycles. In: Wilgus, C.K., Hastings, B.S. Kendall, C.G.ST.C., Posamentier, H., Ross, C.A. & van Wagoner J.C. (eds). *Sea-level Changes: An integrated Approach*. Society of Economic Paleontologists and Mineralogists, Special Publications 42, 71-108

Harman, R.A. 1964. Distribution of foraminifera in the Santa Barbara Basin, California. **Micropaleontology 10**, 81-96

Haynes, J.R. 1981. *Foraminifera*. Mac Millan, London

Haynes, J.R. 1992. Supposed pronounced ecophenotype in foraminifera. Journal **of Micropalaeontology 11,** 59-63

Hayward, B.W., Holzmann, M., Grenfell, H.R.., Pawlowski, J. & Triggs, C.M. 2004. Morphological distinction of molecular types of *Ammonia* – towards a taxonomic revision of the world's most commonly misidentified foraminifera. **Marine Micropaleontology 50**, 237-271

Hecht, A.D., Eslinger, E.V. & Garmon, L.B. 1975. Experimental studies on the dissolution of
planktic foraminifera. **Cushman Foundation Foraminiferal Research. Special Publication 13**, 56–69

Hernandez-Molina, F.J., Llave, E., Somoza, L., *et al.,* 2003. Looking for clues to paleoceanographic imprints: a diagnosis of the Gulf of Cadiz contourite depositional system. **Geology 31,** 19-22

Hernandez-Molina, F. J., Llave, E., Stow, D.A.V., Garcia, M., Somoza, L., Vazquez, J.T., Lobo, F.J., Maestro, A., Del Rio, V.D., Leon, R., Medialdea, T. & Gardner, J. 2006. The contourite depositional system of the Gulf of Cadiz: A sedimentary model related to the bottom current activity of the Mediterranean outflow water and its interaction with the continental margin. **Deep-Sea Research Part Ii-Topical Studies in Oceanography 53 (11-13**), 1420-1463

Hohenegger, J. & Yordanova, E. 2001. Displacement of larger foraminifera at the western slope of Motobu Peninsula (Okinawa, Japan). **Palaios 16,** 53– 72

Holmes, N.A. 1999. The Andrew Formation and "biosteering" - different reservoirs, different approaches. In: Jones, R.W. & Simmons, M.D. (Eds) 1999. Biostratigraphy in Production and Development Geology. **Geological Society of London, Special Publication 152**, 155-166

Holzmann, M. 2000. Species concept in foraminifera: *Ammonia* as a case study. **Micropalaeontology 46,** (Supplement 1), 21-37

Holzmann, M. & Pawlowski, J. 1997. Molecular, morphological and ecological evidence for species recognition in *Ammonia* (Foraminifera). **Journal of Foraminiferal Research 27,** 311-318

Horton, B.P., Edwards, R.J. & Lloyd, J.M. 1999. A foraminiferal based transfer function for sea-level studies. **Journal of Foraminiferal Research 29**, 117-129

Hottinger, L.C. 2000. Functional morphology of benthic foraminiferal shells, envelopes of cells beyond measure. **Micropaleontology 46 (1)**, 57-86

Hottinger, L. 2006. *Illustrated glossary of terms used in foraminiferal research*. Museum of Natural History, CH 4001 Basel, Switzerland. Available online at: http://paleopolis.rediris.es/cg/CG2006_M02/index.html. Accessed 16.09.08

Hohenegger, J. 2005. Estimation of environmental paleogradient values based on presence/absence data: a case study using benthic foraminifera for paleodepth estimation.
Palaeogeography, Palaeoclimatology, Palaeoecology 217, 115– 130

Hosseini,S.A., Shamsai, A. & Ataie-Ashtiani, B. 2006. Synchronous measurements of the velocity and concentration in low density turbidity currents using an Acoustic Doppler Velocimeter. **Flow Measurement and Instrumentation 17**, 59–68

Huthnance, J. M., Humphery, J. D., Knight, P. J., Chatwin, P. G., Thomsen, L. & White, M. 2002. Near-bed turbulence measurements, stress estimates and sediment mobility at the continental shelf edge. **Progress in Oceanography, 52(2-4),** 171–193

Ichron, 2009. Map of Trinidad log positions. E-mailed PDF picture from Nicholas Holmes, Ichron Ltd

Inman, D.L., Nordstrom, C.E. & Reinhard, E.F. 1976. Currents in submarine canyons: An air-sea-land interaction, **Annual Review of Fluid Mechanics 8**, 275–310

Iverson, R. M. 1997. The physics of debris flows. **Reviews of Geophysics 35 (3),** 245–296

Janke, N.C., 1966. Effect of shape upon the settling velocity of regular convex geometric particles. **Journal of Sedimentary Petrology 36,** 370–376

Jimenez, J.A. & Madsen, M. 2003. A simple formula to estimate settling velocity of natural sediments. **Journal of Waterway, Port, Coastal and Ocean engineering, ASCE** 0733-950X (2003) 129:2(70), p70-78

Jimenez, J.A. & Madsen, M. 2004. Discussion of 'simple formula to estimate settling velocity of natural sediments'. **Journal of Waterway, Port, Coastal and Ocean engineering 30 (4),** 219-220

Jones, R.W. 1996. *Micropalaeontology in Petroleum Exploration*. Clarendon Press, Oxford

Jones, R.W. 2006. *Applied Palaeontology*. Cambridge University Press, Cambridge

Jones, R.W. 2011. *Applications of Palaeontology, Techniques and Case Studes*. Cambridge University Press, Cambridge

Jones, R.W., Pickering, K.T., Boudagher-Fadel, M. & Matthews, S. 2005. Preliminary observations on the micropalaeontological characterization of submarine fan/channel sub environments, Ainsa System, south-central Pyrenees, Spain. *In*: Powell, A.J. & Riding, J.B. (Eds). *Recent Developments in Applied Biostratigraphy.* Special Publication of the Micropalaeontological Society 1, 55-68

Jones, R.W. & Simmons, M.D. (eds) 1999. *Biostratigraphy in Production and Development Geology.* The Geological Society, London (Special Publication No. 152).

Jorissen, F.J. 2002. Benthic foraminiferal microhabitats below the sediment-water interface. In: Sen Gupta, B.K. (Ed). *Modern Foraminifera*. Kluwer Academic Publishers, Dordrecht, pp.161-179

Kaminski, M.A. 1985. Evidence for control of abyssal agglutinated foraminiferal community by substrate disturbance: results from the HEBBLE area. **Marine Geology 66,** 113-131

Kaminski, M.A., Gradstein, F.M., Berggren, W.A., Geroch, S. & Beckmann, J.P. 1988. Flysch-type agglutinated foraminiferal assemblages from Trinidad: taxonomy, stratigraphy and paleobathymetry. In: Gradstein, F.M. & Rogl, F. (Eds) 2nd International Workshop on Agglutinated Foraminifera, Vienna 1986, Proceedings. **Abhandlungen Geologische Bundesanst 41,** 155-227

Kaminski, M.A., Cetean, C.G. & Tyszka. J. 2011. Nomenclature to describe the transition from multiserial to uniserial chamber arrangement in benthic foraminifera. **Journal of Micropalaeontology 30,** 7-10

Keigwin, L.D. & Guilderson, T.P. 2009. Bioturbation artifacts in zero-aged sediments. **Palaeoceanography 24**, PA4212, doi:10.1029/2008PA001727

Kelling, G. & Stanley, D.J. 1976. Sedimentation in canyon, slope and basin-of-slope environments. In: Stanley, D.J. & Swift, D.J.P. (Eds) *Marine sediment transport and environment management.* John Wiley, New York. pp.379-435

Kender, S. 2007. *Foraminiferal characterisation and taxonomy of Oligocene – Miocene Congo Fan deep sea sub-environments, offshore Angola*. PhD thesis, University College London.

Kennett,J. & Srinivasan,M.S. 1983. *Neogene Planktonic Foraminifera.* Hutchinson Ross, New York

Kenyon, N.H. & Belderson, R.H., 1973. Bed forms of the Mediterranean Undercurrent Observed with Side-Scan sonar. **Sedimentary Geology 9,** 77-99

Kenyon, N.H., Klaucke, I., Millington, J. & Ivanov, M.K. 2002. Sandy submarine canyon-mouth lobes on the western margin of Corsica abd Sardinia, Mediterranean Sea. **Marine Geology 184,** 69-84

Khripounoff, A. Vangriesheim, A., Babonneau, N., Crassous, P., Dennielou, B. & Savoye, B. 2003. Direct observation of intense turbidity current activity in the Zaire submarine valley at 4000 m water depth. **Marine Geology 194**, 151-158

Klaucke, I., Masson, D.G., Kenyon, N.H. & Gardner, J.V. 2004. Sedimentary processes of the lower Monterey Fan channel and channel-mouth lobe. **Marine Geology 206,** 181-198

Klaucke, I., Savoye, B. & Cochonat, P. 2000. Patterns and processes of sediment dispersal on the continental slope off Nice, SE France. **Marine Geology 162**, 405-422

Knappertsbusch, MW., Binggeli, D., Herzig, A., Schmutz, L., Stapfer, S., Schneider, C., Eisenecker, J. & Widmer, L. 2009. AMOR - a new system for automated imaging of microfossils for morphometric analyses. **Palaeontologia Electronica 12 (2)**, Art. No. 2T 2009

Kneller, B. & Buckee, C. 2000. The structure and fluid mechanics of turbidity currents; a review of some recent studies and their geological implications. **Sedimentology 47**, 62-94

Kneller, B.C. & McCaffrey, W.D. 2003. The interpretation of vertical sequences in turbidite beds: the influence of longitudinal flow structure. **Journal of Sedimentary Research 73**, 706–713

Kneller, B.C., Bennett, S.J. & McCaffrey, W.D. 1999. Velocity structure, turbulence and fluid stresses in experimental gravity currents. **Journal of Geophysical Research 104** (C3), 5381–5391

Knighton, D. 1998. *Fluvial forms and processes.* Arnold, A member of the Hodder Headline Group, London

Koho, K.A., Kouwenhoven, T.J., de Stigter, H.C. & van der Zwaan, G.J. 2007. Benthic
foraminifera in the Nazaré canyon, Portuguese continental margin: sedimentary environments and disturbance. **Marine Micropaleontology 66**, 27-51

Komar, P.D. 1971. Hydraulic jumps in turbidity currents. **Geological Society of America Bulletin 82,** 1477-1488

Komar, P.D. 1977. Computer simulation of turbidity current flow and the study of deep-sea channels and fan sedimentation. In: Goldberg, E.D., McCave, I.N., O'Brien, J.J. & Steele, J.H. (Eds). *The Sea (Ideas and Observations on Progress in the Study of the Seas) Vol.6: Marine Modelling*. John Wiley & Sons, New York, pp 603-621

Komar, P. & Clemens, K. 1986. The relationship between grains settling velocity and threshold of motion under unidirectional currents. **Journal of Sedimentary Petrology 56**, 258-266

Komar, P.D. & Reimers, C.E. 1978. Grain shape effects on settling rates. **Journal of Geology 86,** 193–209

Kontrovitz, M., Snyder, S.W. & Brown, R.J. 1978. A flume study of the movement of foraminifera tests. **Palaeogeography, Palaeoclimatology, Palaeoecology 23**, 141-150

Kotler, E., Martin, R.E & Liddell, W.D. 1992. Experimental analysis of abrasion and dissolution-resistance of modern reef dwelling foraminifera for the preservation of biogenic carbonate. **Palaios 7,** 244-276

Kravtsov, M.V. 1968. Resistance to free steady-state motion of a sphere in a viscous medium. **Journal of Engineering Physics and Thermodynamics 15** (3), 833-838

Krumbein, W.C. 1941. Measurement and geological significance of shape and roundness of sedimentary particles. **Journal of Sedimentary Petrology 11,** 64– 72

Kubo, Y. & Nakajima,T. 2002. Laboratory experiments and numerical simulation of sediment-wave formation by turbidity currents. **Marine Geology 192**, 105-121

Kucera, M. & Darling, K.F. 2002. Cryptic species of planktonic foraminifera: Their effect on palaeoceanographic reconstructions. **Philosophical Transactions of the Royal Society of London Series a-Mathematical Physical and Engineering Sciences 360 (1793),** 695-718

Larsen, A.R. 1976. Studies of recent *Amphistegina:* taxonomy and some ecological aspects. **Israel Journal of Earth-Sciences 25**, 1– 26

Le Roux, J.P., 1997. Comparison of sphericity indices as related to the hydraulic equivalence of settling grains. **Journal of Sedimentary Petrology 67,** 527– 530

Le Roux, J.P. 2002. Application of the Hofmann shape entropy to determine the settling velocity of irregular, semi-ellipsoidal grains. **Sedimentary Geology 149**, 237–243

Le Roux, J.P. 2005. Grains in motion: A review. **Sedimentary Geology 178**, 285–313

Le Roux, J.P. & Brodalka, M. 2004. An Excel-VBA program for the analysis of current velocity profiles. **Computers & Geosciences 30**, 867–879

Leuschner, D.C., Sirocko, F., Grootes, P.M. & Erlenkeuser, H. 2002. Possible influence of *Zoophycos* bioturbation on radiocarbon dating and environmental interpretation. **Marine Micropaleontology 46 (1-2),** 111-126

Leutenegger, S. 1984. Symbiosis in benthic foraminifera: specificity and host adaptations. **Journal of Foraminiferal Research 14**, 16– 35

Levitus, S. & Isayev, G. 1992. Polynomial approximation to the international equation of state for seawater. **Atmosphere and Ocean Technology 9,** 705-708

Li, M.Z. 1994. Direct skin friction measurements and stress partitioning over movable sand ripples. **Journal of Geophysical Research 99**, 791-799

Lin, H-L., Liu, J.T. & Hung, G-W. 2005. Foraminiferal shells in sediment traps: Implications of biogenic particle transport in the Kao-ping submarine canyon, Taiwan. **Continental Shelf Research 25**, 2261–2272

Linke, P. & Lutze, G.F. 1993. Microhabitat preferences of benthic foraminifera: a static concept or a dynamic adaptation to optimize food acquisition? **Marine Micropaleontology 20,** 215-233

Llave, E., Hernandez-Molina, F.J., Somonza, L., Dias Del Rio, V., Stow, D.A.W., Maestro. A. & Alveirinho Dias, J.M. 2001. Seismic stacking pattern of the Faro-Albufeira contourite system (Gulf of Cadiz): a Quaternary record of paleooceanographic and tectonic influences. **Marine Geophysical Researches 22**, 487-508

Lobo, F.L., Sanchez, R., González, R., Dias, J.M.A., Hernandez-Molina, F.J., Fernández-Salas, L.M., Díaz del Río, V. & Mendes, I. 2004. Contrasting styles of the Holocene highstand sedimentation and sediment dispersal systems in the northern shelf of the Gulf of Cadiz. **Continental Shelf Research 24 (4-5)**, 461-482

Loeblich, A.R. Jn., & Tappan, H. 1964. *Treatise on Invertebrate Paleontology, Part C: Sarcodina, Chiefly ('Thecamoebians' and Foraminiferida)*. University of Kensas Press

Loeblich, A.R. & Tappan, H. 1992. Present status of foraminiferal classification. In: Takayanagi, Y. & Saito, T. (Eds) *Studies in Benthic Foraminifera*. Proceedings of the Fourth International Symposium on Benthic Foraminifera, Sendai, 1990 (Benthos '90), Tokai University Press, Tokyo, Japan, 93-102

Loeblich, A.R. Jn., & Tappan, H. 1988. *Foraminifera genera and their classification*. Van Nostrand Reinhold, New York

Loeblich, A.R. Jn., & Tappan, H. 1988a. *Foraminifera genera and their classification - Plates*. Van Nostrand Reinhold, New York

Lorke, A. & Wuest, A. 2005. Application of coherent ADCP for turbulence measurements in the bottom boundary layer. **Journal of Atmospheric and Oceanic Technology 22**, 1821–1828

Loubere, P. & Fariduddin, M. 2002. Benthic foraminifera and the Flux of Organic Carbon to the Seabed. In: Sen Gupta, B.K. (Ed). *Modern Foraminifera*. Kluwer Academic Publishers, Dordrecht, pp.181-199

Lowe, J.J. & Walker, M.J.C. 1997. *Reconstructing Quaternary Environments*. 2nd Edition. Pearson Education Ltd, Harlow, England

Lu, Y. & Lueck, R.G. 1999. Using a broadband ADCP in a tidal channel. Part II: turbulence. **Journal of Atmospheric and Oceanic Technology 16,** 1568–1579

Lueck, R.G., Wolk, F. & Yamazaki, H. 2002. Oceanic velocity microstructure measurements in the 20th century. **Journal of Oceanography 58**, 153–174

Luznik, L., Gurka, R., Zhu, W., Nimmo Smith, W.A.M., Katz, J. & Osborn, T.R. 2007. Distribution of energy spectra, Reynolds stresses, turbulence production and dissipation in a tidally driven bottom boundary layer. **Journal of Physical Oceanography 36**, 1527–1550

Mackensen, A. 1987. Benthische Foraminiferen auf dem Island-Schottland Rucken: Umwelt-Anzeiger an der Grenze zweier ozeanischer-Raume. **Palaontologische Zeitschrfit 61,** 149-179

Madella, M., Powers-Jones, A.H. & Jones, M.K. 1998. A Simple Method of Extraction of Opal Phytoliths from Sediments Using a Non-Toxic Heavy Liquid. **Journal of Archaeological Science 25,** 801–803

Maiklem, W.R. 1968. Some hydraulic properties of bioclastic carbonate grains. **Sedimentology 10**, 101-109

Mantz, P.A. 1977. Incipient transport of fine grains and flakes by fluids. Extended Shields diagram. **Journal of Hydraulic Engineering 103**, 601-615

Martin, R.E. & Liddell, W.D. 1991. The taphonomy of foraminifera in modern carbonate environments: implications for the formation of foraminiferal assemblages. In: Donavan, S.K. (Ed) *The Processes of Fossilisation*. Belhaven Press, London, pp.170-193

Masalo´, I., Reig, L. & Oca, J. 2008. Study of fish swimming activity using acoustical Doppler velocimetry (ADV) techniques. **Aquacultural Engineering 38**, 43–51

Matthews, M.D., 1991. The effect of grain shape and density on size measurement. In: Syvitski, J.P.M. (Ed), *Principles, Methods and Application of Particle Size Analysis*. Cambridge University Press, Cambridge, pp. 22-33

McCave, I.N. & Syvitski, J.P.M. 1991. Principles and methods of geological particle size analysis. In: Syvitski, J.P.M. (Ed), *Principles, Methods and Application of Particle Size Analysis*. Cambridge University Press, Cambridge, pp. 3-21

McLelland, S.J. & Nicholas, A.P. 2000. A new method for evaluating errors in high-frequency ADV measurements. **Hydrological Processes, 14**, 351–366

McNowan, J.S. & Malaika, J. 1950. Effect of particle shape on settling velocity at low Reynolds numbers. **American Geophysical Union Transactions 31,** 74– 82

McNowan, J.S., Malaika, J. & Pramanik, H. 1951. *Particle shape and settling velocity*. Proceedings of the 4th Conference of the International Association of Hydraulic Research, Bombay, pp511-522

Meiburg, E. & Kneller, B. 2010. Turbidity currents and their deposits. **Annual Review of Fluid Mechanics 42,** 135-156

Melhta, A.J., Lee, J. & Christensen, B.A. 1980. Fall velocities of shells as coastal sediments. **Journal of Hydraulic Engineering 106**, 1727-1744

Mendes, I., Gonzalez, R., Dias, J.M.A., Lobo, F. & Martins, V. 2004. Factors influencing recent benthic foraminifera distribution on the Guadiana shelf (Southwestern Iberia). **Marine Micropaleontology 51**, 171– 192

Mendes, I., Rosa, F., Dias, J.A., Schonfeld, J., Ferreira,O. & Pinheiro, J. 2010. Inner shelf paleoenvironmental evolution as a function of land–ocean interactions in the vicinity of the Guadiana River, SW Iberia. **Quaternary International 221**, 58–67

Mendes, I., Dias, J.A., Schonfeld, J. & Ferreira,O. 2010a. *Distribution of the living benthic foraminifera on the northern Gulf of Cadiz continental shelf.* CIMA/CIACOMAR, Edifício 7,Universidade do Algarve, Campus de Gambelas, 8005-139 Faro, Portugal and Leibniz-Institute of Marine Sciences IFM-GEOMAR, Wischhofstr. 1-3, D-24148 Kiel, Germany

Middleton, G.V. 1993. Sediment deposition from turbidity currents. **Annual Review of Earth and Planetary Sciences 21,** 89-114

Middleton, G.V. 1966. Experiments on density and turbidity currents; Part 1. Motion of the head. **Canadian Journal of Earth Sciences 3**, 523-546

Middleton, G.V. & Southard, J.B. 1984. *Mechanics of Sediment Movement.* SEPM. Short Course, 3, 401pp

Miller, M.C., McCave, I.N. & Komar, P.D. 1977. Threshold of sediment motion under unidirectional currents. **Sedimentology 24**, 507-527

Milliman, J.D. 1975. Dissolution of aragonite, Mg-calcite, and calcite in North Atlantic Ocean. **Geology 3 (8),** 461–462

Mitchell, N.C. 2005. Erosion of canyons in continental slopes. In: Hodgson, D.M. & Flint, S.S. (Eds) Submarine Slope Systems: Processes and Products. **Geological Society, London, Special Publications 244**, 131-140

Mohrig, D. & Marr, J.G. 2003. Constraining the efficiency of turbidity current generation from submarine debris flows and slides using laboratory experiments. **Marine & Petroleum Geology 20,** 883-899

Mojtahid, M., Jorissen, F., Lansard, B., Fontanier, C., Bombled, B. & Rabouille, C. 2009. Spatial distribution of live benthic foraminifera in the Rhône prodelta: Faunal response to a continental–marine organic matter gradient. **Marine Micropaleontology** (article in press)

Moraes, M.A.S., Maciel, W.B., Braga, M.S., Viana, A.R. 2007. Bottom-current reworked Palaeocene-Eocene deep-water reservoirs of the Campos Basin, Brazil. In:

Viana, A.R. & Rebesco, M. (Eds) Economic and Palaeoceanic Significance of Contourite Deposits. **Geological Society, London, Special Publications 276**, 81-94

Mulder, T. & Alexander, J. 2001. The physical character of subaqueous sedimentary density flows and their deposits. **Sedimentology 48**, 269–299

Mulder, T., Savoye, B. & Syvitski, J.P.M. 1997. Numerical modelling of a mid-sized gravity flow: the 1979 Nice turbidity current (dynamics, processes, sediment budget and seafloor impact). **Sedimentology 44,** 305-326

Mulder, T., Lecroart, P., Voisset, M., Schonfeld, LeDrezen, J.E., Gonthier, E., Hanquiez, V., Zahn, R., Faugères, J.C., Hernandez-Molina, J., Llave-Barranco, E., & Gervais, A. 2002. Studying past Deep-ocean circulation and the Palaeoclimate record in the Gulf of Cadiz: **EOS, v. 83**, 481-488

Mullenbach, B.L., Nittrouer, C.A., Puig, P. & Orange, D.L., 2004. Sediment deposition in a modern submarine canyon: Eel Canyon, northern California. **Marine Geology 211**, 101–119

Munson, B.R. Young, D.F. & Okiishi, T.H. 2006. *Fundamentals of fluid mechanics*. (5th Edition) John Wiley & Sons, Hoboken, USA

Murray, J.W. 1971. *An Atlas of British Recent Foraminifera*. American Elsevier Publishing Company, Inc., New York

Murray, J.W. 1980. The foraminifera of the Exe estuary. **Devonshire Association Special Volume 2,** 89-115

Murray, J.W. 1987. Biogenic indicators of suspended sediment transport in marginal marine environments: quantitative examples from SW Britain. **Journal of the Geological Society, London 144,** 127-133

Murray, J.W. 1991. *Ecology and Palaeoecology of Benthic Foraminifera*. Longman, Harlow, Essex

Murray, J.W. 1991a. Ecology and distribution of benthic foraminifera. In: Lee, J.J. & Anderson, O.R. (Eds) *Biology of Foraminifera*. Academic press, London, pp.221–253

Murray, J.W. 2000. The enigma of the continued use of total assemblages in ecological studies of benthic foraminifera. **Journal of Foraminiferal Research 30 (3),** 244-245

Murray, J.W. 2001. The niche of benthic foraminifera, critical thresholds and proxies. **Marine Micropaleontology 41**, 1-7

Murray, J. W. 2006. *Ecology and Applications of Benthic Foraminifera*. Cambridge University Press, Cambridge, UK

Murray, J.W. & Alve, E. 1999. Taphonomic experiments on marginal marine foraminiferal assemblages: how much ecological information is preserved? **Palaeogeography, Palaeoclimatology, Palaeoecology 149**, 183–197

Murray, J.W. & Hawkins, A.B. 1976. Sediment transport in the Severn Estuary during the past 8000-9000 years. **Journal of the Geological Society 132**, 385-398

Murray, J.W., Sturrock, S. & Weston, J. 1982. Suspended load transport of foraminiferal tests in a tide- and wave-swept sea. **Journal of Foraminiferal Research 12**, 51-65

Nelson, C.H., Baraza, J. & Maldonado, A. 1993. Mediterranean undercurrent sandy contourites, Gulf of Cadiz, Spain. **Sedimentary Geology 82**, 103–131

Nelson, C. H., Baraza, J., Maldonado, A., Rodero, J., Escutia, C. & Barber J.H. 1999. Influence of the Atlantic Inflow and Mediterranean outflow currents on Late Quaternary sedimentary facies of the Gulf of Cadiz continental margin. **Marine Geology 155**, 99-129

Nguyen, T.M.P., Petrizzo,M.R. & Speijer, R.P. 2009. Experimental dissolution of a fossil foraminiferal assemblage (Paleocene–Eocene Thermal Maximum, Dababiya, Egypt):
Implications for paleoenvironmental reconstructions. **Marine Micropaleontology 73**, 241–258

Nimmo Smith, W.A.M. 2008. A submersible three-dimensional particle tracking velocimetry system for flow visualization in the coastal ocean. **Limnology and Oceanography: Methods 6,** 96–104

Nimmo Smith, W.A.M., Atsavapranee, P., Katz, J. & Osborn, T.R. 2002. PIV measurements in the bottom boundary layer of the coastal ocean. **Experiments in Fluids 33,** 962–971

Nimmo Smith, W.A.M., Katz, J. & Osborn, T.R., 2005. On the structure of turbulence in the bottom boundary layer of the coastal ocean. **Journal of Physical Oceanography 35**, 72–93

Nimmo Smith, W.A.M., Osborn, T.R. & Katz, J. 2004. PIV measurements in the bottom boundary layer of the coastal ocean. In: Gru, J., Liu, P.L.-F., Pedersen, G.K. (Eds.), PIV and **Water Waves, Coastal and Ocean Engineering 9**. World Scientific Publishers, pp. 51–79

Nof, D. 1996. Rotational turbidity flows and the 1929 Grand Banks earthquake. **Deep Sea Research I. Vol. 43 (8),** 1143-1163

Oehmig, R. 1993. Entrainment of Planktonic foraminifera: effect of bulk density. **Sedimentology 40,** 869-877

Ortiz, S., Alegret, L., Payros, A., Orue-Etxebarria, X., Apellaniz, E. & Molina, E. 2011. Distribution patterns of benthic foraminifera across the Ypresian–Lutetian

Gorrondatxe section, Northern Spain: Response to sedimentary disturbance. **Marine Micropaleontology 78**, 1–13

Osborn, T.R., 1974. Vertical profiling of velocity microstructure. **Journal of Physical Oceanography 4,** 109–115

Palaeo-Electronica, 1998. Palaeotologica Electronica, *Elphidium crispum.* Available online at: http://palaeo-electronica.org/1998 Accessed 16.09.08

Palaeo-Electronica, 2001. Palaeotologica Electronica, *Cibicides lobatulus*. Available online at: http://palaeo-electronica.org/2001 Accessed 16.09.08

Palaeo-Electronica, 2002. Palaeotologica Electronica, *Cibicides lobatulus*. Available online at: http://palaeo-electronica.org/2002 Accessed 16.09.08

Palaeo-Electronica, 2002a. Palaeotologica Electronica, *Uvigerina peregrina*. Available online at: http://palaeo-electronica.org/2002 Accessed 16.09.08

Paphitis, D., Collins, M.B., Nash, L.A. & Wallbridge, S. 2002. Settling velocities and entrainment thresholds of biogenic sands (shell fragments) under unidirectional flow. **Sedimentology 49 (1),** 211-225

Parker, G., Fukushima,Y. & Pantin, H.M. 1986. Self-accelerating turbidity current. **Journal of Fluid Mechanics 171,** 145–181

Paterson, A.R. 1997. *A first course in fluid dynamics*. Cambridge University Press, Cambridge

Paull, C. K., Ussler III,W., Greene, H.G., Keaten, R., Mitts, P. & Barry, J. 2003. Caught in the act: The 20 December 2001 gravity flow event in Monterey Canyon, **Geo-Marine Letter, 22,** 227– 232

Peakall, J., Felix, M., McCaffrey, B & Kneller, B. 2001. Particulate gravity currents: perspectives. **Special Publication, International Association of Sedimentologists 31**, 1-8

Peebles, M.W. & Lewis, R.D. 1988. Differential infestation of shallow-water benthic foraminifera by microboring organisms: possible biases in preservation potential. **Palaios 3,** 345–351

Peebles, M.W. & Lewis, R.D. 1991. Surface textures of benthic foraminifera from San Salvador, Bahamas. **Journal of Foraminiferal Research 21**, 285-292

Perry, C.T. 2000. Factors controlling sediment preservation on a North Jamaican fringing reef: a process-based approach to microfacies analysis. **Journal of Sedimentary Research 70,** 633–648

Piper, D. J. W., Cochonat, P. & Morrison, M. L. 1999. The sequence of events around the epicentre of the 1929 Grand Banks earthquake: initiation of the debris flows and turbidity current inferred from side scan sonar. **Sedimentology 46,** 79–97

Pirmez, C. & Imran, J. 2003. Reconstruction of turbidity currents in Amazon Channel. **Marine and Petroleum Geology 20,** 823-849

Platon, E., Sen Gupta, B.K., Rabalais, N.N. & Turner, R.E. 2005. Effect of seasonal hypoxia on the benthic foraminiferal community of the Louisiana inner continental shelf. The 20th century record. **Marine Micropaleontology 54**, 263–283

Prager, E.J., Southard, J.B. & Vivoni-Gallart, E.R. 1996. Experiments on the entrainment threshold of well sorted and poorly sorted carbonate sands. **Sedimentology 43**, 33-40

Prandke, H., Holtsch, K. & Stips, A., 2000. *MITEC technology development: the microstructure/turbulence measuring system MSS*. EUR 19733 EN, European Commission, 2000.

Prather, B.E. 2003. Controls on reservoir distribution, architecture and stratigraphic trapping in slope settings. **Marine and Petroleum Geology 20**, 529-545

Price, J.F. & O'Neil Baringer, M. 1994. Outflows and deep water production by marginal seas. **Progress in Oceanography 33,** 161-200

Prior, D. B., Bornhold, B.D, Wiseman Jr.W.J. & Lowe, D.R. 1987. Turbidity current activity in a British Columbia fjord, **Science 237,** 1330– 1333

Pritchard, D. & Gladstone, C. 2009. Reversing buoyancy in turbidity currents: developing a hypothesis for flow transformation and for deposit facies and architecture. **Marine and Petroleum Geology 26,** 1997-2010

Reading, H.G. 1996. *Sedimentary Environments: Processes, Facies and Stratigraphy*. 3rd Edition, Blackwell Science, Oxford

Reading, H.G. & Richards, M. 1994. Turbidite systems in deep-water basin margins classified by grain size and feeder system. **Bulletin of the American Association of Petroleum Geology 78,** 792-822

Reynolds, O. 1883. An experimental investigation of the circumstances which determine whether the motion of water shall be direct or simuous, and the law of resistance in parallel channels. **Philosophical Transactions of the Royal Society of London 174,** 935– 982

Richards, K.S.1982. *Rivers. Form and process in alluvial channels*. Methuen, London

Rippeth, T.P., Williams, E. & Simpson, J.H. 2002. Reynolds stress and turbulent energy production in a tidal channel. **Journal of Physical Oceanography 32,** 1242–1251

Rippeth, T.P., Simpson, J.H., Williams, E. & Inall, M.E., 2003. Measurement of the rates of production and dissipation of turbulent kinetic energy in an energetic tidal flow: Red Wharf Bay Revisited. **Journal of Physical Oceanography 33,** 1889–1901

Robert, A. 2003. *River Processes: An introduction to fluvial dynamics*. Arnold, Oxford University Press, New York

Robertson, B.E. 1998. *Systematics and paleoecology of the benthic foraminiferida from the Buff Bay section, Miocene of Jamaica*. Micropaleontology, volume 44, supplement 2. Micropaleontology Press, New York

Rodero, J., Pallares, L. & Maldonado, A. 1999. Late Quaternary seismic facies of the Gulf of Cadiz Spanish margin: depositional processes influenced by sea-level change and tectonic controls. **Marine Geology 155**, 131-156

Rogerson, M., van der Zwaan, G.J., Kouwenhoven, T.J., Postma, G., O'Neill, B.J., van der Zwan, C.J., Kleverlaan, K., Tijbosch, H.J., Koho, K., Pluymaekers, M.P.D., Ruhl, M. & Hilgen, F.J. 2005. *Sub-facies characterisation in submarine canyon and fan settings using benthic foraminiferal assemblage data*. University of Utrecht, Faculty of Geoscience. Hi-Res Pragram, Shell International Exploration and Production Inc

Rogerson, M., Kouwenhoven, T.J., van der Zwaan G.J., O'Neill, B.J., van der Zwan, C.J., Postma, G., Kleverlaan, K. & Tijbosch, H. 2006. Benthic foraminifera of a Miocene canyon and fan. **Marine Micropaleontology 60**, 295–318

Rogerson, M., Schonfeld, J. & Leng, M. J. 2011. Qualitative and quantitative approaches in palaeohydrography: a case study from core-top parameters in the Gulf of Cadiz. **Marine Geology, 280 (1-4).** pp. 150-167.

Roth, P.H. & Berger, W.H. 1975. Distribution and dissolution of coccoliths in the South and Central Pacific. **Cushman Foundation for Foraminiferal Research, Special Publication No.13**, 87-113

Sarker, M.A. 1998. Flow measurement around scoured bridge piers using Acoustic-Doppler Velocimeter (ADV). **Flow Measurement and Instrumentation 9**, 217–227

Salles, T., Mulder, T., Gaudin, M., Cacas, M.C., Lopez, S. & Cirac, P. 2008. Simulating the 1999 Capbreton canyon turbidity current with a Cellular Automata model. **Geomorphology 97,** 516-537

Sanchez, M. 2006. Settling velocity of the suspended sediment in three high-energy environments. **Ocean Engineering 33**, 665–678

Schafer, C.T., Cole, F.E. & Syvitski, J.P.M. 1989. Bio- and lithofacies of modern sediments in Knight and Bute inlets, British Columbia. **Palaios 4,** 107-126

Schonfeld, J. 1997. The impact of the mediterranean outflow water (MOW) on benthic foraminiferal assemblages and surface sediments at the southern Portuguese continental margin. **Marine Micropalaeontology 29**, 211-236

Schonfeld, J. 2002. A new benthic foraminiferal proxy for near-bottom current velocities in the Gulf of Cadiz, northeastern Atlantic Ocean. **Deep-Sea Research I 49**, 1853–1875

Schonfeld, J. 2002a. Recent benthic foraminiferal assemblages in deep high-energy environments from the Gulf of Cadiz (Spain). **Marine Micropaleontology 44**, 141-162

Schröder-Adams, C.J., Boyd, R., Ruming, K. & Sandstrom, M. 2008. Influence of sediment transport dynamics and ocean floor morphology on benthic foraminifera, offshore Fraser Island, Australia. **Marine Geology 254 (1-2),** 47-61

Schueth, J.D. & Frank, T.D. 2008. Reef foraminifera as bioindicators of coral reef health: Low Isles Reef, Northern Great Barrier Reef, Australia**. Journal of Foraminifera Research 38, (1)** 11-22

Scoffin, T.P. 1993. The geological effects of hurricanes on coral reefs and the interpretation of storm deposits. **Coral Reefs 12**, 203-221

Selley, R.C. 2004. *Ancient Sedimentary Environments*. 2nd edition. Routledge, London

Sen Gupta, B.K. 2002. *Modern Foraminifera*. Kluwer Academic Publishers, Dordrecht

Sequeiros O.E., Spinewine, B., Beaubouef, R.T., Sun., T., Garcia, M.H. & Parker, G. 2010. Characteristics of velocity and excess density profiles of saline underflows and turbidity currents flowing over a mobile bed. **Journal of Hydraulic Engineering 136 (7),** 412-433

Sequeiros O.E., Spinewine, B., Beaubouef, R.T., Sun., T., Garcia, M.H. & Parker, G. 2010a. Bedload transport and bed resistance associated with density and turbidity currents. **Sedimentology 57,** 1463-1490

Shanmugam, G. 2000. 50 years of the turbidite paradigm (1950s-1990s): deep-water processes and facies models - a critical perspective. **Marine and Petroleum geology 17**, 285-342

She, K., Trim, L. & Pope, D. 2005. Fall velocities of natural sediment particles: A simple mathematical presentation of the fall velocity law. **Journal of Hydraulic Research 43 (2),** 189-195

Shepard, F. P., Marshall, N. F., McLoughlin, P. A., & Sullivan, G. G.1979. Currents in submarine canyons and other sea valleys. **American Association of Petroleum Geologists Studies in Geology No. 8.** Tulsa, Oklahoma, 173 pp.

Shi, Z., Zhou, H.J., Eittreim, S.L. & Winterwerp, J.C. 2003. Settling velocities of fine suspended particles in the Changjiang Estuary, China. **Journal of Asian Earth Sciences 22**, 245–251

Shields, I.A. 1936. *Application of similarity principles and turbulence research to bedload movement.* In: Ott, W. & Van Uchelen, J. (translators). California Institute of Technology, W.M. Keck Laboratory of Hydraulics and Water Resources 26, Berlin

Smith, A.M. & Nelson, C.S. 2003. Effects of early sea-floor processes on the taphonomy of
temperate shell skeletal carbonate deposits. **Earth Science Reviews 63 (1–2),** 1–31

Sneed E.D. & Folk, R.L. 1958. Pebbles in the lower Colorado River, Texas, a study of particle morphogenesis. **Journal of Geology 66 (2),** 114–150

Snyder, S.W., Hale, W.R. & Kontrovitz, M. 1990. Assessment of postmortem transportation of modern benthic foraminifera of the Washington continental shelf. **Micropaleontology 36**, 259-282

Spencer-Cervato, C. & Thierstein, H.R. 1997. First appearance of Globorotalia truncatulinoides: cladogenesis and immigration. **Marine Micropaleontology 30 (4),** 267-291

Spindler, M. 1980. The pelagic gulfweed *Sargassum natans* as a habitat for the benthic foraminifera *Planorbulina acervalis* and *Rosalina globularis*. **Neues Jahrbuch fur Geologie und Palaontolgie Monatheft 9**, 569-580

Sprent, P. 1989. Tests and estimation for two independent samples. In: *Applied nonparametric statistical methods.* Chapman & Hall, London. pp 86-107

Stacy, M.W. & Bowen, A.J. 1988. The vertical structure of density and turbidity currents: theory and observations. **Journal of Geophysical Research 93**, 3528-3542

Stanley, D.J., Culver, S.J. & Stubblefield, W.L. 1986. Petrologic and foraminiferal evidence for active downslope transport in Wilmington Canyon. **Marine Geology 69 (3-4)**, 207-218

Stokes, G. 1851. On the effect of internal friction of fluids on the motion of pendulums. **Transactions of the Cambridge Philosophical Society IX**, 8-106

Stow, D. A. V. & Lovell, J. P. B. 1979. Contourites: their recognition in modern and ancient sediments. **Earth-Science Reviews 14**, 251-291

Stow, D.A.V., Faugeres, J-C., Howe, J.A., Pudsey, C.J. & Viana, A.R. 2002. Bottom currents, contourites and deep-sea sediment drifts: current state-of-the-art. In: Stow, D.A.V., Pudsey, C.J., Howe, J.A., Faugeres, J-C. & Viana, A.R. (Eds.) *Deep-water contourite systems: modern drifts and ancient series, seismic and sedimentary characteristics.* London, UK, Geological Society of London, pp7-20 (Geological Society Memoir 22).

Stow, D.A.V. & Mayall, M. 2000. Deep-water sedimentary systems: New models for the 21st Century. **Marine and Petroleum Geology 17**, 125-135

Stow, D.A.V., Reading, H.G. & Collonson, J.D. 1996. Deep seas. In: Reading H.G. (Ed) *Sedimentary Environments: Processes, Facies and Stratigraphy*. Blackwell Science Ltd, Oxford, 3rd edition, pp395-453

SubSeaIQ, 2011. SubSealIQ offshore field development. Available online at: http://www.subseaiq.com/data/Project.aspx?project_id=587&AspxAutoDetectCookieSupport=1 Accessed 10.10.11

Sumner, E.J., Amy, L.A. & Talling, P.J. 2008. Deposit structure and processes of sand deposition from decelerating sediment suspensions. **Journal of Sedimentary Research 78**, 529-547

Sweetman A.K, Sommer, S., Pfannkuche, O. & Witte, U. 2009. Retarded reponse of macrofuana-size foraminifera to phytodetritus in a deep Norwegian Fjord. **Journal of Foraminiferal Research 39 (1),** 15-22

Talling, P.J., Wynn, R.B., Masson, D.G., Frenz, M., Cronin, B.T. Schiebel, R., Akhmetzhanov, A.M., Dallmeier-Tiessen, S., Benetti, S., Weaver, P.P.E., Georgiopoulou, A., Zuhlsdorff, C. & Amy, L.A. 2007. Onset of submarine debris flow deposition far from original giant landslide. **Nature Vol 450**, doi:10.1038/ nature06313

Tanner, W.F. 1991. Suite statistics: The hydrodynamic evolution of the sediment pool. In: Syvitski, J.P.M. (Ed), *Principles, Methods and Application of Particle Size Analysis*. Cambridge University Press, Cambridge, pp. 225-236

Taylor, K.G. 2005. Sediments and sedimentation. In: Holden, J. (Ed) *Physical geography and the environment.* Pearson Education Ltd., Essex, England

Thomas, F.C. & Schafer, C.T. 1982. Distribution and transport of some common foraminiferal species in the Minas Basin, Eastern Canada. **Journal of Foraminiferal Research 12 (1),** 71-90

Thorpe, S.A., Osborn, T.R., Jackson, J.F.E., Hall, A.J. & Lueck, R.G., 2003. Measurements of turbulence in the upper-ocean mixing layer using Autosub. **Journal of Physical Oceanography 33,** 122–145

Tompkins, M.R., Baldcock, T.E. & Nielsen, P. 2005. Hindered settling of sand grains. **Sedimentology 52,** 1425–1432

Topa, P. & Tyszka, J. 2002. Local minimization paradigm in numerical modelling of foraminiferal shells. **Lecture Notes in Computer Science 2331**, 1095-1115

Tyszka, J. 2006. Morphospace of foraminiferal shells: results from the moving reference model. **Lethaia, Vol. 39 (1),** 1–12

Tyszka, J. & Topa, P. 2005. A new approach to modeling of foraminiferal shells. **Paleobiology 31(3),** 522–537

Ujiie, Y. & Lipps, J.H. 2009. Cryptic diversity in planktic foraminifera in the Northwest Pacific Ocean. **Journal of Foraminiferal Research 39 (3)** 145-154

Umlauf, L. & Burchard, H. 2005. Second-order turbulence closure models for geophysical boundary layers. A review of recent work. **Continental-Shelf Research 25,** 795–827

USGS, 2000. US Geological Survey OFR 00-304: Chapter 9, *Ammonia beccarii.* Available online at: http://pubs.usgs.gov/of/2000/of00-304/htmldocs/chap09/index.htm Accessed 16.09.08

van Weering, T.C.E., de Stigter, H.C., Boer, W. & de Haas, H., 2002. Recent sediment transport and accumulation on the NW Iberian margin. **Progress in Oceanography 52 (2-4),** 349-371

Venec-Peyre, M.T. & Le Calvez, Y. 1986.Etude des foraminiferes de l'herbier a Posidonies de Banyuls-sur-Mer. 106. **Congres national des societes savants, Perignan, 1981, 1,** 191-203

Versteeg, H.K. & Malalasekera, W. 2007. 3. Turbulence and its modeling. In: *An Introduction to Computation Fluid Dynamics, The Finite Volume Method*. (2nd edition). Pearson Education Ltd, England, pp.40-114

Viana, A.R., Almeida Jr, W., Nunes, M.C.V. & BulhoesE.M. 2007. In: Viana, A.R. & Rebesco, M. (Eds) Economic and Palaeoceanic Significance of Contourite Deposits. **Geological Society, London, Special Publications 276**, 1-23

Vilela, C.G. 2003. Taphonomy of benthic foraminiferal tests of the Amazon Shelf. **Journal of Foraminiferal Research 33,** 132–143

Völker, D., Reichel, T., Wiedickie, M. & Heubeck, C. 2008. Turbidites deposited on Southern Central Chilean seamounts: Evidence for energetic turbidity currents. **Marine Geology 251,** 15-31

Wadell, H. 1932. Volume, shape and roundness of rock particles. **Journal of Geology 40,** 443-451

Wadell, H. 1933. Sphericity and roundness of rock particles. **Journal of Geology 41**, 310–331

Wallbridge, S. 1998. *Laboratory determination of the settling, threshold and transport velocities of unusually shaped grains (foraminifera): the effect of shape on grain hydrodynamics.* Unpublished PhD, Department of Oceanography, University of Southampton

Wakefield, M.I., Cook, R.J., Jackson, H. & Thompson, P. 2001. Interpreting biostratigraphical data using fuzzy logic: the identification of regional mudstones within the *Fleming* Field, UK North Sea. **Journal of Petroleum Geology 24(4),** 1-24

Wang, P. & Murray, J.W. 1983. The use of foraminifera as indicators of tidal effects in estuarine deposits. **Marine Geology 51**, 239-250

Wetmore, K.L. 1987. Correlations between test strength, morphology and habitat in some benthic foraminifera from the coast of Washington. **Journal of Foraminiferal Research 17**, 1-13

Wiles, P.J., Rippeth, T.P., Simpson, J.H. & Hendricks, P.J. 2006. A novel technique for measuring the rate of turbulent dissipation in the marine environment. **Geophysical Research Letters 33,** L21608

Williams, J.J. 1996. Turbulent flow in rivers. In: Carling, P.A. & Dawson, M.R. (Eds) *Advances in fluvial dynamics and stratigraphy*. J. Wiley & Sons, Chichester

Williams, J.J. & Rose, C.P. 2001. Measured and predicted rates of sediment transport in storm conditions. **Marine Geology 179 (1-2),** 121-133

Wilson, B., 2006. The environmental significance of some microscopic organisms around Nevis, West Indies. **West Indian Journal of Engineering 28**, 53–64.

Wilson, B. & Wilson, J.I. 2011. Shoreline foraminiferal thanatacoenoses around five eastern Caribbean islands and their environmental and biogeographic implications. **Continental Shelf Research 31**, 857–866

Wolk, F., Yamazaki, H. & Seuront, L. 2002. A new free-fall profiler for measuring bio-physical microstructure. **Journal of Atmospheric and Oceanic Technology 19**, 780–793

Wood, L. 2000. Chronostratigraphy and tectonostratigraphy of the Columbus basin, offshore eastern Trinidad. **American Association of Petroleum Geologists Bulletin 84 (12),** 1905-1928

Wynn, R.B., Weaver, P.P.E., Masson, D.G. & Stow, D.A.V. 2002. Turbidite depositional architecture across the interconnected deep-water basins on the north-west African margin. **Sedimentology 49**, 669-695

Xu, J. P., Noble, M.A., Eittreim, S.L., Rosenfeld, L.K., Schwing, F.B. & Pilskaln, C.H. 2002. Distribution and transport of suspended particulate matter in Monterey Canyon, California, **Marine Geology 181**, 215– 234

Xu, J.P., Noble, M.A. & Rosenfeld, L.K. 2004. In-situ measurements of velocity structure within turbidity currents. **Geophysical research letters 31,** L09311, doi:10.1029/2004GL019718

Yalin, M.S. 1972. *Mechanics of sediment transport*. Pergamon Press, New York

Yamamoto, S., Tokuyama, H, Fujioka, K. Takeuchi, A. & Ujiie, H. 1988. Carbonate turbidites deposited on the floor of the Palau Trench. **Marin Geology 82,** 217-233

Yamashiro, C. 1975. Differentiating dissolution and transport effects in foraminiferal sediments from the Panama Basin. **Cushman Foundation for Foraminiferal Research, Special Publication No.13.,** 151-159

You, Z.-J., 1994. A simple model for current velocity profiles in combined wave–current flows. **Coastal Engineering 23**, 289–304

Yordanova, E.K. & Hohenegger, J. 2007. Studies on settling, traction and entrainment of larger benthic foraminiferal tests: implications for accumulation in shallow marine sediments. **Sedimentology 54**, 1273-1306

Zhang, L., Liddell, W.D. & Martin, R.E. 1993. Hydraulic properties of foraminifera from shallow-water siliciclastic environments: A possible transport indicator in the stratigraphic record. **Geological Society of America Annual Meeting Abstracts with Programs 25,** A428

Zhiyao, S., Tingting, W., Fumin, X. & Ruijie, L. 2008. A simple formula for predicting settling velocity of sediment particles. **Water Science and Engineering 1 (1),** 37– 43

Zhu, L.J. & Cheng, N.S. 1993. *Settlement of Sediment Particles*. Nanjiing: River and Harbour Engineering Department, Nanjiing Research Institute (in Chinese)